DINNER'S SERVED IN THE DEEP SEA

Environmental conditions, organic matter transport, and benthic fluxes at cold-water coral and sponge communities in the deep sea

Evert de Froe

222 UTRECHT STUDIES IN EARTH SCIENCES

Environmental conditions, organic matter transport, and benthic fluxes at cold-water coral and sponge communities in the deep sea

DINNER'S SERVED IN THE DEEP SEA

Evert de Froe

ISBN : 978-90-6266-643-0

Layout: Studio Migle, www.studiomigle.com
Illustrations and cover design: Studio Migle, www.studiomigle.com
Printed in the Netherlands by Ipskamp Printing.

Dinner's Served in the Deep Sea

Environmental conditions, organic matter transport, and benthic fluxes at cold-water coral and sponge communities in the deep sea

Tafeltje dekje in de diepzee

Omgevingsfactoren, transport van organisch materiaal, en benthische fluxen op koudwaterkoraal- en sponsgemeenschappen in de diepzee

(met een samenvatting in het Nederlands)

Proefschrift

ter verkrijging van de graad van doctor aan de
Universiteit Utrecht
op gezag van de
rector magnificus, prof.dr. H.R.B.M. Kummeling,
ingevolge het besluit van het college voor promoties
in het openbaar te verdedigen op

maandag 13 maart 2023 des middags te 12.15 uur

door

Evert de Froe

geboren op 10 juni 1990
te Breda

Promotoren:
Prof. dr. G.J. Reichart
Prof. dr. K.E.R. Soetaert

Copromotor:
Dr. Ir. D. van Oevelen

Beoordelingscommissie:
Prof. dr. J.M. Roberts
Prof. dr. R.N. Glud
Prof. dr. Ir. S. Schouten
Dr. Ir. J.M. de Goeij
Dr. T. Stratmann

This thesis was supported by the European Union's Horizon 2020 Research and Innovation Program under grant agreement no. 678760 (ATLAS).

Voor jou mam

...Voorts is er verzet gerezen van de zijde van de biologen.
Een proces is altijd op zijn beurt een schakel in een meer
omvattend proces en het alles omvattende proces
is het wereldgebeuren...

...Furthermore, opposition has arisen from biologists.
A process is always in turn a chain in a more comprehensive
process and the all-encompassing process is the world event...

Arie de Froe
Van Waarneming tot Oordeel

Contents

Chapter 1

GENERAL INTRODUCTION

The ocean and the deep-sea ecosystem

The oceans cover around 70% of the earth's surface and have an average depth of four kilometres. This seems incredibly deep, but considering that the typical length of an ocean basin is 5,000 to 10,000 kilometres from coast to coast, an ocean has the same dimensions as an A4 sheet of paper (Talley et al., 2011). Oceans regulate the earth's climate system and provide crucial ecosystem functions by e.g., taking up carbon and heat from the atmosphere (Levitus et al., 2005; Friedlingstein et al., 2019), and redistributing heat from the tropics to the polar regions (Talley et al., 2011). Oceans thereby act as a buffer for the on-going climate change and global warming (Reid et al., 2009) and annually take up ~25% of anthropogenic carbon emissions (Sabine et al., 2004; Friedlingstein et al., 2022). Research in the past decades have shown that biological and physical processes in the deep sea, which starts below 200 m depth, are crucial for proper functioning of the ocean.

Phytoplankton (microscopic marine algae), when provided with sufficient sunlight, take up carbon and (inorganic) nutrients, and produce organic carbon by photosynthesis. A fraction of this primary produced organic matter is transported from the ocean surface layer into the ocean interior through physical mixing, vertical migrations of zooplankton and fish, and gravitational settling (Figure 1.1A; Middelburg, 2019; Sarmiento and Gruber, 2013; Volk and Hoffert, 1985). This downward export of organic carbon from the surface layer is known as the biological carbon pump (Ducklow et al., 2001; Boyd and Trull, 2007), and has been linked to past atmospheric CO_2 levels and climate cycles (Volk and Hoffert, 1985; Sigman and Boyle, 2000; De La Rocha and Passow, 2007). Once organic carbon is transferred below the permanent thermocline (~600 metre depth), it is considered sequestered from the atmosphere for centuries to millennia (Falkowski et al., 1998). Although there is large spatial variability between low- and high latitudinal areas, the biological carbon pump is relatively inefficient in transporting organic carbon to the ocean interior and seafloor (De La Rocha and Passow, 2007), as between 5 to 25% of net primary production is exported from the mixed surface layer, and only 1 to 3% reaches the seafloor (e.g., Buesseler, 1998; Martin et al., 1987; Figure 1.1A).

The deep sea, which starts below 200 metres depth, and has a volume of 1,368 * 10^6 km^3 is considered the largest environment on earth (Ramirez-Llodra et al., 2011). To put this into perspective, assuming that terrestrial ecosystems have a maximum vertical magnitude of 50 m (the size of a tall tree), the deep sea comprises 99.5% of the available habitat on earth (Herring, 2002). Despite its size, the deep sea is currently still one of the most understudied ecosystems (Ramirez-Llodra et al., 2011).

The upper 200 metres of the ocean, known as the epipelagic- and euphotic zone (Figure 1.1A), receives sufficient sunlight which enables photosynthesis (Lalli and Parsons, 1997). Below 200 metres however, light levels are too low to support photosynthesis, and therefore life in the deep sea depends, with the exception of chemoautotrophic ecosystems as hydrothermal vents (Karl et al., 1980), on sinking and advection of surface produced organic matter as food source (Gage and Tyler, 1991; Gooday, 2002). As only a small fraction of the surface produced organic matter reaches the seafloor (Buesseler et al., 2007), large parts of the deep sea are considered food limited environments (Smith et al., 2008) and are characterized by low abundances, biomass standing stock and productivity (Rex et al., 2006; Rowe et al., 2008; Figure 1.1A & C). However, food is not homogenously distributed among the deep sea, and regions of high productivity are found where organic matter is concentrated by, for instance, marine canyons, seamounts, and oxygen minimum zones (Levin, 2003; Ramirez-Llodra et al., 2010; Vetter et al., 2010; Levin and Sibuet, 2012; Rogers, 2018). Furthermore, hotspots of biological activity in the deep sea can also be formed by so called ecosystem engineers (*sensu* Jones et al., 1994) such as, cold-water corals and sponges, which provide shelter, structure, and habitat for a wide variety of species (Hogg et al., 2010; Roberts et al., 2009a; Figure 1.1B).

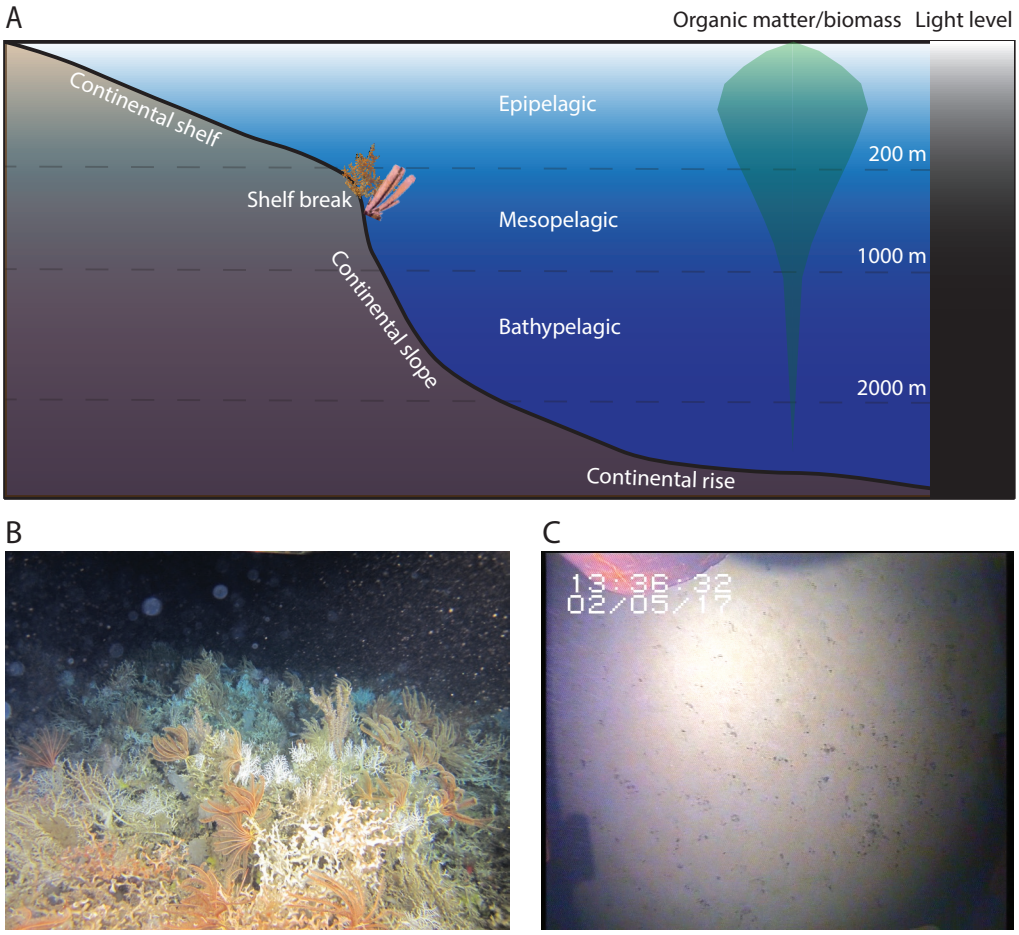

Figure 1.1: A) schematic cross-section of the ocean with its ecological division. B) Example of thriving cold-water coral reef at 750 m depth. C) Example of sediment dominated seafloor.

Cold-water corals and deep-sea sponges

Cold-water corals and deep-sea sponges can form extensive reefs and sponge grounds, respectively, and are important for deep-sea ecosystems in various ways. These hotspots are seen as reservoirs of biodiversity (Roberts et al., 2006; Hogg et al., 2010; Maldonado et al., 2017; Hawkes et al., 2019)., since they support numerous species through their framework or body plan (e.g., Buhl-Mortensen et al., 2010; Jensen and Frederiksen, 1992; Jonsson et al., 2004). Next to supporting high biodiversity, cold-water coral reefs and sponge grounds also increase the biomass of invertebrates (Klitgaard, 1995; Duineveld

et al., 2004) and fish species (Costello et al., 2005; Kenchington et al., 2013; Biber et al., 2014; Beazley et al., 2015). Cold-water coral reefs and sponge grounds trap and mineralize large amounts of organic matter and thereby enhance metabolic activity and carbon/nutrient cycling on the seafloor (Cathalot et al., 2015; van Oevelen et al., 2009). Furthermore, these biological hotspots could act as a refuge for deep-sea species affected by ongoing climate change (Tittensor et al., 2010; Gasbarro et al., 2022).

Cold-water corals belong to the phylum Cnidaria, i.e., Scleractinia (stony corals) and Octocorallia (gorgonian corals; Daly et al., 2007). These corals are distributed globally (Zibrowius, 1980) and highest densities are typically found along the continental margins and shelf breaks (Figure 1.1A, Figure 1.2A; Freiwald et al., 2004). Cold-water corals are passive suspension feeders that trap suspended particulate organic matter (sPOM) with their tentacles (Shimeta and Jumars, 1991; Mortensen, 2001) and by using mucus nets (Murray et al., 2019). In the north Atlantic Ocean, the most common framework building corals are *Desmophyllum pertusum* (Figure 1.2B, C & D; earlier described as *Lophelia pertusa*; Addamo et al., 2016) and *Madrepora oculata*, and non-framework building corals *Desmophyllum dianthus*, and the gorgonian coral *Primnoa resedaeformis* (Figure 1.2E).

The framework building scleractinian corals *D. pertusum* and *M. oculata*, are hermatypic colonial species, or reef-building species, that form branches of different shapes and sizes (Rogers, 1999; Brooke et al., 2009), depending on local hydrodynamic conditions and food supply (Mienis et al., 2012; Sanna and Freiwald, 2021). However, these corals often form bush-like colonies that grow several metres high and consist of thousands of polyps (Figure 1.2B). The coral colonies can grow in patches where the outer part of the patch consists of living cold-water coral tissue and the inner part of the patch, where food supply is relatively reduced, consists of died-off branches and tissue, also known as dead coral framework (Wilson, 1979; Vad et al., 2017). As these colonies grow, the coral framework can join together, cemented by the symbiotic polychaete *Eunice norvegica* (Figure 1.2C; Mueller et al., 2013), and thereby form extensive reefs on the seafloor (Roberts et al., 2009b). If favourable conditions for coral growth persist for a longer time, cold-water coral reefs can form into mounds by baffling of sediment between the branches of cold-water corals. These mounds can be hundreds of metres high and several kilometres wide (de Haas et al., 2009; Titschack et al., 2015). Research on coral mound growth over geological time scales has shown that coral mound growth follows glacial/interglacial cycles and is mainly dependent on sufficient food supply and hydrodynamic forcing (Frank et al., 2011; Hebbeln et al., 2019).

The gorgonian coral *Primnoa* spp. is an ahermatypic, or non-reef building, gorgonian cold-water coral which produces a protein skeleton and can grow several metres high in the water column (Figure 1.2E; Andrews et al., 2002). Although *Primnoa* spp. has a cosmopolitan distribution, the coral is most common in the North Pacific and North Atlantic regions between 100 to 800 metres depth (Krieger and Wing, 2002; Mortensen

and Buhl-Mortensen, 2005). These corals are known for their slow growth and can have a lifespan of several 100s of years (Risk et al., 2002). *Primnoa* spp. provide substrate for high biodiversity habitats (Heifetz, 2002; Krieger and Wing, 2002), supporting commercially important rockfishes and yelloweye (Andrews et al., 2002).

The phylum Porifera currently contains around 9,238 sponge species (Ahyong et al., 2022). Sponges are active filter feeders. They pump large quantities of water through their body plan (Vogel, 1977) and thereby feed on bacteria, dissolved – and, particulate organic matter (e.g., Pile and Young, 2006; Witte et al., 1997). Sponges in the deep sea can occur solitary, but are also found in large aggregations, which are known as sponge grounds. These sponge grounds can be dominated by one sponge species or by a mix of various sponge species, and have a reef-like structure (Kahn et al., 2015; Maldonado et al., 2017). Deep-sea sponge grounds are mainly formed by assemblages of glass sponges (Figure 1.3A) and massive demosponges (Figure 1.3A, C & D). These sponges have a global distribution and are mostly found on seamounts, continental margins, and shelf breaks (Levin and Sibuet, 2012; Figure 1.3E). Glass sponges and massive demosponges can grow up to several metres in diameter and, especially when densely aggregated, filter large volumes of water and thereby have a high impact on ecosystem functioning (Cathalot et al., 2015; Pham et al., 2019; Hanz et al., 2022).

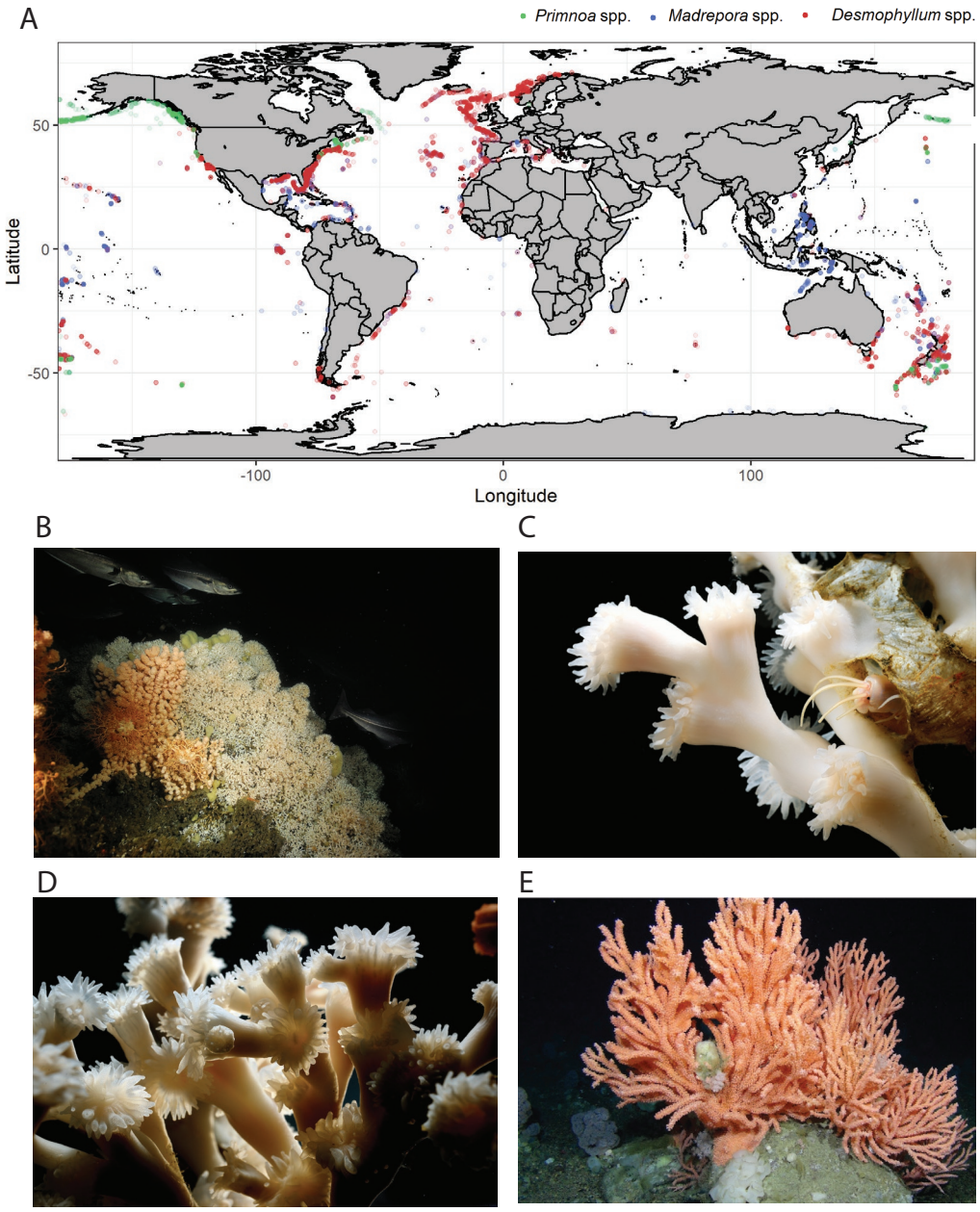

Figure 1.2: A) Global distribution of the cold-water corals Primnoa spp., Madrepora spp., Desmophyllum spp. B) Example of a Cold-water coral reef in Norway © Solvin Zankl, C) D. pertusum with the symbiotic polychaete Eunice Norvegica © Solvin Zankl, D) D. pertusum colony © Solvin Zankl, E) A large specimen of Primnoa spp, credit: DFO-Arcticnet.

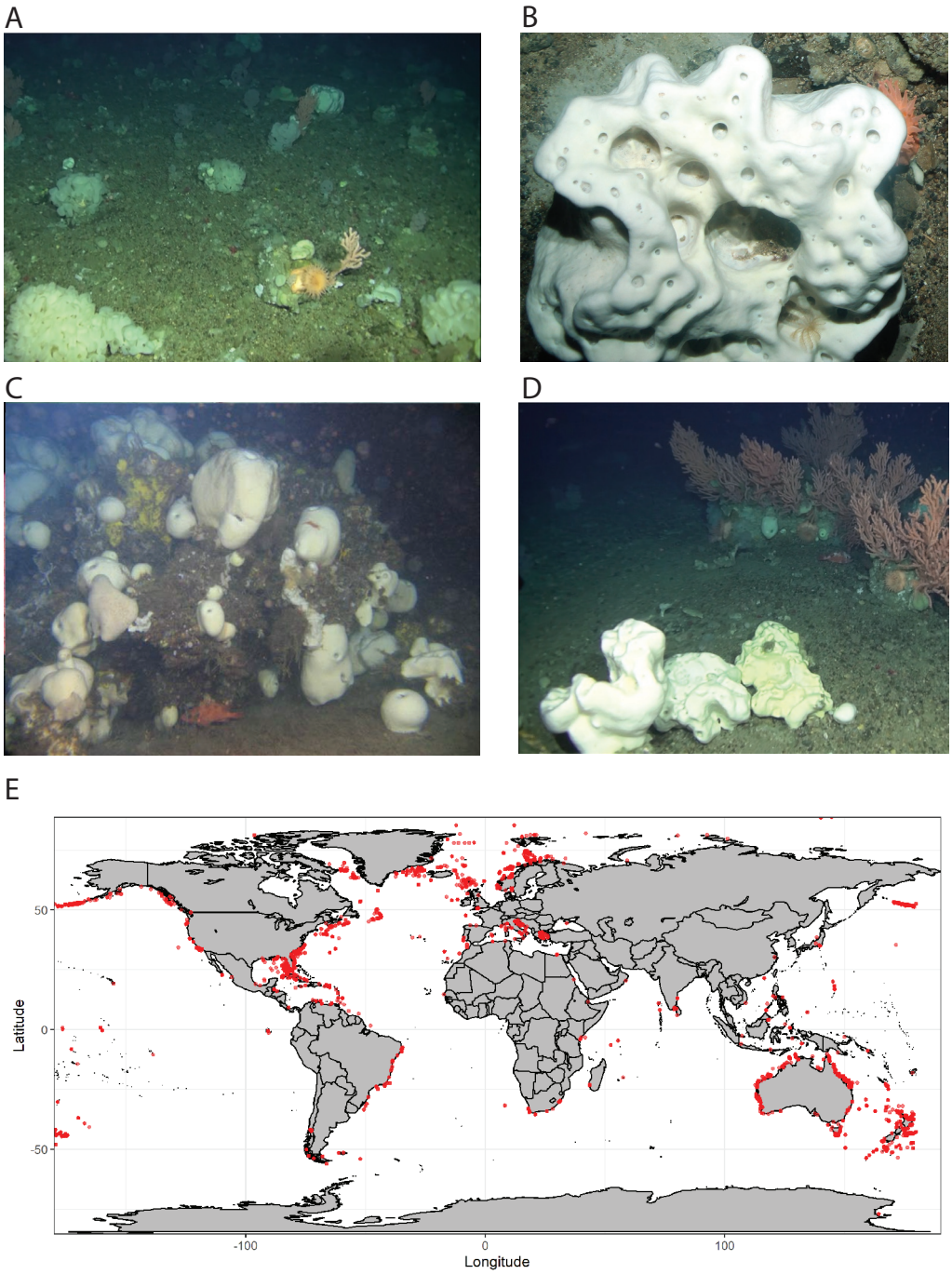

Figure 1.3: A) example of a mixed glass sponge/demosponge sponge ground, B) Geodia baretti, C) A Geodia spp. sponge assemblage, D) Geodia spp. sponges with Primnoa spp. on the background. E) Global distribution of the sponge genus Geodia spp. Credit for photos: DFO/Arcticnet.

Environmental conditions at cold-water coral reefs and deep-sea sponge grounds

The cosmopolitan distribution of cold-water corals suggest that they can be found in a wide variety of environmental conditions. Indeed, *D. pertusum* occurs within a temperature range of 4 – 12 °C and a salinity range of 32 to 39 PSU (Freiwald et al., 2004). In the northeast Atlantic Ocean, thriving *D. pertusum* reefs are linked to specific water masses and are thought to occur within a specific density envelope (Dullo et al., 2008). Although most records of living colonies of this coral species are found at oxygen concentrations of 6.0 – 6.2 ml L^{-1} (Davies et al., 2008), living corals are also found in hypoxic waters off the Angolan margin (Wienberg et al., 2018; Hanz et al., 2019). Framework building scleractinian cold-water corals like *D. pertusum* build their skeleton of aragonite (Allemand et al., 2004; McCulloch et al., 2012b), which is one of the three naturally occurring crystal forms of calcium carbonate ($CaCO_3$). Although these corals can maintain and grow their skeleton in aragonite undersaturated conditions (McCulloch et al., 2012b, 2012a), *D. pertusum* is mostly found above the aragonite saturation horizon (Guinotte et al., 2006). Additionally, thriving cold-water coral reefs have been related to relatively low dissolved organic carbon concentration in bottom waters (Flögel et al., 2014). The gorgonian coral *Primnoa* spp. builds a bimineralic skeleton mainly from aragonite, and calcite (Bostock et al., 2015). The distribution of this coral extends to greater depths, well below the aragonite saturation horizon, and to colder waters than *D. pertusum* and *M. oculata* (Figure 1.2A). Their ability to produce both aragonite and calcite likely protects *Primnoa* spp. from more corrosive waters and therefore enables these corals to survive at greater depths than scleractinian corals (Bostock et al., 2015). Although these abiotic environmental conditions, like temperature, constrain the spatial distribution of cold-water corals, cold-water corals often thrive in areas with strong bottom (vertical) currents that increase the supply of fresh organic matter towards the seafloor (Genin et al., 1986; Roberts et al., 2006; Davies et al., 2009).

Deep-sea sponges, such as glass sponges and massive demosponges, are most commonly found on temperatures ranging from 5 – 7 °C , though their range extends to water temperatures of < 0 to 21 °C (Klitgaard and Tendal, 2004; Howell et al., 2016). These sponges build their body plan with the help of silicious (SiO_2) spicules that form the skeleton and thereby benefit from increased silicic acid concentrations in the bottom water (Maldonado et al., 2011, 2020a). Measurements of near-bed currents have suggest that sponge grounds can occur within- (Hanz et al., 2021a, 2021b) or next to (White, 2003) areas with strong tidal currents.

Food supply towards cold-water coral reefs and deep-sea sponge grounds

Scleractinian cold-water corals feed on a variety of food sources, such as phytoplankton cells (Maier et al., 2019), suspended detrital matter, bacteria (Mueller et al., 2014), dissolved organic matter (Gori et al., 2014), and zooplankton (Mortensen, 2001; Carlier et al., 2009; Naumann et al., 2011). On which food source cold-water corals rely mostly depends on the geographic location and season (Maier et al., 2020a). For example, cold-water corals in Norway depend more on zooplankton as food source (Kiriakoulakis et al., 2005; van Oevelen et al., 2018), while deeper reefs in the North East Atlantic ocean feed on particulate organic matter (Duineveld et al., 2007).

Thriving cold-water coral reefs are found in areas with a relatively elevated quantity (Guinotte et al., 2006) and quality of food particles (Kiriakoulakis et al., 2007). Fresh organic matter can be transported towards the seafloor in various ways (Iversen and Lampitt, 2020). (i) Phytoplankton cells, inorganic minerals, detrital organic matter, and zooplankton faecal pallets can form aggregates. Passive sinking of these aggregates, also called 'marine snow', is thought to be primarily responsible for vertical transport of biogenic material in the water column (Fowler and Knauer, 1986; Alldredge and Gotschalk, 1988; Turner, 2015). (ii) Tidal currents that interact with bottom topography enhance mixing in the water column and promote episodic downward transport of organic matter (Davies et al., 2009; Duineveld et al., 2012). When a (tidal) current encounters an obstacle on the seafloor, like a bank/mound/sill, a hydraulic jump can occur downstream of the obstacle (Juva et al., 2020). This hydraulic jump draws shallow water, which contains fresh organic matter, downward towards the cold-water corals living on the seafloor (Davies et al., 2009). Additionally, high amplitude (>200 m) internal waves propagating along the density gradient of two water layers can also increase organic matter supply to the seafloor (Raddatz et al., 2014). Furthermore, breaking of these internal waves when encountered by bottom topography causes mixing of the water column and enhance vertical transport of organic matter (van Haren and Gostiaux, 2012; Cyr and Haren, 2016). Cold-water coral mounds are examples of such bottom topography that alter local hydrodynamics, enhance water column mixing, and promote food supply toward the seafloor (Cyr et al., 2016; Soetaert et al., 2016a; van der Kaaden et al., 2020). Additionally, the height of the cold-water coral mound is directly related to food supply, a process coined as a positive scale dependent feedback (van der Kaaden et al., 2021). (iii) High quality organic matter can also be supplied to cold-water coral reefs by lateral advection of resuspended, recently deposited fresh organic matter, especially when internal waves collide with bottom topography at a critical angle (White et al., 2005; Mienis et al., 2007). (iv) During spring time conditions, fresh organic matter can be laterally transported cross-slope of conti-

nental shelfs to deeper waters by 'Ekman drainage', which is related to basin scale ocean circulation (White et al., 2005; Simpson and McCandliss, 2013). (v) Finally, particulate matter can also be transported downwards by diel vertical migration of zooplankton, through i.e., a process called the 'lipid pump' (Steinberg, 1995; Jónasdóttir et al., 2015). These different food supply mechanisms provide different types of food to cold-water coral reefs and show distinct organic matter distribution in the water column above a cold-water coral reef. Research so far on organic matter distribution in the water column above cold-water coral reefs focussed on seasonal timescale, or provided a snapshot in time, but few have looked at a timescale of one diurnal tidal cycle.

Deep-sea sponges feed on bacteria, small particulate matter, and dissolved organic matter (Leys et al., 2018; Bart et al., 2021) by actively pumping water through their body plan (Vogel, 1977). Large assemblages of sponges filter large quantities of organic matter from the overlaying water column (Pham et al., 2019), which would quickly become depleted if this organic matter is not replenished at a sufficient rate. Compared to the current knowledge on food supply towards cold-water coral reefs, research on food supply to deep-sea sponge grounds is still in its infancy. Sponge occurrence is also related to the structure of the overlaying water column and the presence of intermediate water layers (Roberts et al., 2021), where internal (tidal) waves travelling across the density gradient between overlaying water masses could enhance food supply towards the sponges. Furthermore, sponge grounds are linked to areas where the interaction of internal waves with sloping boundaries cause turbulence and thereby increase food supply (Rice et al., 1990; Roberts et al., 2018; Davison et al., 2019; Hanz et al., 2021a, 2021b). Therefore, sponges are often found on seamounts, at the continental slope, and shelf breaks, where these processes are known to occur frequently (Roberts et al., 2021).

The effect of climate change and other human induced stressors on the deep sea

Research has shown that on-going climate change alters the conditions in the deep sea (Sweetman et al., 2017). For instance, the warming atmosphere enhances stratification in the upper water layer of the ocean (Li et al., 2020) which could decrease carbon supply to the seafloor (Bopp et al., 2001; Wohlers et al., 2009). The uptake of CO2 by the ocean also results in ocean acidification (Caldeira and Wickett, 2003), which is a threat to calcifying organism as cold-water corals and their reefs (Hennige et al., 2020). Furthermore, changing ocean circulation patterns (Boers, 2021; Caesar et al., 2021), increasing temperatures (Wijffels et al., 2016), and decreasing oxygen levels (Mora et al., 2013) affect marine life and deep-sea ecosystems such as cold-water coral reefs and deep-sea sponge grounds

(Gehlen et al., 2014; Levin and Le Bris, 2015; Brito-Morales et al., 2020; Jorda et al., 2020; Morato et al., 2020). To understand how these changes will affect the cold-water coral reefs and sponge grounds, knowledge on ecosystem functioning, environmental conditions, and spatial distribution of organisms is essential.

As the deep-sea remains a challenging environment to sample, predictive modelling tools are a cost-effective way to analyse how current conditions shape the spatial distribution of biological hotspots and what the effect of future conditions will be. Statistical methods, as habitat suitability modelling, i.e, show that deep-sea sponge distribution in the northwest Atlantic Ocean is related to salinity (Knudby et al., 2013) and CWC biomass is related to terrain variables as the body position index (De Clippele et al., 2021b). Although these types of models can successfully predict suitable habitat of i.e., cold-water corals (Rengstorf et al., 2014a) and deep-sea sponges (Howell et al., 2016), and how this will change in the future (Morato et al., 2020), they provide a limited framework to investigate mechanistically how changing environmental conditions affect distribution patterns, biomass, and ecosystem function. Mechanistic models, in which biological processes are described by physical, chemical, and biological process descriptions, help with this and provide a quantitative approach to investigate what happens to a system if conditions change.

The knowledge gaps

Research efforts in the past decades have vastly improved our understanding on cold-water corals and deep-sea sponges. However, many open questions remain to be answered and it is uncertain how these important ecosystems will react to changing oceanic conditions. To predict or understand the fate of cold-water coral reefs and deep-sea sponge grounds, a mechanistic understanding of the processes that drive their spatial distribution is required. While studies on food supply towards cold-water coral reefs have shown that tidal currents are important in sustaining a cold-water coral reef community, there are few studies that link hydrographic conditions with organic matter distribution in the water column over a relevant timescale of one diurnal tidal cycle (24h). Investigating how tidal waves influence the distribution of organic matter over the full spectrum (e.g., dissolved organic matter, sPOM, zooplankton) in the water column could help us understanding which food supply process (see paragraph above) is vital for cold-water coral reefs. Furthermore, how much food cold-water coral reefs require to sustain itself is currently poorly constrained. Although some studies have measured the benthic metabolism of a cold-water coral reef community in relative shallow reefs (~120-250 m depth), it remains unclear how much food deeper cold-water coral reefs require for maintaining its metab-

olism or support growth. Predicting the spatial distribution of cold-water corals and sponges in the deep sea is currently limited to statistical methods, which provide limited opportunity to quantitatively assess what drives the spatial distribution of these important ecosystems. Finally, in the past decades numerous studies have recorded near-bottom environmental- and hydrodynamic conditions at cold-water coral reefs, but data on sponge grounds remains limited. It is currently not well understood what determines the amount of sponge biomass at sponge grounds.

Aim and outline of this thesis

The main goal of this thesis is to better understand how cold-water coral reefs and sponge grounds can thrive in an otherwise food limited environment as the deep sea. Furthermore, this thesis provides a quantitative approach to further explore the mechanisms behind spatial distributions of cold-water coral reefs and sponge grounds in the deep sea. To this end, the organic matter distribution in the water column above a cold-water coral reef as well as the food supply towards a cold-water coral reef is investigated over a full diurnal tidal cycle (**chapter 2**). Then, the amount of food that a cold-water coral reef needs to sustain its metabolic demand is quantified with help of *in-situ* and *ex-situ* measurements of benthic oxygen and nitrogen fluxes (**chapter 3**). The results of these two data-heavy chapters are consequently used in a mechanistic modelling approach, which predicts cold-water coral biomass based on hydrodynamics, organic matter transport, and cold-water coral physiology (**chapter 4**). Finally, this thesis presents year-long time series of environmental and hydrodynamic conditions at two contrasting high- and low biomass sponge grounds (**chapter 5**).

Chapter 2: *Hydrography and food distribution during a tidal cycle above a cold-water coral mound* investigates how tidal activity influences the organic matter distribution in the water column above a cold-water mound. Cold-water coral reefs are known to occur in areas with high organic matter quality close to the seafloor and in strong tidal currents. However, few studies have quantified the organic matter composition over the full spectrum (DOM, bacteria, sPOM, zooplankton) and tried to link this to local hydrography. Furthermore, while most studies only provided organic matter data as a snapshot or over seasonal timescales, data on organic matter composition and quality over an timescale relevant to tidal activity (24h) is currently limited. In this chapter, a quantitative estimate of the water column organic matter distribution and quality is combined with seawater property measurements over a full diurnal tidal cycle to resolve the effect of tidal forcing on organic matter transport and availability to the cold-water coral reef community.

Chapter 3: *Benthic oxygen and nitrogen exchange on a cold-water coral reef in the North-East Atlantic Ocean* quantifies benthic metabolic rates at several cold-water coral reefs and adjacent sediment area. Although research efforts in the past decades have vastly increased our knowledge on the metabolism of individual cold-water corals, little is known on metabolic demands of whole cold-water coral reef communities. Furthermore, community-based data on benthic nitrogen fluxes of a cold-water coral reef is currently lacking. In this study, benthic fluxes are measured at a deep cold-water coral reef by two methods: *ex-situ* incubation experiments and *in-situ* aquatic eddy covariance oxygen measurements. The results of this study give an estimate of the amount of food that is required by cold-water coral reef communities to sustain their metabolic needs.

Chapter 4: *Modelling cold-water coral biomass and respiration based on physiology, hydrodynamics, and organic matter transport* provides a mechanistic modelling approach to quantitatively investigate the spatial distribution of cold-water coral biomass. Our current capacity to predict the spatial distribution of cold-water corals is based on statistical methods such as habitat suitability modelling. While these models can accurately predict presence/absence of cold-water corals, they provide a limited framework to investigate how changing environmental conditions affect distribution patterns, biomass, and ecosystem functions of cold-water coral reefs. Given that oceanic conditions are currently subject to change, new modelling tools are needed to understand how cold-water corals will respond to future conditions. This study presents a first mechanistic modelling approach predicting cold-water coral biomass based on hydrodynamics, organic matter transport and cold-water coral physiology.

Chapter 5: *Year-long benthic measurements of environmental conditions indicate high sponge biomass is related to strong bottom currents over the Northern Labrador shelf* assesses the environmental- and hydrodynamic conditions at a high– and a low biomass sponge ground for a matching period. Deep-sea sponge grounds are found in a variety of environmental conditions throughout the North Atlantic Ocean. However, currently little is known on what controls sponge biomass on a sponge ground. Furthermore, to date, the environmental conditions of the sponge grounds on the Northern Labrador shelf have not been documented. This chapter presents data on the annual dynamics of near-bed environmental– and hydrodynamic conditions at two contrasting high-and low biomass sponge grounds. The results of this study indicate that high sponge biomass is linked to strong tidal currents on the Northern Labrador shelf.

Chapter 2

HYDROGRAPHY AND FOOD DISTRIBUTION DURING A TIDAL CYCLE ABOVE A COLD-WATER CORAL MOUND

Evert de Froe, Sandra R. Maier, Henriette G. Horn, George A. Wolff, Sabena Blackbird, Christian Mohn, Mads Schultz, Anna-Selma van der Kaaden, Chiu H. Cheng, Evi Wubben, Britt van Haastregt, Eva Friis Moller, Marc Lavaleye, Karline Soetaert, Gert-Jan Reichart, Dick van Oevelen

Published in Deep Sea Research Part I as: de Froe et al. (2022), Hydrography and food distribution during a tidal cycle above a cold-water coral mound. Deep Sea Research Part I: Oceanographic Research Papers, 103854. doi: 10.1016/j.dsr.2022.103854.

Abstract

Cold-water corals (CWCs) are important ecosystem engineers in the deep sea that provide habitat for numerous species and can form large coral mounds. These mounds influence surrounding currents and induce distinct hydrodynamic features, such as internal waves and episodic downwelling events that accelerate transport of organic matter towards the mounds, supplying the corals with food. To date, research on organic matter distribution at coral mounds has focussed either on seasonal timescales or has provided single point snapshots. Data on food distribution at the timescale of a diurnal tidal cycle is currently limited. Here, we integrate physical, biogeochemical, and biological data throughout the water column and along a transect on the south-eastern slope of Rockall Bank, Northeast Atlantic Ocean. This transect consisted of 24-hour sampling stations at four locations: Bank, Upper slope, Lower slope, and the Oreo coral mound. We investigated how the organic matter distribution in the water column along the transect is affected by tidal activity. Repeated CTD casts indicated that the water column above Oreo mound was more dynamic than above other stations in multiple ways. First, the bottom water showed high variability in physical parameters and nutrient concentrations, possibly due to the interaction of the tide with the mound topography. Second, in the surface water a diurnal tidal wave replenished nutrients in the photic zone, supporting new primary production. Third, above the coral mound an internal wave (200 m amplitude) was recorded at 400 m depth after the turning of the barotropic tide. After this wave passed, high quality

organic matter was recorded in bottom waters on the mound coinciding with shallow water physical characteristics such as high oxygen concentration and high temperature. Trophic markers in the benthic community suggest feeding on a variety of food sources, including phytodetritus and zooplankton. We suggest that there are three transport mechanisms that supply food to the CWC ecosystem. First, small phytodetritus particles are transported downwards to the seafloor by advection from internal waves, supplying high quality organic matter to the CWC reef community. Second, the shoaling of deeper nutrient-rich water into the surface water layer above the coral mound could stimulate diatom growth, which form fast-sinking aggregates. Third, evidence from lipid analysis indicates that zooplankton faecal pellets also enhance supply of organic matter to the reef communities. This study is the first to report organic matter quality and composition over a tidal cycle at a coral mound and provides evidence that fresh high-quality organic matter is transported towards a coral reef during a tidal cycle.

Introduction

Framework-building cold-water corals (CWCs) are important ecosystem engineers in the deep sea and provide habitat for numerous species (Roberts et al., 2006). The CWC reefs can form large carbonate mounds ten to hundreds of metres high and several kilometres wide (Kenyon et al., 2003; van Weering et al., 2003). Carbonate mounds alter the surrounding hydrodynamic environment in various ways by enhancing current velocities (Mienis et al., 2007; Mohn et al., 2014), inducing episodic downward transport of waters from shallower depths (Davies et al., 2009; Soetaert et al., 2016a), and breaking of internal waves (van Haren et al., 2014; Cyr et al., 2016). The interaction of the tide (barotropic) with the topography generates internal (baroclinic) tidal processes, which enhance mixing and transport of fresh organic matter, produced at the sunlit surface ocean, to the coral mounds (Duineveld et al., 2004, 2012). Benthic communities on the coral mounds require high-quality organic matter to survive in a food-limited deep-sea environment (Duineveld et al., 2007). Previous work has shown that suspended particulate organic matter (sPOM) in the vicinity of CWCs is of higher quality than at similar water depths in the open ocean (Kiriakoulakis et al., 2007). To date, little is known about the variability of organic matter quality during tidal cycles, and how tidal activity influences the organic matter distribution in the water column close to coral mounds (Duineveld et al., 2007).

The diverse CWC reef communities exhibit a suite of feeding strategies. Scleractinian corals, such as *Desmophyllum pertusum* (formerly *Lophelia pertusa*; Addamo et al., 2016) and *Madrepora oculata*, are opportunistic passive filter feeders that retain a variety of food sources such as fresh phytoplankton (Maier et al., 2019), sPOM, bacteria (Mueller et al., 2014), dissolved organic matter (DOM; Gori et al., 2014), and zooplankton (Carlier et al., 2009; Purser et al., 2010; Naumann et al., 2011; Larsson et al., 2013; Gori et al., 2015). Other passive suspension feeders (i.e. crinoids, stylasterids, ophiuroids, hydrozoans, bryozoans) live in-between or on the coral framework and also trap particles and DOM from the water column (Duineveld et al., 2007; Henry and Roberts, 2007; Maier et al., 2021). The active filter feeders, including sponges and bivalves, pump water to filter particles from the water (Van Soest and Lavaleye, 2005; Bart et al., 2020; Maier et al., 2020a). Polychaetes (i.e. *Eunice norvegica*) feed on larger particles caught by coral polyps but also have a predatory feeding mode (Mortensen, 2001; Roberts et al., 2009a; Mueller et al., 2014; van Oevelen et al., 2018). The breadth and versatility of these feeding strategies suggest that CWC ecosystems can rely on a wide variety of organic matter sources.

A quantitative estimate of organic matter composition and quality in the water column could provide insight into the relative importance of each organic matter component (DOM, bacteria, sPOM, zooplankton) as a food source for the diverse reef community. Additionally, measurements on variability in organic matter composition over a full diurnal tidal cycle could resolve the effect of tidal forcing on organic matter availability

and transport. Few studies have measured the *in-situ* distribution and composition of the whole organic matter spectrum above CWC reefs; sediment traps and long-term moorings have been used to show that food sources such as phytoplankton and zooplankton vary in abundance at CWC reefs on diurnal (Maier et al., 2019; Van Engeland et al., 2019) and seasonal timescales (Duineveld et al., 2004; Mienis et al., 2009a). Furthermore, the combination of physical transport and biotic degradation determine the rate at which sPOM is modified in the ocean interior and the quality of organic matter that reaches the seafloor. Quality of organic matter is an important proxy to determine sPOM palatability for the reef community, as on sinking from the mixed layer, remineralization processes by archaea/bacteria and consumption by zooplankton changes sPOM quality and hence palatability (Cho and Azam, 1988; Lampitt et al., 1993; Steinberg, 1995).

The south-eastern slope of Rockall Bank (Figure 1.1A & B) is an area with numerous coral carbonate mounds hosting thriving CWC reefs (Kenyon et al., 2003). Previous work has described large amplitude (100-200 m) diurnal tidal waves (Mienis et al., 2007; van Haren et al., 2014) and biodiverse benthic communities living in this reefs, which feed primarily on phytodetritus (Duineveld et al., 2007; van Oevelen et al., 2009). Moreover, long-term seasonal studies revealed the arrival of a spring bloom on the seafloor in March/April, and more degraded organic matter in winter (Duineveld et al., 2007; Mohn and White, 2007; Mienis et al., 2009a). A modelling study suggests that there is a large mismatch between the high amount of organic matter required to sustain CWC reef metabolism and the comparatively low organic matter flux to the reef measured by sediment traps (van Oevelen et al., 2009). However, the organic matter transport pathways towards CWC reefs are still in debate. Some studies suggest cross-slope transport of organic matter from a shallower part of the Rockall Bank towards the coral mounds by the presence of intermediate nepheloid layers (Mienis et al., 2007; Bourgault et al., 2014), and 'Ekman drainage' (White et al., 2005; Simpson and McCandliss, 2013). Furthermore, a modelling study indicates the possibility of vertical transport of fresh organic matter during spring tide conditions (Soetaert et al., 2016a).

This study set out to investigate the organic matter distribution along the south-eastern (SE) slope of Rockall Bank and to determine the effect of tidal dynamics on organic matter distribution in the water column. By measuring the hydrography and organic matter composition throughout the water column during a full 24-hour tidal cycle along a transect from the shallow (±450 m) bank to a deep (±800 m) carbonate mound CWC reef, we aim to (i) assess the organic matter distribution in the water column along the transect and (ii) investigate how the tidal activity affects this organic matter distribution. Additionally, (iii) we attempt to unravel the importance of each potential food source (sPOM, bacteria, zooplankton) for the seafloor communities.

Materials and Methods

Study area

The study area is located on the SE Rockall Bank slope, 500 km west of Ireland (Figure 2.1A & B). Rockall Bank is a large submarine bank, with the seafloor mostly composed of soft sediment on the top and coral ridges and mounds are found on the SE slope between 400 and 1000 m water depth (Kenyon et al., 2003; Mienis et al., 2006). These ridges and mounds are formed by reef building corals such as *D. pertusum* and *M. oculata* and host a variety of associated macrofauna (e.g., sponges, crinoids, and polychaetes; van Weering et al., 2003; Van Soest and Lavaleye, 2005; Duineveld et al., 2007; Mienis et al., 2009b). The seafloor around the mounds and ridges in the study area consists mostly of biogenic sandy sediment, pebbles, and boulders (Figure 2.1E; Mienis et al., 2006; de Haas et al., 2009). The flanks of the ridges and mounds are covered by dead coral framework, coral rubble, and patches of living coral, whereas at the mounds summits dense populations of living corals are found (van Weering et al., 2003; De Clippele et al., 2019; Maier et al., 2021). The dominant current direction along the SE Rockall Bank margin is towards the south-west, driven by a cyclonic gyre circling the Rockall Bank (Hansen and Østerhus, 2000; Holliday et al., 2000; Mienis et al., 2007; Schulz et al., 2020). The bottom water temperature between 600 and 1000 m depth varies from 6 to 10 °C and the salinity ranges between 35.1 and 35.4 psu (Mienis et al., 2007). The bottom currents are also mainly in a south-west direction and can peak at 75 cm s^{-1} (Mienis et al., 2009a). A dominant diurnal baroclinic (internal) tide has been measured (van Haren et al., 2014) and can be seen as a modified Kelvin wave (Cyr et al., 2016), which causes cross-slope transport of water over a diurnal tidal cycle (Gerkema, 2019). Internal waves have been observed in the vicinity of these coral mounds (Huthnance, 1973; Mienis et al., 2007; Mohn et al., 2014), along with breaking of internal waves. This breaking of the wave can be caused by the interaction between the tide and the topography, and are especially predicted after the turning of the tide, which is the period of highest turbulence (van Haren et al., 2014; Cyr et al., 2016).

Sampling Stations

We collected data at four different stations along a transect from a shallow part of Rockall Bank to a coral-capped carbonate mound: Bank, Upper slope, Lower slope, and Oreo (~23 km length, Figure 2.1B). Data and samples were collected during two research cruises with the R/V Pelagia, 64PE420OF[1] from 24 April 2017 to 12 May 2017 and 64PE4361F[2] from 29 April 2018 to 10 May 2018; an overview of sampling stations is given in Table 2.1 and Figure 2.1. Station Bank (500 m depth) consists of biogenic sandy sediments located in a sediment wave field (Figure 2.1E). Upper slope (662 m depth) also consists of biogenic sandy sediments and lies north of a small mound cluster. Lower slope (843 m depth) has also biogenic sandy sediment as substrate type, and is located south of a mound cluster, next to a two layered (finer) sediment-filled area. Oreo is a carbonate mound (summit 750 m depth) with a dense thriving CWC reef (Figure 2.1F; **chapter 3**, Mienis et al., 2006). Reef community macrofauna (box core) and organic matter samples (*in-situ* pumps) were obtained during research cruise 64PE420 (2017) at stations Bank and Oreo. CTD-yoyos were performed for 24 hours at the four transect stations during cruise 64PE436 (2018), while water samples were regularly taken from Niskin bottles at five depth intervals (details below). Zooplankton samples were taken using vertical multinet deployments at the 24-hour stations (Table 2.1) for the determination of biomass and species composition. At stations Upper slope and Lower slope, zooplankton multinets were deployed during day and at midnight. Above Oreo, an additional multinet cast was done to obtain zooplankton samples for stable isotope and fatty acid analyses.

[1] Cruise report: 10.5281/zenodo.1454464
[2] Cruise report: 10.5281/zenodo.1454096

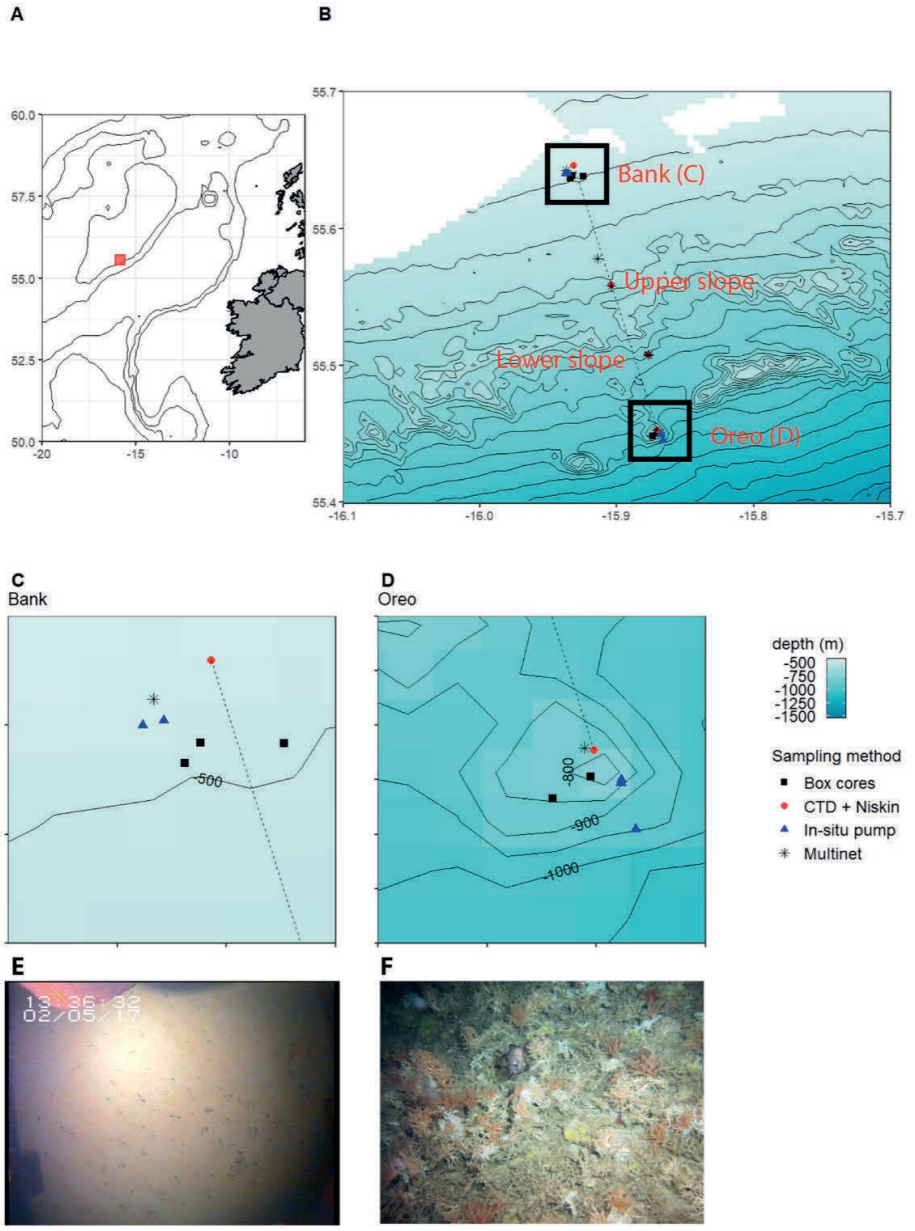

Figure 2.1 Map of the study area showing the transect of the four 24-hour CTD stations, box cores, in-situ pumps, and multinet sampling locations. The length of the transect is approximately 23 km. A) Location of the study area in the Atlantic Ocean. B) Transect along the south-eastern slope of Rockall Bank. C) zoom-in on Bank, D) zoom-in on Oreo, E) example of seafloor at station Bank, F) example of seafloor at station Oreo. Photos are stills taken from a box core deployment video (E) and ROV footage (F). Both videos were taken during research cruise 64PE420[2]F[3]. CTD = conductivity-temperature-depth. Latitude and longitude are given in decimal degrees

[3] Cruise report: 10.5281/zenodo.1454464

Table 2.1 Overview of sampling stations. Latitude and longitude coordinates are displayed in decimal degrees. * = averaged depth of all samples, n = number of samples. Number of Niskin bottles are total number of bottles from all depths combined. SI = stable istotopes.

Sampling	Station	Date	Cruise	Lat	Lon	Depth (m)*	n
In-situ pump system	Bank	3 May '17	64PE420	55.64	-15.94	470	3
"	Oreo	7 May '17	64PE420	55.45	-15.87	740	3
Box core	Bank	30 April '17	64PE420	55.64	-15.93	503	3
"	Oreo	4 May '17	64PE420	55.45	-15.87	838	2
CTD yoyos	Bank	3 – 4 May '18	64PE436	55.65	-15.93	486	53 casts
"	Upper slope	4 – 5 May '18	64PE436	55.56	-15.90	662	39 casts
"	Lower slope	5 – 6 May '18	64PE436	55.51	-15.88	843	25 casts
"	Oreo	2 – 3 May '18	64PE436	55.45	-15.87	757	33 casts
Niskin	Bank	3 – 4 May '18	64PE436	55.65	-15.93	486	35 bottles
"	Upper slope	4 – 5 May '18	64PE436	55.56	-15.90	662	35 bottles
"	Lower slope	5 – 6 May '18	64PE436	55.51	-15.88	843	30 bottles
"	Oreo	2 – 3 May '18	64PE436	55.45	-15.87	757	35 bottles
Multinet zooplankton	Bank	3 – 4 May '18	64PE436	55.64	-15.94	482	5 (day)
"	Upper slope	4 – 5 May '18	64PE436	55.56	-15.90	659	10 (day/ night)
"	Lower slope	5 – 6 May '18	64PE436	55.51	-15.88	844	10 (day/ night)
"	Oreo	2 – 3 May '18	64PE436	55.45	-15.87	755	10 (biomass/ SI)

24-hour CTD yoyo and Niskin bottles

A total of 149 CTD casts were done by yoyoing for 24 hours at each of the four sampling stations with a Sea-Bird 911 plus CTD system mounted on a steel frame in the centre of a Niskin Rosette water sampling unit. The CTD system was equipped with sensors for oxygen (SBE43), and a combined sensor for turbidity and fluorescence (Wetlabs ECO-FLNTU). Data were obtained at 24 Hz, averaged to a resolution of 1dbar using SBE Seasave software, and only downcasts profiles were used in analysis.

At 4-hour intervals, *i.e.,* seven times during the 24-hour cycle, water was sampled by Niskin bottles during the CTD upcast at 5 m above bottom (mab), 50 mab, mid-water, the deep chlorophyll maximum (DCM), and 5 m below the surface. Water samples were collected for nutrient concentration, DOC concentration, bacteria, virus, and phytoplankton cell densities, suspended particulate matter (SPM), sPOM (suspended + sinking POM), and pigment concentrations. On retrieval of the Niskin bottles, water was transferred into 10 L-containers using a silicone tube and moved to a temperature-controlled room (7-9 °C) for further processing.

Nutrient samples (10 mL-syringe) were filtered over a 0.45 µm-mixed cellulose ester filter into 5mL-pony vials and subsequently frozen at -20 °C until analysis in the laboratory at NIOZ, the Netherlands. DOC samples were taken with a pre-rinsed 20 mL-glass syringe over a pre-combusted glass fibre filter (GF/F pore size 0.7 µm; Whatman, GE Healthcare Life Sciences) into 4 mL-glass vials and stored at -20 °C. Samples for flow-cytometric cell counts of (a) bacteria and viruses, and (b) phytoplankton were taken with a 10 mL-syringe. Bacteria-virus samples were placed into 4 mL-cryo vials and fixed with glutaraldehyde (final conc. 0.5%), while phytoplankton samples were placed into a 8 mL-cryo vial and fixed with 18% hexamine-buffered formaldehyde (final conc. 1%). After cooling for 30 min at 4 °C, the flow cytometry samples were flash frozen in liquid nitrogen and stored at -80 °C. The sPOM and pigment samples were taken by filtering 3-5 L of water using a vacuum pump system. Prior to filtering, the 10 L-water container was mixed gently to ensure a uniform distribution of the particulates. The sPOM samples were filtered over a pre-weighed and pre-combusted 0.7 µm-pore size GF/F filter (diameter 47 mm). The filters were then rinsed with approximately 10 mL of an ammonium carbonate solution, stored frozen at -20 °C in a closed petri dish until analysis. Pigment samples were filtered over a GF6 filter (47 mm), wrapped in aluminium foil, flash frozen in liquid nitrogen, and stored at -80 °C.

Multinet zooplankton sampling

Zooplankton samples, both for biomass and stable isotope analysis, were collected by towing a Hydrobios Multinet system (net opening 0.25 m^2) from 10 mab to the surface (100 µm mesh size, speed ~30 m min^{-1}). The multinet sampled at five depth intervals: 10 mab to 50 mab, 50 mab to 100 mab, 100 mab to 100 m depth, 100 m depth to 50 m depth, and 50 m depth to the surface. Samples for zooplankton biomass were fixed in 37% borax-buffered formalin (final conc. 4%). Samples for zooplankton stable isotope and fatty acid analyses were separated in four size fractions by serial sieving on-board: 100 to 200 µm, 200 to 400 µm, 400 to 1000 µm, and > 1000 µm, and stored frozen (-80 °C).

Particulate organic matter sampling with *in-situ* pumps

sPOM *in-situ* pump samples were taken with a McLane Large Volume Water Transfer System Sampler (WTS-LV) *in-situ* pump (McLane Research Laboratories Inc., East Falmouth, MA, USA). Samples were taken at three depths: close to the seafloor (20 mab), at 120 mab, and at 15 m water depth. Each pump was programmed using Crosscut Version 1.0.3 for Windows before deployment. The sample volume was set to 2000 L with an initial flow rate of 7 L min^{-1}. After 50 minutes of filtering, the flow rate was automatically set by Crosscut to 4 L min^{-1} and at a time limit of 4 hrs. The *in-situ* pumps filtered up to 1,400 L of water through an acid-washed 53 µm nylon mesh above a pre-combusted (400ºC; 12 h) 0.7 µm- GF/F filter. Immediately after pump retrieval, the GF/F was photographed and stored at -20 ºC. Larger particles (>53 µm) collected on the nylon mesh were collected by vacuum-filtration using an additional pre-combusted GF/F and stored at -20 ºC.

Box cores benthic fauna sampling

Benthic macrofauna were collected using a cylindric box core (diameter: 50 cm, height: 55 cm, sampling area: ~0.2 m^2) as described in **chapter 3**. Benthic macrofauna were sorted on-board into broad taxonomic groups and stored frozen upon analysis (-20°C).

Laboratory analyses

Nutrients, DOC, sPOM, and plankton

Nutrient samples were analysed using a SEAL QuAATro analyser (SEAL Analytical Inc.) following standard colorimetric procedures. Water samples for DOC concentration were measured by automated UV-wet oxidation to CO_2 using a Formacs^{HT} Low Temperature Total Organic Carbon Analyser in combination with a non-dispersive infrared detector (Skalar). Unfortunately, concentration of NH_4^+ could not be determined accurately due to a technical error.

sPOM samples were freeze-dried, weighed, and analysed for organic carbon content, total nitrogen content, and organic carbon isotopic composition ($\delta^{13}C$) using an elemental analyser (Flash 1112, THERMO Electron Corporation) coupled to an isotope ratio mass spectrometer (EA-IRMS, DELTA-V, THERMO Electron Corporation). Pigment samples were first freeze-dried, then extracted with 90% acetone (Wright et al., 1991), and subsequently quantified by high performance liquid chromatography in combination with a fluorescence detector and a photodiode array absorption detector (Zapata et al., 2000).

Phytoplankton flow cytometry samples were analysed on a BD FACS Canto II flow cytometer (Becton Dickinson, San Jose, California) equipped with a 488 nm argon laser (Brussaard et al., 2013). Based on autofluorescence and sideward scatter signal, we distinguished four phytoplankton groups: nano-eukaryotes (NEUK), cryptophytes (CRYP), pico-eukaryotes (PEUK), and cyanobacteria (CYANO). The bacterial and viral samples were analysed using a BD FACS Calibur following the protocol of Marie et al. (1999) and Brussaard (2004). Samples were diluted with a Tris-EDTA (TE) buffer and subsequently stained with SYBR Green I (Molecular Probes, Invitrogen Inc.). Based on green fluorescence versus sideward scatter signal, we distinguished two groups of bacteria: high DNA containing bacteria (HBAC) and low DNA containing bacteria (LBAC) and three virus groups (vir I, vir II, and vir III). Final measured counts of cells/virions were corrected for a blank containing only TE-buffer and SYBR-Green I prepared and analysed using the same procedure as the samples. Gate settings and an example plot can be found in the supplementary material (Figure S2.1).

Benthic macrofauna and zooplankton

Individual copepods were counted, and the species/genera, stage, and sex were identified by the Institute of Oceanology in Gdansk, Poland (www.iopan.pl). Prosome length was measured for 10 individuals in each species/stage group in all samples. Non-copepod zooplankton groups were identified to genus or species level and counted; their total length was measured.

Benthic macrofauna and zooplankton samples were freeze dried and ground with a pestle and mortar or ball mill to homogenize the samples (list of samples: Supplementary Table S2.1). Subsamples (CWCs ± 20-30 mg, sponges ± 10 mg, ophiuroids, crinoids, and bivalves ± 2 mg) were transferred into silver cups. Carbonate-containing samples were exposed to hydrochloric acid fume (37% HCL) for three days and subsequently acidified in a by drop-wise addition of dilute HCl (2%, 5%, and 30%) prior to analysis. Samples were analysed for organic carbon content, total nitrogen content, and $\delta^{13}C$ and $\delta^{15}N$ on an Elemental Analyser coupled to an Isotope Ratio Mass Spectrometer (EA-IRMS, Thermo flash EA 1112). The $\delta^{13}C$ and $\delta^{15}N$ isotope values are expressed in parts per thousand (‰) relative to the Vienna Pee Dee Belemnite (VPDB) standard and atmospheric nitrogen, respectively.

Total lipids were extracted from macrofauna samples (6 mg to 1 g) with a modified Bligh & Dyer method, incubating the samples in a mix of methanol and chloroform (2 : 1) for two hours at room temperature (Boschker et al., 1999; Maier et al., 2019). The lipid-containing chloroform extract was separated by polarity into neutral-lipid derived fatty acids (NLFAs) and phospholipid-derived fatty acids (PLFAs) over a silicic acid (Merck)

column, then derivatised by mild alkaline methanolysis to fatty acid methyl esters (FAMEs). The respective NLFA/PLFA FAMEs were separated using gas chromatography (GC, HP G1530) on a BPX70 column (SGE Analytical Science) coupled to a Flame Ionization Detector (GC-FID) Trace GC Ultra.

Particulate organic matter sampled by in-situ pumps

The *in-situ* pump sPOM samples were freeze-dried and circles (10 mm diameter <53 µm; 4 mm diameter >53 µm) were punched out from the GF/F filters as subsamples to measure the content of particulate organic carbon (POC, n=2) and particulate nitrogen (PN, n=2). POC samples were de-carbonised prior to analysis (Yamamuro and Kayanne, 1995). POC and PN content was measured on a Thermo Scientific FlashSmart Elemental Analyser. $\partial^{13}C$ and $\partial^{15}N$ of POC and PN were determined on separate punches using an EA-IRMS (COSTECH EA and Delta 5-Advance MS, Thermo-Fisher Scientific). Lipids were extracted following a modified method described in Wolff et al. (1995). In short, sPOM samples were placed in a glass extraction thimble, an internal standard (100 µL of 5α(H)-cholestane; 101 ng μL^{-1}) was added followed by a mixture of dichloromethane and methanol (9:1; 15 mL). The extract was evaporated to dryness under a vacuum, passed through anhydrous sodium sulphate, dried under N_2 gas, and stored (-20 ∞C). Samples were then transmethylated (10% acetyl chloride/methanol; Christie, 1982), passed through a Pasteur pipette potassium carbonate column, and finally derivatised with N,O-Bis(trimethylsilyl)trifluoroacetamide (BSTFA; 30 µL, 40∞C, 30 min), blown down under N_2, and stored (-20∞C) until analysis by gas chromatography-mass spectrometry (GC-MS). Mass data were collected at a resolution of 600 Daltons, cycling every second from 50–600 Daltons, and were processed using Xcalibur software. The relative response factors of the analytes were determined individually for 36 representative fatty acids, sterols, and an alkenone using authentic standards. Response factors for analytes where standards were unavailable were assumed to be identical to those from available compounds of the same compound class.

Data analysis

Partitioning the total particulate organic carbon

To estimate the composition of POC for the 24-hour sampling stations, each of the following components was quantified. Phytoplankton/bacteria/virus cell/particle density, measured by flow cytometry, was multiplied by a cell/particle-to-carbon conversion factor taken from literature (Supplementary Table S2.2). Total phytoplankton C stock was calculated by multiplying the chlorophyll-*a* (chl-*a*) concentration with 40 (de Jonge,

1980). Conversion factors for nanoplankton are uncertain (Ribeiro et al., 2016). Our data consisted of two nanoplankton phototrophic groups (NEUK and CRYP) and two picoplankton phototrophic groups (PEUK and CYANO). Carbon content for CRYP range from 23 to 83 pg C $cell^{-1}$ (i.e. Berggreen et al., 1988; Tarran et al., 2006; Verity et al., 1992). Casey et al. (2013) reported a conversion factor of 2-6 pg C $cell^{-1}$ for eukaryotic phytoplankton, but it is not clear whether PEUK or NEUK were studied. In addition, the sampling location of phytoplankton is also important as cells tend to be smaller in tropical waters compared to temperate regions. We decided to use 50 pg C $cell^{-1}$ for both the CRYP and NEUK groups, 2590 fg C $cell^{-1}$ for PEUK, and 255 fg C $cell^{-1}$ for CYANO. Remaining phytoplankton (i.e. diatoms) C stock was calculated as total phytoplankton stock minus the sum of nanophytoplankton and picophytoplankton. The biomass of bacterioplankton was estimated at 20 fg C $cell^{-1}$ for both HBAC and LBAC (Lee and Fuhrman, 1987; Ribeiro et al., 2016). We used a viral particle-to-carbon conversion factor of 0.2 fg C $particle^{-1}$ (Suttle, 2005). Biomass of copepods and other zooplankton was calculated using length:carbon-weight regressions from literature (see table 1 and 2 in Middelbo et al., 2018; and i.e., Klein Breteler, 1982; Hirche and Mumm, 1992; Sabatini and Kiørboe, 1994; Satapoomin, 1999; Hygum et al., 2000; Madsen et al., 2001). Lastly, the total zooplankton carbon stock was obtained by summing all species/specimens.

The relative contribution of each C stock was obtained via division by POC concentration. The total measured POC concentration minus the sum of phyto-, bacterio, and zooplankton-C stock was then classified as 'detritus'. Here, we assume that the GF/F filter retained the majority of sPOM present in the water, except for viruses. While some studies indicate that a substantial number of bacteria can pass through the GF/F filter used for measuring POC (up to 30% of bacterial biomass; Altabet, 1990), others found a minor effect (<10 % of bacteria passing the filter; Caron et al., 1995). As we calculated bacterial/picophytoplankton C stock from cell counts, the bacterial/picophytoplankton fraction, and thereby the live POC fraction, is likely slightly overestimated in our results. However, this did not affect biomass and cell density estimates of bacteria and picophytoplankton. Furthermore, the viral C stock was divided by POC concentration, but is not accounted in measured detrital POC since viruses do pass through the GF/F filters. The Niskin bottle samples and zooplankton were taken over different timescales and quantities. Therefore, we only used POC and plankton concentrations averaged over the 24-hour cycle.

Organic matter quality indices

Common proxies for organic matter quality in the water column were used. We measured the chlorophyll-a:∑phaeopigment ratio (Lavaleye et al., 2002), where a higher value indicates relatively fresher material. We refer to ∑phaeopigments as the sum of phaeophytin

and phaeophorbide. We also measured the C/N ratio of sPOM, where high values suggest relatively more reworked material and the polyunsaturated fatty acid/monounsaturated fatty acid (PUFA/MUFA) ratio, where higher values suggest relatively fresher material (Kiriakoulakis et al., 2007).

Trophic markers to food sources for benthic communities

To identify potential food sources for the benthic macrofauna, we used stable isotopes and fatty acid/lipid trophic markers. The $\delta^{13}C$ and $\delta^{15}N$ composition of sPOM, zooplankton, and macrofauna were analysed using biplots, and differences between groups were statistically tested with Kruskal-Wallis and Dunn's tests. We did not correct $\delta^{13}C$ values for lipid-$\delta^{13}C$, as this is unusual on deep-sea invertebrates (i.e., Iken et al., 2001; Fanelli et al., 2011b, 2011a; van Oevelen et al., 2018). For benthic macrofauna and zooplankton samples, we used fatty acid trophic markers (FATM) to indicate the consumption of zooplankton, phytoplankton, and bacteria (Supplementary Table S2.3; e.g. Dalsgaard et al., 2003). For *in-situ* sPOM samples, we used total lipid trophic markers (including alcohols and sterols) to estimate the relative contribution of zooplankton, phytoplankton, and bacteria to the sPOM composition (Supplementary Table S2.4). To investigate if sPOM is dominated by diatom or dinoflagellate cells, we also calculated the ratio between $C_{20:5\omega3}$ (eicosapentaenoic acid or EPA), and $C_{22:6\omega9}$ (docosahexaenoic acid or DHA). A high EPA/DHA ratio is generally found in diatoms, while a low ratio is found in dinoflagellates (Dalsgaard et al., 2003).

Tidal model

Barotropic tidal components were estimated with a tidal model to determine the phase and magnitude of the barotropic tidal cycle for each CTD cast. The principal semi-diurnal (M2) and diurnal (K1) harmonics of barotropic tidal currents were extracted from the regional Atlantic Ocean 2011-atlas solution of the Oregon State University Tidal Inversion Software (OTIS; Egbert and Erofeeva, 2002). Atlantic Ocean 2011-atlas is based on a regional 1/12° Atlantic Ocean solution in deep water incorporating high resolution local solutions in a number of coastal areas. Tidal components (M2 and K1) were combined (Supplementary Figure 2.2) and presented for the same period as the 24-hour CTD stations.

Data reporting and statistical tests

Data are reported as mean ± standard deviation. Data were analysed in statistical software program R (R Core Team, 2019), and the R packages: *plot3D*, *OceanView*, *reshape2*, *RNetCDF*, *readxl*, *knitr*, *rmarkdown*, *ggplot2*, *cowplot*, *patchwork*, *oce*, *lubridate*, *dplyr*, *akima*, *FSA*, *RColorBrewer* (Wickham, 2007; Grolemund and Wickham, 2011; Neuwirth, 2014; Wickham, 2016a, 2; Michna and Woods, 2019; Soetaert, 2019b, 2019a; Wickham and Bryan, 2019; Wilke, 2019; Akima and Gebhardt, 2020; Kelley and Richards, 2020; Xie, 2020; Allaire et al., 2021; Ogle et al., 2021; Wickham et al., 2021). Parameter differences between stations were tested for both surface and bottom waters. To increase the statistical power, we pooled the 5 m and deep-chlorophyll maximum samples together for surface waters, and the 50 mab and 5 mab samples for bottom waters. The significance of spatial and temporal differences were first tested for normality with the Shapiro-Wilk test, and subsequently by ANOVA combined with a Tukey's HSD test with normally distributed data and by a non-parametric Kruskal-Wallis test combined with Dunn's test for non-normally distributed data. Lipid concentrations were converted to mole% and transformed by subtracting the mean for each compound. Lipid composition of *in-situ* pump sPOM was analysed by principal component analysis (PCA) and analysis of similarities (ANOSIM) on differences between sites and size classes.

Results

Biogeochemical water-column characteristics during a tidal cycle

Bottom temperature at station Bank showed a semi-diurnal pattern with an amplitude of 20-50 m (Figure 2.2A). Temperature profiles revealed a diurnal tidal cycle with an amplitude of 50-100 m at the Upper slope and of 150-200 m at the Lower slope and Oreo (Figure 2.2B-D) at ~400 m depth. In addition, at Lower slope, an overturning event was apparent just below the DCM, which transported water from 50 to 300 m depth (Supplementary Figure S2.3C). At Oreo, a higher frequency (~6 hour) tidal signal was recorded by the CTD casts superimposed on the diurnal pattern with an amplitude of 200 m (Figure 2.2C). Bottom water temperatures dynamics at the four stations corresponded well with the barotropic tidal current speed and direction (Figure 2.2E-H); when the tidal current speed increased in a northward direction, the bottom water temperature dropped, indicating that colder water was advected upslope, and when tidal currents turned to a southward direction, the opposite effect was seen. These temperature changes were most pronounced at Upper slope, Lower slope, and Oreo. Profiles of seawater density and buoyancy frequency showed that the water column at Bank and Upper slope was more stable than at Lower slope and Oreo (Figure 2.2I-L; Supplementary Figure S2.4). At Oreo, two water column instabilities, at 400 m and 580 m depth, were observed during the full diurnal tidal cycle (Figure 2.2L), while at Lower slope this was observed at 700m depth. No such overturning was apparent at Bank and Upper slope.

Fluorescence and turbidity were the highest in the surface waters and decreased with depth at all stations. At the station Upper slope, Lower slope, and Oreo, turbidity slightly increased again between 400 m depth and the seafloor (Supplementary Figure S2.3I-K). Silicate, nitrate, and phosphate concentrations increased with water depth at all stations (Supplementary Figure S2.5; Figure 2.5). Nutrient concentrations in surface waters were generally lower at Bank and Upper slope than at Lower slope and Oreo. For example, surface nitrate concentrations were significantly lower at Bank (7.89 ± 2.11 µM) and Upper slope (7.69 ± 0.59 µM) than at Oreo (8.73 ± 0.25 µM; TukeyHSD, $p<0.05$). Lower slope surface water showed intermediate nitrate concentrations (8.15 ± 0.55 µM). Silicate values in surface waters at Bank and Upper slope approached zero at the end of the 24-hour cycle. Moreover, the silicate and nitrate concentrations in the surface waters were correlated (0.87 – 1.2, $R^2>0.9$) at all four stations (Supplementary Figure S2.6).

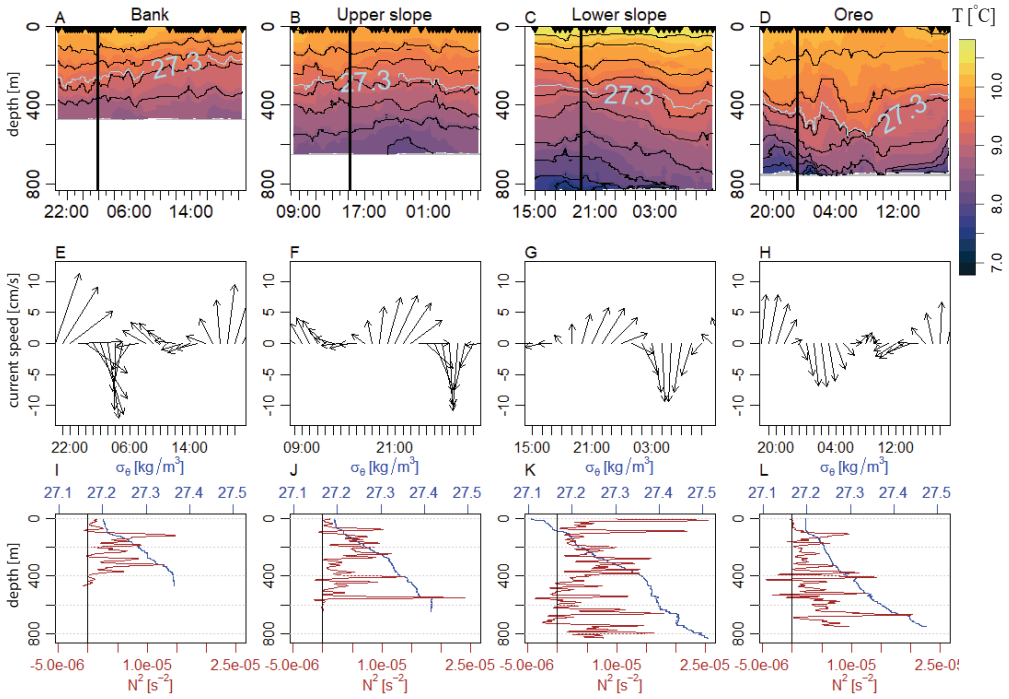

Figure 2.2 Temperature profile during the tidal cycle for Bank (A), Upper slope (B), Lower slope (C), Oreo (D). The contour lines represent density with 0.04 kg m^{-3} difference between each line, and the blue line represents the 27.3 isopycnal. Temperature is expressed in °Celsius. Black triangles at the top of plots A-D show the CTD casts. Barotropic tidal (M2 and K1 combined from tidal model) current speed and direction in cm s^{-1} for Bank (E), Upper slope (F), Lower slope (G) and Oreo (H). CTD profiles of density (in blue) and Buoyancy frequency (in brown) for Bank (I), Upper slope (J), Lower slope (K) and Oreo (K). Sampling time of these CTD profiles is indicated by the black triangles at the top of figures A-D.

Organic matter distribution in the water column during a tidal cycle

Particulate and dissolved organic matter distribution

Suspended particulate matter (SPM) concentrations measured in Niskin bottles were higher in the surface (3.1-3.6 mg L^{-1}) than in bottom samples (2.1-2.7 mg L^{-1}) for all 24-hour stations (Table 2.2; Supplementary Figure S2.7). Surface water POC was significantly higher at Bank and Upper slope compared to Oreo. Fluorescence (Supplementary Figure S2.3E-H) and pigment concentrations (Supplementary Figure S2.8) were likewise higher in the surface water at Bank and Upper slope compared to Lower slope and Oreo. Additionally, bottom water POC concentrations were on average higher at Bank and Upper slope than at Lower slope and Oreo ($p < 0.1$; Table 2.2; Figure 2.3A). Surface POC concentrations measured by *in-situ* pumps were 4 to 20 times lower than in the Niskin bottle samples. Furthermore, the surface POC concentration at Oreo, measured by *in-situ* pumps, was higher compared to the Bank and the material consisted mostly of small sPOM (<0.53 µm). In contrast, the bottom-water POC concentration, measured by *in situ* pumps, was higher at the Bank than at Oreo and consisted mostly of large sPOM (Table 2.2; >0.53 µm; Supplementary Figure S2.10). The mean surface DOC concentration was higher at Oreo compared to the other stations, but differences were not statistically significant (Table 2.2). Moreover, the average bottom DOC concentration was higher at Oreo as compared to Bank, Upper slope, and Lower slope (Dunn's test, $p<0.10$). Lastly, several peaks of DOC concentration of up to 380 µM were observed in the surface and bottom water at Oreo (Figure 2.3A).

Table 2.2 Summary statistics (mean ± standard deviation) for surface water and bottom water samples at the four 24-hour stations for SPM, POC, DOC, and zooplankton (ZP). Letters (a, b) represent statistical groups and indicate which stations were statistically different, where "a" has a higher median than "b". "ab" means the group is not statistical different from group a, and group b. Differences were significant if p value <= 0.05. Krus = Kruskall-Wallis test, Dunn = Dunn's test. * Upper value = Niskin bottles, lower value = in-situ pumps. Colour fills are coherent lwith the statistical groups, to visualize difference between stations.

	Variable	Test	Bank	Upper slope	Lower slope	Oreo
Surface	SPM (mg L^{-1})	Krus	3.2 ± 1.4^{a}	3.2 ± 1.0^{a}	3.6 ± 0.8^{a}	3.1 ± 0.8^{a}
	POC (µM)*	Dunn	16.9 ± 3.4^{a} / 1.1 ± 0.8	17.9 ± 6.4^{a} / -	12.4 ± 3.7^{ab} / -	9.6 ± 3.7^{b} / 2.9 ± 2.6
	DOC (µM)	Krus	93 ± 23^{a}	97 ± 24^{a}	87 ± 17^{a}	116 ± 73^{a}
	ZP (mmol C m^{-3})	Krus	1.1 ± 0.4^{a}	0.7 ± 0.3^{a}	0.6 ± 0.2^{a}	0.5 ± -^{a}
Bottom	SPM (mg L^{-1})	Krus	2.1 ± 0.6^{a}	2.3 ± 0.9^{a}	2.7 ± 0.6^{a}	2.5 ± 0.6^{a}

POC (µM)*	Dunn	2.3 ± 0.8[a] / 1.3 ± 0.8	2.1 ± 0.8[a] / -	1.8 ± 0.6[a] / -	1.8 ± 0.9[a] / 0.3 ± 0.1
DOC (µM)	Krus	92 ± 19[a]	88 ± 31[a]	76 ± 20[a]	128 ± 87[a]
ZP (mmol C m^{-3})	Krus	0.05 ± 0.01[a]	0.02 ± 0.01[a]	0.02 ± 0.02[a]	0.01 ± 0.00[a]

Pigment, nano-, picoplankton, bacteria, and viruses water concentrations

Pigments in the surface water samples at the four stations were composed mostly of chl-*a* and fucoxanthin (Supplementary Figure S2.8). Surface water chl-*a* concentrations, averaged over the full tidal cycle, were significantly higher at the Bank and Upper slope compared to the Lower slope and Oreo (Table 2.3). A non-parametric Dunn's test, which compares medians, showed significantly lower values of chl-*a* concentration for the Lower slope and Oreo compared to the Bank, but average chl-*a* concentration was highest at Oreo due to large variability over the tidal cycle (Table 2.3). Surface water chlorophyllide-a concentration increased during the 24-hour sampling period at Bank and Upper slope (Supplementary Figure S2.9 A & B) Nanophytoplankton consisted mainly of NEUK. Surface water showed higher concentrations of total nanoplankton (NEUK + CRYPT) at Bank than at Lower slope and Oreo (Table 2.3). Nanophytoplankton concentrations (NEUK + CRYPT) decreased with depth at all stations (Supplementary Figure S2.11) and the concentration in the bottom water was significantly higher at Bank than at Upper slope and Lower slope (Table 2.3). Picophytoplankton comprised mostly of PEUK and CYANO and concentrations in the surface waters were significantly higher at Lower slope compared to the Bank, Upper slope, and Oreo. Picophytoplankton concentration decreased with depth (Supplementary Figure S2.11) and was significantly higher at Bank than at Lower slope (Table 2.3).

Bacterial concentrations (HBAC + LBAC) were significantly higher in the surface waters at Bank compared to the Upper slope, Lower slope, and Oreo (Table 2.3). The HBAC:LBAC ratio was around 1:1 for all four stations. Bottom water bacterial concentrations were elevated at the Bank compared to Lower slope. Surface and bottom water viruses were composed mainly of VirII and virIII and concentrations were higher at Bank than Lower slope (Supplementary Figure S2.11). Viral concentrations were most variable at Oreo, with several spikes of high viral densities in the surface water (6-8 · 10^6 particles mL^{-1}) and bottom water (4-5 · 10^6 particles mL^{-1}), coinciding with high DOC concentrations (Supplementary Figure S2.12).

Table 2.3 Summary statistics (mean ± standard deviation) for surface water and bottom water samples at the four 24-hour stations. Letters (a, b) represent statistical groups and indicate which stations were statistically different, where "a" has a higher median than "b". "ab" means the group is not statistical different from group a, and group b. Differences were significant if p value <= 0.05. Krus = Kruskall-Wallis test, Dunn = Dunn's test. * Upper value = Niskin bottles, lower value = in-situ pumps. Colour fills are coherent with the statistical groups, to visualize difference between stations. Chl-a = chlorophyll-a, nano = nanophytoplankton, pico = picophytoplankton, bact = bacteria.

	Variable	Test	Bank	Upper slope	Lower slope	Oreo
Surface	Chl-a (µg L^{-1})	Tukey	2.0 ± 0.4^{a}	2.2 ± 0.5^{a}	1.2 ± 0.3^{b}	1.5 ± 0.5^{b}
	Nano ($\cdot 10^3$ cells mL^{-1})	Dunn	1.21 ± 0.40^{a}	1.17 ± 0.27^{ab}	0.97 ± 0.25^{b}	0.73 ± 0.37^{b}
	Pico ($\cdot 10^3$ cells mL^{-1})	Dunn	2.83 ± 0.91^{b}	2.37 ± 0.44^{b}	5.80 ± 1.97^{a}	3.06 ± 1.51^{b}
	Bact ($\cdot 10^5$ cells mL^{-1})	Tukey	8.0 ± 2.5^{a}	5.0 ± 1.6^{b}	5.7 ± 1.0^{b}	4.6 ± 1.5^{b}
	Virus ($\cdot 10^6$ cells mL^{-1})	Dunn	6.5 ± 1.2^{a}	5.4 ± 1.5^{ab}	4.5 ± 0.6^{b}	5.5 ± 1.4^{ab}
Bottom	Chl-a (µg L^{-1})	-	0.04 ± 0.010.03	0.06 ± 0.140.02	0.04 ± 0.080.02	0.07 ± 0.190.02
		Dunn	[median]^{a}	[median]^{ab}	[median]^{b}	[median]^{b}
	Nano ($\cdot 10^3$ cells mL^{-1})	Dunn	0.064 ± 0.054^{a}	0.043 ± 0.062^{b}	0.034 ± 0.039^{b}	0.054 ± 0.076^{ab}
	Pico ($\cdot 10^3$ cells mL^{-1})	Dunn	0.50 ± 0.26^{a}	0.35 ± 0.07^{ab}	0.37 ± 0.31^{b}	0.42 ± 0.25^{ab}
	Bact ($\cdot 10^5$ cells mL^{-1})	Dunn	1.6 ± 0.4^{a}	1.5 ± 0.4^{ab}	1.2 ± 0.4^{b}	1.6 ± 0.8^{ab}
	Virus ($\cdot 10^6$ cells mL^{-1})	Dunn	3.0 ± 0.3^{a}	2.6 ± 0.7^{ab}	2.2 ± 0.6^{b}	2.8 ± 1.1^{ab}

Zooplankton communities

The zooplankton community was dominated (>85 % of total biomass) by calanoid copepods (primarily *Calanus* spp and *Metridia lucens*) at all stations. Zooplankton-carbon concentrations were the highest in surface waters (Table 2.2). Surface water zooplankton-carbon concentration (strata 0-50 m) was higher at Bank (1.4 mmol C m^{-3}) than at Lower slope (0.7/0.8 mmol C m^{-3}, day/night, respectively), Upper slope (0.5/1.0 mmol C m^{-3}, day/night), and Oreo (0.5 mmol C m^{-3}). At Upper slope, a shift in carbon concentration at 300 m depth (from 0.2 to 0.05 mmol C m^{-3}) and surface waters (from 0.5 to 1.1 mmol C m^{-3}) was observed between day and night, respectively (Supplementary Figure S2.13). Bottom zooplankton carbon concentration was generally low, ranging from <0.01 mmol C m^{-3} at Oreo to 0.05 mmol C m^{-3} at the Bank.

Partitioning of particulate organic carbon

The bottom water at Oreo mound had the highest living POC fraction of bottom water at the four sampling stations (26%/37%, 5 mab/50 mab), together with the 50 mab-sample at the Bank (31%), while the lowest live POC was measured at 5 mab at the Upper slope (22%; Figure 2.3B). Detritus, the non-living fraction, comprised the largest fraction of POC in deeper water, ranging from 63 to 78% in bottom waters. The nanoplankton fraction of surface POC ranged from 24% for the surface water (5m) sample at Upper slope to 35% for the DCM sample at Oreo (Figure 2.3), and its contribution decreased with depth 5-15% in bottom waters. Picoplankton accounted for a small fraction of the POC throughout the water column (1% to 7%) and was highest in the surface water at Lower slope (7%). Remaining phytoplankton fraction was low at Lower slope (0-10%) but ranged throughout the water column from 17% to 33% for the stations Bank, Upper slope, and Oreo. Bacterioplankton dominated the POC in deeper waters (mid water, 50 mab and 5 mab), ranging from 10% at Bank to 15% at Oreo, where it also was the largest fraction of living POC. Zooplankton carbon was a small (0 – 5%) fraction of the POC throughout the water column, with higher contributions in surface (2-5%) than deeper waters (0-1%). Viruses represented only a small fraction of POC throughout the water column (2-3%).

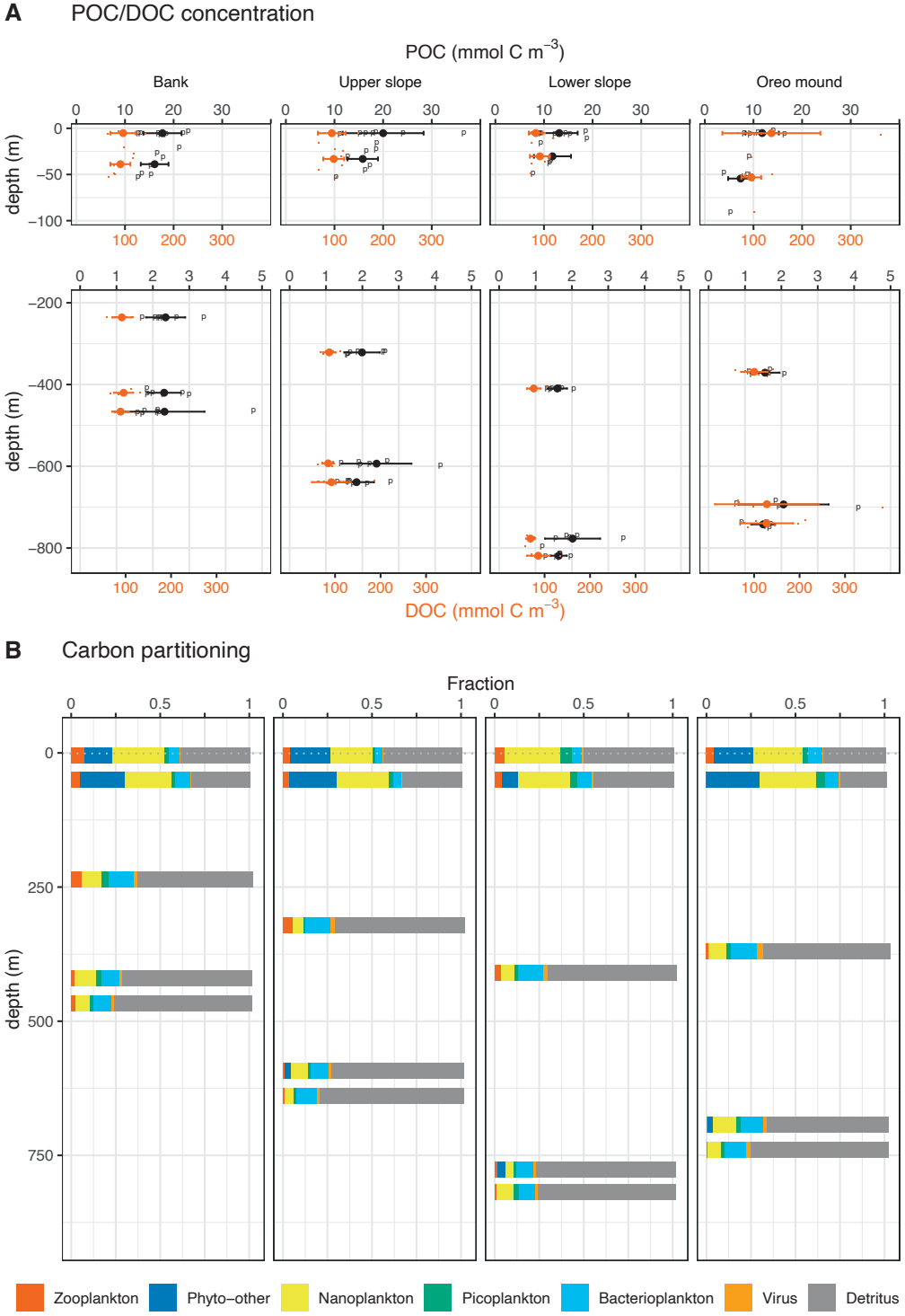
A
POC/DOC concentration
POC (mmol C m^{-3})
Bank
Upper slope
Lower slope
Oreo mound
depth (m)
DOC (mmol C m^{-3})
B
Carbon partitioning
Fraction
depth (m)
Zooplankton
Phyto–other
Nanoplankton
Picoplankton
Bacterioplankton
Virus
Detritus

← **Figure 2.3** A) POC (in black) and DOC (in orange) concentrations plotted over depth for the four sampling stations. Top x-axis is POC concentration, bottom x-axis indicates DOC concentration. Note the different scale for POC in the top and bottom plot of subplot to visualise bottom water differences. B) Carbon partitioning over indicated groups for the four stations.

Organic matter quality along the transect

Organic matter quality indices

Surface water chl-*a*:∑phaeopigment ratio was on average lower at the Bank compared to the other stations, but this difference was not statistically significant (Table 2.4). Bottom water chl-*a*:∑phaeopigment ratio was significantly lower at Bank than at Oreo. Surface water C:N ratio of sPOM was significantly higher at Oreo than at Bank and Upper slope, while the bottom water C:N ratio of sPOM did not differ significantly between stations (Table 2.4), although variability was higher at Oreo compared to the other stations. In the surface water *in-situ* pump samples (small and large fraction pooled), the PUFA/MUFA ratio was not significantly different between the Bank and Oreo. The bottom water PUFA/MUFA ratio was on average higher at Oreo compared to Bank (TukeyHSD, $p < 0.1$).

Table 2.4 Organic matter quality indices of sPOM samples from the four stations along the transect. To increase statistical power, bottom samples are combined the 5 mab and 50 mab samples for Niskin bottles, and deployments at 10 mab and 120 mab for the in-situ pumps. In cases that two values are provided, upper value refers to samples from Niskin bottles and the lower value to samples from in-situ pumps. PUFA = polyunsaturated fatty acid, MUFA = monounsaturated fatty acid. Differences were considered significant if p <=0.05. Letters (a, b) represent statistical groups and indicate which stations were statistically different, where "a" has a higher median than "b". "ab" means the group is not statistical different from group a, and group b. Differences were significant if p value <= 0.05. Krus = Kruskall-Wallis test, Dunn = Dunn's test. * Upper value = Niskin bottles, lower value = in-situ pumps. Colour fills are coherent with the statistical groups, to visualize difference between stations

		Test	Bank	Upper slope	Lower slope	Oreo
Chl-a:Phaeo ratio	Surface	Krus	2.48 ± 1.74^{a}	3.25 ± 1.85^{a}	3.50 ± 2.38^{a}	3.26 ± 1.34^{a}
	Bottom	Dunn	0.58 ± 0.35^{a}	1.01 ± 1.05^{ab}	0.95 ± 0.91^{ab}	1.42 ± 1.06^{b}
C/N ratio*	Surface	Dunn	5.89 ± 0.46^{b} /	5.86 ± 0.46^{b} /	6.47 ± 0.58^{ab} /	7.73 ± 2.84^{a} /
			3.11 ± 1.73^{a}	-	-	3.55 ± 1.04^{a}
	Bottom	Krus	7.5 ± 2.6^{a} /	6.6 ± 1.8^{a} /	7.6 ± 1.8^{a} /	7.8 ± 4.0^{a} /
			5.6 ± 1.1^{a}	-	-	4.7 ± 0.9^{b}
PUFA/MUFA ratio	Surface	Krus	4.54 ± 4.12^{a}	-	-	1.91 ± 1.74^{a}
	Bottom	Krus	1.83 ± 0.53^{a}	-	-	2.27 ± 0.49^{a}

Lipid composition from in situ pump sPOM

The lipid concentration showed a similar trend over depth as the POC and PN, with elevated values close to the sea floor at Bank, while values decreased with depth at Oreo (Supplementary Figure S2.14). Lipids in the bottom water sPOM, for both the small fraction (0.7 – 53 µm) and the large fraction (>53 µm), were dominated by the fatty acid $C_{16:0}$ and PUFA and MUFA such as $C_{18:1}$, $C_{18:2}$, $C_{18:3}$, $C_{20:5\ \omega3}$ (eicosapentaenoic acid or EPA), and $C_{22:6\ \omega9}$ (docosahexaenoic acid or DHA), with minor amounts of sterols. PCA showed that the small fraction (0.7 – 53 µm) and the large fraction (>53 µm) separate along the PCA1 axis (ANOSIM; r = 0.785, p < 0.001; Figure 2.4). This separation is driven largely by (1) a higher abundance/contribution of $C_{18:3\ (cis\text{-}6)}$ (diatom-fatty acid trophic marker) in the large particles, pointing to abundance of diatom aggregates, and (2) higher abundance/contribution of $C_{18:1}$ alcohols (zooplankton fatty-acid trophic marker). Differences along the PCA2 axis are driven primarily by (1) higher contribution of EPA + DHA for the high values, and (2) lower contribution of C_{16} alcohols. However, there was no significant difference in lipid composition of sPOM between the two stations (ANOSIM; r = -0.0219; p = 0.596). PUFA concentration in the bottom water was higher at the Bank compared to Oreo in both the large (140 ± 28 and 8 ± 4 ng L^{-1}, respectively) and small (299 ± 164 and 92 ± 37 ng L^{-1}, respectively) size fractions.

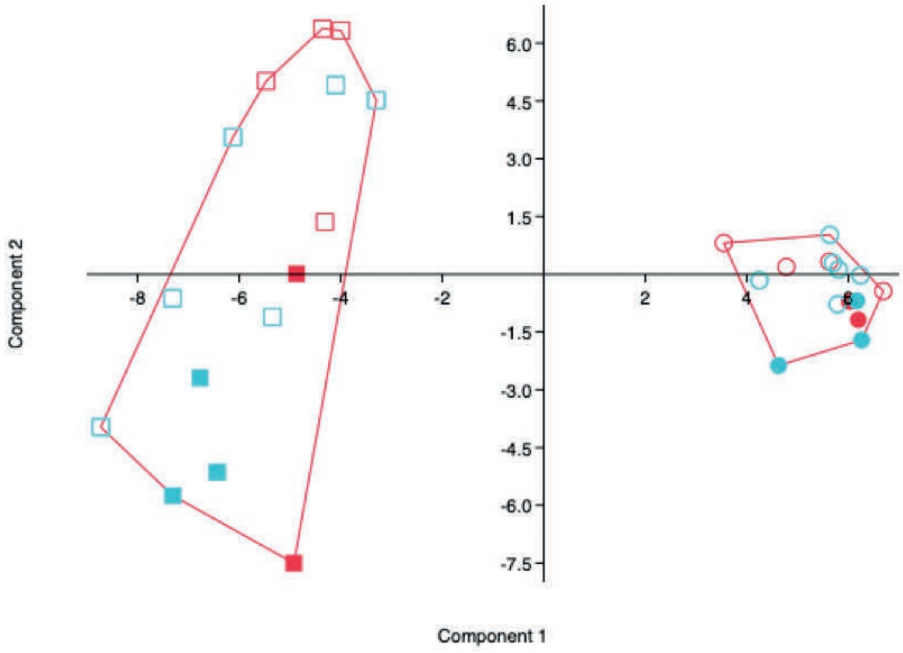

Figure 2.4 sPOM lipid composition. Squares >53 µm, circles 0.7 – 53 µm; filled – surface, open – deep, red is Bank, cyan is Oreo. PC1 and PC2 scales show Eigenvalues.

Tidal effect and organic matter quality

At Oreo, we observed a possible effect of an internal tidal wave on organic matter composition/quality near the coral mound seafloor. After the internal wave passed (23:00), the 50 mab water samples at Oreo (Figure 2.5) showed an increase in all measured sPOM variables (i.e., POC, chl-*a*, picophytoplankton), and a decrease in nutrient concentration (Figure 2.5). There was also a second peak in picophytoplankton at 22:30, with a corresponding lower nutrient concentration. Accordingly, the bottom water was more oxygen-rich and warmer after the tidal wave passed (Figure 2.5 E&F, Figure 2.2 D&H).

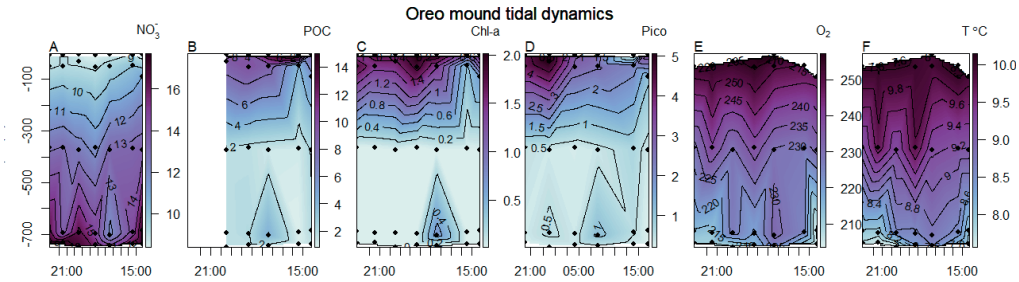

Figure 2.5 Interpolated profiles of Oreo mound during a tidal cycle with A) Nitrate concentration in µM, B) particulate organic carbon concentration in µM, C) chl-a concentration in µg L^{-1}, D) total picophytoplankton concentration in $\cdot 10^3$ cells mL^{-1}, E) oxygen concentration in µmol L^{-1}, and F) temperature in degrees Celsius. The x axis shows sampling time, the y axis shows depth in metres. Note that the first two samples for POC were not available due to a sampling error.

Linking organic matter in the water column to the macrobenthos

Isotopes and C/N ratios of sPOM, zooplankton, and seafloor community

The POC from the *in-situ* pumps tended to have higher $\delta^{13}C$ values than the POC from the 24-hour Niskin bottle-deployment. Bottom water POC collected by Niskin bottles showed a significantly higher $\delta^{13}C$ on the Bank (-23.9 ± 2.3 ‰) compared to Upper slope (-25.9 ± 1.4 ‰), and Lower slope (-26.0 ± 0.8 ‰). At Oreo, bottom water $\delta^{13}C$ of POC (-24.5 ± 2.9 ‰) was significantly higher compared to Lower slope (-26.0 ± 0.8 ‰; Dunn's test, $p<0.05$). The POC collected by *in-situ* pump showed a higher $\delta^{13}C$ at Oreo than at the Bank (Supplementary Figure S2.15, Figure S2.16, and Figure S2.17). Niskin bottle POC became depleted in ^{13}C with depth while the *in-situ* pump POC became enriched in ^{13}C with depth. The POC sampled by *in-situ* pump showed a similar $\delta^{15}N$ at the Bank and at Oreo in the surface and bottom waters, despite a difference of 300 m in depth for the latter (Supplementary Figure S2.17). The large fraction sPOM showed around 1 ‰ lower $\delta^{15}N$ values than the small fraction.

Zooplankton $\delta^{13}C$ ranged from -26.5 and -20.5 ‰ and differed between the size classes (Supplementary Figure S2.18C). Bottom-water zooplankton samples were depleted in $\delta^{13}C$ compared to surface-water samples. The $\delta^{15}N$ value of zooplankton increased with depth and showed a clear distinction between size classes (Supplementary Figure S18B). The largest zooplankton (>1000 µm) in bottom samples have higher $\delta^{15}N$ values (8.0 – 8.5‰) than the smaller zooplankton (100-400 µm; 4.1 – 4.6‰). The C/N ratio of smaller zooplankton classes (100-400 µm) increased markedly with depth (Supplementary Figure S2.18E). In contrast, the C/N ratio of the largest zooplankton class (1000 µm) stayed rather constant from surface to 50 mab but was increased at the bottom.

The $\delta^{13}C$ of sediment and benthic macrofauna at the Bank ranged from -23.9 to -19.1‰ and at Oreo from -22.9 to -13.2‰. The surface sediment (0-1 cm) at Oreo was on average higher in $\delta^{13}C$ (-20.6 ± 0.3 ‰) than the sediment at the Bank (-22.0 ± 1.2 ‰), but the differences were not statistically significant (ANOVA, $p > 0.05$). Likewise, bivalves showed a higher $\delta^{13}C$ at Oreo (-16.3 ‰) compared to the Bank (-19.7 ± 0.4 ‰). The sediment was higher in $\delta^{15}N$ at Bank (5.3 ± 0.4 ‰) compared to Oreo (4.9 ± 0.4 ‰), but this difference was not significant (ANOVA, $p > 0.05$). Bivalves at the Bank had a similar $\delta^{15}N$ as the sediment and were enriched in ^{15}N by 2.6 ‰ relative to sPOM. The $\delta^{15}N$ value of framework building CWCs (~8.0 ‰) were significantly enriched compared to the *in-situ* pump sPOM samples (3.0 ‰). Ophiuroidea, *E. norvegica*, and sponges showed the highest $\delta^{15}N$ and $\delta^{13}C$ values overall (Figure 2.6B).

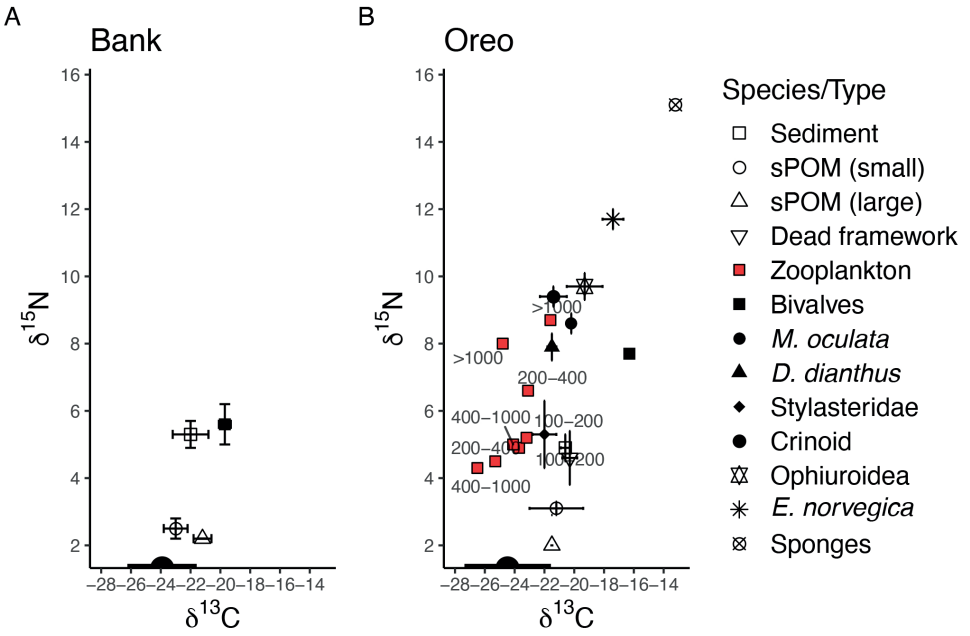

Figure 2.6 $\delta^{13}C$ and $\delta^{15}N$ stable isotope biplots for stations Bank (A) and Oreo (B). Size classes of zooplankton are shown inside the plot area (e.g., 400 - 1000 µm). sPOM samples, both small and large, are from the in-situ pump system. Niskin bottle sPOM $\delta^{13}C$ values (no $\delta^{15}N$ data available) are shown on the x-axis. Only bottom water sPOM and zooplankton are included in the plot.

Fatty acids/lipids of suspended and seafloor communities

Phytoplankton biomarkers were the largest fraction of sPOM lipids throughout the water column and at both sites (Bank, bottom-water: 44.9 ± 12.0% of lipids; Oreo, bottom-water: 44.0 ± 9.3% of lipids). Bacterial and zooplankton biomarkers in bottom sPOM samples were on average higher at the Bank (1.6 ± 0.5 % and 21.1 ± 7.6% of lipids, respectively) than at Oreo (1.0 ± 0.4 % and 16.9 ± 6.4% of lipids, respectively), but the differences were not significant (Kruskall, $p>0.05$). Zooplankton lipids were consistently higher in the small fraction sPOM than the large fraction (Figure 2.7A & B), and zooplankton lipids in sPOM increased with depth, especially at Oreo (Figure 2.7B).

Phytoplankton FATM were higher in the PLFA fraction of benthic organisms compared to the NLFA fraction, except for *E. norvegica*. The macrofauna *M. oculata*, *E. norvegica,* and Ophiuroidea contained more zooplankton FATM in their PLFA pool compared to Stylasteridae. Zooplankton in bottom-waters contained mostly FATM for zooplankton and phytoplankton (Figure 2.7C & D). Sponges showed higher bacterial FATM in their NLFA pool compared to the other benthic organisms. In addition, the EPA/DHA ratio of sPOM differed

between the small (0.7 – 53 µm) and the large (>53 µm) fraction (Supplementary Figure S2.19). The small sPOM fraction had an EPA/DHA ratio between 0.8 and 1.2, indicating no specific domination by any one phytoplankton group. The large sPOM fraction showed mostly an EPA/DHA ratio above 1, which suggests that the phytoplankton community is dominated by diatom cells. The CWCs had an EPA/DHA ratio above 1 in the NLFA fraction, but <1 in the PLFA fraction. The bivalve sample from the Bank station showed an EPA/DHA ratio close to zero in both the NLFA and PLFA fractions, indicating a dinoflagellate-rich diet. DHA was not detectable in most zooplankton samples.

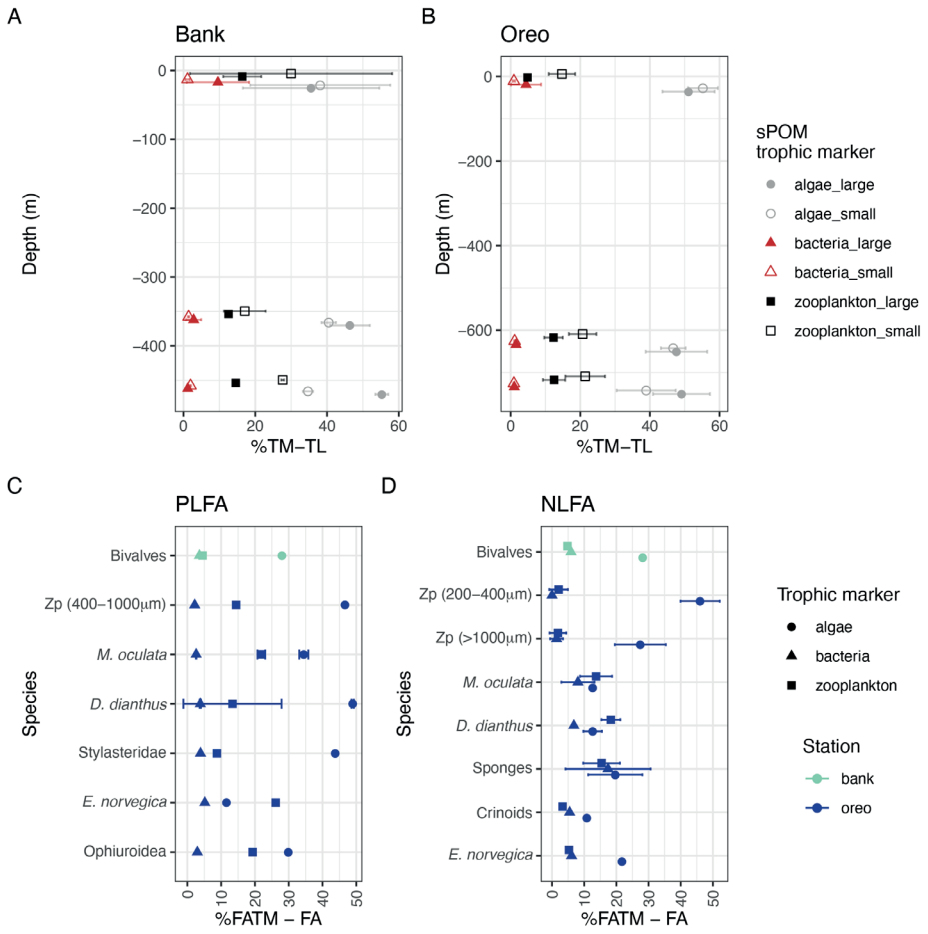

Figure 2.7 Lipid trophic markers of total lipids in the sPOM (small – and large fraction separately) at A) Bank and B) Oreo. %TM-TL = percentage trophic marker of total lipids. C) Fatty acid trophic markers in phospholipid-derived fatty acids (PLFAs) in benthos D) Fatty acid trophic markers in neutral-lipid derived fatty acids (NLFA) in benthos. Zp = zooplankton. Benthos species differ between the PLFA fraction and the NLFA fraction due to a technical error in the laboratory and a limited number of available samples, therefore not all macrofauna groups present in PLFA data are present in the NLFA data, and viceversa.

Discussion

We attempted to gain a better understanding of the transport and availability of organic matter during a full tidal cycle above a CWC mound and the subsequent utilization of this organic matter by benthic macrofauna. In the following sections, we discuss (1) water column dynamics, (2) surface phytoplankton communities, (3) organic matter supply and quality at the coral mound, (4) organic matter distribution in the water column, and (5) the relevance of different organic matter sources as food for the benthic communities.

Water column dynamics on the south-eastern slope of Rockall Bank

Coral mounds are often found in areas with increased internal tidal activity (Mohn et al., 2014; van der Kaaden et al., 2021). The interaction between the barotropic tide and bottom topography can cause energetic hydrodynamic features, e.g., hydraulic jumps and internal bores (Hosegood and van Haren, 2004; Juva et al., 2020). Coral presence and coral mound growth is likewise linked to the combined presence of an intermediate water layer and high internal wave activity (e.g. Raddatz et al., 2014; Rüggeberg et al., 2016). We measured a relatively small (50 m) amplitude tidal wave at 400 m depth on the Bank, but a larger amplitude wave (100 to 200 m) with a period of approximately 24 hours on the other three stations (Figure 2.2A-D). This is consistent with earlier 24-hour CTD yoyos performed in the area (Mienis et al., 2007). We recorded an internal wave at Oreo (~400 m depth) with an amplitude of 200 m (Figure 2.2D; Figure 2.5; Figure 2.8, process 2a). This wave passed by after the turn of the tide and likely formed by the interaction between the barotropic tide and the coral mound (Cyr et al., 2016). Alternatively, it could be a freely propagating internal wave, which are common in this area (Mohn et al., 2014).

Furthermore, coral growth and flourishing CWC reefs in the NE Atlantic have also been linked to a steep density gradient in a short bathymetric range and a narrow density envelope of sigma-theta (σ_θ) = 27.35 to 27.65 kg m^{-3} (Dullo et al., 2008). Here, density of the bottom water at Oreo falls within this proposed envelope and shows a steep density gradient at times during the 24h tidal cycle (Supplementary Figure S2.4D). Our temperature-salinity data indicate the presence of Wyville Thompson Overflow Water (WTOW) below 600 metres at Oreo (see Schulz et al., 2020). The WTOW is a water mass that is considered crucial for CWC presence on the slopes of Rockall Bank, transporting food, nutrients, and coral larvae to the seafloor (Johnson et al., 2010; Schulz et al., 2020). Schulz et al. (2020) note that sPOM in WTOW is of low quality, and that it is therefore unlikely that WTOW provides food directly. Indeed, our results also show high quality sPOM was mostly present in water with a density of σ >27.4 kg m^{-3}, which is beyond the upper density limit of WTOW (Johnson et al., 2010, 2017). Therefore, we argue that it is unlikely that

the WTOW itself carries high-quality sPOM (see also Schulz et al., 2020), but the WTOW pycnocline can play a role in causing turbulence and water column mixing above the coral mound (Vic et al., 2019). Internal waves that propagate along this pycnocline can cause increased horizontal currents and vertical displacements (White et al., 2007; Pomar et al., 2012). Large variability in variables as temperature, density, and nutrient concentrations are therefore also seen as a proxy for internal wave activity (Davison et al., 2019).

Our measurements showed that the bottom water at Oreo was highly dynamic over the tidal cycle (Figure 2.8, process 3a), *i.e.,* density, salinity, and buoyancy frequency there showed the highest variability close to the seafloor (Supplementary Figure S2.4). This suggests that the water column above the mound is partly stratified and partly well-mixed during a 24-hour tidal cycle, which could be the result of breaking internal waves on or over the steep topography. Similarly, intensified diurnal tidal waves have been observed close to the seafloor at Haas mound, a large CWC mound ± 5 km to the north-east of Oreo mound (van Haren et al., 2014; Schulz et al., 2020). In addition, variability in nutrient concentrations was high in the bottom water at Oreo (e.g., range in NO_3^-: 12 – 18 µM), which was also found previously at other CWC reefs on Rockall Bank and Norway (McGrath et al., 2012; Findlay et al., 2014; Juva et al., 2021). Therefore, our data confirm that the water column at Oreo mound is more dynamic than at the top of Rockall bank (e.g., Mienis et al., 2007, 2009, 2012; Findlay et al., 2014), likely due to vertical water displacements by internal (tidal) waves. These vertical displacements would benefit the CWCs and associated community in two ways (Findlay et al., 2014): First, flushing of CWC reef bottom water with nutrient-rich colder water prevents build-up of low oxygen and nutrient conditions close to the CWC reef. Second, downward transport of warmer water containing fresh sPOM supplies high quality food to the CWC reef, thereby also preventing bottom water depletion of high quality sPOM by the reef community (Lavaleye et al., 2009; Wagner et al., 2011).

Phytoplankton community dominated by diatoms

Primary productivity was higher in the surface waters at Bank and Upper slope compared to the Lower slope and Oreo, as indicated by higher concentrations of POC, chl-*a*, and CTD fluorescence. This is consistent with satellite data for chl-*a*, which shows that organic matter is retained on Rockall bank, while chl-*a* concentration decreases in surface waters in southward cross-slope direction (Mohn and White, 2007). The surface waters in the study area were dominated by diatoms, as shown by the dominance of fucoxanthin (Wright and Jeffrey, 1987; Barlow et al., 1993; Renaud et al., 2008) and the high EPA/DHA ratio in the *in-situ* pump samples, which compares well with previous work (Mojica et al., 2015). The chl-*a*:∑phaeopigment ratio of samples in the euphotic zone could be

used to determine the growth phase of a phytoplankton community, where a ratio of >10 is indicative of growing healthy algae cells, and a ratio of 1:1 represents degraded material (Bianchi et al., 2002; Lomas and Moran, 2011). Furthermore, a high chlorophyllide-a concentration is indicative of senescent diatom cells (Bianchi et al., 2002; Jeffrey et al., 2005). Our results suggest that the diatom communities were at the Bank and Upper slope were in a senescent phase (chl-*a*:∑phaeopigment ratio: ~1.3 and 0.7 respectively; increasing chlorophyllide-a concentrations), while actively growing at Lower slope and Oreo (chl-*a*:∑phaeopigment ratio: 2.6 and 3.98 respectively; Supplementary Figure S2.20). However, caution should be applied as high zooplankton grazing could also lower chl-*a*:∑phaeopigment ratio of surface water samples, and with the higher zooplankton biomass at Bank and Upper slope, this would suggest higher grazing activity at these sites (Louda et al., 2002).

Our findings also suggest that silicate is a limiting nutrient for phytoplankton growth in the euphotic zone. The near-1:1 correlation between surface nitrate and silicate concentrations (Supplementary Figure S2.6) suggests that nitrate is taken up almost solely by diatoms (Brzezinski, 1985), implying that diatoms are largely responsible for new primary production in the euphotic zone, and that other phytoplankton species utilise regenerated nitrogen in the surface waters (Dugdale and Goering, 1967; Dugdale and Wilkerson, 1998). At the end of the 24-h cycle at Bank and Upper slope, surface water silicate concentrations became depleted, but the POC concentration and cryptophyte abundance still increased, suggesting regenerated production, and minimal diatom growth (Sonnekus et al., 2017).

The station Oreo exhibits shoaling of nutrient-rich water in the top 100 metre surface layer during the tidal cycle (Figure 2.8, process 1a; Figure 2.5A; Supplementary Figure S2.5), which could be the result of the diurnal tidal semi-enclosed Kelvin wave. The tidal wave likely supplies silicate to the surface layer and stimulates new primary production (Figure 2.8, process 1b; Dugdale and Wilkerson, 1998). If this diurnal tidal wave reoccurs and replenishes nutrients in the surface layer at each tidal cycle along the slope of Rockall Bank, then new primary production could be elevated along the slope of Rockall Bank, and thus could be advected into the coral mound area from an upstream region (White et al., 2005; Soetaert et al., 2016a). New primary production is equal to export production at steady state (i.e. Middelburg, 2019). As the sinking of ungrazed, large diatom cells and the formation of diatom aggregates are considered key mechanisms in export of POC to the deep sea (Boyd and Newton, 1999), these aggregates could enhance carbon export towards the coral mound (Figure 2.8, process 1c). Previous research in the study area found that SPM in intermediate and bottom waters consisted mainly of biogenic material, such as diatoms and coccoliths, indicating this organic matter transport route can be important in the area (Mienis et al., 2007).

Increased organic matter quality at the coral mound and organic matter transport pathways

Food quantity and quality are drivers of benthic communities and food webs (Pearson and Rosenberg, 1978; Campanyà-Llovet et al., 2017). We report increased bottom water sPOM quality at the Oreo mound compared to the Bank site on a variety of temporal scales (12- and 24-hour) and variables (C/N ratio, chl-*a*/phaeopigments, PUFA/MUFA). The difference in sPOM quality between the stations along the transect is substantial, with a bottom-water chl-*a*:∑ phaeopigments ratio at Bank (0.57 ± 0.35) comparable with degraded sPOM from the Porcupine Abyssal Plain (North East Atlantic) at 4000 m depth, while at Oreo, the respective ratio (1.42 ± 1.06) is indicative of fresh/high quality material (Witbaard et al., 2000). The low quality sPOM at the Bank might be the result of organic matter retention on top of Rockall Bank, due to anticyclonic circulation of surface water around the bank summit (Mohn and White, 2007). The high variability of C/N ratios and $\delta^{13}C$ at Oreo, collected using Niskin bottles within the tidal cycle, indicates that the material originated from different sources, i.e., resuspended versus fresh sPOM (Figure 2.8, processes 2b & 3b; Supplementary Figure S2.16).

The higher organic matter quality at Oreo compared to the other stations is remarkable since the station is deeper than stations Bank and Upper slope. Nevertheless, high quality organic material can reach the seafloor through various pathways (Iversen and Lampitt, 2020), which are here demonstrated in a schematic illustration (Figure 2.8): (i) Via advective downward transport of water from shallower depth which is especially important for small particles such as picoplankton (Figure 2.8, process 2b; Richardson, 2019). (ii) High quality organic matter can also be transported towards the coral mound by lateral advection of resuspended, recently deposited fresh organic matter (Mienis et al., 2007). (iii) Organic matter can be transported downward cross-slope from the top of Rockall Bank to deep waters by 'Ekman drainage' (Simpson and McCandliss, 2013). (iv) Via formation and sinking of aggregates (Figure 2.8, process 1c; Thiem et al., 2006). (v) Finally, zooplankton can also transport carbon to the seafloor by diel vertical migration (DVM; Steinberg, 1995).

Here, we observed a spike in organic matter quality and quantity of bottom-water sPOM, shortly after an internal wave passed the CWC mound (Figure 2.5). Previous studies suggest a connection between internal tidal waves and organic matter freshness in the water column at CWC reefs (White et al., 2005; Mienis et al., 2007; Davies et al., 2009; Findlay et al., 2013; Soetaert et al., 2016a), and link fluorescence with cross-slope tidal currents (Duineveld et al., 2007). High quality sPOM in bottom waters has been observed at several CWC mounds and reefs in the NE Atlantic (Kiriakoulakis et al., 2007). Furthermore, tidal downward transport of fresh sPOM to the seafloor has been recorded previously for shallow CWC reefs (~100 to 200 m depth) as Mingulay Reef (Davies et al.,

2009; Duineveld et al., 2012) and Tisler Reef (Lavaleye et al., 2009). This study, when particularly looking at the nutrient data (Figure 2.5, Supplementary Figure S2.5), provides evidence that water from shallower depth (~300 m), characterized by low density, low nutrient concentration, high sPOM quality, and increased picoplankton concentration, is advected downward to the CWC mound after the passing of a 200-metre amplitude internal wave (Figure 2.8, processes 2a & 2b). To our knowledge, this is the first study to report this for a relatively deep (750 m) CWC reef. A steady tidal supply of high-quality food particles is thought to be a key factor for healthy CWC reefs (Juva et al., 2020). Although there is currently no quantitative assessment of the state of the CWC reef on Oreo mound available, the images from an exploratory ROV dive and box core deployment videos suggest the presence of a flourishing CWC reef (**chapter 3**, Figure 2.1 F). The presence of a healthy reef suggests downward advection of high-quality organic matter occurs more frequently throughout the year.

In this study, we found no evidence for strong resuspension and consecutive 'Ekman drainage' across the SE slope of Rockall Bank. Although the *in-situ* pump data showed enhanced POC quantity at the Bank seafloor, which is consistent with the turbid bottom mixed layer observed during time of sampling3F, no prominent benthic nepheloid layer was present cross-slope the Rockall Bank during both sampling campaigns (as in Thorpe and White, 1988; Simpson and McCandliss, 2013). This turbid layer on the Bank contained a relative high concentration of PUFAs in the large-fraction (>53µm), which suggests bottom POC included large diatom-rich sPOM which had settled on the seafloor recently (Zimmerman and Canuel, 2001). Our CTD data did record slightly elevated turbidity in the bottom 200-300 metres across the slope or Rockall Bank (Supplementary Figure S2.3I-K). This could be the result of resuspension events caused by interaction of bottom current with other coral mounds located on the SE slope of Rockall Bank and would enhance organic matter transport across the slope towards the coral mound. However, although our data only provides a snapshot (24 h) in time, values are generally low and therefore large particulate matter transport seem unlikely. Furthermore, the slightly higher turbidity concentration at Oreo mound could also be advected by WTOW (Vlasenko and Stashchuk, 2018; Schulz et al., 2020).

The formation of diatom aggregates and their fast sinking through the water column relative to individual plankton (and their waste products) enhances transport of fresh organic material to the seafloor (Thiem et al., 2006; Iversen and Ploug, 2010). Support for this organic matter transport route at Oreo mound is found in the high EPA/DHA ratio in large sPOM in bottom waters, indicating the presence of diatoms. Accordingly, the lower $\delta^{15}N$ values of large sPOM compared to small sPOM at depth suggest that the large particles were fresher and hence transported faster to the bottom water. Additionally, micro- and mesozooplankton consume sPOM, thereby producing faecal pellets which, like aggregates, sink faster to the seafloor than smaller-sized sPOM (Youngbluth et al.,

1989; Turner, 2015). The high concentration of zooplankton lipid biomarkers in bottom water sPOM (Figure 2.7B), particularly in the small fraction (15-25 mol% of total lipids), indicate the presence of these pellets, and imply that that the zooplankton generate small sized sPOM by mechanically breaking up larger sPOM/diatom aggregates. Alternatively, as zooplankton may store large amount of energy as lipids (Lee et al., 2006), the higher zooplankton lipid biomarker concentration in small sPOM could also be a result of high lipid content in bottom water zooplankton, which is supported by their high C/N ratio (Supplementary Figure S2.18E). Finally, DVM was seen at Upper slope, with higher zooplankton biomass at the surface during the night and below 100 m depth during the day, but we could not verify the occurrence of DVM at Oreo due to sampling restrictions due to heavy weather. However, it is highly likely DVM took place at Oreo since the dominant zooplankton (calanoid copepods) are well known to migrate vertically (e.g. Zaret and Suffern, 1976; Bandara et al., 2021).

Organic matter composition and plankton densities over depth

In the bottom water, POC largely consists of detrital material, while phytoplankton-C stock contributes less than 10% (Fuhrman et al., 1989; Caron et al., 1995; Roman et al., 1995). However, caution should be applied in interpreting this estimation since the chl-*a*:POC ratio (1:40, de Jonge, 1980) can show high variability depending on the season, phytoplankton community, and nutrient availability (de Jonge, 1980; Murray et al., 1994; Taylor et al., 1997; Sathyendranath et al., 2009; Mojica et al., 2015). Although bacteria comprised the largest living fraction of POC in bottom waters, which was also found by Roman et al. (1995), phytoplankton was occasionally the largest fraction, for example, in the high organic matter quality sample from Oreo mound. This high phytoplankton fraction of POC measured at Oreo (compared to the Bank, Upper slope, and Lower slope) indicate transport of fresh organic matter to depth.

The high plankton density (nano-, pico-, bacterioplankton, and virus particles) in the bottom water above Oreo Mound compared to the other stations on the slope demonstrates an increased availability of fresh planktonic food. The bacterial density in the bottom water at Oreo ($1.6 \pm 0.8 \cdot 10^5$ cells mL^{-1}) was on average slightly lower than prokaryotic abundance in the bottom-water at a shallow CWC reef in the Skagerrak ($3.2 \pm 0.1 \cdot 10^5$ cells mL^{-1};Weinbauer et al., 2012) and at other deep coral mounds close to our transect (range 3.1 to $4.9 \cdot 10^5$ cells mL^{-1}; Maier et al., 2011; van Duyl et al., 2008). Viral particle density at Oreo ($2.8 \pm 1.1 \cdot 10^6$ cells mL^{-1}) was lower than that measured at Skagerrak ($1.1 \pm 0.1 \cdot 10^7$ mL^{-1}; Weinbauer et al., 2012) and at other coral mounds in the study area ($5.7 - 8.4 \cdot 10^6$ mL^{-1}; Maier et al., 2011). In the present study, the variability in cell/particle density was larger than at the Skagerrak reef and in earlier Rockall Bank measurements (van Duyl

et al., 2008; Maier et al., 2011; Weinbauer et al., 2012). As zooplankton mostly feed on phytoplankton (Mauchline, 1998), their spatial distribution at the surface was closely linked to the chl-*a* concentration, with higher zooplankton biomass at Bank than at Oreo. We found decreasing zooplankton biomass with depth, consistent with observations on other North Atlantic zooplankton communities during spring (Gislason, 2018; Krumhansl et al., 2018). Overall, these findings show that, next to high variability in physical conditions (Juva et al., 2021) and higher sPOM quality, the plankton densities are increased close the CWC reef, indicating more food is available for suspension feeders living on the reef. Additionally, plankton densities were also highly variable over a single diurnal tidal cycle, a factor to consider in future sampling campaigns.

Food sources for the benthic communities

Our isotope and fatty acid data show that CWCs feed on a mixture of fresh phytodetritus, detritus, and smaller zooplankton, in agreement with previous work (Duineveld et al., 2007; van Oevelen et al., 2009; Galand et al., 2020). The $\delta^{15}N$ value of CWCs is comparable with previous observations at Rockall bank (8 - 8.5‰; Duineveld et al., 2007; Kiriakoulakis et al., 2005) and in the Mediterranean (Carlier et al., 2009), but lower compared to CWCs at Galicia bank (~9.5‰; Duineveld et al., 2004) and in Norwegian fjords (~10-11‰; Maier et al., 2020a). In the food web, CWCs are situated more than one trophic level above sPOM (assuming a 3.4‰ $\delta^{15}N$ enrichment per trophic level; Fry, 2006), indicating a mixed diet of sPOM and organisms of a higher trophic level, such as zooplankton (Mortensen, 2001). With respect to our third research objective, we could not, unfortunately, determine how important zooplankton is for the diet of CWCs. The stable isotopic signal of CWCs and presence of zooplankton-FATM imply CWCs might feed on zooplankton. Nevertheless, the observed presence of zooplankton-FATM in the CWC PLFAs alone is not enough to indicate a zooplankton diet, since CWCs can synthesize zooplankton-FATMs de novo (Mueller et al., 2014). Furthermore, at Rockall Bank, opposed to other CWC areas, zooplankton biomass in bottom waters in spring is low (present study, Duineveld et al., 2007). Nevertheless, the high food quality of lipid rich zooplankton (Lee et al., 2006), could imply CWCs only have to feed low amount of zooplankton to alter their trophic level. Alternatively, while CWC samples represent a longer time-integrated signal, the stable isotopic signal of sPOM and zooplankton biomass may vary on seasonal or annual scale. sPOM from sediment traps deployed at Oreo showed a higher $\delta^{15}N$ value in winter (~8 ‰) compared to spring (Korte et al., *in prep*), and more zooplankton were likely present in the bottom waters during winter and early spring when zooplankton (e.g. *Calanus* spp) are known to overwinter at depth (Heath et al., 2004). Therefore, the high trophic level of CWCs could originate from consumption of more degraded sPOM or higher zooplankton consumption

in winter, as CWCs may switch their diet with seasonally changing food availability (Maier et al., 2020a). Nevertheless, a diet of mostly zooplankton appears unlikely. In addition, the corals may consume resuspended organic matter, as the sedimentary $\delta^{15}N$ (~5 ‰) was precisely one trophic level lower than the CWC samples. In comparison with CWCs, zooplankton could still be of importance for the CWC reef community, as the polychaete *E. norvegica*, which lives in symbiosis with *D. pertusum* and builds tubes within the coral framework (Mueller et al., 2013), showed relatively high concentration of zooplankton FATM and the $\delta^{15}N$ value (11-12‰) was one trophic level higher than large zooplankton (8‰). This compares well with literature (Duineveld et al., 2007; Mueller et al., 2013; van Oevelen et al., 2018) and the observation that the polychaete can feed on suspended particles with their body extended up to 30 cm from the coral framework and steal food particles/zooplankton from polyps (Mortensen, 2001).

A further possible food source for the reef community is (labile) DOC, that can be taken up by a variety of deep-sea invertebrates (Rix et al., 2016; Maier et al., 2020b). We found elevated DOC concentrations in the bottom water (116 ± 73 µM) above Oreo as compared to the Bank (93 ± 23 µM). This higher DOC concentration at Oreo could originate from the sediment (Papadimitriou et al., 2002) and/or from reef biota such as CWCs (Wild et al., 2008; Maier et al., 2019). Other studies have also reported enhanced DOC concentrations above CWC reefs in the same study area (van Duyl et al., 2008; de Froe, unpublished data) and in the Skagerrak (Weinbauer et al., 2012) compared to open-ocean concentrations, indicating that CWC reefs are a source of DOC in the deep-sea (Wagner et al., 2011).

Conclusion

In summary, we have shown that the water column is more dynamic above a CWC mound at Rockall Bank in multiple ways. Our results suggest the presence of three organic matter transport mechanisms towards the coral mound. (1) Fresh organic matter of high quality is transported from mid-water depth to the seafloor by advection with internal waves (process 2a & 2b, Figure 2.8). (2) Furthermore, the replenishment of surface nutrients may enhance new primary production of diatoms, which aggregate and sink to mid-water depth and ultimately the seafloor (process 1b & 1c, Figure 2.8). (3) Lastly, zooplankton faecal pellets (and likely migration) may also enhance vertical transport of organic matter. The relative contribution of either of these mechanisms in fuelling the cold-water coral reef community remains to be clarified. Our study confirms that the reef benthic community feeds on a variety of food sources, yet ultimately depends on surface primary production.

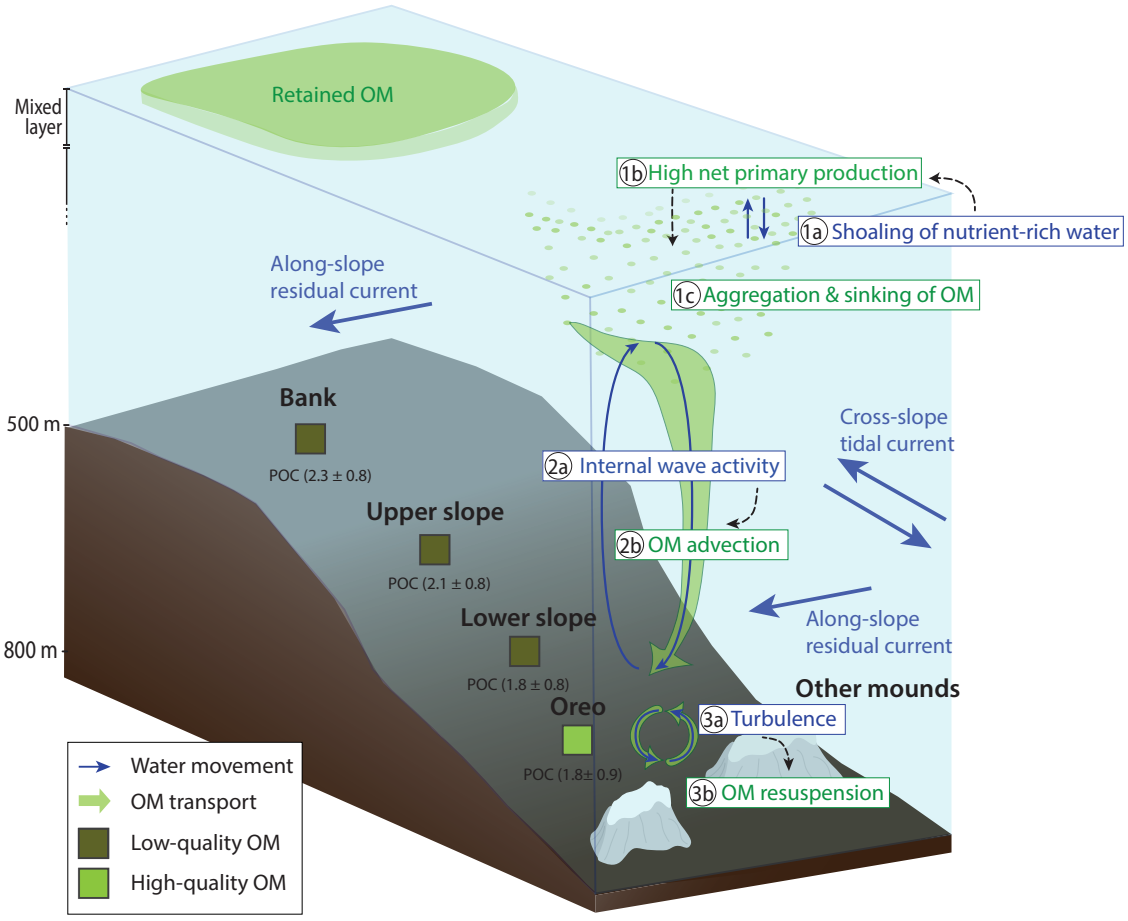

Figure 2.8 Schematic illustration of the investigated transect. This illustration is not to scale and only indicates the organic matter-related transport processes argued in the current study. Hydrodynamic processes are indicated with blue arrows. Organic matter-related transport processes are indicated in green. OM = organic matter, POC = particulate organic matter concentration, in mean ± SD. Turbulence is here interpreted as a more dynamic bottom water caused over a tidal cycle. Along slope and cross slope transport arrows is based on Cyr et al. (2016) and Schulz et al. (2020).

Supplementary material *Chapter 2*

Figures

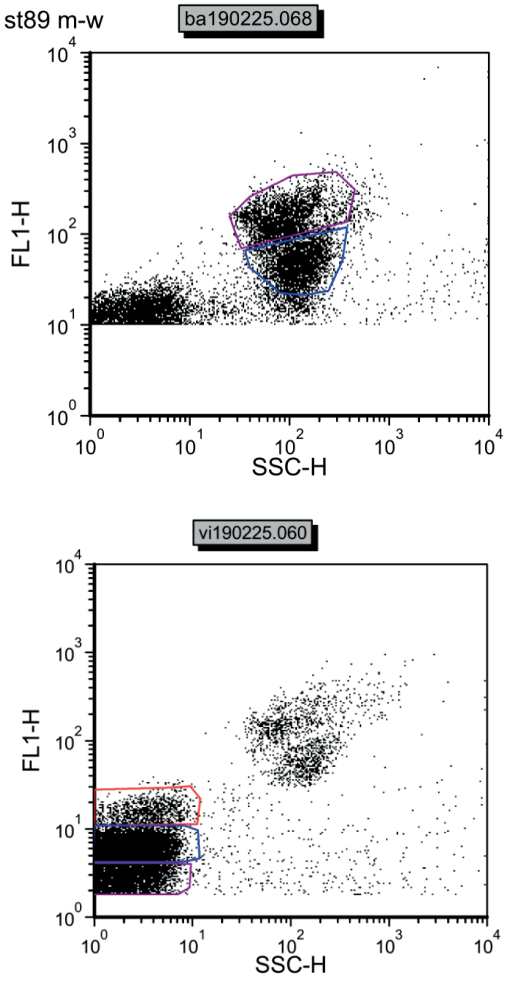

Figure S2.1 Example of gate settings for bacteria samples (left panel). In purple the high DNA bacteria (HBAC), in blue the low DNA bacteria (LBAC). Virus samples (right panel) show in virI (purple), virII (blue) and virIII (red)

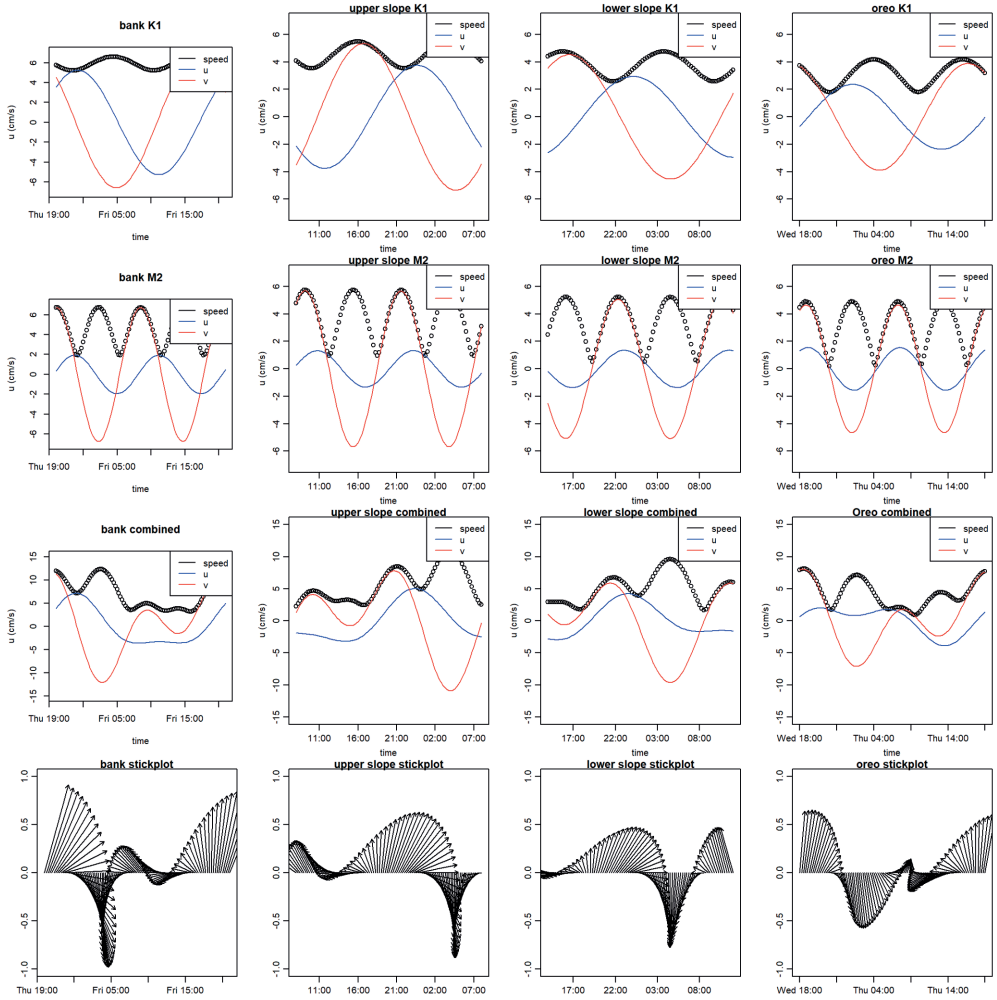

Figure S2.2 Tidal constituents of the four 24-hour stations. Only the K1 (diurnal lunar tide) and the M2 (lunar semi-diurnal tide) are considered

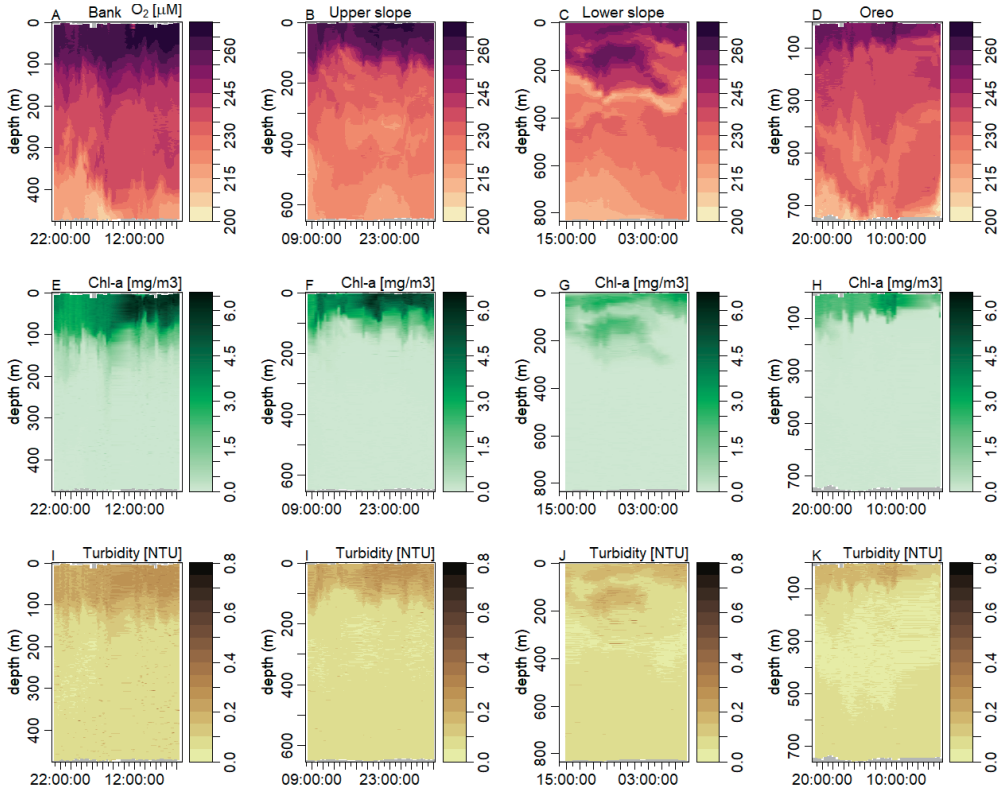

Figure S2.3 Oxygen (top row), chlorophyll-a (middle row), and Turbidity (bottom row) profiles for the stations (from left to right) Bank, Upper slope, Lower slope, and Oreo

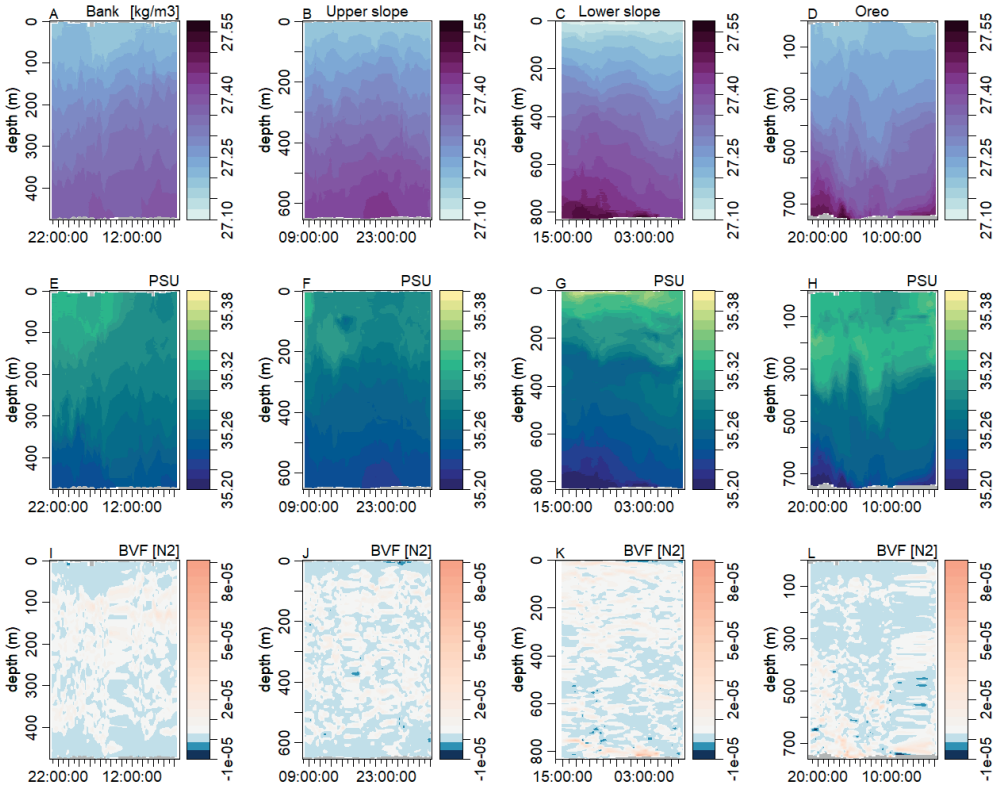

Figure S2.4 Density (top row), salinity (middle row), and buoyancy frequency (bottom row) profiles for the stations (from left to right) Bank, Upper slope, Lower slope, and Oreo

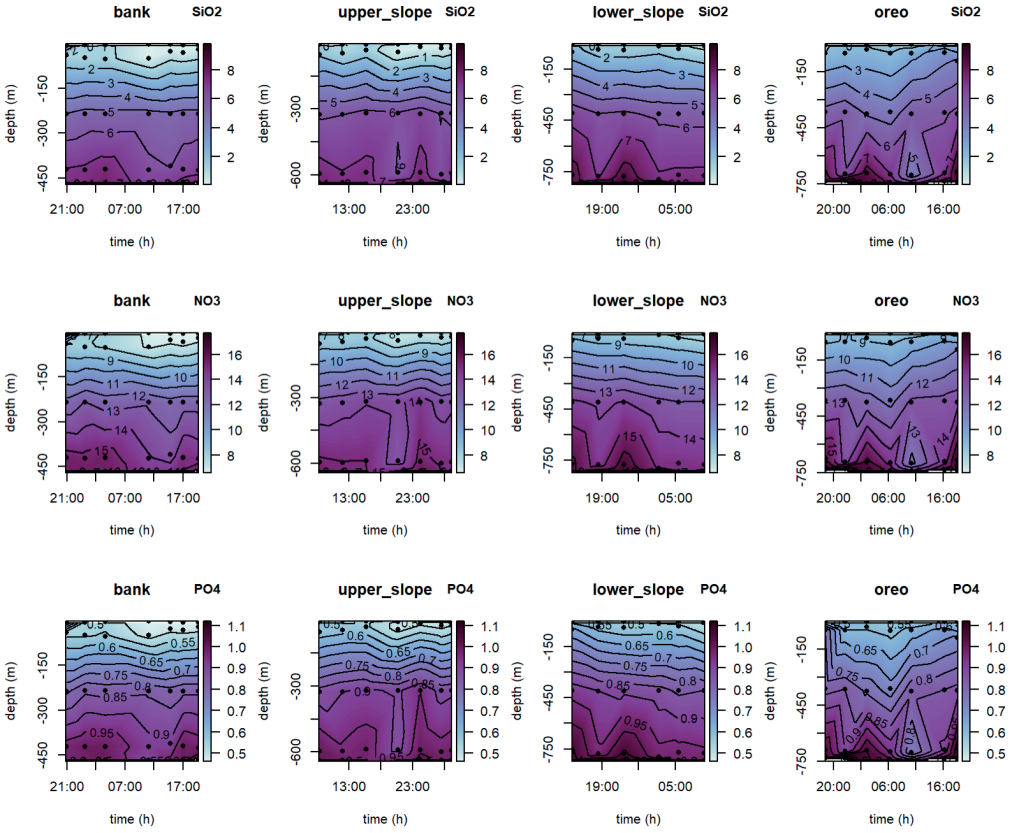

Figure S2.5 Profiles for Silicate (SiO_2), Nitrate (NO_3), and Phosphate (PO_4). Values are in µM

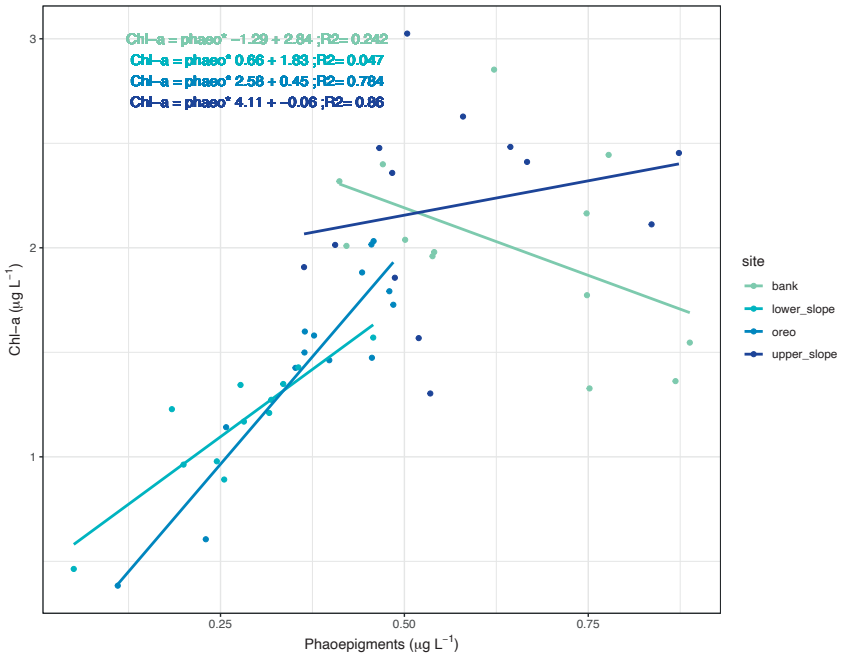

Figure S2.6 Nitrate versus silicate, only for the surface samples for the four 24-hour sampling stations. Top left text shows the linear equation per station, and the top middle text shows the Pearson coefficient and p-value

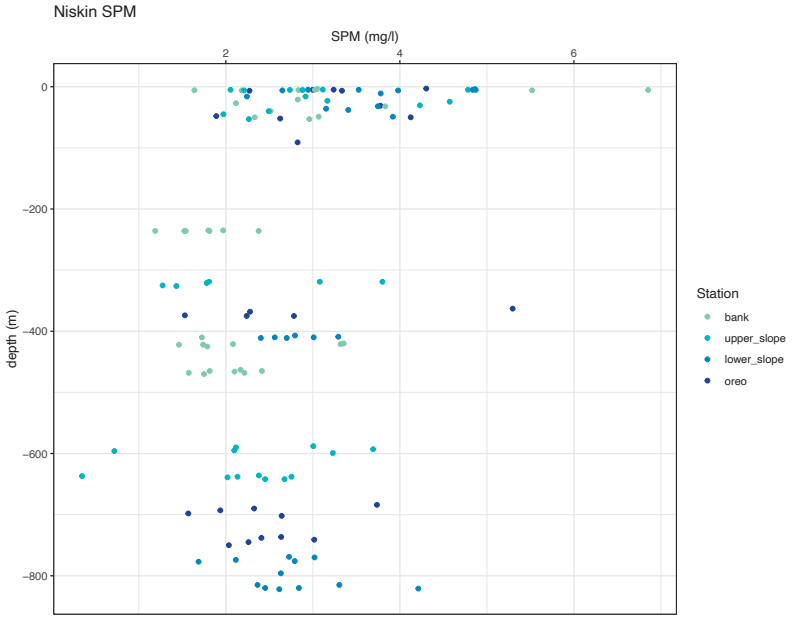

Figure S2.7 Suspended particulate matter (mg L^{-1}) for the four 24-hour CTD stations

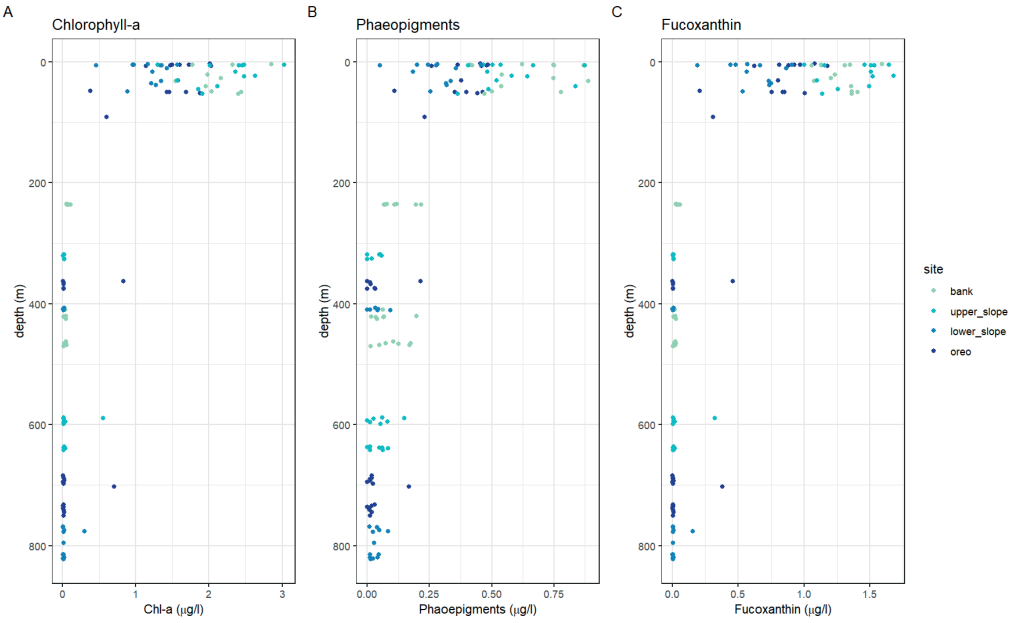

Figure S2.8 pigment concentrations over depth for the four 24-hour stations with A) chlorophyll-a, B) phaeopigments, and C) Fucoxanthin

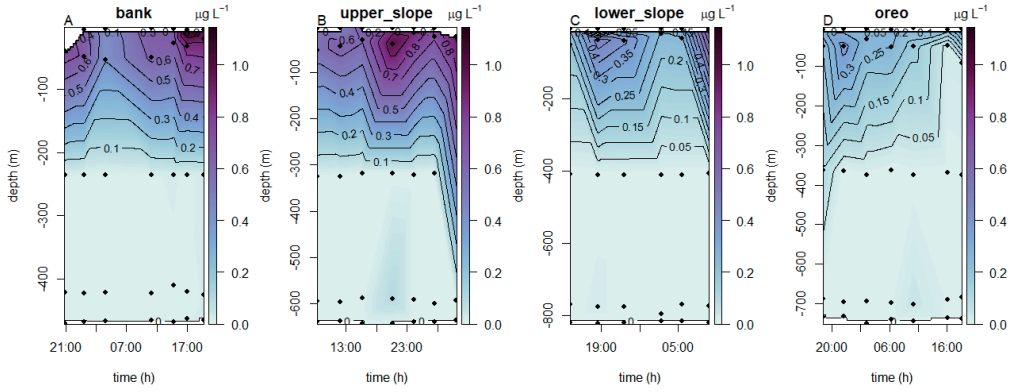

Figure S2.9 Chlorophyllida-a concentration over the 24--hour sampling period

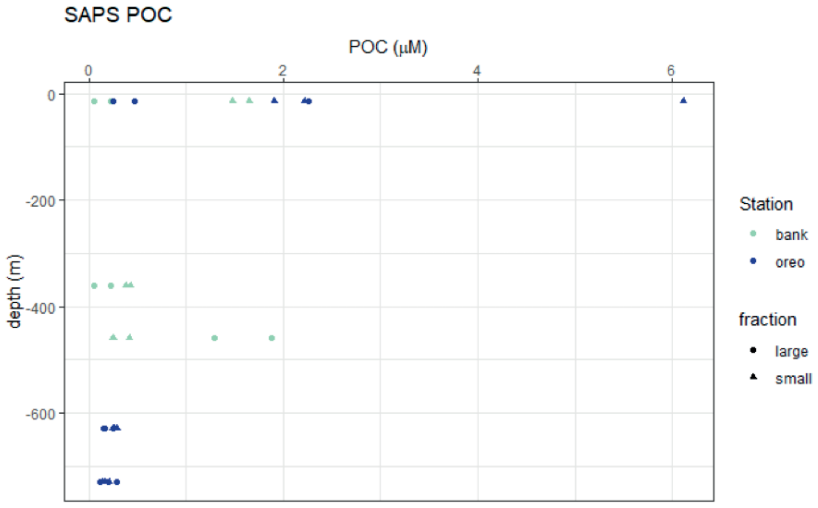

Figure S2.10 Particulate organic carbon (POC) concentration as measured by a semi-automated pumping system

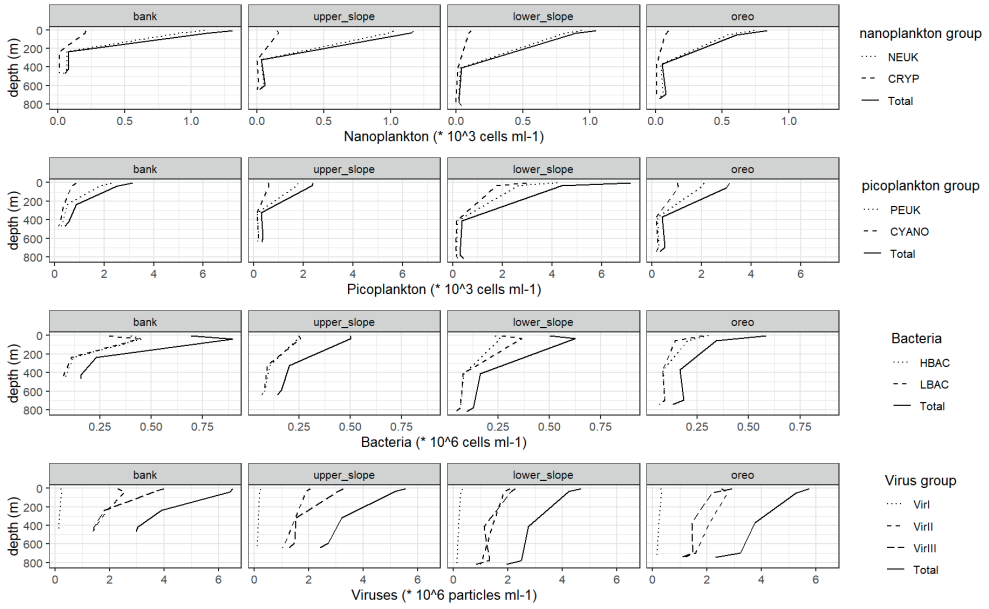

Figure S2.11 Profiles of nanoplankton, picoplankton, bacteria, and virus densities. Values are averaged over the 24-hour sampling period. NEUK = nano-eukaryotes, CRYP = cryptophytes, PEUK = pico-eukaryotes, CYANO = Cyanobacteria, HBAC = high DNA containing bacteria, LBAC = low DNA containing bacteria, VirI = virus group 1, Vir2 = virus group 2, Vir3 = virus group 3

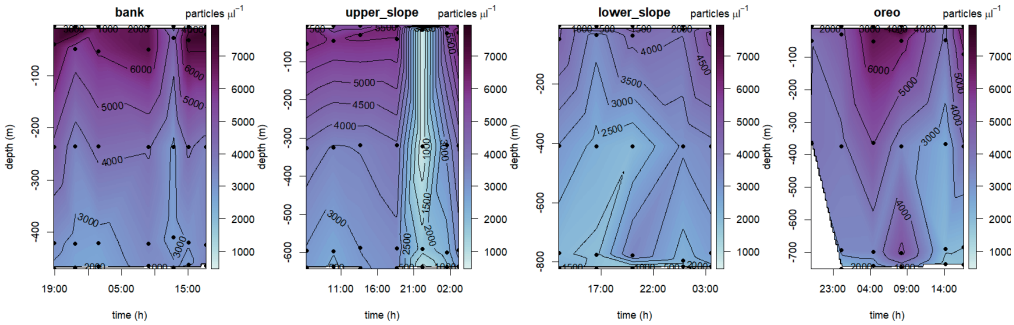

Figure S2.12 Virus concentration in particles μl^{-1} (virI, virII, virIII combined) over the tidal cycle at the four sampling station

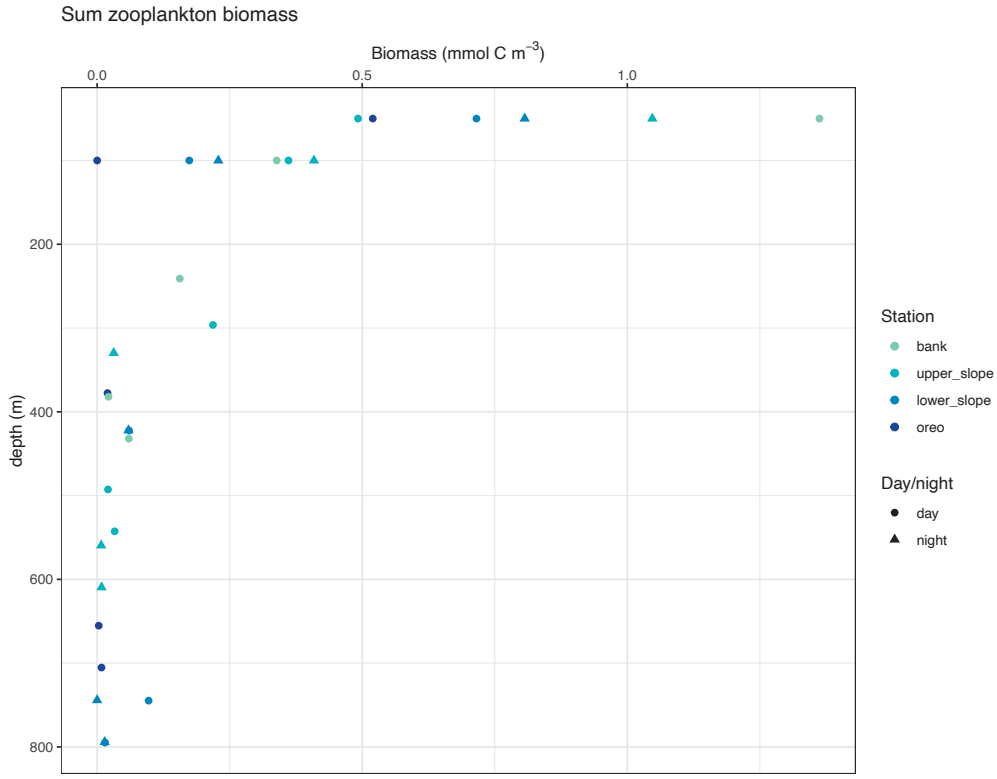

Figure S2.13 Zooplankton biomass versus depth per station and sampling time (day/night)

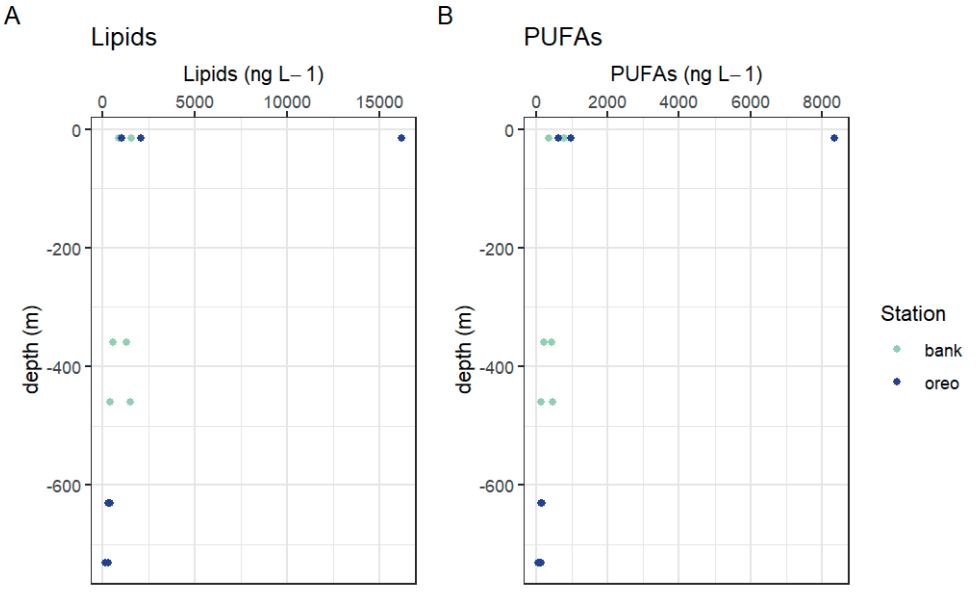

Figure S2.14 In-situ pump total lipids (A) and PUFA (B) concentration over depth. Small and large fraction combined

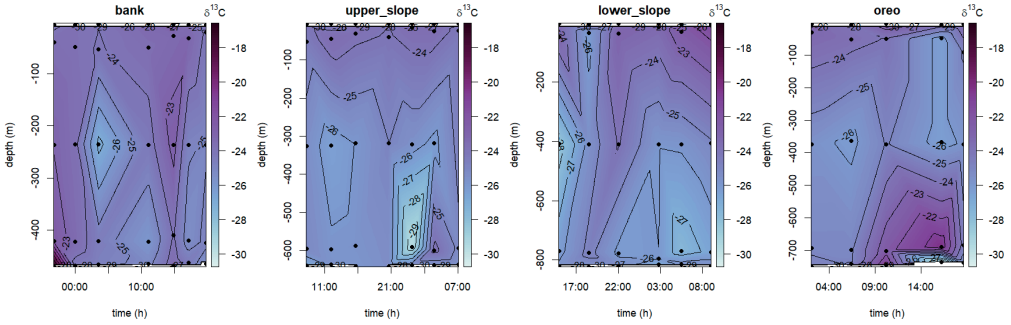

Figure S2.15 Tidal dynamics of $\delta^{13}C$ at the four 24-hour sampling stations. Note the different depth range on the y axis. Oreo mound and Lower slope do not span full 24 hours

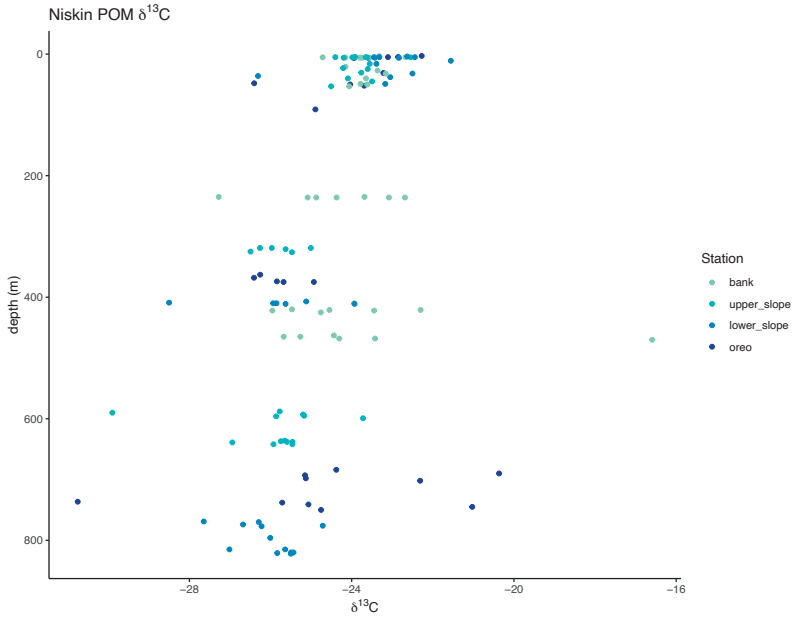

Figure S2.16 Niskin bottle POC $\delta^{13}C$ profiles for the four 24-hour stations

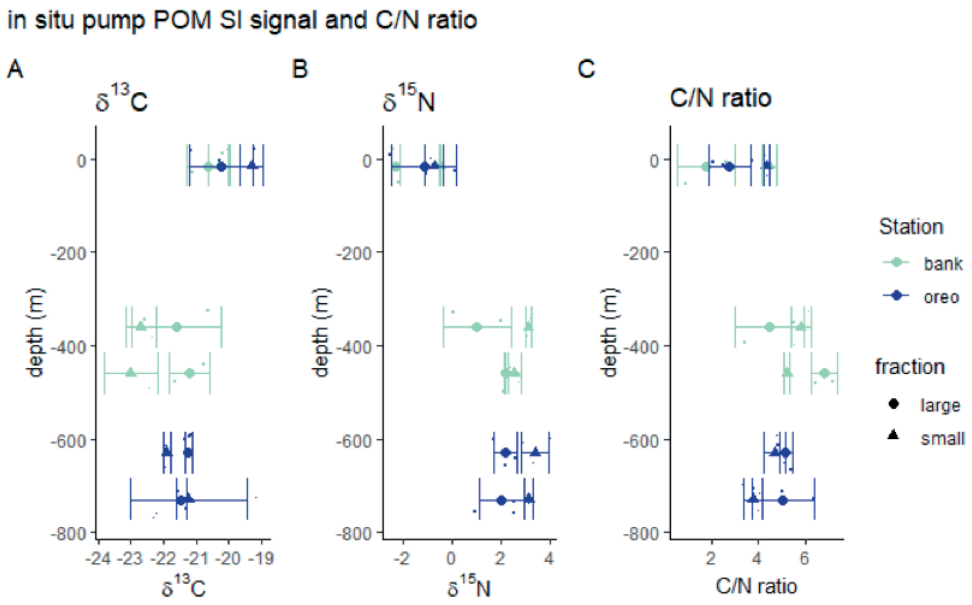

Figure S2.17 SPOM, sampled by in-situ pump system, stable isotopes (A, B) and C/N ratio (C) over depth. This plot only shows the small (<0.53 µm) fraction

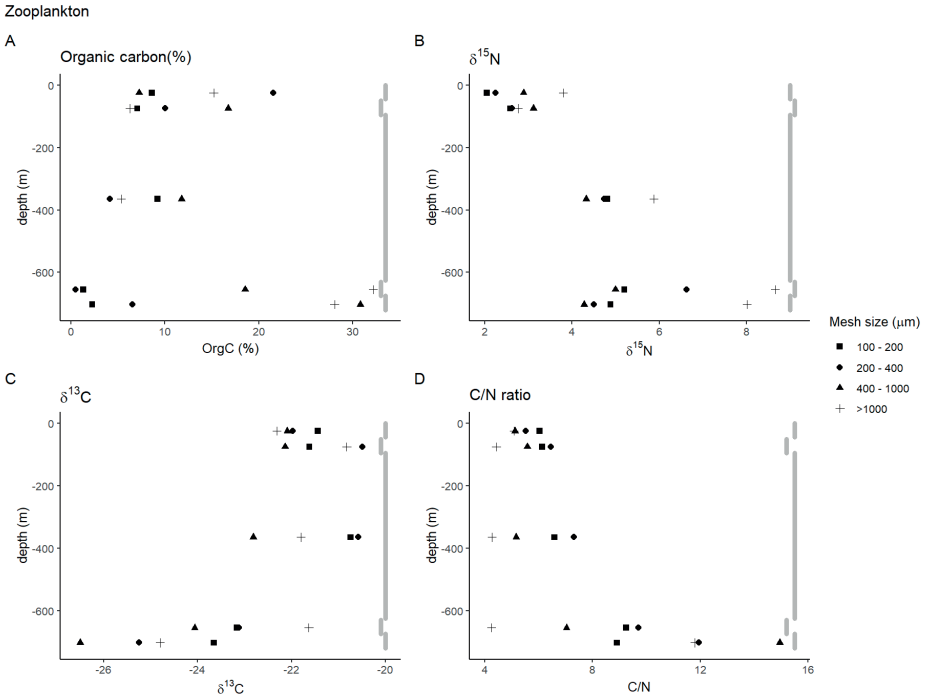

Figure S2.18 Zooplankton (A) organic carbon content), (B) $\delta^{15}N$ ratio, (C) $\delta^{13}C$ ratio, and (D) C/N ratio. Points indicate the middle of the depth interval from which the samples were taken, the grey line shows the depth interval

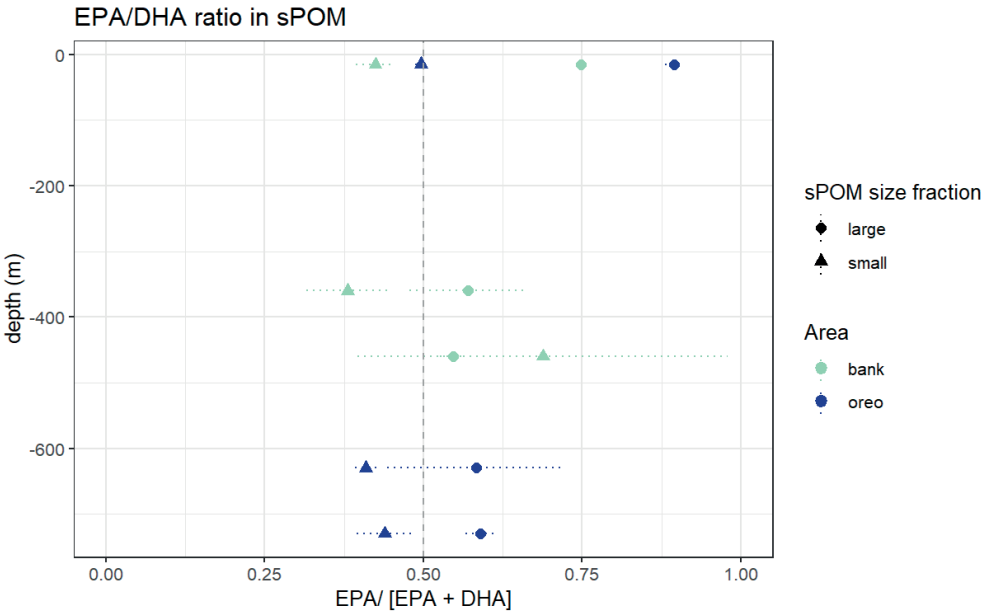

Figure S2.19 the EPA/DHA ratio of the sPOM over depth, Vertical dashed line represents a 1:1 EPA/DHA ratio

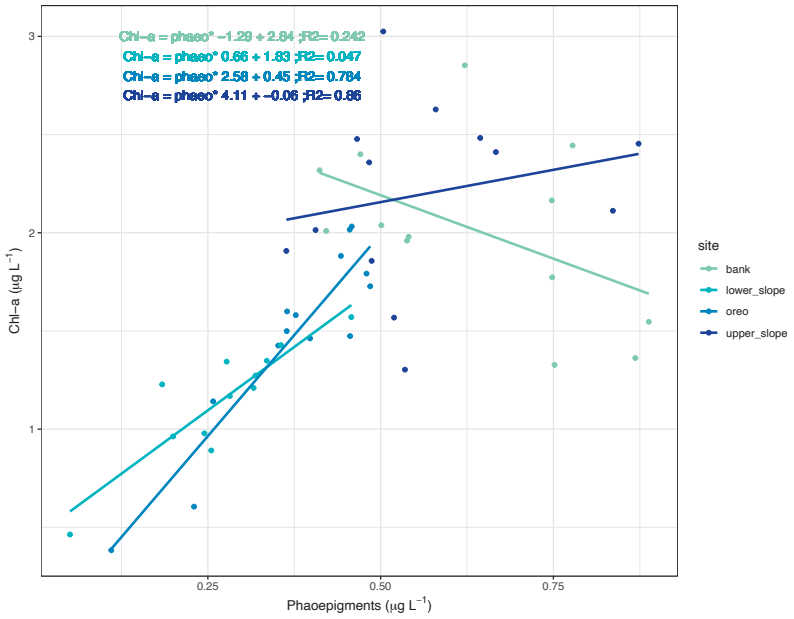

Figure S2.20 Phaeopigments vs chlorophyll-a, with linear models fitted for each 24-hour station. Only surface and midwater samples are used. The chl-a:∑phaeo ratio, for which >10:1 is indicative of healthy algae cells and a 1:1 ratio represents degraded material (Bianchi et al., 2002; Lomas and Moran, 2011), shows that the phytoplankton community at Bank and Upper slope was in a senescent phase (slope coefficients -1.29 and 0.66 respectively), and actively growing at the stations Lower slope and Oreo (slope coefficients 2.58 and 3.98, respectively)

Tables

Table S2.1 List of benthic fauna and zooplankton sampled for stable isotope and lipid analysis

Group	Station	Depth	Replicates
Bivalves	bank	benthic	7
Sediment	bank	benthic	5
Sponge	oreo	benthic	1
Bivalves	oreo	benthic	1
Crinoids	oreo	benthic	3
Madrepora oculata	oreo	benthic	6
Desmophyllum dianthus	oreo	benthic	2
Ophiuroidea	oreo	benthic	6
Eunice norvegica	oreo	benthic	5
Stylasteridae	oreo	benthic	3
Dead framework	oreo	benthic	6
Sediment	oreo	benthic	2
Zooplankton (100- 200 µm)	oreo	50m-0m	1
Zooplankton (200- 400 µm)	oreo	50m-0m	1
Zooplankton (400- 1000 µm)	oreo	50m-0m	1
Zooplankton (>1000 µm)	oreo	50m-0m	1
Zooplankton (100- 200 µm)	oreo	100m - 50m	1
Zooplankton (200- 400 µm)	oreo	100m - 50m	1
Zooplankton (400- 1000 µm)	oreo	100m - 50m	1
Zooplankton (>1000 µm)	oreo	100m - 50m	1
Zooplankton (100- 200 µm)	oreo	100mab - 100m	1
Zooplankton (200- 400 µm)	oreo	100mab - 100m	1
Zooplankton (400- 1000 µm)	oreo	100mab - 100m	1
Zooplankton (>1000 µm)	oreo	100mab - 100m	1
Zooplankton (100- 200 µm)	oreo	50mab - 100mab	1
Zooplankton (200- 400 µm)	oreo	50mab - 100mab	1

Zooplankton (400- 1000 µm)	oreo	50mab - 100mab	1
Zooplankton (>1000 µm)	oreo	50mab - 100mab	1
Zooplankton (100- 200 µm)	oreo	10mab - 50mab	1
Zooplankton (200- 400 µm)	oreo	10mab - 50mab	1
Zooplankton (400- 1000 µm)	oreo	10mab - 50mab	1
Zooplankton (>1000 µm)	oreo	10mab - 50mab	1

Table S2.2 Carbon conversion factors used to calculate the carbon partitioning of POC

Group	Description	Carbon content	Unit	Source
NEUK	Nano-eukaryotes	50	pg $cell^{-1}$	(Berggreen et al., 1988; Verity et al., 1992; Tarran et al., 2006; Casey et al., 2013)
CRYPTO	Cryptophytes	50	pg $cell^{-1}$	(Berggreen et al., 1988; Verity et al., 1992; Tarran et al., 2006; Casey et al., 2013)
PEUK	Pico-eukaryotes	2590	fg $cell^{-1}$	(Buitenhuis et al., 2012)
CYANO	Cyanobacteria, e.g., Synechoccus	255	fg $cell^{-1}$	(Buitenhuis et al., 2012)
HBAC	High DNA bacteria	20	fg $cell^{-1}$	(Lee and Fuhrman, 1987)
LBAC	Low DNA bacteria	20	fg $cell^{-1}$	(Lee and Fuhrman, 1987)
Vir1	Viruses gate 1	0.2	fg $cell^{-1}$	(Suttle, 2005)
Vir2	Viruses gate 2	0.2	fg $cell^{-1}$	(Suttle, 2005)
Vir3	Viruses gate 3	0.2	fg $cell^{-1}$	(Suttle, 2005)

Table S2.3 Fatty acid trophic markers used in this study for the zooplankton and macrofauna PLFA/NLFA samples

Fatty acid	Trophic marker	Source
iC14:0	bacteria	(Dalsgaard et al., 2003)
C15:0	bacteria	(Kelly and Scheibling, 2012)
iC15:0/C14:1w5c	bacteria	(Dalsgaard et al., 2003)
aiC15:0	bacteria	(Dalsgaard et al., 2003)
iC16:0/C15:1w5c (coeluting)	bacteria	(Dalsgaard et al., 2003)
10-MeC16:0	bacteria	(Blaud et al., 2012)
C17:0	bacteria	(Kelly and Scheibling, 2012)
iC17:0	bacteria	(Dalsgaard et al., 2003)
C17:0/3-OH C12:0 (coeluting in PLFAs)	bacteria	(Dalsgaard et al., 2003)
aiC17:0	bacteria	(Dalsgaard et al., 2003)
C18:1w7c	bacteria	(van Oevelen et al., 2018)
10-MeC18:0	bacteria	(Blaud et al., 2012; Maier et al., 2020a)
C18:2w6	algae	(Kelly and Scheibling, 2012)
C18:2w6c	algae	(van Oevelen et al., 2018)
C18:3w3	algae	(van Oevelen et al., 2018)
C18:4w3	algae	(Kelly and Scheibling, 2012)
C20:5w3 (EPA)	algae	(Volkman et al., 1989; Dalsgaard et al., 2003; Tolosa et al., 2004; Parrish, 2013)
C20:4w6	algae	
C22:6w3 (DHA)	algae	(Volkman et al., 1989; Dalsgaard et al., 2003; Tolosa et al., 2004; Parrish, 2013)
C16:4w3	algae	(Volkman et al., 1989; Dalsgaard et al., 2003; Tolosa et al., 2004; Parrish, 2013)
C18:5w3	algae	(Volkman et al., 1989; Dalsgaard et al., 2003; Tolosa et al., 2004; Parrish, 2013)
C18:3w4	algae	(Volkman et al., 1989; Dalsgaard et al., 2003; Tolosa et al., 2004; Parrish, 2013)
C20:3w6	algae	(Dalsgaard et al., 2003)
C22:5w3	algae	(Dalsgaard et al., 2003)

C20:1w9c	zooplankton	(Falk-Petersen et al., 2002; Sheridan et al., 2002; Howell et al., 2003; Alfaro et al., 2006; Dodds et al., 2009; Ravet et al., 2010)
C22:1w9c	zooplankton	(Falk-Petersen et al., 2002; Sheridan et al., 2002; Howell et al., 2003; Alfaro et al., 2006; Dodds et al., 2009; Ravet et al., 2010)
C22:1w9	zooplankton	(Falk-Petersen et al., 2002; Sheridan et al., 2002; Howell et al., 2003; Alfaro et al., 2006; Dodds et al., 2009; Ravet et al., 2010)
C22:1w11	zooplankton	(Falk-Petersen et al., 2002; Sheridan et al., 2002; Howell et al., 2003; Alfaro et al., 2006; Dodds et al., 2009; Ravet et al., 2010)

Table S2.4 Lipid biomarker table used for the in-situ pump sPOM analysis

Lipid	Indicator	Source
C13:0	bacteria	
C15:0	bacteria	(Sheridan et al., 2002; Dalsgaard et al., 2003; Parrish, 2013)
C17:0	bacteria	(Sheridan et al., 2002; Dalsgaard et al., 2003; Parrish, 2013)
C19:0	bacteria	(Sheridan et al., 2002; Dalsgaard et al., 2003; Parrish, 2013)
iC15:0	bacteria	(Sheridan et al., 2002; Dalsgaard et al., 2003; Parrish, 2013)
aiC15:0	bacteria	(Sheridan et al., 2002; Dalsgaard et al., 2003; Parrish, 2013)
iC17:0	bacteria	(Sheridan et al., 2002; Dalsgaard et al., 2003; Parrish, 2013)
aiC17:0	bacteria	(Sheridan et al., 2002; Dalsgaard et al., 2003; Parrish, 2013)
C19_iso?	bacteria	(Sheridan et al., 2002; Dalsgaard et al., 2003; Parrish, 2013)
C18:1w9c	zooplankton	(Sheridan et al., 2002; Tolosa et al., 2004)
C18:1w9t	zooplankton	(Sheridan et al., 2002; Tolosa et al., 2004)
C20:1w9c	zooplankton	(Sheridan et al., 2002; Tolosa et al., 2004)
C22:1_iso	zooplankton	(Sheridan et al., 2002; Tolosa et al., 2004)
C22:1w9	zooplankton	(Sheridan et al., 2002; Tolosa et al., 2004)
C14_alc	zooplankton	(Sheridan et al., 2002; Dalsgaard et al., 2003)
C16_alc	zooplankton	(Sheridan et al., 2002; Dalsgaard et al., 2003)
C18_alc	zooplankton	(Sheridan et al., 2002; Dalsgaard et al., 2003)
C18:1_unsat_alc	zooplankton	(Sheridan et al., 2002; Dalsgaard et al., 2003)
C20:1_unsat_alc	zooplankton	(Sheridan et al., 2002; Dalsgaard et al., 2003)
C22:1_unsat_alc	zooplankton	(Sheridan et al., 2002; Dalsgaard et al., 2003)

C27d5	zooplankton	(Sheridan et al., 2002)
C27d5_22	zooplankton	(Sheridan et al., 2002)
C16:4	algae	(Volkman et al., 1989; Dalsgaard et al., 2003; Tolosa et al., 2004; Parrish, 2013)
C16:3	algae	(Volkman et al., 1989; Dalsgaard et al., 2003; Tolosa et al., 2004; Parrish, 2013)
C18:5	algae	(Volkman et al., 1989; Dalsgaard et al., 2003; Tolosa et al., 2004; Parrish, 2013)
C18:3w6	algae	(Volkman et al., 1989; Dalsgaard et al., 2003; Tolosa et al., 2004; Parrish, 2013)
C18:3_iso	algae	(Volkman et al., 1989; Dalsgaard et al., 2003; Tolosa et al., 2004; Parrish, 2013)
C18:2w6	algae	(Volkman et al., 1989; Dalsgaard et al., 2003; Tolosa et al., 2004; Parrish, 2013)
C18:3w3	algae	(Volkman et al., 1989; Dalsgaard et al., 2003; Tolosa et al., 2004; Parrish, 2013)
C20:5w3 (EPA)	algae	(Volkman et al., 1989; Dalsgaard et al., 2003; Tolosa et al., 2004; Parrish, 2013)
C22:6w3 (DHA)	algae	(Volkman et al., 1989; Dalsgaard et al., 2003; Tolosa et al., 2004; Parrish, 2013)
C16:1_iso1	algae	(Volkman et al., 1989; Dalsgaard et al., 2003; Tolosa et al., 2004; Parrish, 2013)
C16:1w7	algae	(Volkman et al., 1989; Dalsgaard et al., 2003; Tolosa et al., 2004; Parrish, 2013)
C16:1_iso2	algae	(Volkman et al., 1989; Dalsgaard et al., 2003; Tolosa et al., 2004; Parrish, 2013)
C28d5_22	algae	(Sheridan et al., 2002)


O_2
O_2
O_2
O_2
O_2
O_2
O_2
NH_4^+
NO_3^-
NO_3^-
NH_4^+

Chapter 3

BENTHIC OXYGEN AND NITROGEN EXCHANGE ON A COLD-WATER CORAL REEF IN THE NORTH-EAST ATLANTIC OCEAN

Evert de Froe, Lorenzo Rovelli, Ronnie N. Glud, Sandra R. Maier, Gerard Duineveld, Furu Mienis, Marc Lavaleye, Dick van Oevelen

Published in Frontiers in Marine Sciences as: de Froe et al. (2019), Benthic Oxygen and Nitrogen Exchange on a Cold-Water Coral Reef in the North-East Atlantic Ocean. Front. Mar. Sci. 6:665. doi: 10.3389/fmars.2019.00665

Published as: ***de Froe E****, Rovelli L, Glud RN, Maier SR, Duineveld G, Mienis F, Lavaleye M and van Oevelen D (2019) Benthic Oxygen and Nitrogen Exchange on a Cold-Water Coral Reef in the North-East Atlantic Ocean. Front. Mar. Sci. 6:665. doi: 10.3389/fmars.2019.00665*

Abstract

Cold-water coral (CWC) reefs are distributed globally and form complex three-dimensional structures on the deep seafloor, providing habitat for numerous species. Here, we measured the community O_2 and dissolved inorganic nitrogen (DIN) flux of CWC reef habitats with different coral cover and bare sediment (acting as reference site) in the Logachev Mound area (NE Atlantic). Two methodologies were applied: the non-invasive *in situ* aquatic eddy co-variance (AEC) technique, and *ex situ* whole box core (BC) incubations. The AEC system was deployed twice per coral mound (69 h in total), providing an integral estimate of the O_2 flux from a total reef area of up to 500 m^2, with mean O_2 consumption rates ranging from 11.6 ± 3.9 to 45.3 ± 11.7 mmol O_2 m^{-2} d^{-1} (mean ± SE). CWC reef community O_2 fluxes obtained from the BC incubations ranged from 5.7 ± 0.3 to 28.4 ± 2.4 mmol O_2 m^{-2} d^{-1} (mean ± SD) while the O_2 flux measured by BC incubations on the bare sediment reference site reported 1.9 ± 1.3 mmol O_2 m^{-2} d^{-1} (mean ± SD). Overall, O_2 fluxes measured with AEC and BC showed reasonable agreement, except for one station with high habitat heterogeneity. Our results suggest O_2 fluxes of CWC reef communities in the North East Atlantic are around five times higher than of sediments from comparable depths and living CWCs are driving the increased metabolism. DIN flux measurements by the BC incubations also revealed around two times higher DIN fluxes at the CWC reef (1.17 ± 0.87 mmol DIN m^{-2} d^{-1}), compared to the bare sediment reference site (0.49 ± 0.32 mmol DIN m^{-2} d^{-1}), due to intensified benthic release of NH_4^+. Our data indicate that the amount

of living corals and dead coral framework largely contributes to the observed variability in O_2 fluxes on CWC reefs. A conservative estimate, based on the measured O_2 and DIN fluxes, indicates that CWC reefs process 20% to 35% of the total benthic respiration on the southeasterly Rockall Bank area, which demonstrates that CWC reefs are important to carbon and nitrogen mineralization at the habitat scale.

Introduction

Benthic solute exchange and carbon mineralization have been studied extensively in the past decades (e.g. (Glud, 2008). However, the importance of reef structures, including cold-water corals (CWCs), for benthic carbon and nitrogen cycling is still poorly resolved. CWC reefs are topographically complex structures supporting high biomass and species richness of macro- and megafauna (Jonsson et al., 2004; Roberts et al., 2006). These CWC reefs can trap and mineralize large amounts of particulate organic matter (POM) and are presumed to act as carbon cycling hotspots (van Oevelen et al., 2009; Cathalot et al., 2015). However, quantification of mineralization rates remain few due to the complications of sampling and incubation intact CWC communities.

Most studies on the metabolism and nitrogen cycling of CWCs investigate individuals or nubbins of corals that are incubated *ex situ* in experimental chambers (Purser et al., 2010; Maier et al., 2011; Orejas et al., 2011). These approaches have concluded that CWCs act as a deep-sea source of dissolved inorganic nitrogen (DIN) as NH_4^+ and, presumably due to an active nitrifying community associated with the CWC microbiome, NO_3^- (Khripounoff et al., 2014; Middelburg et al., 2015). These observations hint at the presence of a dynamic nitrogen cycle on CWC reefs, especially given the identification of archaea in the microbial assemblage of cold-water corals (Van Bleijswijk et al., 2015). Assessments of community-based nitrogen fluxes in these habitats, however, have yet to be performed.

Upscaling results from laboratory incubations to the scale of CWC reefs is problematic given i) the natural complexity and the spatial heterogeneity in faunal density and biomass distribution and ii) potential recovery/sampling effects on community performance. Only three quantitative studies on O_2 fluxes at CWC reefs have been conducted, and these were focused on relatively shallow CWC communities at ~100-200 m depth (White et al., 2012; Cathalot et al., 2015; Rovelli et al., 2015). These studies have suggested that the organic carbon turnover at CWC reefs is enhanced compared to soft-sediment habitats at equivalent depths, but also show extensive variations in reef activity. The drivers of such variability are still poorly constrained, and it is currently unknown to what extent the resolved range can be extrapolated to other and deeper CWC reef communities.

Here, we combine two methodologies to quantify the O_2 and DIN flux of CWC reef communities, located in the North East Atlantic between 500 – 900 m depth. We used the non-invasive Aquatic Eddy Covariance (AEC) technique to quantify the *in situ* O_2 flux at CWC reef communities and *ex situ* whole-box core incubations to measure the O_2 and DIN flux of CWC reef communities and at a bare sediment reference site. Our primary aims are to i) provide robust measurements of the O_2 flux of a CWC reef community, ii) compare the invasive versus the non-invasive methodology iii) provide a first estimate of DIN solute exchange of a CWC reef community and iv) quantify the importance of sediment, dead coral framework and living CWC in driving the whole CWC reef community O_2 and DIN flux.

Material and Methods

Study site and Sampling

The Logachev mound province is located on the SE slope of Rockall Bank, approximately 500 km NW of Ireland (N 55.55, W 15.80, Figure 3.1A). In this area, coral mounds are present in a 90 km x 60 km area between 500 and 1000 m water depth (Kenyon et al., 2003; Mienis et al., 2006). The cold-water coral communities on the mound consist of framework-building *Lophelia pertusa* and *Madrepora oculata* with associated macrofaunal such as polychaetes (e.g. *Eunice norvegica)*, sponges (e.g. *Hexadella dedritifera*), and crinoids (Van Weering et al., 2003; Van Soest and Lavaleye, 2005). Ambient bottom water temperatures on the coral mounds vary between 7-9 °C. The area is characterized by high bottom current velocities, internal tidal waves and hydraulic jumps (Mohn et al., 2014; Van Haren et al., 2014; Cyr et al., 2016).

This study targeted three sites: the Haas mound, which is 360 m high and the largest carbonate mound in the region; the Oreo mound, a smaller carbonate mound SW of the Haas mound with the summit at 750 m water depth; and an off-mound bare sediment reference site at 500-m water depth further upslope Rockall Bank (Figure 3.1B-D; (Mienis et al., 2006). Previous work on the Logachev mound province showed a large habitat heterogeneity on the CWC reefs; with patchy distribution of live coral, bare sediments and coral rubble on the summit of the Haas mound, and a dense thriving CWC reef on the southern flank of the Haas- and Oreo mound (Duineveld et al., 2007; de Haas et al., 2009; Van Bleijswijk et al., 2015).

During the R/V Pelagia research cruise 64PE420[5] (30/04/2017 to 07/05/2017), twelve box cores were collected along with three parallel deployments of the NIOZ ALBEX lander (Duineveld et al., 2004), equipped with the Aquatic Eddy Covariance (AEC) system. To cover the above-mentioned habitat heterogeneity of the CWC reef communities in the region, AEC deployment and box core sampling was performed at the following sites (Table 3.1): i) two box cores and one AEC deployment at the summit of the Haas mound, ii) four box cores and one AEC deployment at the southern flank of the Haas mound, iii) three box cores and one AEC deployment at the summit of the Oreo mound and iv) three box cores at the bare sediment reference site (Figure 3.1B-D). Eight of the eleven box-cores were used for the incubation experiments, while six were subsampled to characterize the surface sediment. Table 3.1 provides an overview of the applied methodological approaches at the respective stations.

[5] Cruise report DOI: 10.5281/zenodo.1454465

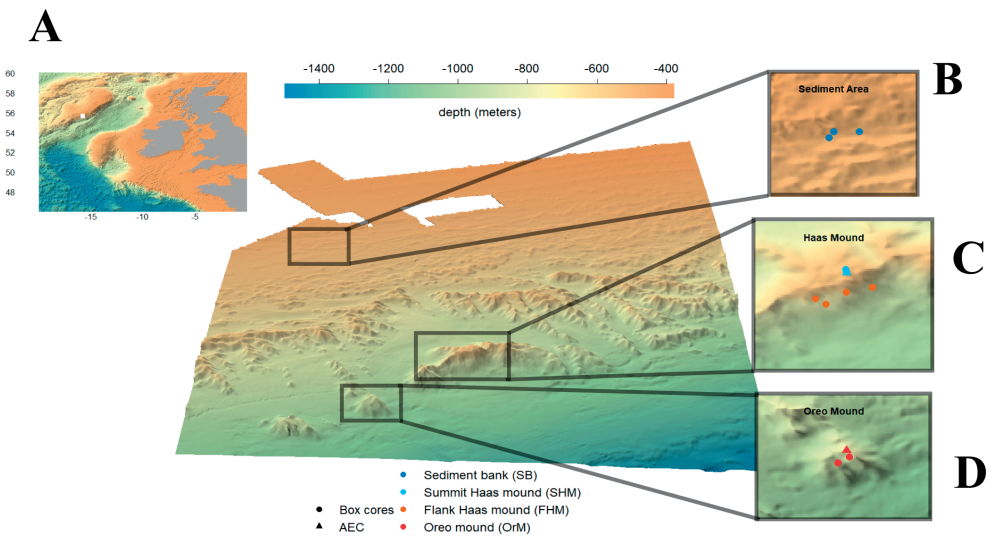

Figure 3.1: Multibeam map of the Logachev mound province with as insets: (A) Location of Logachev mound province at the SE Rockall Bank, NE Atlantic (GEBCO, 2013), (B) sampling locations at the bare sediment reference site, (C) sampling locations at Haas mound, (D) sampling locations at Oreo mound. Plot produced with R package plot3D (Soetaert, 2017).

Table 3.1 Station characteristics; date, depth, latitude, longitude, and applied methods. SHM = Summit Haas Mound, SB = Sediment Bank reference site, FHM = Flank Haas Mound, OrM = Oreo Mound; BC = box core incubation, SC = sediment characteristics, AEC = Aquatic Eddy Covariance technique

Station	Date	Depth (m)	Latitude	Longitude	Method
SHM 1	30/04/2017	536	N 55° 29.71'	W 15° 47.98'	BC
SHM 2	30/04/2017	539	N 55° 29.74'	W 15° 47.99'	BC; SC
SHM 3	30/04/2017	536	N 55° 29.69'	W 15° 47.98'	AEC
FHM 1	04/05/2017	747	N 55° 29.16'	W 15° 48.30'	BC; SC
FHM 2	05/05/2017	639	N 55° 29.25'	W 15° 48.47'	BC
FHM 3	06/05/2017	616	N 55° 29.36'	W 15° 47.98'	SC
FHM 4	06/05/2017	719	N 55° 29.45'	W 15° 47.57'	SC
OrM 1	06/05/2017	838	N 55° 26.89'	W 15° 52.43'	BC; SC
OrM 2	07/05/2017	757	N 55° 27.01'	W 15° 52.22'	BC; SC
OrM 3	07/05/2017	744	N 55° 27.14'	W 15° 52.28'	AEC
SB 1	02/05/2017	495	N 55° 38.30'	W 15° 55.94'	BC; SC
SB 2	02/05/2017	501	N 55° 38.19'	W 15° 56.03'	BC; SC
SB 3	02/05/2017	503	N 55° 38.29'	W 15° 55.48'	SC

Aquatic Eddy Covariance (AEC) technique

The AEC system consisted of an Acoustic Doppler Velocimeter (ADV Vector, Nortek, Norway), an underwater amplifier (see McGinnis et al., 2011) with two fast Clark-type O_2 microelectrodes and a dedicated battery canister allowing up to 5 days of continuous sampling at 64 Hz. The AEC system was mounted on a leg of the NIOZ ALBEX lander using a metal extension (Figure 3.2).

Figure 3.2: The ALBEX lander (Duineveld et al. 2004) equipped with A) the AEC instrument; B) Fluorescence sensor.

This design ensured that the system was positioned 0.5 m outside the lander frame to minimize any potential flow disturbance by the frame itself. To protect the AEC system, an aluminum caging was mounted around the ADV (Figure 3.2). The ADV sampling volume was positioned at a measurement height (*h*) of 80 – 86 cm above the sea bed. This ensured that AEC measurements were performed well above large coral patches which could otherwise damage the sensors and lead to local disturbance of the flow field.

The O_2 and velocity time series were processed following established AEC protocols as outlined in detail in (Attard et al., 2014; Rovelli et al., 2015). Key steps included i) sensor reading calibration, ii) data averaging and despiking, iii) rotation of the flow velocity

coordinate system, iv) computation of the turbulent fluctuations, v) alignment of the O_2 and vertical velocity fluctuations, and vi) quantification of O_2 fluxes. Raw readings from the O_2 microelectrodes were *in situ* calibrated based on concurrent O_2 measurements from a factory-calibrated Rinko optical dissolved O_2 meter (JFE Advantech Co., Ltd., Japan). Each flow velocity time series was screened to identify periods where the ambient flow measured by the AEC had been disturbed by the lander frame and these were removed from subsequent processing. Turbulent fluctuations of O_2 and vertical velocity were obtained over a time interval of 5 min using linear detrending, which was found to be the most suitable for the given bottom roughness. Both fluctuation time series and O_2 fluxes were computed using the Fortran program suite Sulfide-Oxygen-Heat Flux Eddy Analysis (SOHFEA) version 2.0 (available from www.dfmcginnis.com/SOHFEA; McGinnis et al., 2014). To relate the O_2 flux rates to the respective benthic communities and their heterogeneity, the footprint area of the AEC was estimated for each deployment based on *h* and the bottom roughness length scale (z_0; Berg et al., 2007). Mean values for z_0 were derived assuming Law-of-the-Wall as described in (Inoue et al., 2011).

Box core (BC) incubations

Box cores (BCs) were taken from the reef framework and bare sediment with a NIOZ-designed box corer (Figure 3.3A). The BC consisted of a cylindrical barrel of 50 cm diameter and 55 cm height and sampled an area of 0.2 m^2. A camera was mounted on the BC and recorded the seafloor just before sampling. After collection, the cores, with reef community and bottom water, were sealed with plexiglass lids, placed in a temperature-controlled water reservoir to maintain *in situ* temperature, covered in black plastic sheets, and subsequently incubated after an acclimatization period of ~2 h (Figure 3.3A-B). *In situ* temperatures were recorded by repeated CTD casts during the cruise. PreSens© O_2 and temperature sensors were installed in the lid, along with a magnetic stirrer (Figure 3.3C). The mixing efficiency of the stirring device was tested prior to the cruise by adding ~10 ml of a uranine solution (1 g L^{-1}) to a BC with dead coral framework. Uranine fluorescence was measured with a Cyclops® 7 fluorescence sensor (Turner Designs, Inc) and revealed homogeneous mixing already after ~3 minutes (data not shown). The BCs taken at the bare sediment reference site were subsampled with a 12 cm diameter- plexiglass incubation core, and incubated in a temperature-controlled room (8-10 °C). The use of smaller subsampled incubation cores for bare sediment reference site was preferred since the porous marine sediment caused problems in closing the base of the large BCs during incubation.

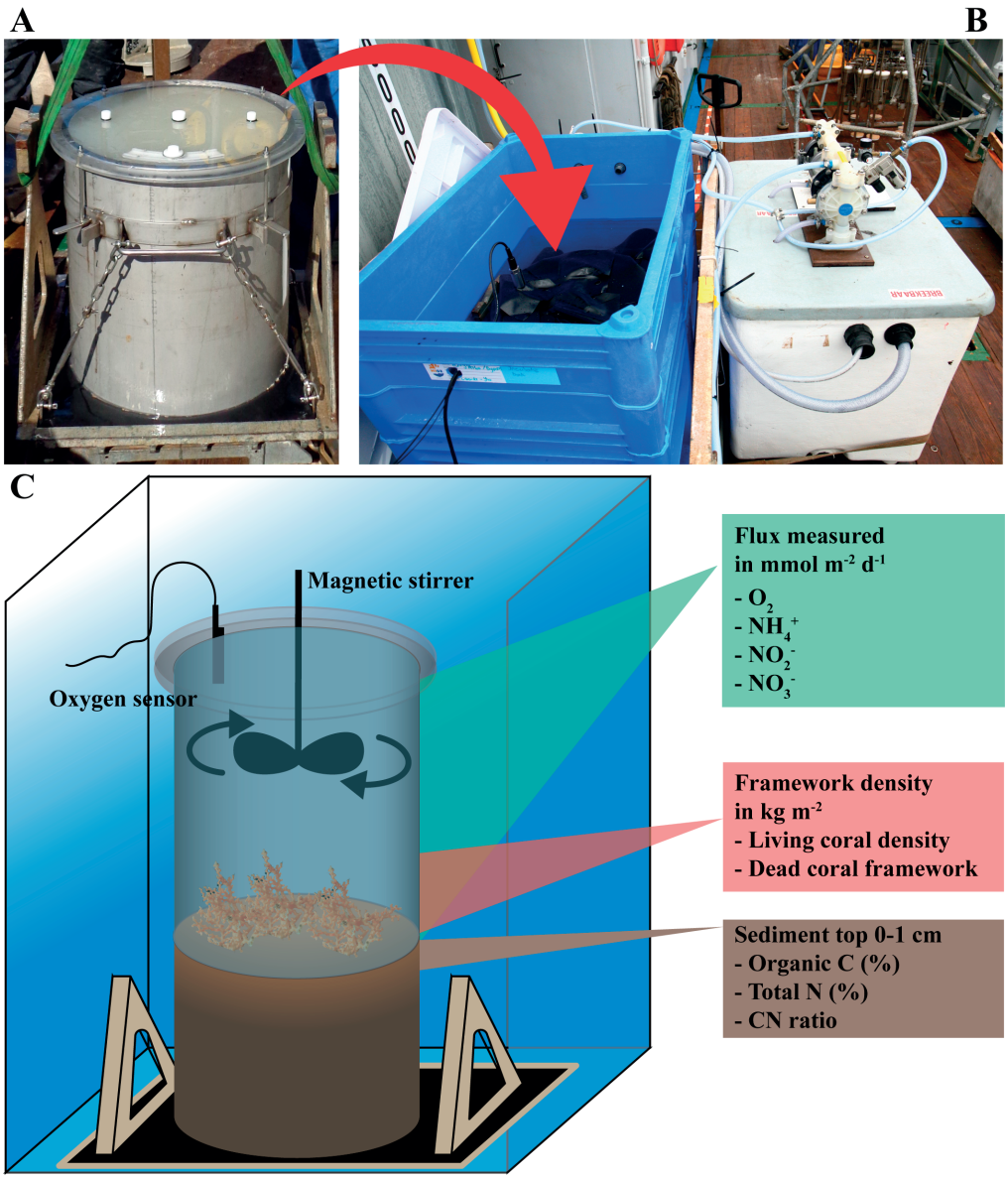

Figure 3.3A: A) Box core after closure with lid, B) incubation set-up, C) schematic view of incubation set-up and measured variables.

In both procedures the O_2 concentration of the overlying water was measured continuously at 30 s intervals. The O_2 saturation did not drop by more than 20% of the start O_2 value during the incubation. Samples for dissolved inorganic nitrogen (DIN), i.e. NH_4^+, NO_3^- and NO_2^-, were taken in triplicate by 10 ml syringes through a sampling port in the lid

at the start and at the end (~24 h later) of each incubation. In six of the nine incubations a third intermittent measuring point was included. DIN samples were filtered through 0.45 µm cellulose membranes filters (Acrodisc® 25 mm filter, 0.45 µm HT Tuffryn ®membrane) and frozen (-20 °C) until analysis eight weeks later in the laboratory at NIOZ. Sampled water was replaced by bottom water retrieved with the CTD rosette from the respective sampling station. After the incubation, the water was drained, and the living CWC and dead coral framework stored frozen (-20 °C). Dead coral framework is here defined as dead coral branches with associated biofilm, epifauna and endofauna. A sediment sample of the top cm layer was taken by a plastic liner (i.d. 5 cm) for analysis of grain size and organic carbon and nitrogen content (Figure 3.3C). Due to large amounts of coral fragments in the sediment layer, it was not possible to sample the sediment of stations SHM 1 and FHM 2.

Concentration of DIN was measured using a SEAL QuAAtro analyzer (Bran+Luebbe, Norderstedt, Germany). Corals were freeze-dried, and dead coral framework was oven-dried at 55 °C, to constant weight. Corals and dead coral framework were weighed (i.e. dry weight) and subsampled for organic carbon analysis. Subsamples (~2 g, 3 per incubation) were ground and homogenized to fine powder using a ball mill at a 30 s^{-1} frequency (MM301, Retsch). About 20 mg of coral powder was subsampled into silver measuring cups, exposed to hydrochloric acid fume (HCl, 37%) for three days, and subsequently acidified with increasing levels of concentrated HCl (2%, 5%, and 30%) until all inorganic carbon was removed (Maier et al., 2019). Another set of tin cups was filled with ~20 mg of coral powder for total nitrogen analysis and was not acidified. The acidified and non-acidified cups were pinch closed and respectively analyzed for total organic carbon and total nitrogen with an element analyzer (Thermo Electron Flash EA 1112 Analyzer). To determine the sediment grain size distribution, sediment samples were freeze-dried, sieved through a 2 mm mesh to remove small coral fragments, and analyzed by laser diffraction technique (Mastersizer 2000; Malvern Instruments Ltd, Malvern, UK; measurement range 0.02-2000 µm). In addition, ground sediment samples were analyzed for organic carbon and nitrogen content as described above.

Absolute O_2 concentrations were calculated with the *marelac* R package from the percent O_2 air saturation measured by the O_2 sensors (Weiss, 1970; Soetaert et al., 2016b). The O_2 and DIN fluxes (mmol m^{-2} d^{-1}) were subsequently calculated from the slope of a linear regression fitted to the observed concentration change and corrected for box core volume and surface area (Glud, 2008). To unravel the contribution of living corals, dead coral framework and sediment to the total O_2 and DIN flux, we performed a planar regression of the observed benthic flux from the box core incubations against the predictor variables 'living coral biomass' (kg dry weight m^{-2}) and 'dead coral framework' (kg dry weight m^{-2}; n = 6), of which the intercept is interpreted as sedimentary benthic flux. Specifically, we resolved the regression model: $flux = a \cdot CWC + b \cdot Framework + c$, in which is the measured flux of O_2 or DIN (mmol m^{-2} d^{-1}), is the parameter representing the dry-mass-specific ben-

thic flux for living corals (i.e. mmol kg DW^{-1} d^{-1}), *CWC* is the dry weight of living cold-water corals in the box core scaled up to m^{-2} (kg DW m^{-2}), is the dry-mass-specific flux for dead coral framework (mmol kg DW^{-1} d^{-1}), *Framework* is the dead coral framework density (kg DW m^{-2}), and is the sediment flux (mmol m^{-2} d^{-1}). Hence, we actually used the differences in the living coral biomass and dead coral framework in each box core to quantify the contribution of 'living coral biomass', 'dead coral framework' and 'sediment' to the total flux in each incubation. All statistics were performed in the statistical software program R (R Development Core team, 2018). The R packages *ggplot2* and *plot3D* were used to produce Figure 3.6 and Figures 3.1 and 3.7, respectively (Wickham, 2016b; Soetaert, 2017).

Results

Site description

The bare sediment sites were characterized by a smooth surface with occasional drop stones (Figure 3.4A). In contrast, recordings at the summit of the Haas Mound showed a patchy distribution of coral colonies, dead coral framework and bare sediment patches (Figure 3.4B). On the southern flank of the Haas and Oreo Mounds, a thick framework of thriving coral reef was observed (Figure 3.4C-D).

Sediment characteristics and coral density of box core incubations

The surface sediment at the reference site was mainly composed of fine to medium sand (grain size between 63 – 630 µm), with a low organic matter content (i.e. 0.19% organic carbon and 0.03% organic nitrogen; Table 3.2). Surface sediment on the coral mounds was substantially finer than at the reference site and was composed mainly of silt and very fine sand (grain size between 2-200 µm). Consistent with the finer particle sizes, the organic nitrogen and carbon content was higher on the mounds as compared to the reference site. The [molar] CN ratio of the sediments was similar among the four sampling sites (Table 3.2).

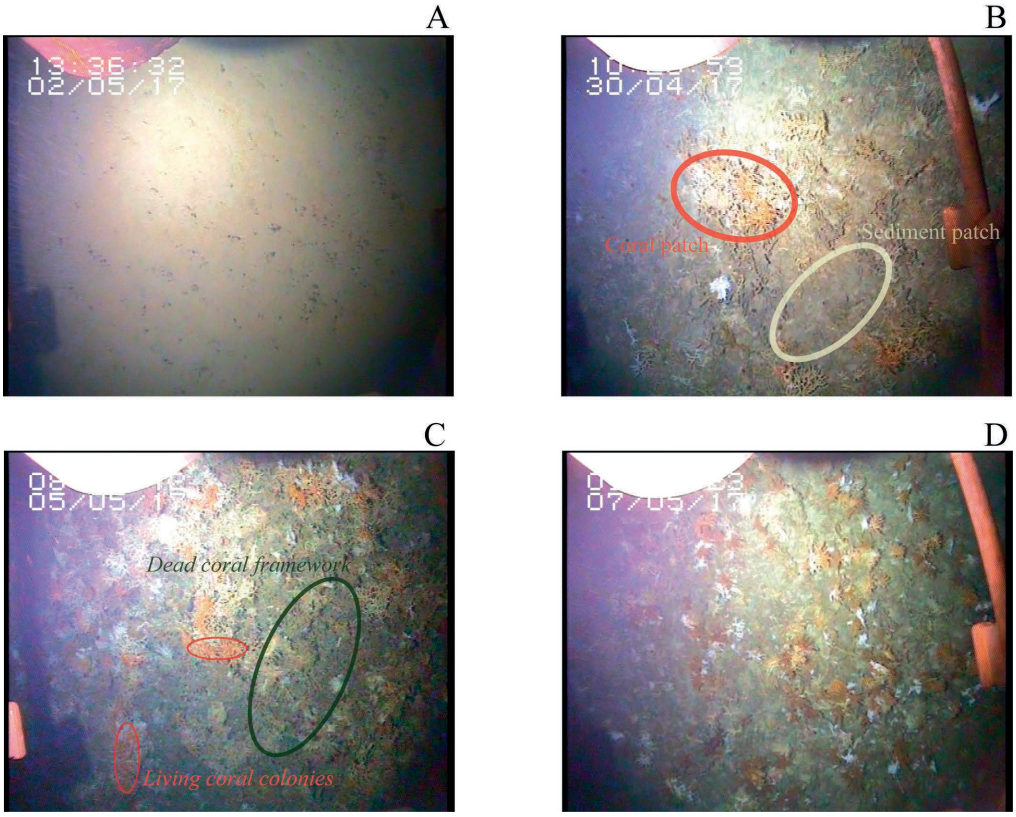

Figure 3.4A: Stills extracted from the video that was mounted on the boxcore displaying the four habitats sampled by box core. A) Reference site on Rockall Bank, B) The summit of Haas Mound, note the patchy distribution of coral framework and sediment and C, D) southern flank of Haas and Oreo Mound, respectively, showing a thick layer of living coral and dead coral framework.

Table 3.2 The sediment characteristics median grain size (µm), organic nitrogen content (%), organic carbon content (%) and molar C/N ratio. Values are presented in mean ± SD, SD only if n >1

	Sediment	Summit Haas	Flank Haas	Oreo Mound
Median grain size (µm)	224.9 ± 28.8	41.6 ± -	62.8 ± 6.1	74.1 ± 17.4
Organic nitrogen	0.03 ± 0.00	0.09 ± -	0.06 ± 0.00	0.06 ± 0.00
Organic carbon	0.19 ± 0.01	0.51 ± -	0.32 ± 0.05	0.32 ± 0.06
C/N ratio	6.77 ± 0.71	6.26 ± -	6.08 ± 0.83	6.15 ± 0.77

In all box cores used for incubations, the density of dead coral framework was substantially (on average 27 times) higher than the density of living coral (Table 3.3). Three scleractinian CWC species were present in the six box cores: two colonial species of *Lophelia pertusa* and *Madrepora oculata*; and the solitary *Desmophyllum dianthus*. The organic carbon and nitrogen content of the dead coral framework was three to four times lower as compared to the living corals. The Haas Mound summit showed the largest range of living coral density (0.01 – 3.31 kg DW m^{-2}). The Haas Mound flank was characterized by a low living coral density (0.00 – 0.08 kg DW m^{-2}) and comparatively high dead framework (19.59 – 85.97 kg DW m^{-2}). On the Oreo mound, only living corals of the species *M. oculata* and small amounts of *D. dianthus* were found (0.45 – 0.98 kg and 0.01 – 0.05 kg DW m^{-2} respectively). The amount of dead coral framework on the Oreo mound (5.00 to 9.54 kg DW m^{-2}) was comparable to that of the summit of the Haas mound.

Table 3.3 The density (kg dry weight m^{-2}), organic carbon content (%) and organic nitrogen content (%) of the living corals and dead coral framework for box core (mean ± SD, SD only if n >1), n.d. = not detected, * not measured due to technical error

		Summit Haas Mound		Flank Haas Mound		Oreo Mound	
		SHM 1	SHM 2	FHM 1	FHM 2	OrM 1	OrM 2
L. pertusa	Density	n.d.	3.31	0.05	n.d.	n.d.	n.d.
	Organic carbon	-	0.67 ± 0.09	0.34	-	-	-
	Organic nitrogen	-	0.17 ± 0.02	0.11	-	-	-
M. oculata	Density	0.01	0.09	0.01	n.d.	0.98	0.45

	Organic carbon	0.79	0.71 ± 0.08	*	-	1.43 ± 0.35	1.27 ± 0.18
	Organic nitrogen	0.19	0.19 ± 0.03	*	-	0.33 ± 0.08	0.31 ± 0.05
D. dianthus	Density	n.d.	n.d.	0.02	n.d.	0.01	0.05
	Organic carbon	-	-	1.14 ± 0.01	-	1.16	2.11
	Organic nitrogen	-	-	0.24 ± 0.01	-	0.25	0.41
Dead framework	Density	5.85	6.95	19.59	85.97	9.54	5.00
	Organic carbon	0.12 ± 0.04	0.19 ± 0.08	0.14 ± 0.01	0.14 ± 0.02	0.14 ± 0.01	0.22 ± 0.03
	Organic nitrogen	0.06 ± 0.01	0.08 ± 0.02	0.07 ± 0.02	0.07 ± 0	0.06 ± 0.01	0.09 ± 0.01

O_2 fluxes measured by the AEC technique

The two AEC deployments provided a total of 28h and 41h of unobstructed useful measurements, respectively. During the 28-h deployment on the summit of Haas Mound (i.e. SHM3, Table 3.1), the lander was deployed diagonally to the main flow axis and the lander structure affected 25% of the measurements, which were therefore excluded from the analysis. Undisturbed flow velocities ranged between 0 and 23 cm s^{-1} (average 9.8 cm s^{-1}). The dominant flow direction changed during the deployment (Figure 3.5A), suggesting that the O_2 flux measured with the AEC technique is representative of different CWC community patches. This was confirmed by particle path analysis (data not shown), and by the fact that the cumulative flux analysis found distinctly different integrated O_2 fluxes (11.5 ± 3.6 (mean ± SE) and 22.35 ± 5.6 mmol m^{-2} d^{-1}, respectively) for the different footprints (Figure 3.5B). The site-representative bottom roughness length scale (z_0) was 3.1 cm for both AEC footprints.

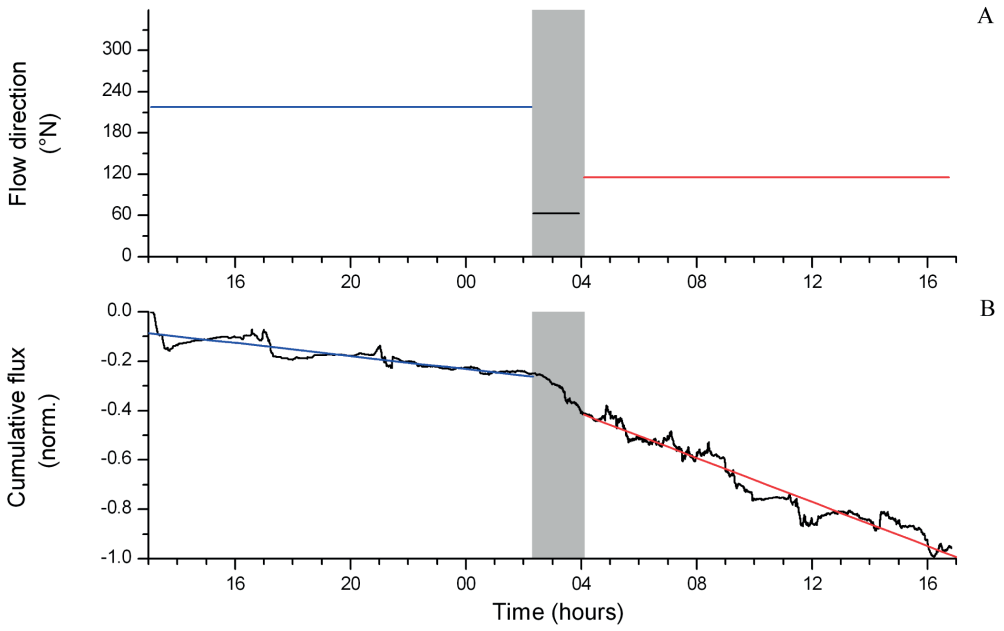

Figure 3.5 A) Dominant flow direction during the deployment at summit of Haas Mound (i.e. AEC01), B) normalized cumulative O_2 flux at summit of Haas mound (AEC01). Note that a linear change of the cumulative flux over time indicates stable conditions and thus well-developed fluxes. Linear sections (red and blue lines) indicate the main flux contributions from the two AEC footprints. The shaded time frame represents a transitional period in the flow direction which resulted in flow disturbances by the lander structure and overall unstable flux conditions. Deployment time is in hours after 30-Apr 00:00 UTC

The AEC deployment on top of Oreo mound (OrM 3, Table 3.1) revealed a strong directional flow with velocities ranging from 0.047 m s^{-1} up to 1.8 m s^{-1} (average 0.89 m s^{-1}). The lander structure affected 42% of the measurements, but the values obtained during unobstructed flow came from one distinct AEC footprint and gave an O2 flux of 45.3 ± 11.7 mmol m^{-2} d^{-1}. The site-representative z_0 was 5.1 cm, reflecting a rougher benthic surface than at the summit of Haas mound.

O_2 fluxes measured by BC incubations

Temperature during the box core incubations ranged between 7.6 and 9.4 °C, which corresponds well to the range of *in situ* water temperature (8.7- 9.0 °C). Leakage at the base of the box corer created an occasional air bubble under the lid of the core, and the ship movement caused the air bubble to mix with the incubation water, and induced periods

of O_2 perturbation (Figure 3.6). When an air bubble was observed, it was eliminated by adding bottom water. The period during which the O_2 concentration was visually perturbed was omitted from the linear regression. After removal of the air bubble, the O_2 decreased continued in a comparable way to before the presence of the air bubble (Figure 3.6).

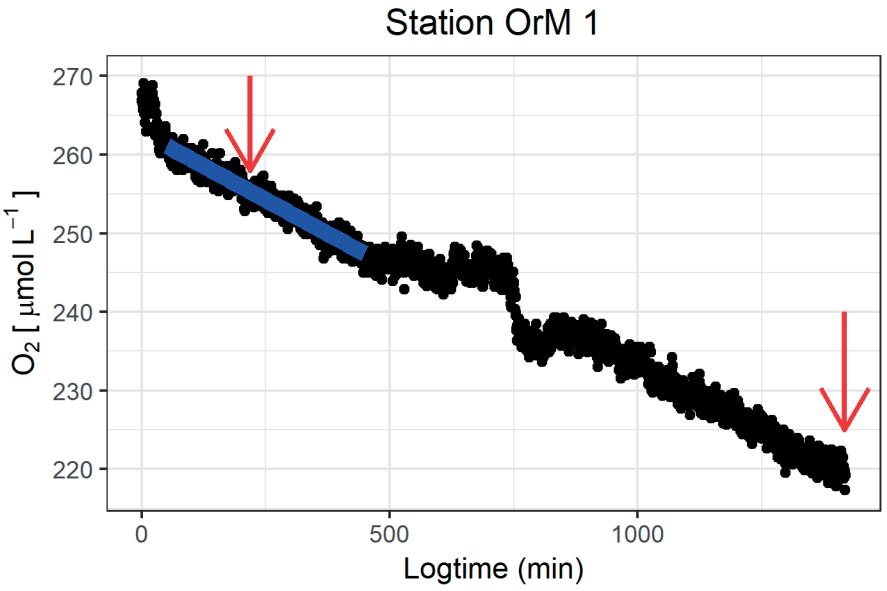

Figure 3.6 Representative O_2 concentration series during a boxcore incubation (OrM 2), with the black dots representing the O_2 concentration (µmol L^{-1}) and the blue line the resulting linear regression which was used to calculate the O_2 flux. The red arrows indicate sampling of DIN. The disturbance caused by air bubble development is visible between minute 500 and 800

The O_2 flux at the reference sediment site ranged from 0.6 to 3.2 mmol O_2 m^{-2} d^{-1} (mean ± SD: 1.9 ± 1.4 mmol O_2 m^{-2} d^{-1}; Table 3.4). The O_2 flux of the CWC reef communities ranged from 5.7 to 28.4 mmol O_2 m^{-2} d^{-1} (mean ± SD: 14.6 ± 8.4 mmol O_2 m^{-2} d^{-1}). The variability in CWC reef community O_2 flux was higher on the summit of the Haas mound than on the flank and at Oreo mound (Summit Haas = 17.0 ± 16.0 mmol O_2 m^{-2} d^{-1}, Flank Haas = 15.5 ± 6.9 mmol O_2 m^{-2} d^{-1}, Oreo = 11.2 ± 2.8 mmol O_2 m^{-2} d^{-1}; Table 3.4).

Table 3.4 Benthic O_2 uptake rate and DIN fluxes measured from the BC incubation experiments expressed in mmol m^{-2} d^{-1}. Values are reported as flux ± SD, values in bold are significant fluxes ($p < 0.05$)

	Summit Haas		Flank Haas		Oreo		Sediment		
	SHM 1	SHM 2	FHM 1	FHM 2	OrM 1	OrM 2	SB 1	SB 2A	SB 2B
O_2	**5.7 ± 0.3**	**28.4 ± 2.4**	**10.7 ± 0.9**	**20.5 ± 0.8**	**13.1 ± 0.7**	**9.2 ± 1.2**	**3.2 ± 0.0**	**1.9 ± 0.0**	**0.6 ± 0.0**
NH_4^+	0.02 ± 0.02	**0.98 ± 0.16**	0.16 ± 0.10	0.00 ± 0.02	**0.22 ± 0.02**	**0.06 ± 0.02**	0.01 ± 0.06	-0.11 ± 0.10	-0.02 ± 0.02
NO_3	**0.93 ± 0.09**	**2.04 ± 0.30**	**1.12 ± 0.10**	**0.54 ± 0.05**	**0.58 ± 0.09**	**0.38 ± 0.08**	**0.15 ± 0.04**	**1.04 ± 0.23**	0.40 ± 0.22

Nitrogen fluxes measured by BC incubations

During all incubations, the concentration and flux of NO_2^- were negligible, hence we present only the results for NH_4^+ and NO_3^-. The initial NH_4^+ concentrations ranged from 0.3 to 0.5 µmol L^{-1} while values at the end of incubation were between 0.3 and 2.0 µmol L^{-1} and NO_3^- concentrations during incubations increased from 10.0 – 17.0 µmol L^{-1} to 11 – 20 µmol L^{-1}. Due to the occasionally high variation within the triplicate samples, the calculated fluxes were not always significant (Table 3.4). However, the average DIN (NO_3^- + NH_4^+) flux of CWC reef communities (1.17 ± 0.87 mmol N m^{-2} d^{-1}) was around two times higher than that of bare sediment reference site (0.49 ± 0.32 mmol N m^{-2} d^{-1}). At the bare sediment reference site, NO_3^- fluxes were relatively more important than the NH_4^+ fluxes for the overall DIN flux. Generally, the DIN fluxes of box core incubations were mainly driven by NO_3^- except for incubations containing CWC colonies, in these cores the NH_4^+ fluxes were a significant part of the DIN fluxes.

Unravelling the biogeochemical fluxes

Planar regression of the box core O_2 fluxes against living coral and dead coral framework, with the intercept representing the contribution of the sediment, showed a robust relation (R^2- adj: 0.99, Figure 3.7, Table 3.5), indicating that the dry-mass-specific O_2 flux of living coral is >30 times higher than that of the coral framework. For the NH_4^+ flux, living coral density was the only significant descriptor (R^2-adj = 0.94, Table 3.5) and contributions from the sediment and dead coral framework were non-significant. The NO_x flux was not significantly related to the amount of live or dead coral framework, and only the intercept (i.e. sediment activity) was significant. Note that the regression could only be based on the box core incubations, as data on the coral and dead coral framework density in the AEC footprint are lacking.

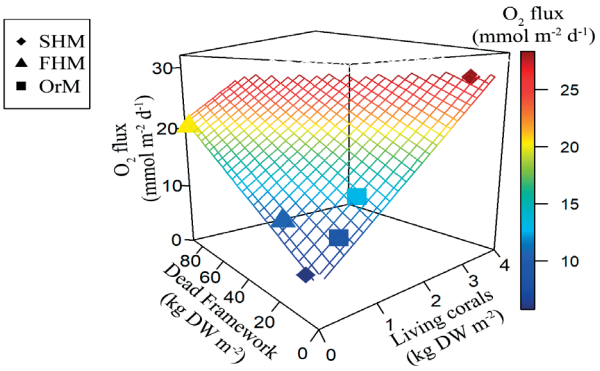

Figure 3.7 Planar regression of the O_2 flux (mmol m^{-2} d^{-1}) against the predictor variables living coral density (kg dry weight m^{-2}) and dead coral framework density (kg dry weight m^{-2}), of which the intercept is interpreted as sedimentary O_2 flux. The six incubated boxcores are plotted as individual datapoints and plane represents results of the regression model. Note that the symbols in the plot are shape according to their location (see legend) and colored according to the observed O_2 flux. Plot produced with R package plot3D (Soetaert, 2017)

Table 3.5 Planar regression of the benthic flux, i.e. *flux* = $a \cdot CWC + b \cdot Framework + c$ (n=6), with a = 'Living coral' rate, b = 'Dead coral framework' rate and c = 'Sediment' rate. Significant model parameters are highlighted in bold

	Living coral (mmol O_2 kg^{-1} DW d^{-1})	Dead coral framework (mmol O_2 kg^{-1} DW d^{-1})	Sediment (mmol O_2 m^{-2} d^{-1})	Model fit (R_2 – adj)
O_2	**6.39 ± 0.32**	**0.18 ± 0.01**	**5.32 ± 0.59**	0.99
NH_4	**0.28 ± 0.03**	0.00 ± 0.00	0.01 ± 0.06	0.93
NO_3	0.36 ± 0.17	0.00 ± 0.01	0.64 ± 0.32	0.37

Discussion

Constraining O_2 exchange rates at CWC reefs

This study provides the first concurrent O_2 flux measurements from box core (BC) incubations and aquatic eddy-covariance (AEC) and contributes to the small database for O_2 fluxes of whole CWC reef communities (Table 3.6). The mean O_2 flux derived by AEC generally aligns well with the flux derived by chamber incubations for homogenous cohesive sediments in shallow water and deep sea settings (Berg et al., 2003, 2009; Glud et al., 2016). In complex benthic habitats such as permeable sand, maerl beds, reefs or megafauna enriched sediments, the O_2 exchange obtained by the two approaches often diverges (Glud et al., 2010; Attard et al., 2014, 2016). This discrepancy has been ascribed to mesoscale heterogeneity that might be poorly represented during chamber deployments, or to changes of flow characteristics or food availability during chamber enclosure (Attard et al., 2015). However, deep water AEC deployments in complex habitats such as CWC reefs come with logistical challenges and often require access to a work-class remotely operated vehicle for accurate positioning (Rovelli et al., 2015), which limits the applicability of the approach. Moreover, in dynamic settings such as CWC reefs, the AEC approach requires a relatively long deployment time of 12 – 24 h to integrate the inherent short-term variations associated to changes in flow direction and velocity (Holtappels et al., 2013; Glud et al., 2016).

Our study measured the O_2 flux at sites that visually differed in their density of living coral and dead coral framework. While the BC incubations showed no site differences, the regression analysis showed that two variables, namely the quantity of living coral and dead coral framework, explained most variability in the O_2 flux at all three investigated coral sites. The congruence of the O_2 fluxes by the AEC and BC method for the summit of Haas mound, which showed a patchy distribution of living corals and bare sediment, suggests that the habitat variability of the ~500 m^2 large AEC footprint was reasonably represented by the replicate ~0.2 m^2 large BC incubations. In contrast, at the deeper (~750 m) Oreo mound we encountered a higher near-bottom flow velocity, and the average O_2 flux derived by the AEC technique was four times higher than that obtained with the BC incubations. Data on the density of living coral and dead framework in the AEC footprint is unfortunately not available, so it remains difficult to judge what caused the high AEC O_2 flux at Oreo mound. As the AEC data from Oreo mound were of high quality and represented a large footprint (~500 m^2), we believe that the AEC value presumably provides the more robust O_2 flux estimate on a CWC community scale and that the two box core incubations poorly represented the natural habitat variability or compromised the natural flow conditions. It should also be noted, that a higher O_2 flux at Oreo mound was a priori anticipated given the higher coral density previously observed on video transects and

on the boxcore videos (Figure 3.4B-D).

The measured O_2 fluxes of the summit of Haas mound compare well with those reported for the shallower CWC communities at the Mingulay Reef Complex and Stjernsund (Norwegian glacial sound; Rovelli et al., 2015). The AEC-based O_2 flux at Oreo mound is however ~3 times higher, which underlines the large spatial metabolic variability that may exist between mounds of the same mound province. The highest O_2 flux reported for CWC reefs was reported for a 'cigar-shaped' reef at the Træna marine protected area in Norway (Cathalot et al., 2015). That O_2 flux, however, is representative for the head section of these reefs, which are known for having a very dense cover of live *Lophelia pertusa* (Cathalot et al., 2015) and this may not be directly comparable to the other CWC mounds. Furthermore, the measurements at the Træna marine protected area were based on a short measuring period of a few hours (~2h) and may thus not fully represent average flux conditions at the measuring site. Excluding that value, the available AEC-based O_2 uptake rates of CWC communities converge towards 28.7 mmol m^{-2} d^{-1}, which is a factor of 5 higher than the O_2 uptake for soft bottom systems at similar depths (Andersson et al., 2004; Glud, 2008).

The dry-mass-specific O2 flux for living corals (inferred from planar regression model) of 6.39 ± 0.32 mmol O2 kg-1 DW d-1 compares well with O2 fluxes measured for L. pertusa or M. oculata obtained during laboratory incubations (Dodds et al., 2007; Larsson et al., 2013; Khripounoff et al., 2014), suggesting limited disturbance induced by the sampling. The coral framework consists of eroding dead branches that provide a substrate for biofilm, consisting of microbial biomass, and sessile and mobile fauna. Fauna encountered in the box cores (data not shown) belonged to the classes/phyla: Echinoidea, Polychaeta, Porifera, Crustacea, Actiniaria, which also previously have been identified as dominant in NE Atlantic CWC communities (e.g. (Duineveld et al., 2007; Henry and Roberts, 2007). The inferred dry-mass-specific O2 flux for dead coral framework (0.2 mmol O2 kg-1 DW d-1) was more than 30 times lower than the flux for living corals. However, as all box cores contained substantially more framework than living corals, especially at the southern flank of the Haas mound, the framework still contributed significantly, ranging from 10% to 75% of the total benthic O2 flux.

The organic carbon content (~0.35%) and median grain size (~ 63 µm) of sediment on the coral mounds is in line with previous work in the same area (Mienis et al., 2009b, 2009d), while being slightly lower than found in sediments underneath a CWC reef in Norway (Wehrmann et al., 2009). The dominance of fine and comparatively organic-rich sediment below the CWC framework is presumably caused by baffling of the water flow by the coral branches that leads to the accumulation of fine sediment particles between the coral framework (Dorschel et al., 2005a; de Haas et al., 2009). (Mienis et al., 2019) recently showed with a laboratory flume study that the current velocity was strongly reduced within and behind (i.e. wake effect) coral framework patches, inducing the settlement of inorganic and organic particles. In addition, the enhanced trapping of suspended organic

matter by the filter-feeding faunal community, and subsequent deposition as (pseudo) feces, may additionally enrich the organic carbon concentration on coral mounds (Maier et al., 2021). The reference site in contrast, lacks the baffling effect of the framework and (most of) the filter-feeding activity, which leaves a coarser sediment with lower organic carbon content.

Table 3.6. Overview of O_2 fluxes (mmol m^{-2} d^{-1}) of CWC communities based on various methods. For comparison, mean sediment community oxygen consumption (SCOC) for soft sediments for the respective depth is provided from published regressions.

Site	Depth (m)	O_2 flux	Method	SCOC	Reference
Summit Haas mound, Rockall Bank	539 536 - 539	17.0[b]17.0 ± 16.0	AEC BC	2.7 / 7.1	this study
Flank Haas mound, Rockall Bank	639 - 747	15.5 ± 6.9	AEC BC	2.1 / 6.4	this study
Oreo mound, Rockall Bank	744 757 - 838	45.3 ± 11.7 11.2 ± 2.8	AEC BC	2.1 / 6.4	this study
Mingulay Reef Complex (Scotland)	128	27.8 ± 2.3	AEC	7.8 / 9.2	Rovelli et al. (2015)
Stjernsund (Norway)	220	24.8 ± 2.6	AEC	5.2 / 6.4	Rovelli et al. (2015)
Træna marine protected area (Norway)	280 280	121.5 ± 9.9[c]81.7 ± 9.8	AEC In situ incubation and upscaling	4.2 / 5.8	Cathalot et al. (2015)
Guilvinec & Croisic canyons (France)	850	7.7	In situ incubation and upscaling	1.9 / 4.4	Khripounoff et al. (2014)
Tisler Reef (Norway)	102 - 150	37.1	Water retention time combined with O_2 change	7.9 / 9.6	White et al. (2012)

[a] Global regression of O_2 flux for soft sediment at comparable depths after Glud (2008) / Andersson et al. (2004). Note that Glud (2008) only included O_2 fluxes obtained *in situ*, while Andersson et al. (2004) included both in situ and *ex situ* data

[b] Average of two AEC footprints, 22.4 ± 5.6 and 11.5 ± 3.6 mmol m^{-2} d^{-1}, respectively[c] based on two short AEC deployments of 2 h each

To date, little is known on O_2 flux mediated by the sediment underneath a CWC reef. Microbially mediated processes are presumably more active in sediment underlying a CWC reef as compared to bare sediments (Wehrmann et al., 2009). Our findings support this idea in two ways. Firstly, the sediment on the coral mounds consists of finer and more organically rich material than the reference site, likely due to the baffling effect of the coral framework discussed above, suggesting that mineralization will be higher. Secondly, from the planar regression we inferred an O_2 flux of 5.3 mmol m^{-2} d^{-1} for the sediment underlying the coral framework, which is indeed a factor ~3 higher than the average O_2 flux measured at reference site. The O_2 flux of the CWC-sediment inferred in this study is substantially lower than the O_2 flux of 33.2 ± 10 mmol m^{-2} d^{-1} (mean ± SD) that was measured in a food web model of the cold-water coral community at Rockall Bank (van Oevelen et al., 2009). This might reflect a true difference among sites, but in addition to spatial and temporal variability, methodological differences may contribute to this difference, as the latter authors measured the O_2 flux in a core that was taken from a box core after the overlying coral and dead framework was removed.

CWC reef communities appear to be hotspots of carbon mineralization on the seafloor. A habitat suitability model suggest a CWC habitat cover of 4.7% for the Logachev mound province (areal extent of 60 x 90 km; Rengstorf et al., 2014). Assuming the remaining 95.3% in the area consists of soft-sediments, we can calculate the benthic soft-sediment respiration with the depth-dependent power equation developed by (Glud, 2008). Using the median CWC community O_2 uptake rate obtained from the BC incubations (11.9 mmol O_2 m^{-2} d^{-1}), and the AEC technique (24.8 mmol O_2 m^{-2} d^{-1}), we estimate that CWC reefs are responsible for 20% to 35% of the total benthic respiration in the Logachev mound province, depending on which median O_2 uptake rate is used. This percentage is in line with calculations of the relative importance of CWC reefs in benthic OM cycling on the Norwegian Margin (36% of total benthic respiration; (Cathalot et al., 2015) and indicates that the CWC mounds in the Logachev mound province play an important role in regional carbon cycling.

Nitrogen fluxes of a CWC reef community

The present study reports the first nitrogen flux measurements of intact CWC communities and allows a comparison with sediment communities. The nitrogen fluxes measured from the bare sediment reference site incubations showed a variable release of NO_3^- into the overlying water and negligible NH_4^+ efflux. This pattern is consistent with many earlier studies on nitrogen cycling in deep water, aerobic sediments, which have shown that NH_4^+ produced by organic matter mineralization generally is oxidized by different nitrifying microorganisms to NO_2^- and subsequently to NO_3^- which diffuses out of the sediment

(Thamdrup and Dalsgaard, 2008; Libes, 2009).

The inorganic nitrogen fluxes from the incubations including a CWC reef community are markedly different. Firstly, the 2.4 times higher NO_3^- efflux by the CWC reef community, compared to the sediment, is consistent with its higher O_2 flux/consumption. The significant production of NH_4^+ by the CWC reef community indicates that the NH_4^+ typically produced by the reef fauna (Wright, 1995), like sponges (Hoffmann et al., 2009; Leys et al., 2018) and *Lophelia pertusa* (Middelburg et al., 2015), is only partly nitrified, presumably by reef-associated micro-organisms including archaea (Van Bleijswijk et al., 2015). CWC reef communities, in contrast to soft sediment communities, hence increase the NH_4^+ concentration of the bottom water. This modification of the nitrogen cycle by CWC reef communities is consistent with the observations of elevated NH_4^+ concentrations in the water column above the CWC mounds at Rockall Bank (Findlay et al., 2014).

The inferred dry-mass-specific NH_4^+ release rate for living corals in our study (0.29 ± 0.03 mmol NH_4^+ kg^{-1} DW d^{-1}) compares favorably with the reported *in-situ* values and *ex-situ* rates of 0.10 – 0.40 mmol NH_4^+ kg^{-1} DW d^{-1} (Khripounoff et al., 2014; Middelburg et al., 2015; Maier et al., 2019). Our results also show that the living cold-water corals are primarily responsible for the observed NH_4^+ release, as the dry-mass-specific dead coral framework DIN fluxes are found to be negligible. This is consistent with the planar regression of the O_2 flux data, which showed that the dry-mass-specific O_2 flux of living corals is >30 times higher than that of dead coral framework.

In conclusion, we show that the O_2 flux of CWC reef communities in the North-East Atlantic Ocean is on average ~5 times higher than that of soft sediments from comparable depths. This implies that also deep CWC reefs, in addition to earlier findings for relatively shallow (<200 m depth) CWC reefs, are hotspots of carbon cycling on continental margins. Moreover, despite a dominance of dead coral framework in the reef community, the living cold-water corals appeared to be the major driver of this high O_2 flux. The first CWC reef community-based dissolved inorganic nitrogen fluxes to-date show that the CWC reef community, specifically the living cold-water corals, alter benthic nitrogen cycling compared to bare sediment, by largely circumventing nitrification and releasing NH_4^+ directly into the ambient water. This implies that CWC reefs are not only hotspot of carbon cycling, but are also hotspots of nitrogen cycling.

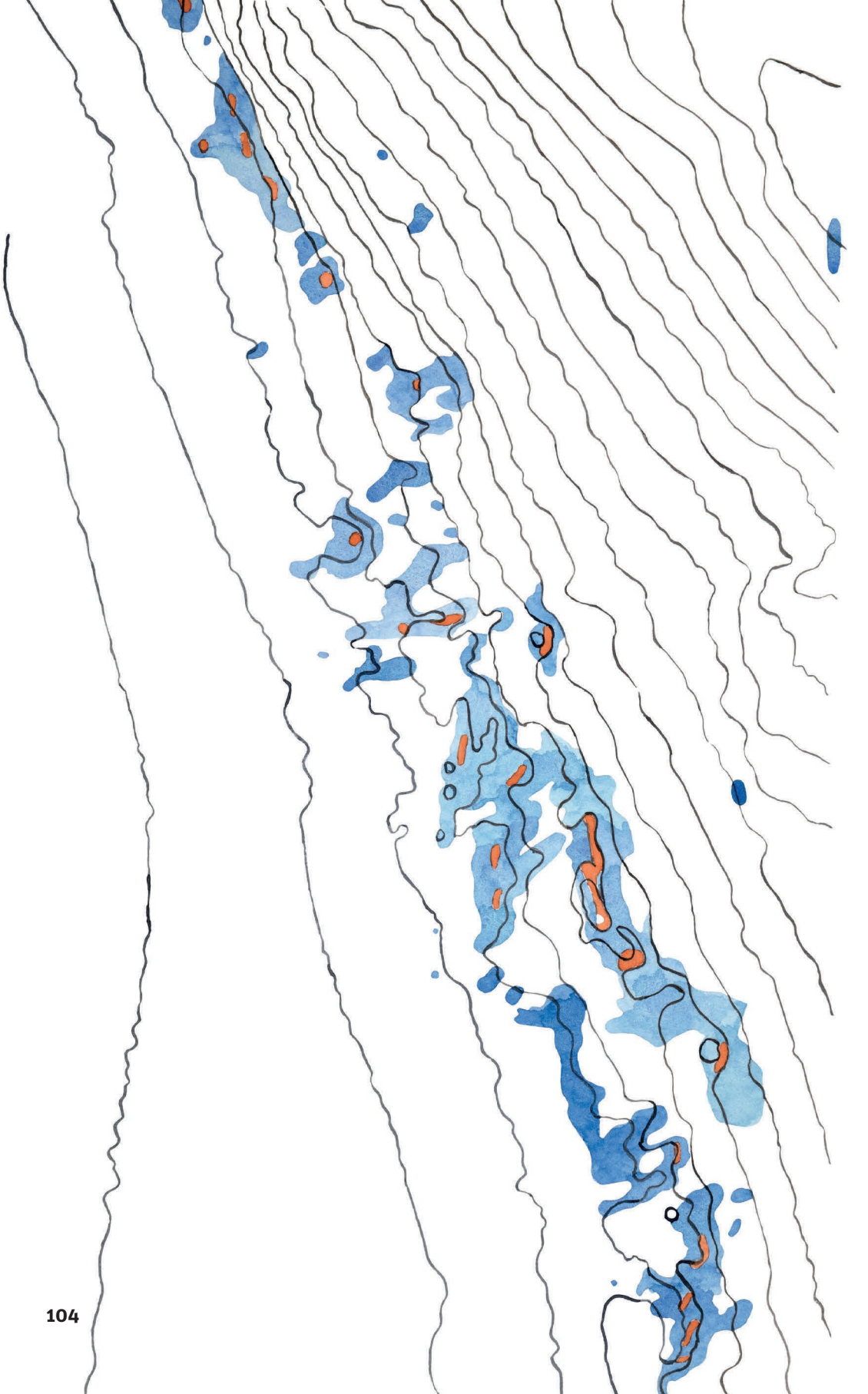

Chapter 4

MODELLING COLD-WATER CORAL BIOMASS AND RESPIRATION BASED ON PHYSIOLOGY, HYDRODYNAMICS, AND ORGANIC MATTER TRANSPORT

Evert de Froe, Christian Mohn, Karline Soetaert, Anna van der Kaaden, Gert-Jan Reichart, Laurence H. De Clippele, Dick van Oevelen

To be submitted to Scientific Reports

Abstract

Cold-water corals form complex three-dimensional structures on the seafloor, providing habitat for numerous species and act as a carbon cycling hotspot in the deep-sea. Although these ecosystems are recognized as important deep-sea habitats, our capacity to predict their distribution and ecosystem functions relies largely on statistical habitat suitability models in which coral occurrence is merely predicted from variables such as terrain characteristics, temperature, salinity, and surface productivity. Here, we present the results of a mechanistic process-based model in which coral biomass and respiration is predicted from a 3D coupled transport-reaction-model for the south-east Rockall Bank (NE Atlantic Ocean). Hydrodynamic forcing is provided by a high-resolution ROMS (Regional Ocean Modelling System) model, which drives the transport of reactive suspended particulate organic matter in the region. The physiological cold-water coral model, with coral food uptake, assimilation, and respiration as key variables, is coupled to the reactive transport model of suspended organic matter. The cold-water coral biomass predictions agree with biomass and benthic respiration observations in the study area and coral occurrences comply with predictions from previously published habitat suitability models. Coupling the pelagic organic matter transport model with the cold-water coral model proved to be essential to produce realistic coral biomass estimates in our modelling approach. Furthermore, the organic matter concentration in the benthic boundary layer was strongly determined by coral- or filter feeding activity. This mechanistic modelling approach has the advantage over statistical predictions that it can be used to obtain a mechanistic understanding of the effect of changing environmental conditions such as ocean temperature, surface production export, or ocean currents on cold-water coral biomass distribution and can be applied to other study areas and/or species.

Introduction

Scleractinian cold-water corals (CWCs) are ecosystem engineers in the deep-sea that build reefs of high biodiversity and biomass (Jonsson et al., 2004; Roberts et al., 2006; Henry and Roberts, 2007). These reefs are considered hotspots of organic matter remineralization in the deep-sea (**chapter 3**, Cathalot et al., 2015; Rovelli et al., 2015), and can form carbonate mounds over geological timescales (Dorschel et al., 2005b; van der Land et al., 2014; Wienberg et al., 2020). These mounds and CWCs are distributed globally (Davies and Guinotte, 2011), and can be found in a wide range of environmental conditions, e.g., temperature and oxygen (Dullo et al., 2008; Mienis et al., 2012; Flögel et al., 2014; Hanz et al., 2019), but typically with high bottom currents (Genin et al., 1986; Mienis et al., 2007; Davies et al., 2009; Juva et al., 2020). Thriving CWC reefs have been linked to relatively low dissolved inorganic carbon (DIC) concentrations, i.e., a low carbonate saturation state (Flögel et al., 2014), strong tidal currents (Juva et al., 2020), and an above-average quantity (Guinotte et al., 2006) and quality supply of food (**chapter 2**, Kiriakoulakis et al., 2007). These CWC reefs, and deep-sea habitats in general, are currently under threat by ongoing climate induced oceanic changes (Gehlen et al., 2014; Jones et al., 2014; Levin and Le Bris, 2015; Brito-Morales et al., 2020; Morato et al., 2020), such as ocean acidification (Caldeira and Wickett, 2003; Hennige et al., 2015, 2020), enhanced stratification (Li et al., 2020), increasing temperatures (Wijffels et al., 2016), altered large ocean circulations (Boers, 2021; Caesar et al., 2021), and decreased carbon export from the surface layer (Laws et al., 2000; Bopp et al., 2001; Wohlers et al., 2009). However, predicting how these environmental changes will affect deep-sea habitats remains challenging due to, for instance, the technical constrains in sampling possibilities, and new tools and models are needed to understand how CWCs will be influenced by a changing marine environment.

The current capacity to predict the spatial distribution of CWCs is limited to statistical approaches, such as habitat suitability models, which predict the probability of CWC occurrence based on a broad set of environmental variables (i.e., terrain variables, depth, pH, temperature, salinity; Guinotte and Davies, 2014; Morato et al., 2020; Rengstorf et al., 2014). These models use observations of CWC presence (and absence) and accompanying environmental conditions to spatially extrapolate the probability of CWC occurrences to areas without observations. These statistical models are used to predict suitable habitat and likelihood of presence, and can be used to understand the consequences of climate change (as in Morato et al., 2020), but the output depends heavily on the availability of high-quality data and mostly predict presence/absence rather than cover or biomass. While machine learning classification based biomass modelling exists (De Clippele et al., 2021b, 2021a), to date, a mechanistic model that predicts CWC biomass is lacking.

Mechanistic modelling efforts so far have been able to model hydrodynamics at CWC mounds (Mohn et al., 2014; van der Kaaden et al., 2021), as well as organic matter trans-

port in the water column (Soetaert et al., 2016a). The development of a mechanistic model requires sufficient knowledge of the functioning of an ecosystem and data availability on the relevant species' physiology and food supply mechanisms. Recently, surface productivity, food supply, and local hydrodynamics have been identified as the most important factors in coral growth (Fink et al., 2013; Hebbeln et al., 2019), where the range in other environmental conditions (i.e. temperature, oxygen) act as mere limits to CWC survival (e.g. Dullo et al., 2008; Hanz et al., 2019). Modelling work has shown how coral mounds alter local hydrodynamics (Cyr et al., 2016; van der Kaaden et al., 2021), thereby enhancing water column mixing and consequently food supply toward the mounds (Soetaert et al., 2016a; van der Kaaden et al., 2020). Filtering activity of CWC reefs has also been shown to deplete POC in surrounding bottom waters (Lavaleye et al., 2009; Wagner et al., 2011), which leads to spatial self-organization of cold-water coral mounds (van der Kaaden et al., 2020). Our understanding of CWC reefs and CWC physiology has vastly improved in the past decades. Laboratory experimental work has allowed us to understand CWC's feeding behaviour in more depth and have reported data on CWC food uptake rates (Gori et al., 2014), basal- and total respiration rates (Dodds et al., 2007; Larsson et al., 2013; Maier et al., 2019), feeding behaviour under altering current speeds (Orejas et al., 2016a), and *in situ* polyp behaviour (Osterloff et al., 2019). Here we use these insights to build on an earlier developed modelling framework (Mohn et al., 2014; Soetaert et al., 2016) to predict the spatial distribution of CWC biomass, benthic respiration, and sediment organic matter content in a CWC mound region.

The CWC mounds and ridges on the south-eastern (SE) slope of Rockall Bank (north Atlantic Ocean) provide an excellent case study to develop a mechanistic model of CWC biomass and respiration. This area hosts numerous CWC mounds between 500 – and 1000-metre depth, which have been studied extensively for several decades (e.g., Kenyon et al., 2003; van Weering et al., 2003; Mienis et al., 2006; Duineveld et al., 2007). The mounds are formed by the framework building CWC species *Desmophyllum pertusum* (previously known as *Lophelia pertusa*, Addamo et al., 2016) and *Madrepora oculata*, for which a large amount of physiological data is available. Past mechanistic modelling efforts at Rockall Bank include a local high-resolution setup of the 3D Region Ocean Modelling Software model (ROMS – AGRIF; Mohn et al., 2014) and an organic matter transport model (Soetaert et al., 2016a). More recently, new 3D hydrodynamic ROMS output has been developed to investigate changes of the Atlantic Meridional Overturning Circulation (AMOC; Mohn et al., *submitted*), and to study how coral mound size affects local hydrodynamics (van der Kaaden et al., 2021). Furthermore, recent observational studies on benthic carbon cycling (**chapter 3**), video transects (De Clippele et al., 2019; Maier et al., 2021), and hydrodynamics (Schulz et al., 2020) can be used to validate model predictions. Finally, the presence of a habitat suitability model (Rengstorf et al., 2014) and a biomass mapping model (De Clippele et al., 2021b) that were developed for this area offer the opportunity

to validate our mechanistic modelling approach with statistical modelling methods.

This study provides a first mechanistic model approach to predict CWC biomass based on a coupling of models for hydrodynamics, POC transport and CWC physiology. Our main goal was to assess to what extent the spatial distribution of CWC biomass can be predicted by this set of drivers. With this, we aim to contribute to the development of a modelling approach which can be used to investigate how CWCs will be affected by changing oceanic conditions and which can be adapted for other study areas or benthic species. Below, we first present the study area, the model species, and our modelling approach. Then, we compare our predictions with available data on 1) hydrodynamics, 2) POC concentration and transport, 3) CWC distribution, and 4) respiration. Subsequently, we discuss the spatial distribution of predicted CWC biomass in the model domain, compare our model predictions with statistical modelling methods, and discuss the implications, limitations, and prospects of our model results.

Material and Methods

Study area

Our study area is situated on the south-eastern (SE) slope of Rockall Bank (north-east Atlantic; Figure 4.1A). The substrate in this area is characterized by biogenic soft sediment at the shallow part of Rockall Bank (300 – 500 m depth) and coral capped carbonate mound and ridges found on the slope between 500 – 1000 m depth. The area in between the carbonate mounds and in the deeper part of the Rockall Bank slope (>1000 m depth) comprises mainly of biogenic soft sediments (Kenyon et al., 2003; Mienis et al., 2006). The current direction throughout the water column is predominantly to the southwest, driven by the clockwise gyre circling the Rockall Bank (Hansen and Østerhus, 2000; Holliday et al., 2000; Mienis et al., 2007; Schulz et al., 2020). This area is subject to internal waves with amplitude of several 100s of metres and high bottom current speeds (i.e., >50 cm s^{-1}; Mienis et al., 2007; Mohn et al., 2014). Interaction of tidal currents with mound topography cause breaking of internal waves (Cyr et al., 2016) with subsequent downward transport of organic matter (**chapter 2**, Duineveld et al., 2007; Soetaert et al., 2016a;). In this area, coral ridges are found in the north-eastern part, while numerous coral mounds, known as the Logachev mound province, are found in the southwest (Figure 4.1B). For readability, we will refer to the coral mounds and ridges in this area as 'CWC mounds'. The largest CWC mound in the model domain is called "Haas mound" which is around 500 metres high, one to two kilometres wide, five kilometres long, and shaped parallel to the Rockall Bank slope.

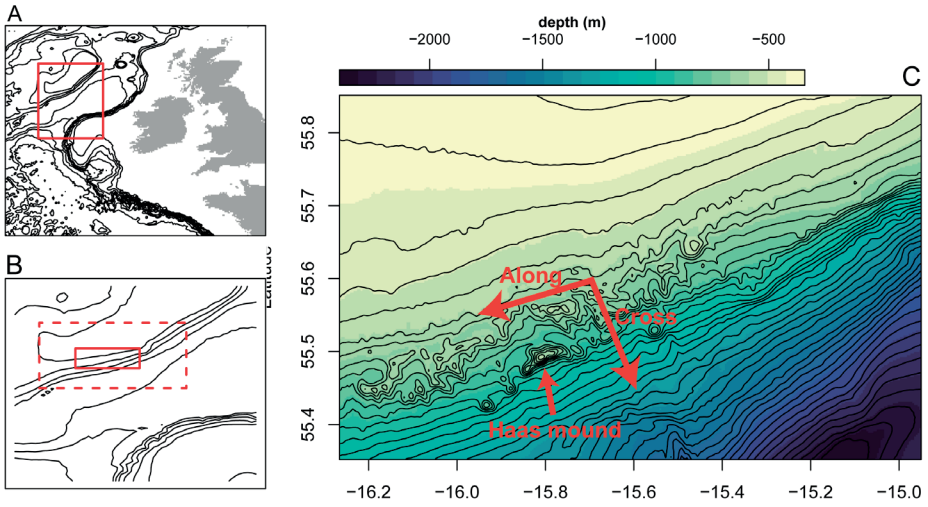

Figure 4.1 Study area and model domain. (A) location study area in the Atlantic Ocean, the red line marks the plot boundaries of panel B, (B) location of parent grid (dashed lines) and the embedded child grid (solid line), (C) model domain with dimensions of 83 x 55 km, and 450 – 2300 m depth range. The arrows indicate the location of Haas mound and the direction of along- and cross slope transport of water and POC (Schulz et al., 2020)

Model species: *Desmophyllum pertusum*

The carbonate ridges and mounds in the study area are formed by the framework building CWCs *Desmophyllum pertusum* and *Madrepora oculata* (van Weering et al., 2003; Duineveld et al., 2007; Maier et al., 2021). These corals are framework building, and form bush-like colonies that can grow several metres high consisting of thousands of coral polyps (Roberts et al., 2009b). In this study, *D. pertusum* is used as model species for multiple reasons. First, *D. pertusum* is considered a keystone species, providing numerous associated macrofauna species suitable habitat (Jensen and Frederiksen, 1992; Freiwald et al., 2002; Husebø et al., 2002; Costello et al., 2005). Second, framework building corals in our study area are important contributors to reef metabolism (**chapter 3**). The coral species feeds on a mixture of particulate organic matter and zooplankton, but CWCs in the Rockall Bank area likely primarily feed on particulate organic matter (Duineveld et al., 2007), as zooplankton density there is relatively low (**chapter 2**). Therefore, suspended particulate organic carbon (POC) is likely a good food source proxy for *D. pertusum* in this region.

Modelling approach

This study was set-up by coupling three models (details provided below): first, hydrodynamic output was extracted from a local setup of the ROMS-AGRIF model, which was previously developed and validated for the Rockall Bank study region (Mohn et al., 2014; Mohn et al., *in review*). Secondly, these hydrodynamics forced a POC reactive-transport model following Soetaert et al. (2016a). Finally, a new benthic CWC and sediment model was developed, fuelled by POC dynamics, via suspension feeding and sedimentation. This model was used to predict CWC biomass, sediment organic matter content, and CWC and sediment respiration.

Hydrodynamic model

See Mohn et al. (2014) for a detailed description of the hydrodynamical modelling set-up. In short, the ROMS-AGRIF model domain encompasses an area of 86 x 58 km, which was divided into 336 grid cells in longitudinal direction and 228 grid cells in meridional direction, resulting in a horizontal resolution of 250 metres (depth range 320-2500 metres; Figure 4.1B). This child model grid was nested inside a parent grid with a 750 m resolution that encompassed an area of 190 x 188 km (Figure S4.1). Both models were run on a staggered Arakawa-C grid with a terrain-following stretched sigma grid of 32 vertical levels (Figure S4.1) which provides a higher vertical resolution at the surface and seafloor (Shchepetkin and McWilliams, 2005). Tidal forcing was prescribed using the TPXO7 global tidal inverse solution (Egbert and Erofeeva, 2002). Here we used hydrodynamic output (horizontal currents) data for the period March 1979, which was simulated and validated in a separate study investigating the influence of contrasting AMOC states on benthic hydrodynamics at different CWC sites (Mohn et al., *in review*). This specific time period was chosen for two purposes: first, fresh POC arrives at CWC reefs in the study area in spring (Duineveld et al., 2007). Second, in the year 1979 the AMOC showed a weak signal (Böning et al., 2016). Given that the AMOC state is currently at its weakest of the last millennium (Caesar et al., 2021), and may weaken further under global carbon emission projections (Bakker et al., 2016; Caesar et al., 2018), using modelled properties of a weak AMOC year provides a good representation of future large scale circulation patterns and hydrodynamic conditions (Mohn et al., *submitted*). The hydrodynamic output, stored at 3-hour intervals, was then used to model POC dynamics in the water column.

Organic matter transport model

A detailed description of the organic matter transport model can be found in Soetaert et al. (2016a). In this model, we use particulate organic carbon (POC) as proxy for organic matter. In short, POC is advected throughout the model domain based on the 3-hour interval output from the ROMS-AGRIF model. A zero-gradient boundary condition is assumed on the model domain boundaries, a constant input (i.e., export from the photic zone) of POC is assumed at the upper boundary and passive settling of POC on the seafloor (i.e., the lower boundary of the model domain). Furthermore, POC is subject to constant first-order decay. To decrease computation time, vertical flow was calculated from the flux divergence of the horizontal flow and assuming a constant free-surface or zero elevation (η). Comparing the vertical flow from this method with ROMS output vertical flow, the spatial pattern of vertical velocities compares favourably (Supplementary Figure S4.2). The reactive-transport model is implemented as:

$$\frac{dH_z \bullet POC}{dt} = -\frac{d(H_z \bullet u \bullet POC)}{dx} - \frac{d(H_z \bullet v \bullet POC)}{dy} - \frac{d(H_z \bullet w \bullet POC)}{dz} - \frac{d(H_z \bullet w_s \bullet POC)}{dz} - k \bullet H_z \bullet POC \quad (1)$$

Where H_z is the grid cell thickness in metres, POC is the concentration POC in each grid cell in mmol C m^{-3}, w_s is the passive sinking velocity of POC in the water column in m d^{-1}, k is the first-order decay rate of POC in d^{-1}. Henson et al. (2015) provided a model analysis of the carbon export and export efficiency in the ocean. POC export from the photic zone is based on the annual primary production and export efficiency in the study area and we used an annual primary production and export efficiency for the Rockall Bank area of 200 g C m^{-2} and 25 % respectively (Henson et al., 2015), resulting in an export of 12 mmol C m^{-2} d^{-1}. The degradation rate of sinking POC is defined as $k = 0.016 * 1.066^T$ (Yool et al., 2011; Henson et al., 2015), in which T is temperature in °C. Temperature ranges from 4 °C at 2000-metre depth to 15 °C in the summer periods at the surface. Therefore, we used a water column temperature of 10°C which corresponds to a k of 0.03 d^{-1}. Sinking of POC was set to 10 m d^{-1} which is considered representable for slow sinking suspended particles (Riley et al., 2012).

The POC transport model was numerically solved with POC concentration in the centre of each box and exchange fluxes defined on the grid cell interfaces. The flow velocity data from the hydrodynamic model were linearly interpolated in time to obtain flow velocities at every model integration step. The model was numerically integrated using a variable-order Adams-Moulton predictor-corrector scheme, as implemented in the R-package deSolve (Soetaert et al., 2010; R Core Team, 2019). Advection was implemented using simple first-order upwind differencing; due to the numerical dispersion that this method generates, no horizontal or vertical diffusion was imposed.

Cold-water coral biomass and sediment model

We imposed a CWC biomass- and sediment organic matter model at the bottom boundary layer of the model domain. The CWC biomass model is based on organic matter uptake and CWC physiology. We express CWC biomass in C-units based on the metabolically active organic carbon and exclude carbon stored in inorganic calcium carbonate skeletons. Corals use their polyps and tentacles to feed on POC in the bottom layer of the model. To take the physical constraints of a coral into account, we use several efficiency parameters, and a surface-to-biomass conversion factor as follows:

$$\frac{\mathrm{dCWC}_b}{\mathrm{dt}} = \mathrm{CWC_b} \bullet \left(1 - \frac{\mathrm{CWC_b}}{\mathrm{CC_{CWC}}}\right) \bullet \mathrm{POC_{bbl}} \bullet \mathrm{v_{bbl}} \bullet \mathrm{A_{CWC}} \bullet AE_{cwc} \bullet NGE_{CWC} \bullet CE_{CWC} \bullet \mathrm{FP_{CWC}}(\mathrm{v_{bbl}}, p, k_v) - \mathrm{m_{CWC}} \bullet \mathrm{CWC_b} \quad (2)$$

Where dCWC_b/dt is the change in CWC biomass over time, CWC_b is the CWC biomass on the seafloor (mmol C m^{-2}) and CC_{CWC} is the approximated carrying capacity of CWCs (mmol C m^{-2}). POC_{bbl} is the organic matter concentration in the bottom layer grid cell (mmol C m^{-3}), v_{bbl} is the bottom layer grid cell current speed (m d^{-1}), A_{CWC} is the surface-to-biomass ratio of a CWC or the biomass-specific feeding area of CWC (m^2 (mmol C coral)$^{-1}$), AE_{CWC} is a dimensionless assimilation efficiency parameter, NGE_{CWC} is the net-growth-efficiency parameter, CE_{CWC} is a dimensionless parameter describing organic matter capturing efficiency by CWC polyps, FP_{CWC} is a function estimated the fraction of open CWC polyps based on bottom current speed and scaling parameters p and k_v. m_{CWC} is the basal CWC respiration rate in d^{-1}. The fraction of extended polyps (FP_{CWC}) is modelled as:

$$FP_{CWC} = FP_{max} \bullet \left(1 - \frac{{v_{bbl}}^p}{{v_{bbl}}^p + {k_v}^p}\right) \quad (3)$$

Where FP_{max} is the maximum fraction of extended polyps, as measured in situ by Osterloff et al. (2019), p is a dimension fitting parameter, k_v is the current speed at which half of the CWC polyps are open (m d^{-1}).

The sediment organic matter model on the bottom of the model domain receives POC from the benthic boundary layer by passive settling, and from deposition of the non-assimilated POC uptake of cold-water corals. The change in organic matter concentration in the sediment over time (in mmol C m^{-2} d^{-1}) is calculated as:

$$\frac{dPOC_{sed}}{dt} = w_s \bullet POC_{bbl} + (1 - AE_{cwc}) \bullet CWC_{in} - k_{sed} \bullet POC_{sed} \quad (3)$$

Where $dPOC_{sed}$/dt is the change in sediment organic matter concentration (POC_{sed}) in the sediment top layer, w_s is the passive sinking rate of POC in the bottom layer (m d^{-1}), POC_{bbl} is the organic matter concentration in the bottom layer grid cell (mmol C m^{-3}), AE_{CWC}

is a dimensionless assimilation efficiency parameter of cold-water corals, CWC_{in} is the organic matter uptake by CWCs (in mmol C m^{-2} d^{-1}, i.e., first term in Equation 2) and *ksed* is the sedimentary organic matter respiration (d^{-1}).

As CWCs extract POC from the bottom layer of the model, the POC reactive-transport model in the bottom layer of the model domain is governed as follows:

$$\frac{dPOC_{bbl}}{dt} = \frac{dH_{bbl} \bullet POC_{bbl}}{dt} - \frac{CWC_{in}}{dH_{bbl}} \quad (4)$$

Where POC_{bbl}/dt is the change in POC concentration in the bottom boundary layer (mmol C^{-3} d^{-1}), (dH_{bbl} • POC_{bbl})/dt is the change in bottom layer POC concentration due to advection and passive settling (see Equation 1), and CWC_{in} / dH_{bbl} is the uptake of POC by the CWCs (in mmol C m^{-2} d^{-1}) divided by the height of the bottom layer (m).

The parameters and values are chosen as follows (see Table 4.1): the surface-to-biomass ratio (A_{CWC}) is defined as the biomass-specific feeding area, or the polyp area, per mmol C of coral and is expressed in m^2 (mmol organic C)$^{-1}$. *D. pertusum* has 2.40 ± 0.99 polyps (g dry weight)$^{-1}$ (mean ± SD; n = 15; Gori et al., 2014), and consists for 1.36% ± 0.35 of organic carbon per dry weight (**chapter 3**, Larsson et al., 2013; Maier et al., 2019). Therefore, *D. pertusum* contains 2.12 ± 0.87 polyps (mmol C)$^{-1}$. The polyps of *D. pertusum* have a surface area of 35.3 ± 2.0 mm^2 $polyp^{-1}$ (Purser et al., 2010) and multiplying the polyp surface area with the number of polyps per coral biomass gives 7.48 * 10^{-5} m^2 (mmol C)$^{-1}$. This surface-to-biomass ratio represents the maximum feeding surface, but not all polyps of a colony are always fully extended, e.g. flow speed influences polyp behaviour of corals (Osterloff et al., 2019). At high flow speeds, corals can retract their polyps to reduce the force drag on their tissue. We implemented this behaviour by fitting experimental data of polyp extension versus current velocity to estimate the fraction of extended polyps at a given bottom current speed (Equation 3; Figure S4.3; Orejas et al., 2016)

Additionally, not all extended polyps are successful in capturing a food particle. A study of a hydroid coral showed that between 5 and 60% of polyps were successful in capturing a food particle, depending on the flow regime and coral morphology. Here, we introduce this parameter as CE_{CWC}, and as the mean capturing efficiency for an elongated coral colony ranged from 0.10 to 0.30, we set its value to an intermediate value of 0.15 (Hunter, 1989).

CWCs can also experience intra-colonial polyp competition, i.e. inner polyps of a colony may filter water which was already partially filtered by polyps on the outside of the colony (Kim and Lasker, 1998; Galli et al., 2016). This effect is approximated by introducing a carrying capacity (CC_{CWC}) or maximum population density. The carrying capacity is calculated in the benthic model as: $\left(1 - \frac{CWC_b}{CC_{CWC}}\right)$ so coral growth rate approaches zero when the population density reaches the carrying capacity. The maximum CWC density measured in a box core

in the study area was 1,800 mmol C m^{-2} (**chapter 3**), in which living corals covered ~20% of the box core (De Clippele et al., 2021b). A video transect found maximum coverage of 60% of the seafloor on a large coral mound in the study area (Maier et al., 2021). Based on these data, we set the carrying capacity of CWCs to 6,000 mmol C m^{-2}. Food particles captured by corals are divided into a digestible and a non-digestible fraction with the assimilation efficiency (AE_{CWC}). Direct measurements of the assimilation efficiency for CWCs are not available as experimental measurements are often difficult because the non-assimilated part of the food is often mixed with particulate mucus (Wild et al., 2008). However, the release of particulate organic matter (i.e. non-assimilated matter and mucus) is found to be small compared to the food uptake (Maier et al., 2019) and the AE_{CWC} is therefore set to 0.8, consistent with values reported for tropical corals (Anthony, 1999). The assimilated food is used for growth and for the maintenance metabolism. The fraction of carbon incorporated into the tissue compared to the assimilated carbon is known as the net growth efficiency (*NGE*). Although data on NGE for CWCs is scarce, two studies estimate the *NGE* for *D. pertusum* to be between 0.05 and 0.3 (van Oevelen et al., 2016; Maier et al., 2019). Therefore, the *NGECWC* is set to 0.1, which is low compared to better-studied taxa like zooplankton (>0.5) and shallow-water anemones (0.3 – 0.6; Anderson et al., 2005; Zamer and Shick, 1987). However, a low growth efficiency and slow growth are typical for long-lived species as *D. pertusum* (Roberts et al., 2009b).

Table 4.1 model parameter values, conversion factors, and respective sources

Parameter	Description	Value	Unit	Source
FO	Water column POC upper boundary export production	12	mmol C m^{-2} d^{-1}	(Henson et al., 2015)
K_{poc}	Water column POC decay rate	0.030	d^{-1}	(Yool et al., 2011; Henson et al., 2015)
w_s	Water column POC passive sinking speed	10	m d^{-1}	(Riley et al., 2012)
A_{CWC}	CWC surface-to-biomass ratio	7.48 * 10^{-5}	m^2 mmol C^{-1}	(**chapter 3**, Purser et al., 2010; Larsson et al., 2013; Gori et al., 2014; Maier et al., 2019)
CE_{CWC}	CWC capture efficiency, fraction of polyps that capture a food particle	0.15	-	(Hunter, 1989)

AE_{CWC}	CWC assimilation efficiency, fraction digestible POC	0.80	-	(Anthony, 1999)
NGE_{CWC}	CWC net-growth efficiency, fraction digested POC used for growth	0.10	-	(van Oevelen et al., 2016; Maier et al., 2019)
FP_{max}	CWC maximum fraction of extended polyps	0.90	-	(Orejas et al., 2016; Osterloff et al., 2019)
p	CWC scaling parameter, fraction extended polyps related to bottom current speed	1.5	-	(Orejas et al., 2016); this study
k_v	CWC flow speed at which half of polyps are rectracted	0.40/86400	m d^{-1}	(Orejas et al., 2016)
CC_{CWC}	CWC carrying capacity, maximum biomass density	6000	mmol C m^{-2}	(**chapter 3**; Maier et al., 2021)
m_{cwc}	CWC basal respiration rate	0.0035	d^{-1}	(Larsson et al., 2013)
k_{sed}	Sediment respiration rate	4.1 * 10^{-2}	d^{-1}	(Westrich and Berner, 1984)

Procedure to solve the coupled model

Model spin-up of the fully coupled model proved to be computer intensive, as CWC growth and hydrodynamics operate on different timescales. While CWC growth is relatively slow (~years), the simulation runs could do with a large integration time step. At the same time, hydrodynamics change on short (~hourly) time scales, requiring short integration time steps.

In the end, the model was solved in these three-step procedure (see Figure 4.2 for a workflow diagram). Interestingly, this approach provided unexpected predictions of the control of CWCs on the suspended matter concentration in the benthic boundary layer, which will be discussed in section 3.2. The three-step procedure comprised of (1) organic matter transport initialization, (2) benthic biomass initialization, and (3) coupled benthic-biogeochemical model runs. In step 1, the POC concentration was imposed by an exponential decrease with water depth (Figure 4.2A; Martin et al., 1987). Then,

advective transport of organic matter is spin-up by running the organic matter transport model for three consecutive months. The output of step 1 is used as input to initialize the CWC biomass (Figure 4.2B) by taking the average bottom layer POC and average bottom current speed to calculate the initial CWC biomass (see Equation 2) and sediment POC concentration (see Equation 3) for each grid cell (Figure 4.2C & D). The output of steps 1 and 2 (Figure 4.2B & D) are then finally used as initial conditions for the fully coupled model (Figure 4.2E). During this run, it appears that using the average bottom layer POC concentration and bottom current speed overestimates the amount of CWC biomass in the model (Figure 4.2D), as the coupling of the benthic model with the organic matter model caused a rapid decline of POC in the bottom layer (Figure 4.2F), and thereby declining CWC biomass throughout the model domain. As CWCs are slow growing organisms, it takes considerable time to reach a (dynamic) biomass equilibrium in the coupled model. To speed up computation, we (1) divided initial CWC biomass from step 2 by three and used that as initial benthic biomass, and (2) ran the coupled model for a total of five consecutive months with a coral growth/decline enhancement factor of 12. A method that is also used in sediment transport modelling approaches (Ranasinghe et al., 2011). Finally, two months were run without the growth- enhancement to arrive at the final output, in which $dCWC_b$ / dt was close to steady-state.

Data sources for model-data comparison

Recent observational studies in the study area provide a good opportunity for model validation (Figure 4.3A & B). For the water-column, two moorings were placed in the study area for a full year which measured current profiles, turbidity, and fluorescence measurements (Schulz et al., 2020). Benthic organic matter remineralization rates were quantified on two mounds in the Logachev mound province, and an adjacent sediment area (**chapter 3**) using on-board incubation experiments and the eddy covariance technique. In addition, the cover of living CWC, dead framework, and sediment was quantified from video frames along the slopes and top of Haas mound (Maier et al., 2021) and other CWC mounds in the area (De Clippele et al., 2019). Finally, a statistical habitat suitability model has been developed for the same model domain (Rengstorf et al., 2014), as well as a machine learning classification based biomass maps (De Clippele et al., 2021b). The results of these studies are used for model validation and to discuss our findings.

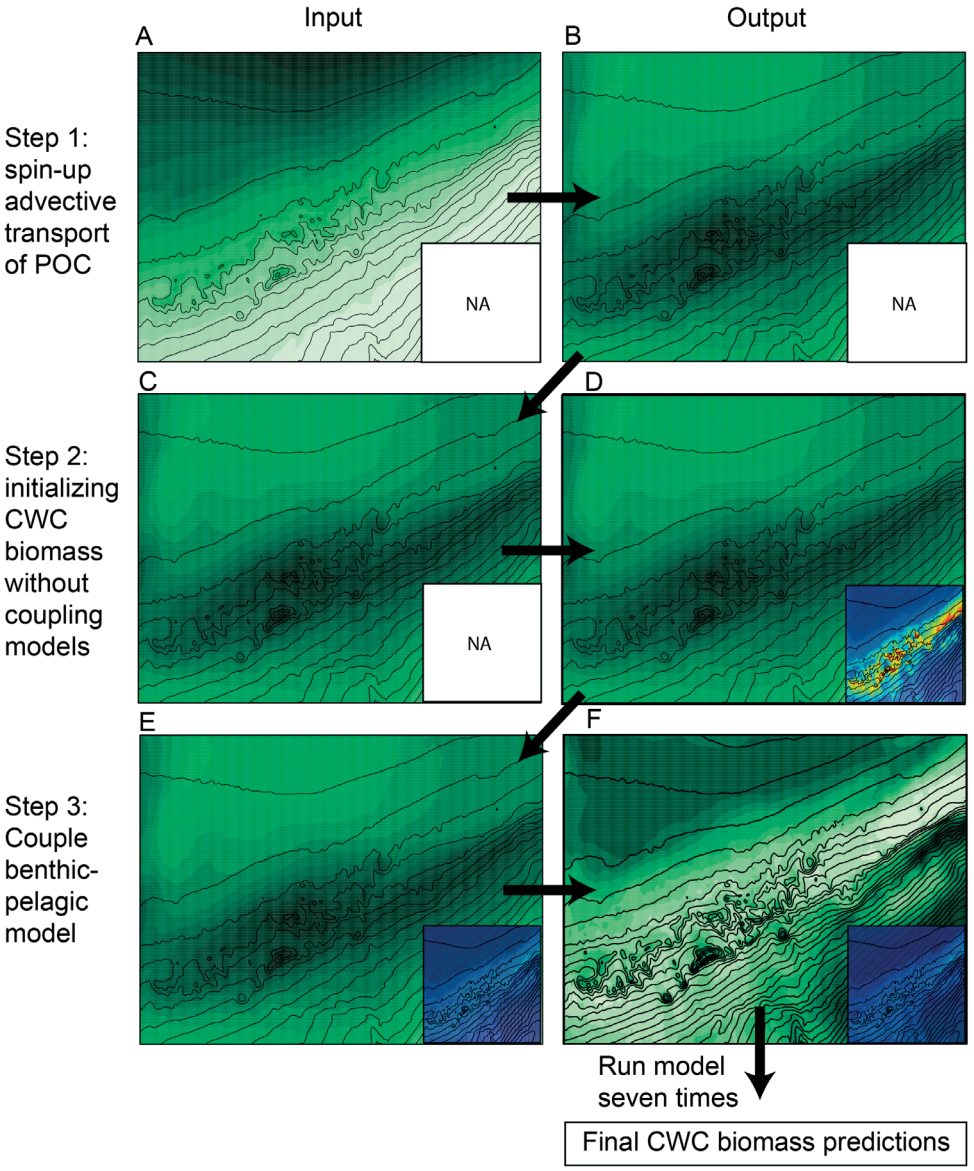

Figure 4.2 Workflow diagram describing the steps used to spin up the coupled model with the large panels showing the average POC concentration in the bottom layer across the model domain and the small inset panel shows the spatial cold-water coral biomass. 'NA' means that predictions of the CWC biomass are not yet available at that stage. A) initial bottom layer POC concentration based on the Martin's curve Martin et al. (1987), B) bottom layer POC concentration after spin-up of POC transport by advection, which is used as input (C) for initializing benthic biomass. Initialized cold-water coral biomass used as input (E) to couple the POC transport model with the benthic model. F) Intermediate snapshot (after one week of running the model) of POC in bottom layer and CWC predictions. This shows POC depletion in the bottom water column after running the coupled model with one week of data. Running the coupled model for seven times results in our final CWC biomass predictions

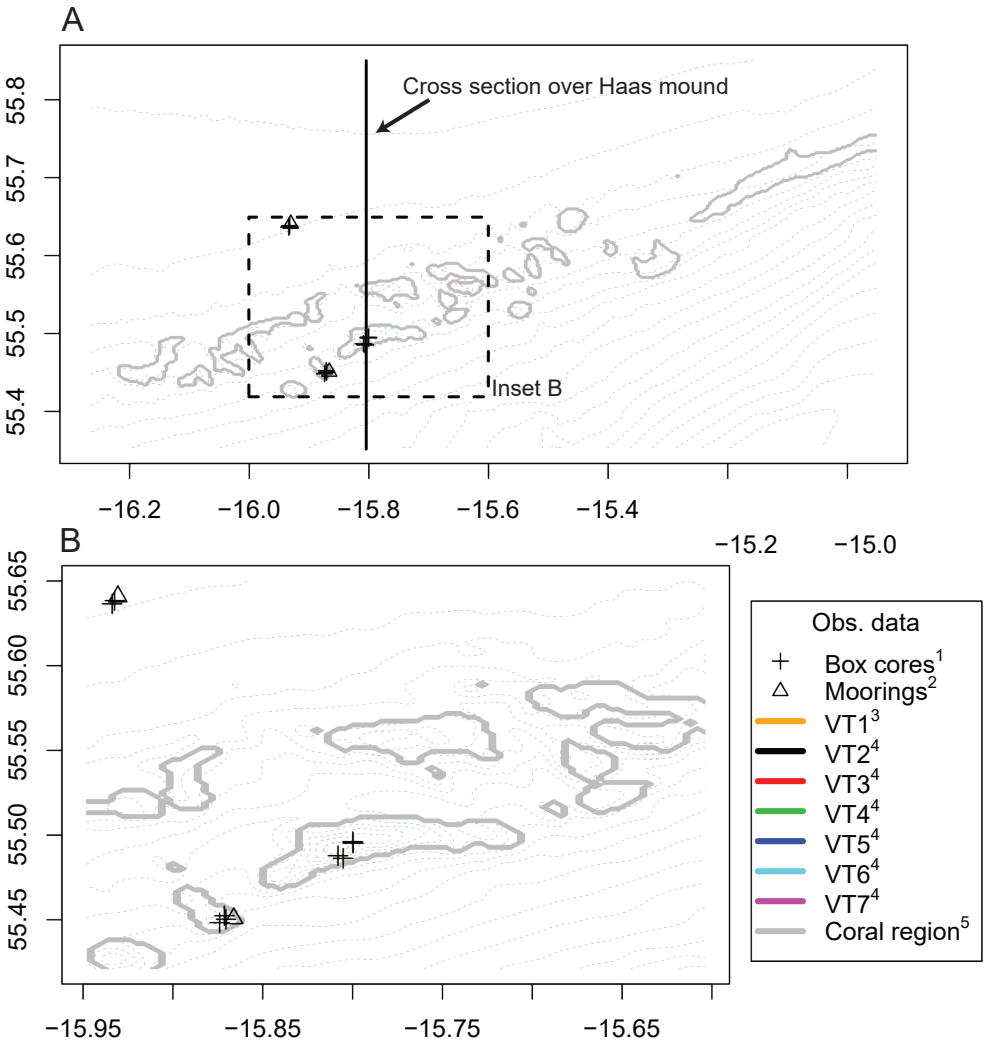

Figure 4.3 Observational data locations used to validate the model results. A) Map of whole model domain with dotted lines illustrating the bathymetry and the black line indicates the cross-section over Haas mound used for Video S2. B) expanded detail on where most data was collected. Box cores data is used to validate benthic respiration and biomass, mooring data is used to validate hydrodynamics and POC transport, Video transect (VT) data are used to validate CWC biomass predictions, "Coral presence" lines are the contours of area within which suitable habitat is predicted by Rengstorf et al. (2014). **chapter 3**, [2] Schulz et al. (2020), [3] Maier et al. (2021), [4] De Clippele et al. (2019), [5] Rengstorf et al. (2014)

Results & discussion

Comparing model performance with observations

Hydrodynamic forcing of our 3D model shows that the general or residual current in the model is directed south-westerly along the slope of Rockall Bank (Figure S4.4). This is a result of anti-cyclonic circulation circumventing Rockall Bank (e.g., Ellett et al., 1986; Holliday et al., 2000; Johnson et al., 2010). The area is subject to a dominant diurnal tidal system where barotropic diurnal tidal waves are trapped, causing cross-slope transport with a diurnal periodicity (Huthnance, 1973; Pingree and Griffiths, 1984). These tidal currents cause high vertical velocities on the flanks and summits of the coral mounds following a diurnal and spring-neap tidal cycle (Figure S4.2B; Mohn et al., 2014). The hydrodynamic forcing is validated in Mohn et al. (*in review*) with the observational current velocity data from various moorings in the region (see Schulz et al, 2020) and White et al., 2007). The general direction of POC transport in our model domain was in southwest direction (Video S1) as also measured by Schulz et al. (2020). The vertical currents above the CWC mounds caused episodic transport of POC towards the seafloor (Video S2), a process which was observed in earlier modelling- (Soetaert et al., 2016a) and observational studies (**chapter 2**; Duineveld et al., 2007).

The CWC biomass density was predicted to be highest on the summits and south- and southwestern upper flanks of the CWC mounds (Figure 4.4). These results match video transect CWC data of benthic cover data generally well (De Clippele et al., 2019; Maier et al., 2021), with highest predicted CWC biomass in areas with high cover of live CWCs/dead coral framework and low predicted biomass in areas with high sediment cover (Figure 4.5; Figure 4.6). From the seven video transects, only transect VT7 showed a large discrepancy between modelled and observed CWC biomass/cover (Figure 4.6F). This discrepancy was likely caused by large differences between model and video transect depth (Supplementary Figure S4.6). Although only a qualitative comparison between video data and model predictions can be made due to the different units that are used for biomass quantification, interesting observations surface from this comparison. First, although our predicted CWC biomass shows good agreement with cover of living CWCs, the CWC biomass predictions match even better with the seafloor cover of dead coral framework.

Dead coral framework is skeleton without a cover of coral tissue, and is an important part of a CWC reef (Freiwald and Wilson, 1998), responsible for a substantial part of benthic respiration (**chapter 3**) and hosts a complex nitrogen cycle (Maier et al., 2021). CWCs are thought to grow in patches (Wilson, 1979), where the living polyps extend their tentacles in the water column to feed on suspended particles, and the polyps closer to the seafloor eventually die-off and become buried by baffling of sediment (Mienis et

al., 2009c; Roberts et al., 2009b). The presence of dead coral framework on the mound therefore suggests that this site used to have favourable conditions for coral growth. Our model CWC predictions are solely based on hydrodynamics and POC concentration and could therefore be loosely interpreted as 'locations favouring CWC growth' over longer periods of time. Currently, to our knowledge, generally little is known on the temporal and spatial dynamics between living CWCs and dead coral framework. For example, it is yet unknown how long a CWC colony lives before it dies-off and becomes dead coral framework, or if dead coral framework prevents coral growth in the surrounding area by filtering POC from the water layer (Maier et al., 2021). A possible explanation of the match between our CWC predictions and dead coral framework cover could therefore be that living CWCs could grow at locations indicated by our model but died off due to conditions that are not included in our model (i.e., infection, predation, temperature, ocean acidification). Died-off coral branches are not included in our model. However, it would be an interesting addition to include a mortality rule (as in Hennige et al. 2021), whereby dead coral cover or density could be predicted over longer timescales, with living CWCs growing on top of the dead coral framework. Living CWC to dead framework ratio on a CWC reef is measured between 0.10 and 0.30 (Vad et al., 2017). Extrapolating this observation would suggest a high amount of framework is projected in areas where the model now predicts high CWC biomass density. Indeed, large thickets of dead coral framework are seen on the southern slope of Haas mound (**chapter 3**; Maier et al., 2021).

Although predicted CWC biomass and live coral/dead coral framework cover compare well, the model predicts that CWC extend more to the south than is observed (Figure 4.5B). This mismatch could have several causes: first, the resolution (250m) of the model does not allow for modelling hydrodynamic processes on the scale of metres, which could be important for coral growth on the top of the Haas mound flank. Second, a patchy distribution of live CWC colonies could cause the video transect to overlook live CWC on the southern flank. Nevertheless, our modelling results show CWCs can successfully be predicted based solely on local hydrodynamics and organic matter transport, even without considering environmental conditions as temperature, salinity, or oxygen concentration. This further strengthens the hypothesis that a steady food supply or influx is a key indicator for CWC growth and occurrence (Hebbeln et al., 2019; Portilho-Ramos et al., 2022).

In the model, benthic respiration ranges between 3.7 and 40.9 mmol C m^{-2} d^{-1} and closely follows the CWC biomass spatial distribution (Figure 4.7A), indicating that CWCs are largely responsible for the benthic respiration (up to 70%) in areas with high CWC biomass (Figure 4.7B). Sediment carbon content and sediment-based respiration is enhanced in areas with high CWC biomass (Figure S4.6A & B), due to organic matter deposition on the underlying sediment and a higher POC concentration in the bottom layer. Modelled benthic respiration in the model domain compares generally well with observational data (**chapter 3**; Figure 4.7C), and the modelled benthic respiration on coral mounds (10 – 40

mmol mmol C m^{-2} d^{-1}) is comparable with observational data from CWC reefs in the north-east Atlantic (White et al., 2012; Khripounoff et al., 2014; Cathalot et al., 2015; Rovelli et al., 2015). Although some of the physiological parameters for CWC, such as 'assimilation efficiency' and 'net growth efficiency', are presently only rudimentary constrained, our modelled benthic respiration rates are in a similar order of magnitude as measured values.

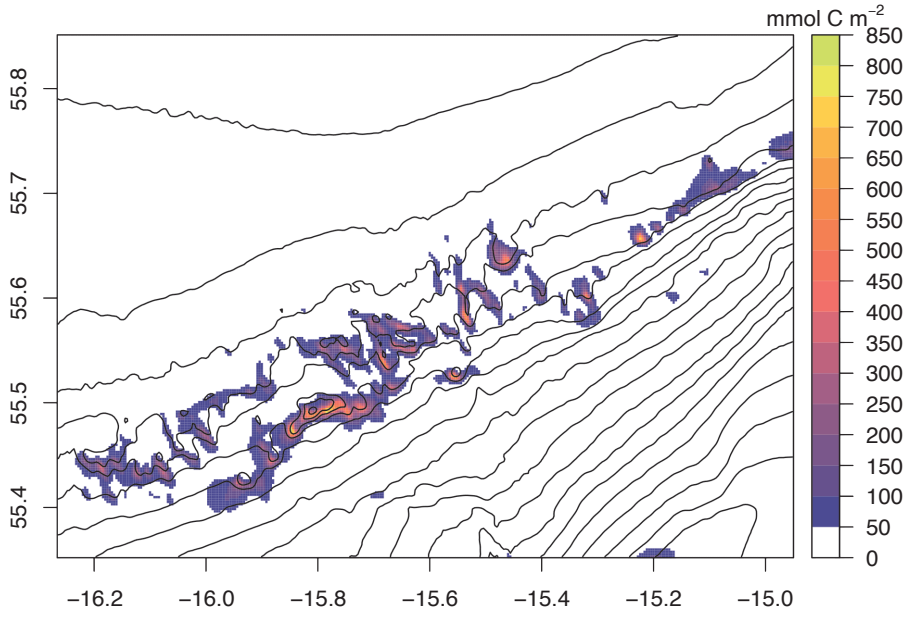

Figure 4.4 predicted CWC biomass in mmol C m^{-2}. Black lines indicate the bathymetry of the model domain (see Figure 4.1 for depth indices)

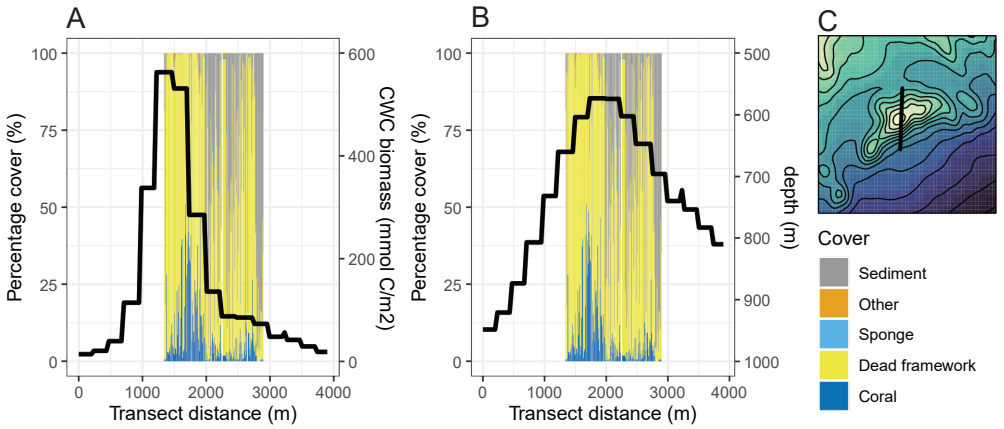

Figure 4.5 Comparison between model prediction and video transect data (VT1, Figure 4.3) from Maier et al. (2021). Cover is in percentages, category "Other" includes other macrofauna species. A) predicted CWC biomass indicated by the black line and the scale on the right Y-axis, B) depth of model domain along the video transect indicated by the black line and scale on the right Y-axis, C) Location of video transect over Haas moun

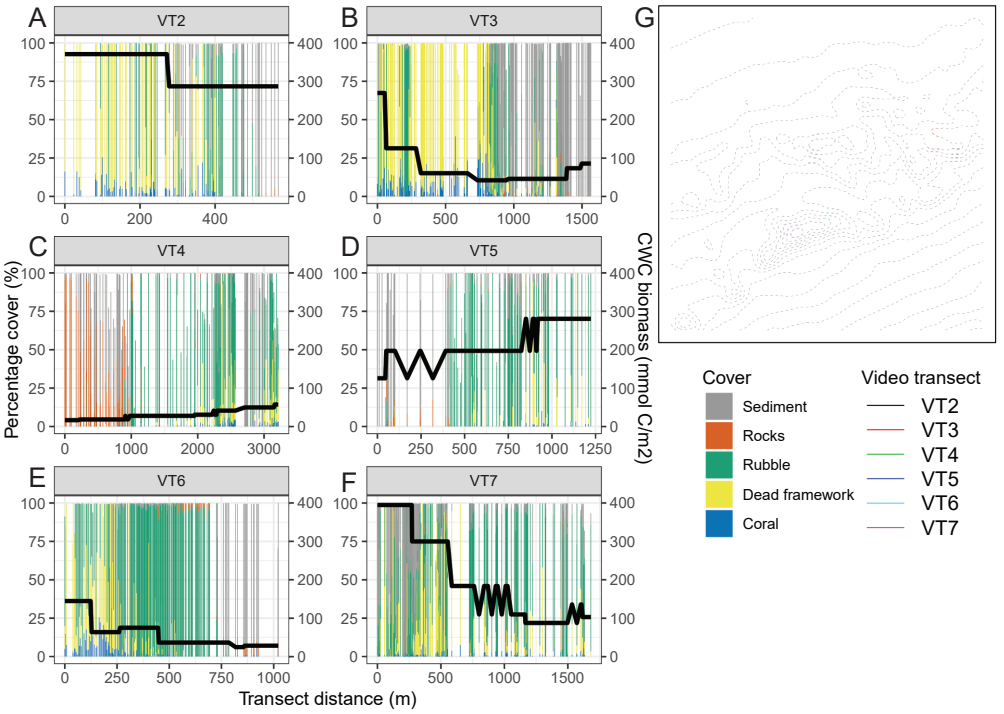

Figure 4.6 Comparison between model prediction and video transect data (VT2 – VT7, Figure 4.3) from De Clippele et al. (2019).Model predictions are indicated by black line and biomass scale is on the right Y-axis. A) VT2, B) VT3, C) VT4, D) VT5, E) VT6, F) VT7, G) locations of the video transects in the model domain

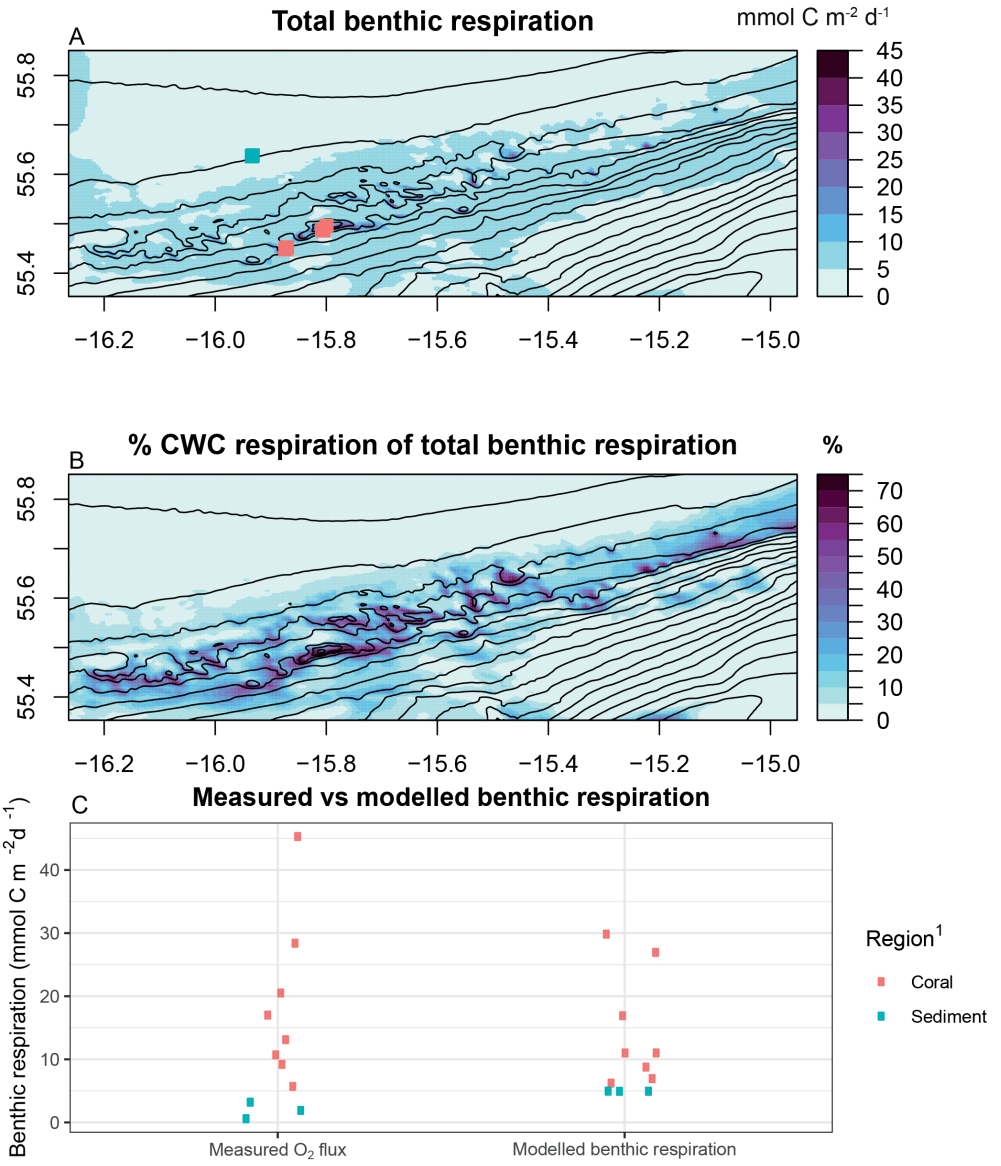

Figure 4.7 Modelled benthic respiration compared to observational data from **chapter 3**. A) total benthic respiration and measurement locations indicated in coloured points, B) percentage of total benthic respiration caused by cold-water coral respiration, C) measured versus modelled benthic respiration. [1] regions are based on **chapter 3** and Rengstorf et al. (2014)

Spatial distribution of cold-water corals related to hydrodynamics and organic matter transport

The spatial distribution of CWC predictions in our model is shaped by three processes on which we elaborate in the following section: (i) the presence of relatively high bottom current speeds, (ii) bottom POC depletion by CWC feeding, (iii) vertical downward POC transport to the seafloor by tidal advection. First (i), high enough bottom current speeds allow CWCs to filter food particles out of the bottom water (White et al., 2007; Purser et al., 2010; Hebbeln et al., 2016). Spinning up the model in step 2, predicted CWC biomass based solely on bottom current speed and bottom water POC concentrations without coupling the organic matter transport model with the benthic model (Figure 4.2D Inset; Equation 2). This overestimated the amount of CWC biomass in our model along the Rockall Bank slope between 500 – 1000 m depth (Figure 4.2D inset). Second (ii), coupling the two models (Figure 4.2E & F) caused strong POC depletion in the layers above the high CWC biomass areas, except above the CWC mounds (Figure 4.2F). Third (iii), above these mounds, tidally induced vertical currents transported POC towards the seafloor (Video S2; Soetaert et al., 2016a), replenishing bottom water POC levels during each tidal cycle. Therefore, high CWC biomass is predicted on the upper flanks of the CWC mounds where bottom water POC is regularly replenished, and relatively high bottom current speeds are found (Supplementary Figure S4.4). These findings suggest vertical transport of POC is vital for CWC growth and support the idea that tidal dynamics are crucial for sufficient food supply to the CWC reefs on these mounds (**chapter 2**; van Haren et al., 2014; Soetaert et al., 2016a; Juva et al., 2020). However, interestingly, relatively increased POC concentration persisted above the whole CWC mounds while high CWC biomass was predicted on the south- and southwestern flanks. In the following section, we elaborate on this discrepancy.

The south-westerly residual along-slope current and tidally induced cross-slope currents cause POC to be advected up- and down the slope between 500 – 1000 m depth in the model domain, while the net POC transport is still in a southwest direction (Video S1). The combined effect of these currents is that POC concentration is relatively frequently replenished above the CWC mounds summits and subsequently transported along their south- and southwestern flanks (Figure 4.8A). Under these favourable conditions, high CWC biomass is predicted on the upper flanks of the CWC mounds (Figure 4.4, Figure 4.8). In addition, bottom currents that encounter a mound or ridge are directed southward due to Coriolis force (Figure 4.8A; Supplementary Figure S4.7) further promotes CWC growth on the southern flanks. Furthermore, north of Haas mound we found an area with low bottom current speed where suspended/organic matter is trapped in an eddy circulation (Supplementary Figure S4.7). This enhance sediment deposition and compares well with the sediment infill found in this area (Mienis et al., 2006).

Besides that CWCs were mostly predicted on the south- and southwestern flanks of the CWC mounds, highest biomass was found specifically close to the summits and on the upper side of the flanks. This pattern was caused by depletion of POC in the bottom layer by CWCs which decreased the quantity of available food for CWCs located downstream (Figure 4.7B). Bottom water depletion by filtering activity of CWCs has also been observed in the field (Lavaleye et al., 2009; Wagner et al., 2011), and can be interpreted as a negative scale dependent feedback on CWC growth (van der Kaaden et al., 2020), a mechanism derived from the theory of spatial self-organization (van de Koppel et al., 2005; Rietkerk and van de Koppel, 2008). This mechanism of bottom water POC depletion proved to be key in successfully predicting CWC biomass. Hence, we argue that the spatial distribution of CWCs in our study area is shaped by a combination of current dynamics, food supply, and scale-dependant feedbacks.

Our mechanistic modelling approach and CWC biomass predictions could also be used to examine CWC mound development and morphology. Although CWC growth and mound development operated on a different timescale and our model does not include sedimentation or baffling of sediment, our CWC predictions can indicate in which direction a mound will likely develop. CWC mound development and morphology depends on a complex interplay between CWC growth, sedimentation, hydrodynamics, and scale-dependent feedbacks (van der Kaaden et al., 2020). The presence of CWC framework promotes mound development by providing structure and baffling of sediment (Dorschel et al., 2007; Mienis et al., 2007; Titschack et al., 2015). CWC mounds are globally found in a wide variety of shapes and relative orientation to the general current direction. For example, CWC mounds can be shaped parallel (Hebbeln et al., 2014; De Clippele et al., 2017; Matos et al., 2017) or perpendicular (Correa et al., 2012) to the general current direction. Furthermore, the distribution of CWCs can differ greatly per mound and region. CWCs are found facing the current direction (Buhl-Mortensen et al., 2012; Correa et al., 2012) but are also found on summits, flanks and leeward sides of CWC mounds (Dorschel et al., 2007; Lim et al., 2017; Conti et al., 2019). The CWC mounds in our model domain are mostly elongated in shape, perpendicular to the general current direction, except for Haas mound, which is elongated parallel to the current direction, and was formed on a pre-existing hump (Mienis et al., 2006). Our CWC biomass predictions fit well with the mound morphologies in the model domain. For instance, in the northwest of the model domain, the CWC ridges shaped perpendicular to the general current direction show high CWC biomass on the southern side (Figure 4.7C). This suggests that these ridges will develop further in this direction and might provide an explanation to why these CWC mounds are shaped perpendicular to the current and slope. This agrees well with findings from White et al. (2007): CWC mounds are often aligned with the major axis of the tidal current oscillation, which is across-slope in this area.

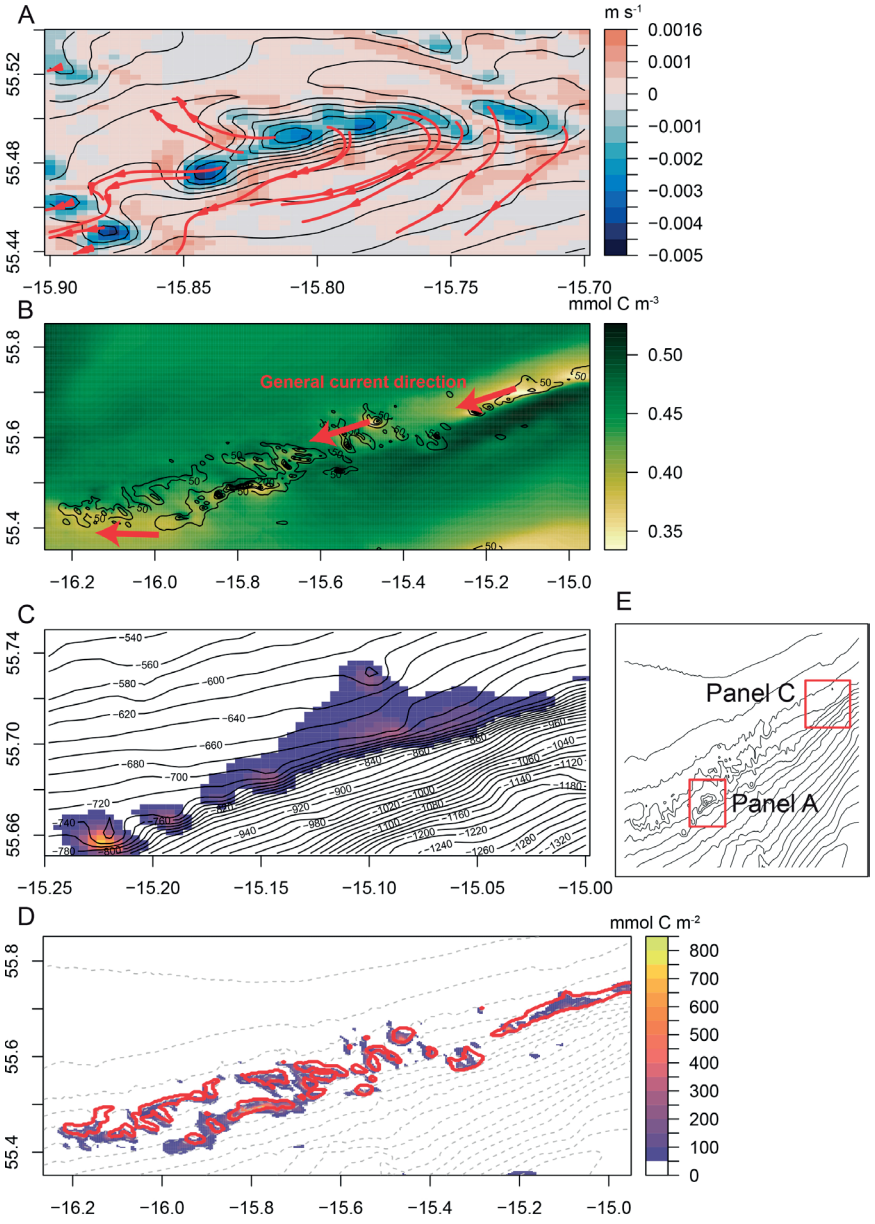

Figure 4.8 A) General transport direction of organic matter in the bottom layer above Haas mound, with colour overlay representing averaged vertical velocity in bottom layer, black lines indicate the bathymetry, and red lines show the predicted flow paths of neutrally buoyant particles that were released on the summits. B) POC depletion by CWCs, colour overlay represents averaged POC concentration in the bottom layer, black lines show predicted CWC biomass, and red arrows show the general current direction in the bottom layer. C) Detail of CWC predictions on the ridges in the northeast of the model domain. D) comparison between CWC predictions and the coral region of Rengstorf et al. (2014) indicated by the red line, E) location of subpanels A and C in this figure.

Mechanistic cold-water coral predictions compared to statistical methods

Our modelling approach allows for a more quantitative estimate of the spatial distribution of CWCs than habitat suitability models developed earlier for this area (Rengstorf et al., 2014). Rengstorf et al. (2014) underline the importance of including hydrodynamic variables in predicting the area of suitable habitat for CWCs, their model predictions for suitable habitat are somewhat shifted northeast compared to this study. Our predicted CWC biomass showed high variability inside their area with >0.9 probability of CWC presence (Figure 4.7D). The importance of including hydrodynamic variables in habitat suitability models is being recognized (Lim et al., 2020), as including variables as bottom current speed and vertical velocity improves model performances (Rengstorf et al., 2014; Bargain et al., 2018; Pearman et al., 2020). Here we show that the spatial distribution of CWCs also depends on organic matter replenishment and conditions in the surrounding areas due to interaction between CWC growth and bottom water POC. Therefore, competition for resources should be taken into account in high resolution habitat suitability models. A novel approach in mapping CWC biomass by a combination of habitat suitability modelling and field measurements (De Clippele et al., 2017, 2021b), identified body position index (BPI) as most important predictor for CWC biomass in our study area and predicted that CWC biomass was highest on the summits and crests of the mounds and ridges (De Clippele et al., 2021b). As this compares well with the biomass found on the summit and southern flanks of the mounds, BPI, the relative height of an area compared to its surroundings, might be a good proxy for areas where CWCs experience little competition for resources. However, our findings emphasize the need to include oceanographic variables and spatial competition when understanding and predicting suitable habitat of CWCs in the deep sea with statistical methods.

An important ecosystem function that cold-water corals fulfil is benthic respiration (Cathalot et al., 2015). Assuming that modelled benthic respiration is representative throughout the year, the model domain seafloor would respire in total 104,845 tonnes C per year. Of this, CWCs are responsible for 11,260 tonnes C yr^{-1} of benthic respiration, or 10.7% of the total benthic respiration in the model domain, while only on 2.8 % of the model domain CWC biomass > 100 mmol C m^{-2} is predicted. CWC based respiration is similar, but at the upper end of a recent carbon turnover estimate of 5763 to 9260 tonnes C yr^{-1} of the CWC suitable habitat model (De Clippele et al., 2021; Rengstorf et al., 2014). The benthic respiration in areas with high CWC biomass exceeds the export flux supported by surface primary production (e.g., 12 mmol C m^{-2} d^{-1}; Henson et al., 2015), suggesting CWCs require organic matter production from a wider area to survive and grow. Furthermore, our model-derived benthic respiration estimates on the CWC mounds confirm that CWC reef depend on suspension feeding of POC that arrives by advective transport (Soetaert et al., 2016a).

Implications, limitations, and future work

This study presents the first mechanistic modelling approach to predict CWC biomass based on organic matter transport and hydrodynamics. As research on the spatial distribution of CWCs in the deep sea is restricted mostly by ship-time and observational constraints, the model predictions provide a good opportunity to investigate the mechanisms behind the spatial distribution of CWCs in the deep sea. We show that our model successfully predicts CWC occurrence. The spatial distribution of CWCs on the south-eastern slope of Rockall Bank is driven by the horizontal bottom water POC flux, POC replenishment, and spatial competition. Depletion of organic matter in the bottom water layer by CWCs was key in adequately predicting CWC biomass. The good fit between video observations and modelled CWC biomass strengthens the hypothesis that food supply is the prime predictor for CWC growth (Hebbeln et al., 2019) and abiotic environmental variables (e.g. temperature, salinity; Dullo et al., 2008; Rüggeberg et al., 2011) might be of less importance for the spatial distribution of CWCs than previously thought.

The CWC biomass predictions compare reasonably well with video observations but there are several limitations to the model that should be considered. First, we only used one month of hydrodynamic data to spin-up and run the model, while seasonal variability in environmental/hydrodynamic conditions affect CWC growth (Maier et al., 2020a). As we used spring conditions, in which CWC growth is likely enhanced, the CWC biomass estimates could be an overestimation. Furthermore, the metabolic cost of reproduction is also included in the benthic model, which results probably in CWC biomass overestimation as well. Second, CWC framework has complex interactions with bottom hydrodynamics which could change the food supply mechanisms towards the reefs (Guihen et al., 2013; Mienis et al., 2019). In addition, POC concentration is elevated in the benthic boundary layer, close to the seafloor, due to resuspension (Adams and Weatherly, 1981). Although resolving these small-scale processes for such a large area can be challenging and would require resolving spatial scales <<250 m, future work might need to take the interaction between CWC framework and hydrodynamics into consideration.

This modelling approach provides a framework to study the effect of changing temperatures, currents, pH, and nutrients on the spatial distribution of CWCs in the deep sea. As CWCs might be severely impacted by rising temperatures and ocean acidification (Gori et al., 2016), this model can be used to study this by, for example, coupling CWC respiration to water temperature or simulating the higher cost of calcification under ocean acidification by increasing basal CWC respiration (Dodds et al., 2007; McCulloch et al., 2012b; Gori et al., 2016). In addition, although computationally heavy and beyond the scope of this study, POC remineralization in the water column could be coupled to the water temperature. Further, nitrogen cycling could be added to the model in the form of inorganic nutrients or particulate organic nitrogen. As surface produced POC export to

the deep-sea could be reduced with climate change (Bopp et al., 2001), this could affect CWC reefs and decrease benthic biomass in general (Smith et al., 2008; Jones et al., 2014; Puerta et al., 2020). Our model could be used to examine this effect by reducing POC export from the upper boundary layer/condition. Furthermore, our CWC biomass predictions matched dead coral framework observations well. Predictions of dead coral framework could be performed by adding a mortality rule in the CWC model (as in Hennige et al., 2021). Finally, with the prerequisite of having sufficient physiological data available, our model could also be applied to other suspension feeders. In summary, our study improves the understanding of the mechanisms driving the spatial distribution of CWCs in the deep sea and provides a tool to investigate this under changing oceanic conditions.

Conclusion

This study set out to investigate what drives the spatial distribution of cold-water coral biomass by developing a first mechanistic model based on hydrodynamics, organic matter transport, and CWC physiology. Our model approach successfully predicted CWC biomass on the coral mounds and ridges of the south-eastern slope of Rockall Bank, northeast Atlantic Ocean. High CWC biomass was predicted in regions with strong bottom currents and sufficient replenishment of bottom water organic matter. Benthic respiration on the CWC mounds is mostly driven by CWCs. Coupling the pelagic organic matter transport model with the benthic CWC biomass and sediment model proved to be key for predicting CWC biomass. This model can be used as a tool in future work investigating the effect of changing ocean conditions on the spatial distribution of CWCs or other suspension feeders in the deep sea.

Supplementary material *Chapter 4*

Figures

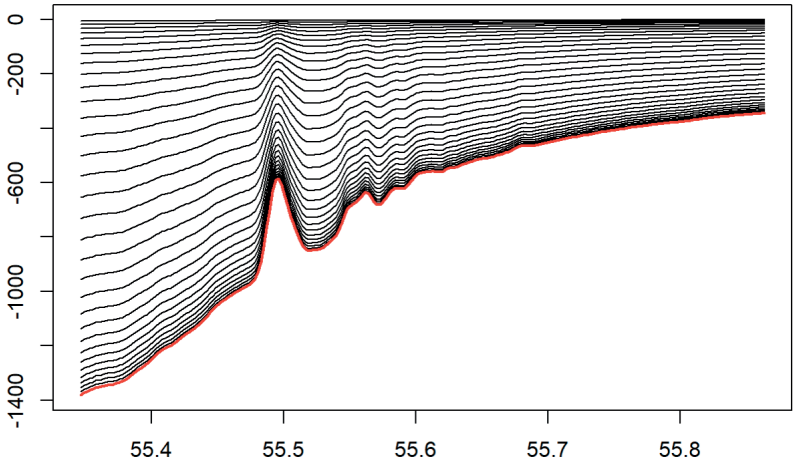

Figure S4.1 Latitudinal cross-section of model sigma grid over Haas mound. Example of sigma grid

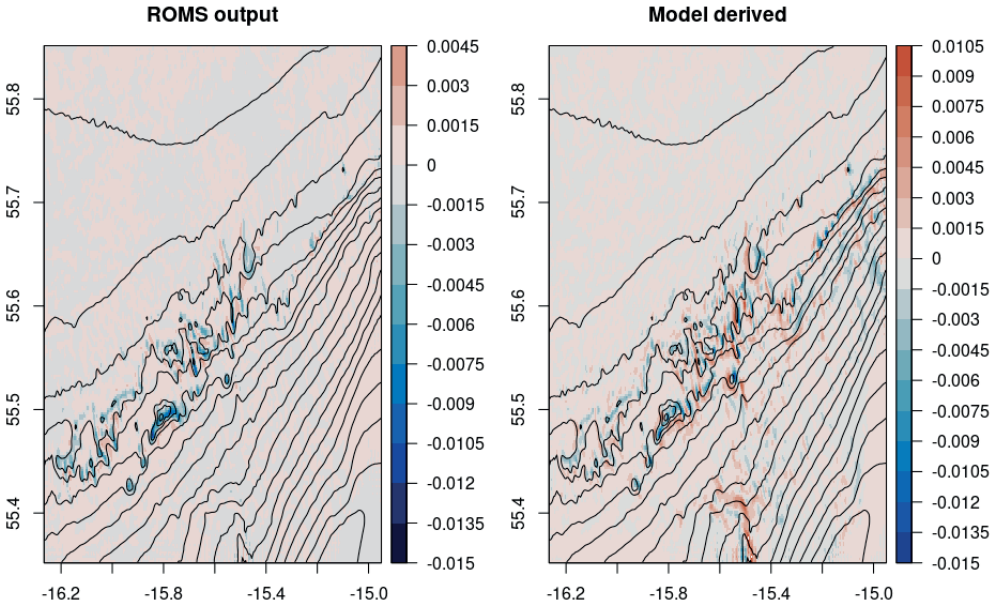

Figure S4.2 water column averaged vertical velocities (A) from ROMS output and (B) calculated from the horizontal currents

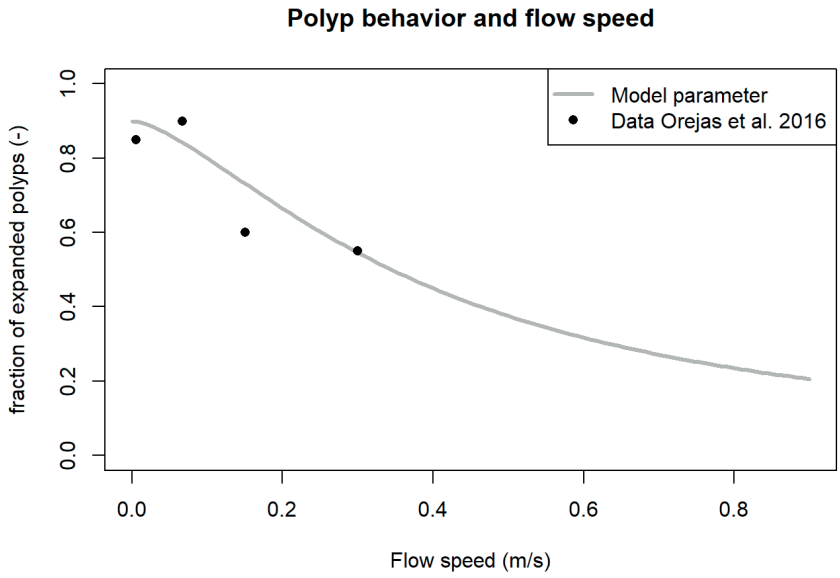

Figure S4.3 Fitted effect of flow speed on polyp behaviour in a Lophelia pertusa colony

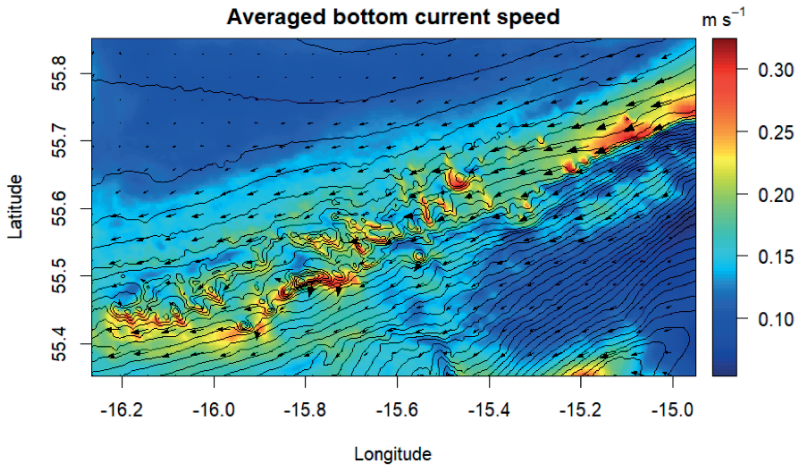

Figure S4.4 Averaged current speed of bottom layer and direction

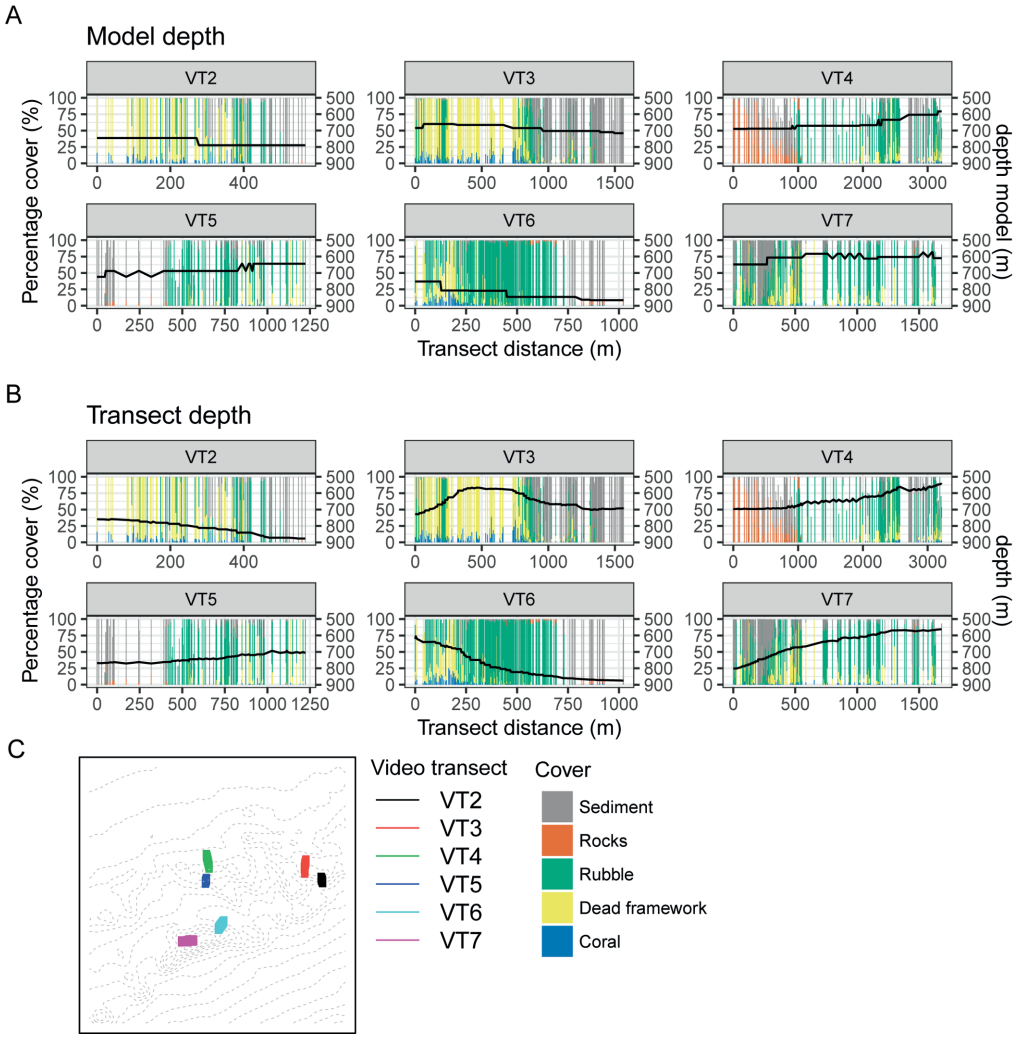

Figure S4.5 comparison between model and video observations from De Clippele et al. (2019) with A) model depth, B) video transect depth, and C) a map of the transect locations

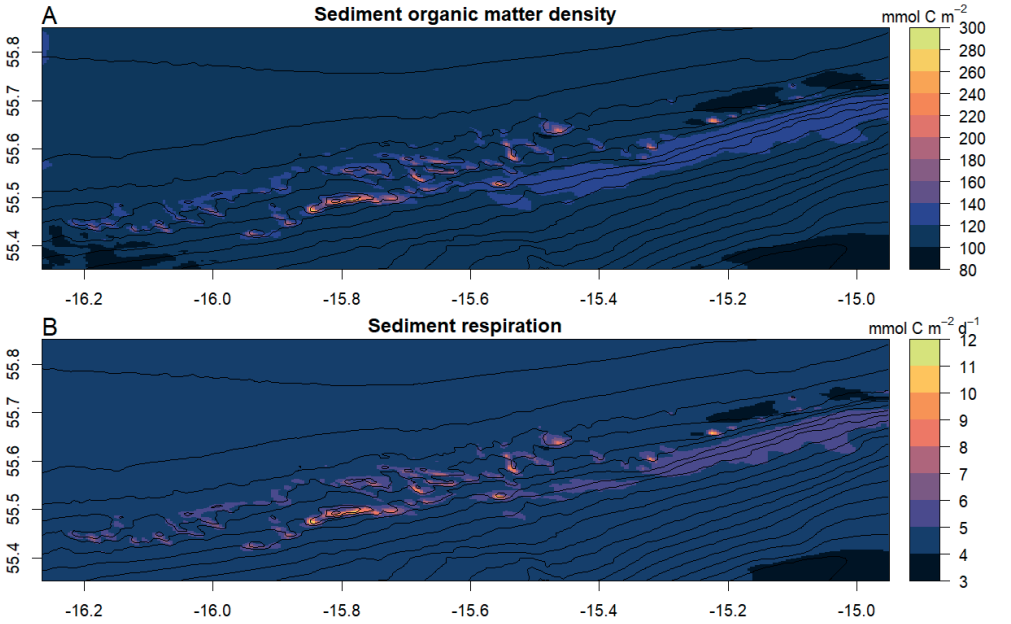

Figure S4.6: A) sediment organic carbon density or biomass, B) sediment respiration.

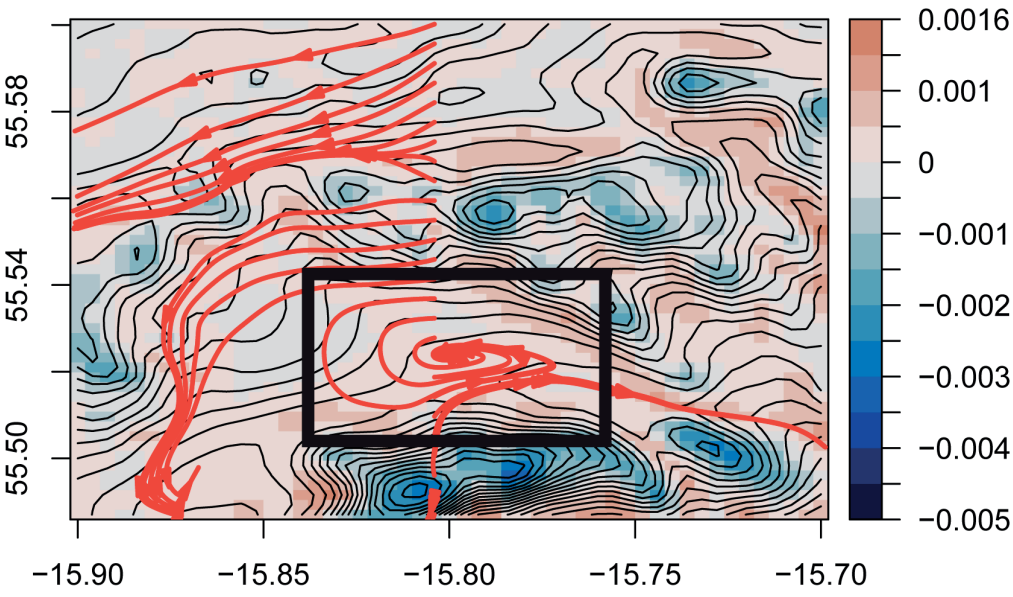

Figure S4.7 general direction of organic matter in the bottom layer released along a latitudinal cross-section. Black box indicates where organic matter follows cyclonic circles. The colours represent vertical velocity in m s^{-1}

Videos

Video S1 depth averaged particulate organic carbon concentration in the water column. Note the overall southwestward direction of the particulate matter, and the north-south sloshing by tidal currents, see: https://doi.org/10.5281/zenodo.7510506

Video S2 vertical velocity and particulate organic carbon concentration over the Haas mound cross-section. The arrows indicate the north-south direction of the current. See: https://doi.org/10.5281/zenodo.7510506

Chapter 5

YEAR-LONG BENTHIC MEASUREMENTS OF ENVIRONMENTAL CONDITIONS INDICATE HIGH SPONGE BIOMASS IS RELATED TO STRONG BOTTOM CURRENTS OVER THE NORTHERN LABRADOR SHELF

Evert de Froe, Igor Yashayaev, Christian Mohn, Johanne Vad, Furu Mienis, Gerard Duineveld, Ellen Kenchington, Erica Head, Steve W. Ross, George A. Wolff, Sabena Blackbird, Murray Roberts, Barry McDonald, Graham Tulloch, Dick van Oevelen

To be submitted to Progress in Oceanography

Abstract

Deep-sea sponge grounds are distributed globally and are considered hotspots of biological diversity and biogeochemical cycling. To date, little is known about the environmental constraints that control where deep-sea sponge grounds occur and what conditions allow high sponge biomass in the deep sea. Here, we characterize oceanographic conditions at two contrasting high- and low sponge biomass sites off the northern Labrador Shelf near Canada. Data were collected by year-long benthic lander deployments equipped with current meters, turbidity and chlorophyll-*a* sensors, and sediment traps. Additional CTD casts were taken to describe the water mass structures across the two shelf break stations and stable isotopes of the benthic fauna were analysed to identify potential food sources. Our results revealed strong (0.26 ± 0.14 m s^{-1}; mean ± SD) semidiurnal tidal currents at the high sponge biomass site and less stronger currents (0.14 ± 0.08 m s^{-1}; mean ± SD) at the low sponge biomass site. These tidal currents cause periodic temperature fluctuations, sediment resuspension, and during spring, transport of organic material to the seafloor during a diurnal tidal cycle. Fluctuations in bottom water temperature indicates transport across the shelf break at the high sponge biomass site. Furthermore, bottom nutrient concentrations were relatively high at the high biomass sponge ground due to advection of nutrient-rich bottom water from Baffin Bay. The arrival of chlorophyll-*a* rich material in spring at both sponge grounds demonstrated tight benthic-pelagic

coupling prior to the onset of stratification. Mass fluxes of trapped material were higher and consisted of less degraded material at the high sponge biomass site. Stable isotope signatures indicated that soft corals (*Primnoa resedaeformis*) fed on suspended particulate organic matter, while massive sponges (*Geodia* spp.) likely utilized required additional food sources, e.g. dissolved organic matter, at the high sponge biomass site. Our results imply that strong tidal currents benefit the benthic community and favour development of sponge biomass on the northern Labrador Shelf by increasing food supply to benthic fauna and replenishing nutrients, oxygen, and dissolved organic matter in bottom waters.

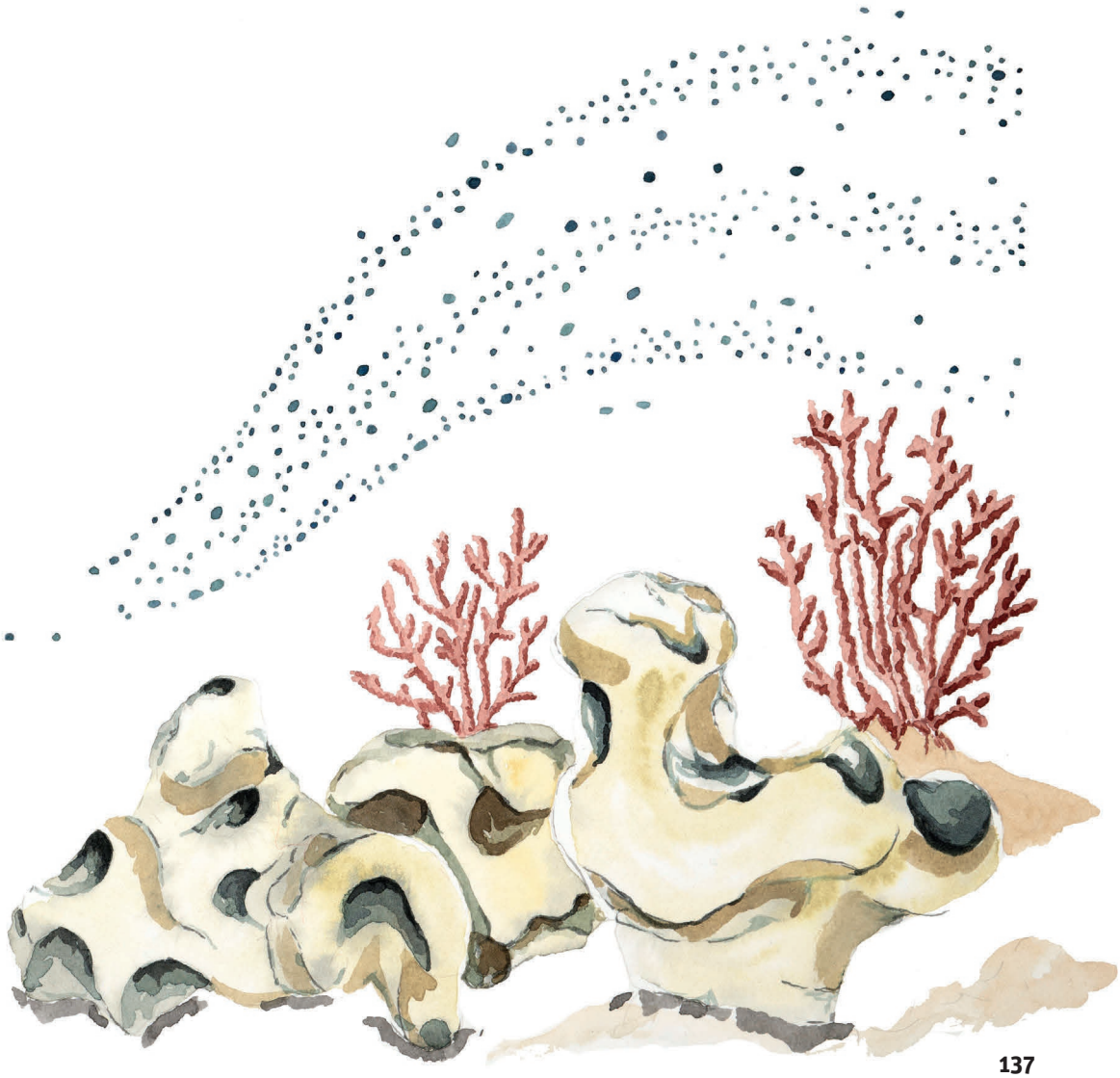

Introduction

Sponges are an ancient group of sessile filter feeders capable of pumping large quantities of water through their bodies (Vogel, 1977; Bergquist, 1978; Leys et al., 2011), thereby exchanging significant amounts of particulate- and dissolved organic matter and nutrients with the water column (e.g. van Duyl et al., 2008; Maldonado et al., 2012; Kahn et al., 2015; Rix et al., 2016). In the deep sea, sponges can form dense aggregations, known as sponge grounds, which are considered hotspots of macrofaunal diversity and abundance (Klitgaard, 1995; Buhl-Mortensen et al., 2010; Beazley et al., 2013; McIntyre et al., 2016), carbon- and nutrient cycling (Kutti et al., 2013; Cathalot et al., 2015; Maldonado et al., 2020a), and benthic-pelagic coupling (Pile and Young, 2006). Sponge grounds are often classified as Vulnerable Marine Ecosystems (VMEs) as defined by the Food and Agriculture Organization of the United Nations (FAO, 2009). They form complex habitats that provide breeding grounds and shelter for commercially important fish species, increasing demersal fish biomass and diversity (Kenchington et al., 2013; Kutti et al., 2015; Meyer et al., 2019).

These valuable ecosystems are currently under threat from anthropogenic disturbances such as deep-water bottom trawling and ongoing climate change. Pham et al. (2019) found that large quantities of sponges (~4% of total stock) have been removed by bottom trawling from sponge grounds on the Flemish Cap. Deep-sea sponges are especially vulnerable to bottom fishing due to the sponges` longevity and slow growth (Leys and Lauzon, 1998; Hogg et al., 2010). Benthic trawling reduces the density and diversity of deep-sea sponge grounds (Colaço et al., 2022), and recovery of disturbed sponge habitats can take decades to centuries (Vieira et al., 2020). Recent studies suggest that climate change also impacts deep-sea benthic fauna (Brito-Morales et al., 2020; Jorda et al., 2020). A recent modelling study predicted that the suitable area for *Vazella pourtalesii* on the Scotian Shelf would increase four-fold in the coming years due to warming of colder waters around its current habitat (Beazley et al., 2021). Nevertheless, research on the effect of climate change on deep-sea sponges is still in its infancy and to predict the effects of environmental change on sponge grounds, a mechanistic understanding is needed of the environmental conditions that favour their occurrence.

In the past decades, research on deep-sea sponges has focussed on physiological processes and feeding behaviour (e.g. Leys and Lauzon, 1998; Yahel et al., 2007; Kahn et al., 2015; Kazanidis et al., 2018; Maier et al., 2020b; Bart et al., 2020; de Kluijver et al., 2021), and modelling their spatial distributions using habitat suitability models (Knudby et al., 2013; Howell et al., 2016; Beazley et al., 2018; Murillo et al., 2018). More recently, data on the environmental conditions where sponge grounds are found have been gathered using long-term measurements from lander-mounted equipment. These data indicate that sponge grounds are found in areas with internal waves (Davison et al., 2019) and comparatively strong tidal currents which flush the seafloor with oxygen and nutrient-rich

water, and with a high suspended particle matter load near the seabed (Roberts et al., 2018; Hanz et al., 2021a, 2021b). The spatial distribution of sponge grounds is also linked to gamete/larval dispersal and food availability (Abelson and Denny, 1997; Robertson et al., 2017). In addition, sponges can alter the hydrodynamic conditions of the benthic boundary layer by increasing the bottom roughness, creating conditions favourable for larval recruitment, suspended particle deposition, and increasing the effective radius of pumping (Culwick et al., 2020). These studies show that sponge grounds can be found in areas having a variety of environmental conditions, but little is known of the mechanisms controlling their spatial distribution or what controls their biomass.

The Canadian Atlantic continental shelf breaks and upper slopes, including the northern Labrador Shelf, host extensive sponge grounds (Kenchington et al., 2010; Knudby et al., 2013). Sponge assemblages occur over a large depth range (200 – 1800 m) and are often aligned along depth contours with presumably similar environmental conditions (Murillo et al., 2012; Knudby et al., 2013). On the northern Labrador Shelf and upper slope, sponge assemblages consist mostly of *Geodia* spp. and glass (hexactinellid) sponges (Kenchington et al., 2010) but with strongly varying sponge biomass among areas. Therefore, this region provides an interesting setting to study which environmental conditions favour high sponge biomass, and to provide insight into the factors that drive the spatial distribution of sponge assemblages on the eastern Canadian Shelf. Also, research on present environmental conditions on the seafloor is timely as the Labrador Shelf region is one of the fastest warming large marine ecosystems globally (~1 °C decade^{-1}; Belkin, 2009), and water mass properties there could change by 2100 in terms of temperature, particulate organic carbon, pH, and aragonite saturation state (Puerta et al., 2020). This study presents a valuable reference dataset for the upper slope of the Northern Labrador Shelf against which future changes can be evaluated.

To obtain a better understanding of the environmental conditions and ecosystem functioning of sponge grounds on the upper slope of the northern Labrador Shelf, this study specifically aimed to examine at the high- and low- sponge biomass sites: (i) differences in seawater properties, (ii) the annual dynamics of near-bed environmental and hydrodynamic conditions, and (iii) differences in organic matter flux and food sources for sponges and associated macrofauna. This study is the first to collect long-term hydrodynamic and environmental data simultaneously at a high- and a low biomass sponge ground.

Material and methods

Oceanographic setting and the study area

The study area comprises the northern Labrador Shelf and upper slope and extends from the southeastern Hudson Strait outflow region to the base of the Labrador slope (Figure 5.1A). This region is known for intense mixing and water mass transformation (Dunbar, 1951; Kollmeyer et al., 1967; Griffiths et al., 1981; Drinkwater and Jones, 1987; Yashayaev, 2007) and four distinct flow components can be identified (Figure 5.1A; Smith et al., 1937; Yashayaev, 2007; Straneo and Saucier, 2008; Curry et al., 2011, 2014): first, the cold and relatively fresh Arctic outflow, passing through the Davis Strait via the Baffin Island Current (BIC), enters the region from the north as Arctic Water (AW) and Baffin Bay Water (BBW; Sherwood et al., 2021); second, the West Greenland Current (WGC) approaches our study site from the northeast; third, Irminger Water (IW), a warmer and saltier water mass, can often be seen underneath the WGC, usually below 150 m depth; and fourth, Hudson Strait outflow water which enters the region from the west. The resulting aggregated boundary current joins the Labrador Current (LC) flowing southward along the Labrador shelf/slope, effectively forming and maintaining a baroclinic transition between the less-saline shelf water and the more-saline deep-basin water (Yashayaev, 2007).

The northern Labrador Shelf hosts multiple sponge grounds with contrasting sponge community composition, density, and biomass (Kenchington et al., 2010; Dinn et al., 2020). We selected a high sponge biomass (HSB; 410 m depth) site in the north and a low sponge biomass (LSB; 558 m depth) site in the south of the study area (Table S5.1; Figure 5.1B), which were approximately 130 km apart. The seafloor at HSB was characterized by large-sized massive demosponges (e.g. *Geodia* spp.) and glass sponges (e.g. *Asconema* spp.), the large gorgonian corals (*Primnoa resedaeformis)*, and rock boulders (Figure 5.2A & B; Kenchington et al., 2010; Dinn et al., 2020). At LSB the seafloor mainly consisted of sediment, boulders, and small sponge structures (e.g., *Mycale* spp.; Figure 5.2C & D). The HSB lander was located on the shelf on a 2° slope and slope aspect was directed westward at 82°. The LSB lander was located on the upper slope, east of the shelf break, on a 7° slope and aspect was directed northwest at 62° (Figure S5.1). The west-to-east slope angle was directed downhill, and north-to-south slope angle was directed uphill at both lander sites (Figure S5.2).

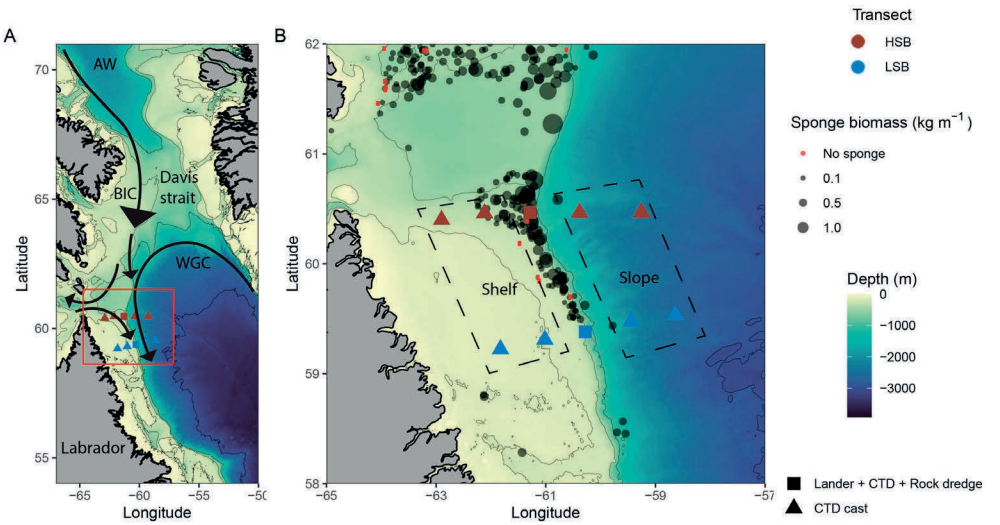

Figure 5.1 Map of the study area with (A) the general circulation pattern (Curry et al., 2014). Cold Artic Water (AW) flows southward through the Davis Strait and continues as the surface-intensified Baffin Island Current. The warmer, more saline West Greenland Slope Current (WGC) of North Atlantic origin largely follows the continental slope in the depth range 150 – 800 m and is deflected westward at approximately 64° N. Cold and fresh water leaves Hudson Strait and joins the BIC and WGC to form the offshore branch of the Labrador Current (Straneo and Saucier, 2008). (B) Location of lander deployments and CTD-casts, with sponge biomass (in kg m^{-1}) based on Kenchington et al. (2010). Dotted line boxes indicate the shallow shelf and deeper slope stations at both sites. HSB = high sponge biomass transect (red symbols), LSB = low sponge biomass transect (blue symbols)

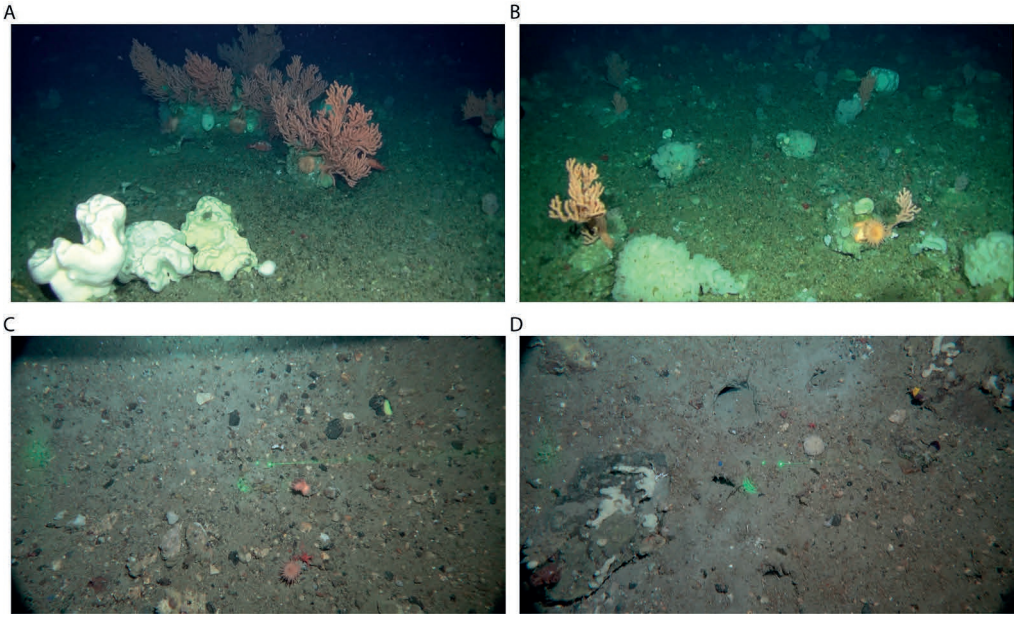

Figure 5.2 Images of benthic lander deployment sites, at the high sponge biomass (HSB) site (A,B) and low sponge biomass (LSB) site (C, D). Photographs were taken by drop camera at LSB and by ROV at HSB. ROV image credits: ArcticNet/CSSF/DFO, CSSF = Canadian Scientific Submersible Facility, DFO = Department of Fisheries and Oceans

Sampling methodology

Near-bed lander deployment

Landers were deployed during research cruise Amundsen 2018 leg 2c (27 July 2018) and retrieved during research cruise Amundsen 2019 leg 1b (4 July 2019). The landers were each equipped with a 2 mHz ADCP (upward-looking, Nortek Aquadopp), a sediment trap, and chlorophyll-*a* (chl-*a*) and optical backscatter sensors (Wetlabs – FLNTU; Table S5.1). The ADCPs collected an ensemble average of the 3D velocity field and echo intensity (acoustic backscatter signal) every 600 seconds over one year along with pressure, temperature and data from altitude sensors including heading, pitch, and roll. The ADCP was mounted 2 m above the bottom, the blanking distance was 1.14 m, and the ADCP was programmed to measure velocities at the first bin closest to the transducer head. Velocity data were recorded in beam coordinates and transformed to ENU coordinates (East, North, Up) after recovery using the transformation matrix provided by the manufacturer. The chl-*a* and optical backscatter sensors were programmed to measure every 600 seconds over the one-year period. Sediment traps (PPS 4/3, Technicap Inc.) with a surface area of 0.05 m^2 were equipped with twelve bottles for particle collection. Collection started at 15/08/2018 and lasted until the end of the deployment. Different time intervals of bottle rotation were set to increase sampling resolution during spring and summer months. The bottles rotated every 15 days from mid-August to mid-September 2018, every 30 days from mid-September to mid-November 2018, every 60 days from mid-November to mid-March 2019, then every 30 days from mid-March to mid-May 2019, and every 15 days again from mid-May to mid-July 2019. Prior to deployment, a 4% solution of formalin in brined seawater (40 psu) was added to each bottle.

Water column and benthic sampling

Conductivity-Temperature-Depth (CTD) casts were performed over two cross-shelf transects at the high- and low sponge biomass sites (Coté et al., 2018; Figure 5.1; Table S5.1). Two CTD casts were carried out on the shelf and three over the slope, where the third or middle cast was performed above each benthic lander deployment. The CTD was equipped with a Seabird SBE 911*plus* system, which contained sensors to measure temperature (Seabird SBE 3plus), conductivity (Seabird SBE 4), pressure (Paroscientific Digiquartz®), dissolved oxygen (Seabird SBE 43), fluorescence (Seapoint), and a rosette water sampler with 12 Niskin bottles (12L each). CTD data were processed and "cleaned" with the *Sea-Bird SBE Data Processing* software (Guillot, 2018). Water samples were taken from Niskin bottles at five depths (5 m, 50 m, mid-water, 50 m above bottom, 10 m above bottom) for the determination of nutrients (NH_4^+, NO_2^- + NO_3^-, PO_4^{3-}, SiO_2), and suspended

particulate organic matter (sPOM).

Benthic macrofauna samples for stable isotope analysis were collected at the two lander locations using a rock dredge on retrieval of the benthic landers (Coté et al., 2019; Table S5.2). A description of the species found at the two locations can be found in Coté et al. (2019) and Vad et al. (*in prep*). The rock dredge (7 mm mesh size) was deployed in "drift" mode at HSB, with a maximum speed of two knots (~4 km h^{-1}) for 10-20 minutes, and "tow" mode at LSB, with the ship moving at one knot for 10 minutes. On deck, the dredge was rinsed, and the catch was subsampled and deposited in fish totes (64 L). The remaining material was sieved through a 2 mm mesh for analysis of invertebrates and fishes. The total catch was photographed and preserved for species identification and quantification. Samples for stable isotopes were frozen (-20 °C) for further analysis at the Netherlands Institute for Sea Research (NIOZ).

Laboratory analysis

Water column nutrient concentrations were analysed with a SEAL QuAATro analyser (Bran + Luebbe, Norderstedt, Germany) following standard colorimetric procedures. POM samples were freeze-dried, weighed, and analysed for organic carbon content, total nitrogen content, and $\delta^{13}C$ using an elemental analyser (Flash 1112, THERMO Electron Corporation) coupled to an isotope ratio mass spectrometer (EA-IRMS, DELTA-V, THERMO Electron Corporation).

Sediment trap samples were filtered through a 1 mm sieve to remove large particles and swimmers, then split into five sub-samples using a McLane WSD-10 rotary splitter, rinsed with demineralized water to remove salts and formalin and subsequently freeze-dried and weighed (Newton et al., 1994; Mienis et al., 2012). Lipids were extracted and analysed following the method of Kiriakoulakis et al. (2004). Briefly, samples were spiked with internal standard (5a(H)-cholestane), extracted by sonication in dichloromethane:-methanol (9:1; x3). The solvent was removed and samples were first trans-methylated (Christie, 1982) and then treated with bis-trimethylsilyltrifluoroacetimide: trimethylsilane (99:1; 30-50 µL; 60 °C; 1 h) prior to analysis by gas chromatography-mass spectrometry (GCMS). GCMS analyses were conducted using a GC Trace 1300 fitted with a split-splitless injector and column DB-5MS (60m x 0.25mm (i.d.), with film thickness 0.1 µm, non-polar stationary phase of 5% phenyl and 95% methyl silicone), using helium as a carrier gas (2 mL min^{-1}). The GC oven was programmed after 1 minute to rise from 60°C to 170°C at 6°C min^{-1}, then from 170°C to 315°C at 2.5 °C min^{-1} and was then held at 315 °C for 15 min. The eluent from the GC was transferred directly *via* a transfer line (320 °C) to the electron impact source of a Thermoquest ISQMS single quadrupole mass spectrometer. Typical operating conditions were: ionisation potential 70 eV; source temperature 215°C; trap

current 300 µA. Mass data were collected at a resolution of 600, cycling every second from 50– 600 Daltons and were processed using Xcalibur software.

Compounds were identified either by comparison of their mass spectra and relative retention indices with those available in the literature and/or by comparison with authentic standards. Quantitative data were calculated by comparison of peak areas of the internal standard with those of the compounds of interest, using the total ion current (TIC) chromatogram. The relative response factors of the analytes were determined individually for 36 representative fatty acids, sterols and an alkenone using authentic standards. Response factors for analytes where standards were unavailable were assumed to be identical to those of available compounds of the same class.

Sponges and other benthic fauna collected using a rock dredge were freeze-dried and homogenized with a pestle mortar/ball mill. Subsamples (*ca.* 10 mg) were transferred into silver cups and acidified by addition of dilute HCL (2%, 5%, and 30%) to remove carbonates. Organic carbon and $\delta^{13}C$ were analysed on acidified subsamples, and total nitrogen and $\delta^{15}N$ were analysed on non-acidified subsamples using an Electron Analyser coupled to an Isotope Ratio Mass Spectrometer (Thermo flash EA 1112). $\delta^{13}C$ and $\delta^{15}N$ isotope values are expressed in parts per thousand (‰) relative to the Vienna Pee Dee Belemnite (VPDB) standard and atmospheric nitrogen, respectively.

Data processing

The transformation of beam coordinates to ENU coordinates for the ADCP data was carried out in Matlab (MATLAB, 2010), and all other data processing steps used R (Wickham, 2007, 2016a; Grolemund and Wickham, 2011; Neuwirth, 2014; signal developers, 2014; Michna and Woods, 2019; Pedersen, 2019; R Core Team, 2019; Wickham and Bryan, 2019; Wilke, 2019; Kelley and Richards, 2020; Stoffer, 2020; Vaughan and Dancho, 2020; Xie, 2020; Lovelace et al., 2022). Occasionally, pitch and roll data from the ADCP sensor at HSB were shifted for a small period of the deployment, implying the lander was occasionally moving a bit. However, removing these datapoints did not change the outcome of any of the analyses, statistical tests, or descriptive statistics and these datapoints were therefore retained in the HSB time series. Chl-*a* (in µg L^{-1}) and turbidity (in NTU) concentrations were calculated from ping counts as described in the manual of the manufacturer. To investigate connectivity in environmental variables between the two benthic landers, and correlations between hydrodynamic- and environmental conditions, a cross-correlation analysis with time lag was performed. Spectral analysis on lander data was performed to examine recurring patterns or periodicity in the time-series data (e.g. Shumway et al., 2000), and coherence analysis was carried out to assess correlation in periodicity between landers and variables (Bloomfield, 2004). Spectral and coherence analyses were

based on a Fourier transformation on unfiltered data (Bloomfield, 2004). Prior to these analyses, time series data were smoothed using a modified lowpass Daniell filter (Bloomfield, 2004). The magnitude and direction of ADCP-recorded tidal currents were analysed with least-squares harmonic analysis, using the t_tide MATLAB toolbox (Pawlowicz et al., 2002). Bottom currents and direction were compared to model derived barotropic tidal currents, retrieved from the Oregon State University (OSU) Tidal Inversion Software (OTIS; Egbert and Erofeeva, 2002). Correlations between sediment trap variables (mass, $\delta^{15}N$, etc.) and time-series data were investigated by averaging the ADCP+FLNTU data over each sediment bottle period, using Pearson correlation analysis. Sea-ice cover above the two benthic landers was extracted from weekly ice charts (Canadian Government). Statistics are presented as means ± standard deviations.

Results

Seawater properties over the northern Labrador shelf and slope

The CTD casts, performed July 2018, revealed a difference in seawater properties between the two transects (Figure 5.3, Figure S5.3). The surface water at the time of survey was relatively warm (2 – 6 °C) and fresh (31.2 to 33.8 psu) yet showed a significant offshore increase in temperature and salinity. From the surface to the depth of 20-70 m, depending on the transect and location, temperature decreased to sub-zero or near-zero at the shelf locations, to 3 °C at the slope locations, and then increased again to 2.8 °C at 250 m depth on the shelf and to 4.3°C at 150 m on the slope. The temperature changes from cooling to warming with depth signify the Cold Intermediate Layer (CIL). Salinity in the CIL increased nearly monotonically with depth across all stations. The stations at LSB were more saline overall than those on the HSB transect.

The oxygen concentration was highest in the surface waters (0 – 50 m) on the shelf and decreased for all CTD stations with depth (Figure 5.4A). The bottom oxygen concentrations at the lander stations were, for both transects, relatively depleted compared to the deep water CTD transects at similar depth. Concentrations of nitrate, phosphate, and silicate were lowest above the thermocline (0 – 3 µM) and increased with depth, while ammonium and nitrite were higher near the surface than at depth (Figure 5.4B & C, Figure S5.4). The HSB station exhibited relatively high nitrate, phosphate, and silicate concentrations at 10 and 50 metres above bottom compared to similar depths at shelf and deep stations (Figure 5.4B & C, Figure S5.4). This increased nutrient concentration in the bottom waters was also apparent at the LSB station, but to a lesser degree. Chl-*a* profiles showed a deep

chlorophyll maximum along both transects at 50 m, and near-zero concentrations in the bottom waters (Figure S5.3D). Particulate organic carbon (POC) concentrations were highest in the surface waters (8 – 38 µmol POC L^{-1}) and on the shelf (Figure S5.5). POC concentrations decreased with depth, and concentrations 10 m above bottom were 1.48 µmol POC L^{-1} at HSB, and 5.95 µmol POC L^{-1} at LSB.

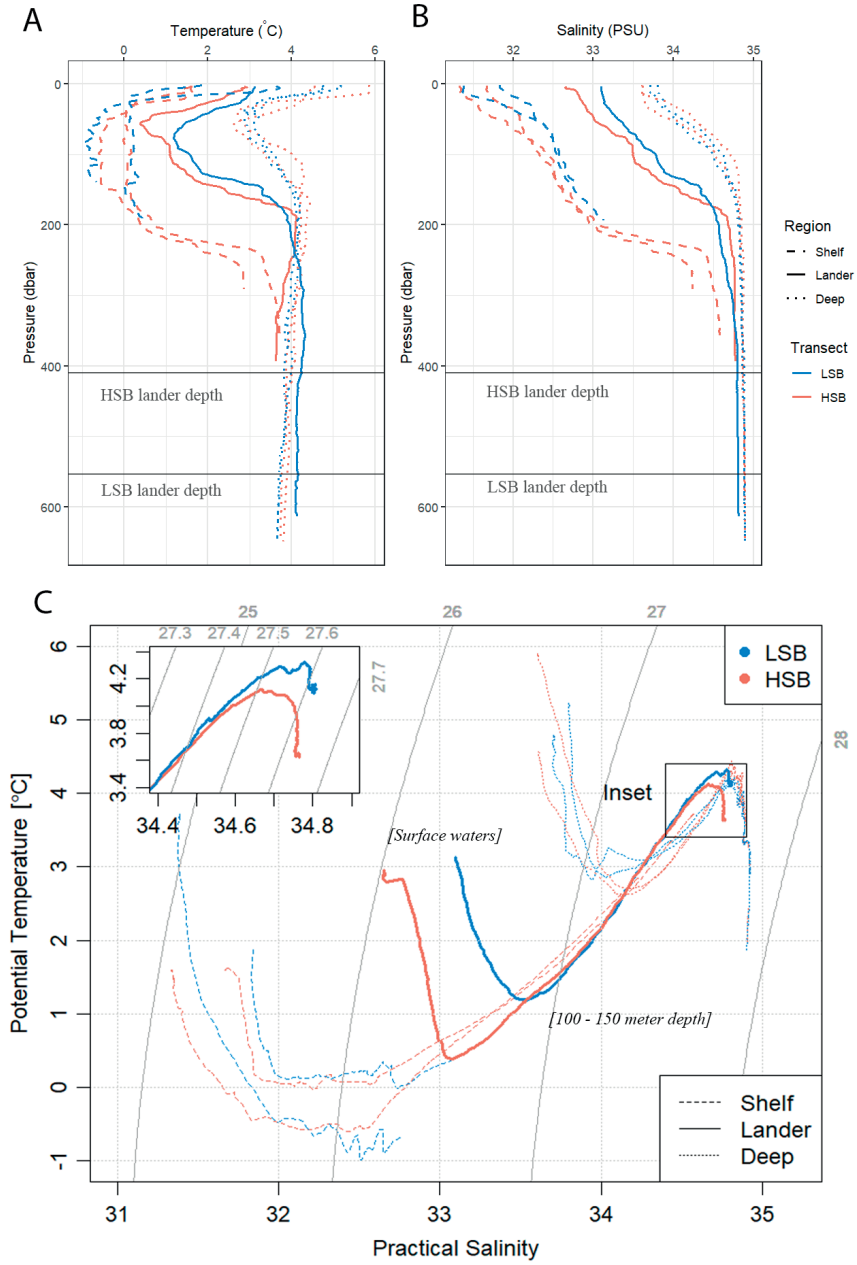

← **Figure 5.3** Hydrographic conditions in the study area: (A) temperature, (B) salinity and (C) temperature – salinity (TS) plots for the two transects. LSB = low sponge biomass, HSB = high sponge biomass. Depths of landers are indicated by the horizontal grey lines in A and B. Temperature and salinity profiles in A and B only show top 600 m, while TS plots include the entire water column

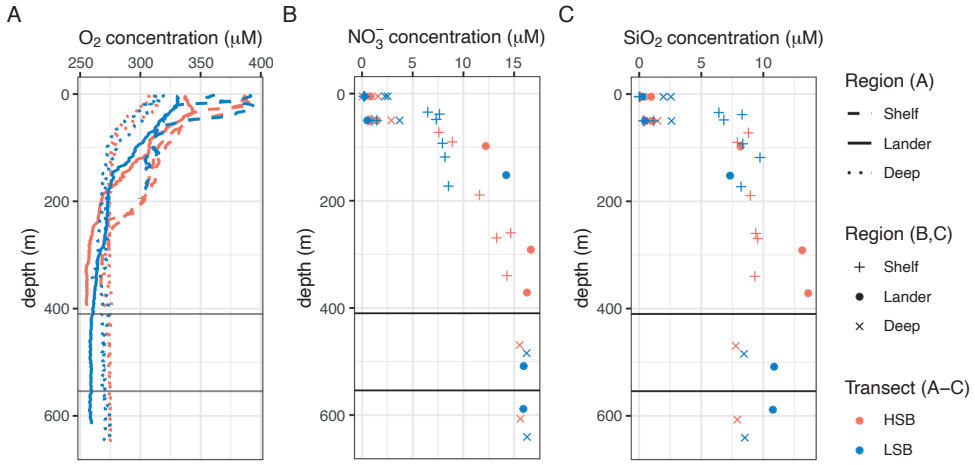

Figure 5.4 Oxygen (A), nitrate (B), and silicate (C) concentration profiles for the two transects. HSB = high sponge biomass site, LSB = low sponge biomass

Long-term near-bottom measurements

Near-bottom current velocities

In general, bottom current speeds were higher at the HSB compared to the LSB station (Table 5.1; Figure 5.5). The eastward velocity (*u*) was more eastward at HSB than at the LSB site and northward velocity (*v*) was comparable between sites and directed southward. The residual current was south-easterly at HSB and south-south-westerly at LSB (Figure 5.6, Figure S5.6). Vertical velocity (*w*) was on average upwards and comparable between HSB and LSB, but the range in vertical velocity was higher at HSB (-0.35 to 0.32 m s^{-1}) compared to LSB (-0.11 to 0.21 m s^{-1}). Bottom currents were twice as high at HSB than at the LSB (Table 5.1), and peak bottom current speeds were 0.75 m s^{-1} (HSB) and 0.65 m s^{-1} (LSB), with the third quantile at 0.33 m s^{-1} (HSB) and 0.18 m s^{-1} (LSB). The pressure signal, a proxy for sea surface height, showed peaks in variance preserving spectrum periodicity at the semidiurnal (M2, S2, N2), and diurnal tidal harmonics (K1, O1; Figure 5.7A). Bottom current speeds showed semi-diurnal and spring-neap tidal patterns, with bottom currents peaking every fortnight for both sites (Figure 5.5C; Figure 5.7B). The major axes of the semidiurnal tidal ellipses were directed in a northwest-southeast direction at HSB and a north-south direction at LSB, and were aligned with the continental shelf and slope,

respectively (Figure 5.7D; Figure S5.6). The M2 and S2 major axes at the HSB station (0.28 m s^{-1} and 0.05 m s^{-1}) were a factor of five larger than the corresponding magnitudes at the LSB station, whereas diurnal major axes were small (< 1 cm s^{-1}) and of similar magnitude at both locations. Frequency distributions of spectral variance showed highest variability in semidiurnal periodicity for bottom current components at both sites, but the peak in the variance-preserved spectrum was higher at HSB than at LSB. Furthermore, spectral density for the HSB bottom current components also peaked at shorter frequencies (3-6 h) and at the fourteen-day spring-neap tide (Figure 5.7B). In addition, a superimposed seasonal pattern can be seen at both sites, where the bottom current speed gradually increased from July 2018 to March 2019 and decreased again from March 2019 to July 2019. The slope aspect was directed at 82° at HSB and 62° at LSB, which results in a net down- and up-slope transport over the course of a year, respectively (Figure 5.6). High downward velocities were recorded during periods having south-easterly and north-westerly current direction at HSB. High upward velocities at LSB were recorded when current direction was south or south-westerly (Figure 5.8).

Near-bottom environmental conditions

Bottom temperature was slightly warmer at HSB compared to LSB and increased at both sites (0.2 – 0.3 °C) during December and January (Figure 5.9). Acoustic backscatter signal (ABS) was similar for the two stations (Table 5.1; Figure 5.9B) and showed higher values in winter months. Chl-*a* remained low from October to early March when a spring peak was observed for both landers (Figure 5.9C). Maximum chl-*a* concentration was lower at HSB (2.24 µg L^{-1}) than at the LSB (5.41 µg L^{-1}). The HSB station showed spring bloom conditions from mid-March to the end of May, while at the LSB station the spring bloom lasted from mid-March to early May. Turbidity was comparable at the two sites, and was elevated at HSB from February to April, and at LSB from December to January. Turbidity increased at high south-easterly current velocities at HSB and high southerly current velocities at LSB (Figure S5.8). The higher variability in chl-*a* and turbidity at the LSB site over the year (Table 5.1) was caused by several peaks in chl-*a* and turbidity that were an order of magnitude higher than average values (Figure S5.9).

Daily temperature fluctuations were higher at HSB than at LSB. Cross and along slope water transport influenced bottom temperature. For example, in the first week of September, temperature decreased when the current was directed northwest and increased when the current was directed southeast (Figure 5.8A-D; Figure 5.9A-E). Temperature showed a reoccurring tidal signal, with higher peaks in spectral density for the semidiurnal periodicity at HSB than at LSB (Figure 5.7C). An occasional drop in temperature was observed after high downward vertical velocities in southeast direction at HSB (e.g. first week of

March; Figure S5.7). Cross-correlation showed that near-bottom temperatures (daily averaged) were correlated between the two landers with a lag of five days (R^2 = 0.52). ABS (Acoustic Backscatter Signal) increased often at the turning of the tide and at high south-easterly current velocities at HSB while ABS increased with high south-easterly, along-slope, current velocity at LSB (Figure 5.10F; Figure S5.8A & B). Cross-correlation showed ABS was weakly correlated with bottom current speed at HSB (R^2 = 0.34) and LSB (R^2 = 0.44). During the spring bloom, bottom chl-*a* concentration increased at strong south-easterly current velocities at HSB (Figure S5.10) and showed a periodic reoccurring signal (Figure S5.11A).

Temperature, chl-*a*, ABS, turbidity, all showed a reoccurring tidal signal, with higher peaks in spectral density for the semidiurnal periodicity at HSB than at LSB (Figure 5.7C). Ice cover seemed to affect the peak of chl-*a* concentration at the seafloor (Figure S5.11). However, both sites were located at the sea-ice border in the study area and had highly variable sea-ice coverage. Only during January coverage was above 70% at both sites. The Hudson Strait froze up in early December and opened again in early June. During the spring bloom, between the end of March and early May, sea-ice coverage tended to be higher at HSB than at LSB (Figure S5.11D).

Table 5.1 Summary statistics for the long-term near-bottom measurements. Values are given as mean ± standard deviation. HSB = high sponge biomass lander, LSB = low sponge biomass lander. ABS = acoustic backscatter signal.

Variable	HSB	LSB
u (eastward velocity; m s^{-1})	0.05 ± 0.22	-0.01 ± 0.09
v (northward velocity; m s^{-1})	-0.07 ± 0.16	-0.09 ± 0.11
w (vertical velocity; m s^{-1})	0.03 ± 0.05	0.02 ± 0.03
Bottom current speed (m s^{-1})	0.26 ± 0.14	0.14 ± 0.08
Temperature (°C)	3.70 ± 0.17	3.58 ± 0.17
Daily temperature variability (Δ°C d^{-1})	0.25 ± 0.16	0.17 ± 0.1
ABS (counts)	98.1 ± 9.8	96.6 ± 11.0
Chl-a concentration (µg L^{-1})	0.11 ± 0.03	0.08 ± 0.10
Turbidity (NTU)	0.20 ± 0.10	0.21 ± 0.27

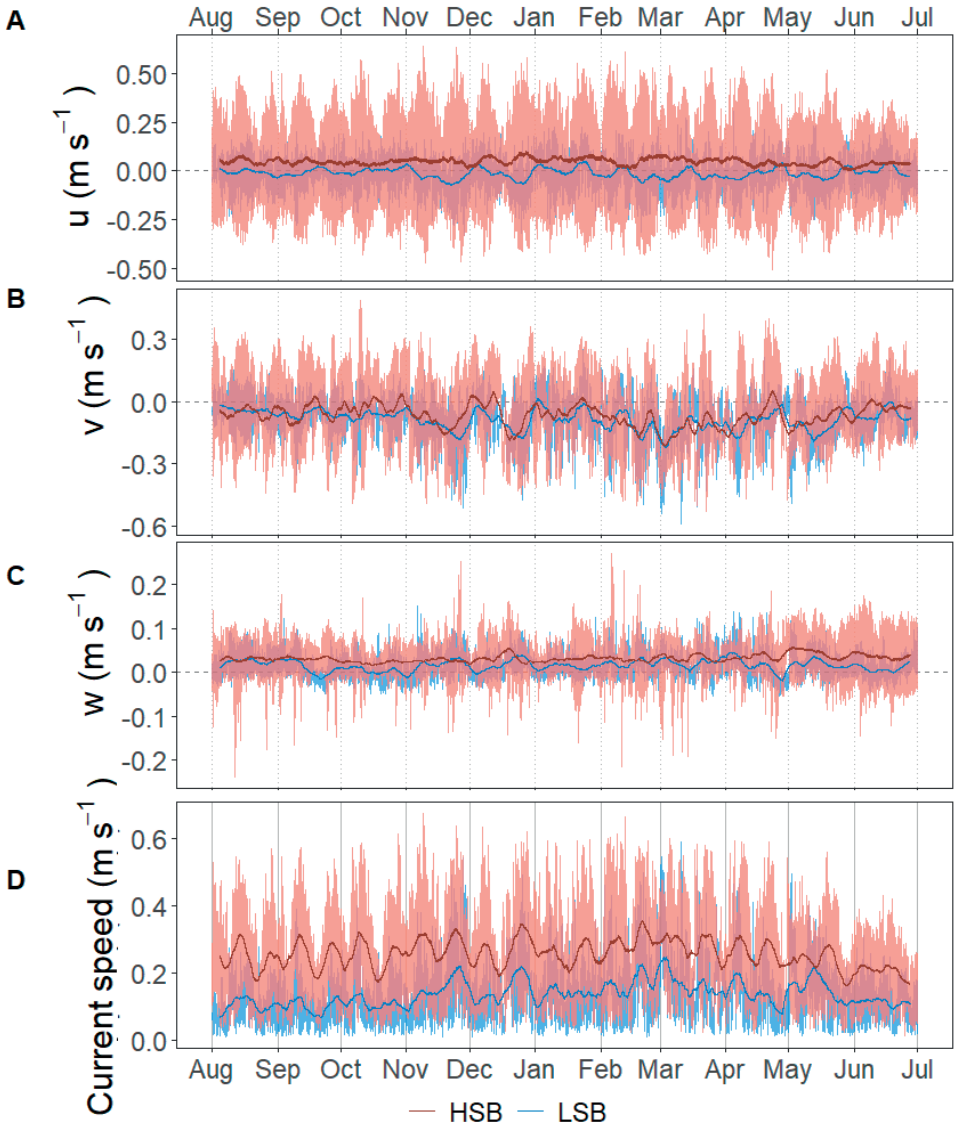

Figure 5.5 Time series of the flow velocities with eastward u velocity (A), northward v velocity (B), vertical w velocity (C), and bottom current speed (D). Plots show the hourly averaged data as transparent lines and the seven-day rolling means as solid lines

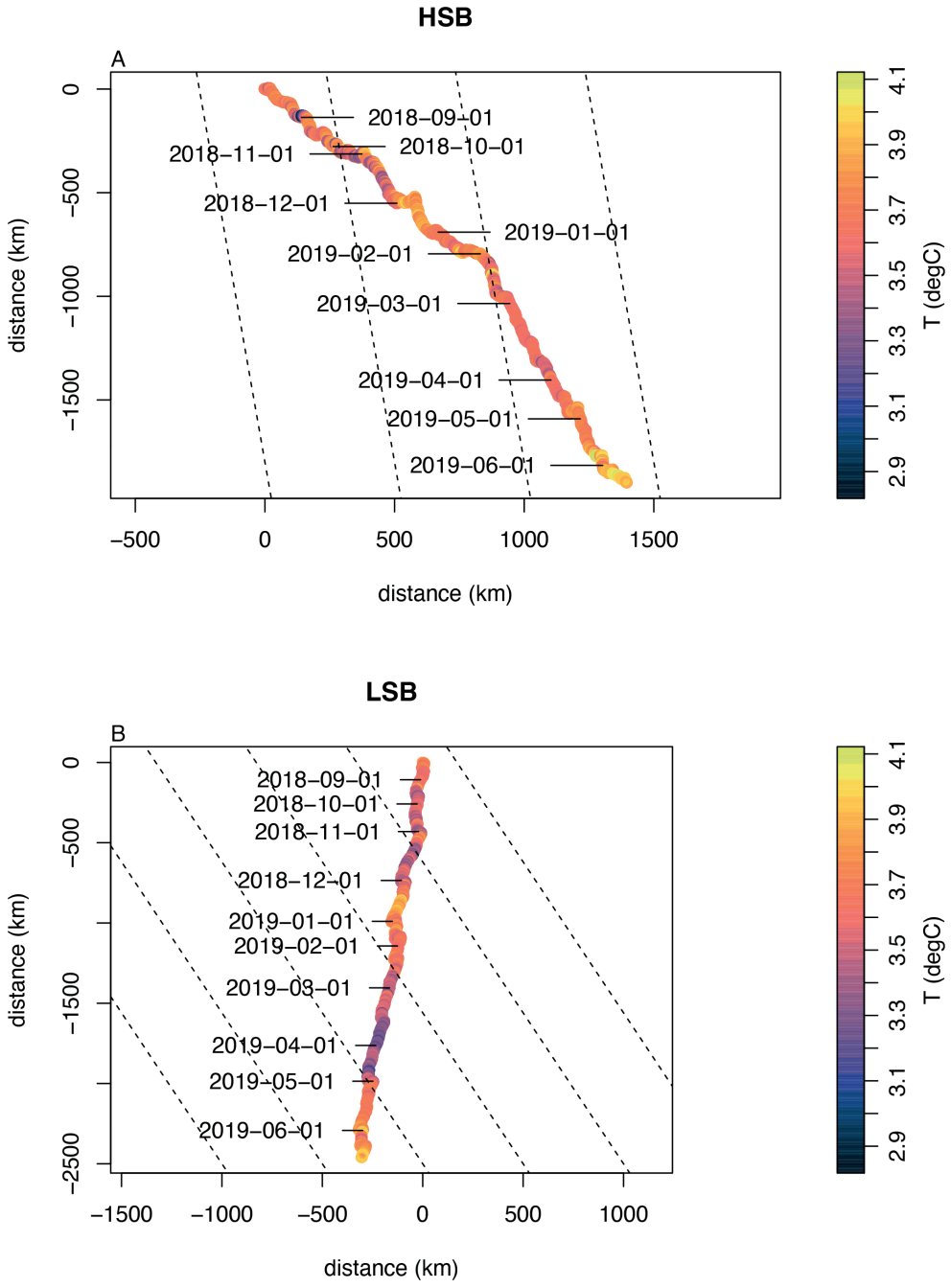

Figure 5.6 Progressive vector plots with temperature as colour variable for (A) the high-sponge biomass (HSB) lander and (B) the low sponge biomass (LSB) lander. The dotted lines indicate the along-slope direction at both lander sites

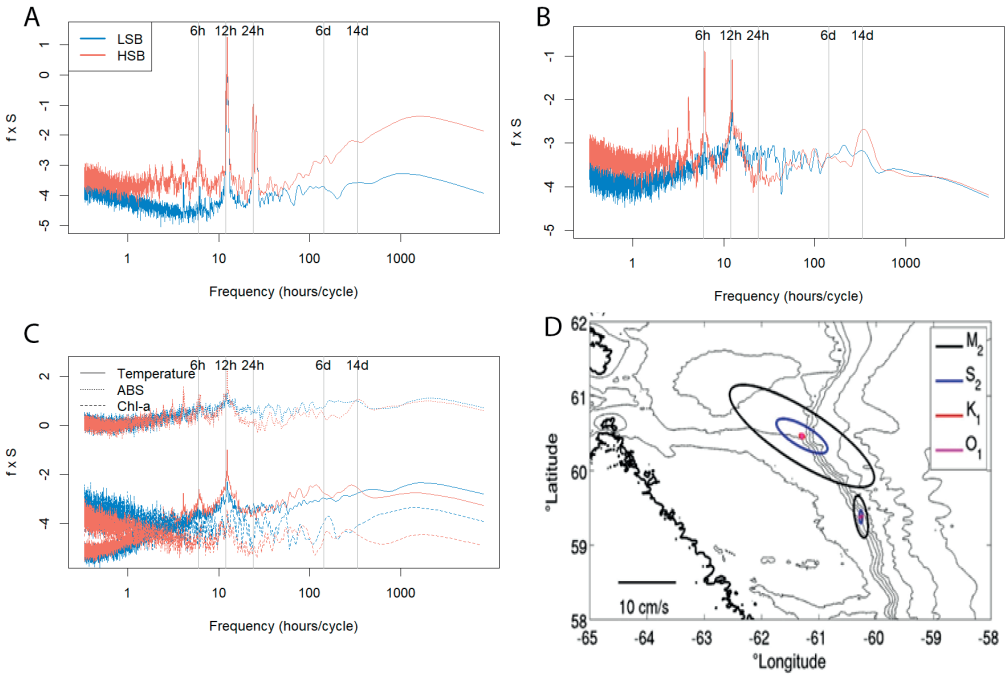

Figure 5.7 Variance preserving spectra for (A) pressure, (B) bottom current speed, (C) temperature, acoustic backscatter signal (ABS), and chl-a, and (D) resulting tidal current ellipses for the two dominant diurnal and semidiurnal tidal harmonics derived from the unfiltered ADCP velocities

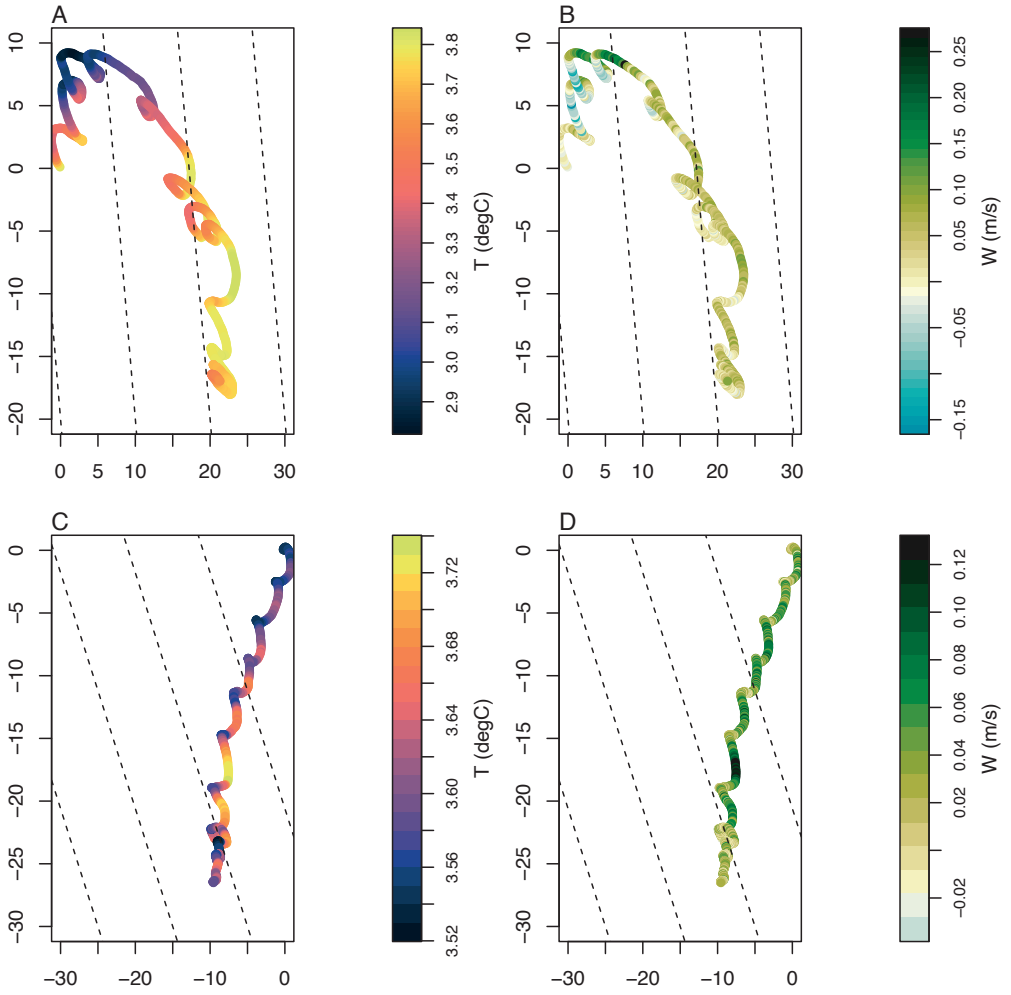

Figure 5.8 Progressive vector plot for 1 September to 7 September for the high-sponge biomass site, HSB (A, B) and low sponge biomass site, LSB (C, D), with temperature (A, C) and vertical velocity (C, D) as colour variable. The dotted line indicates the along-slope direction at both lander sites. X- and y-axes represent distance in km

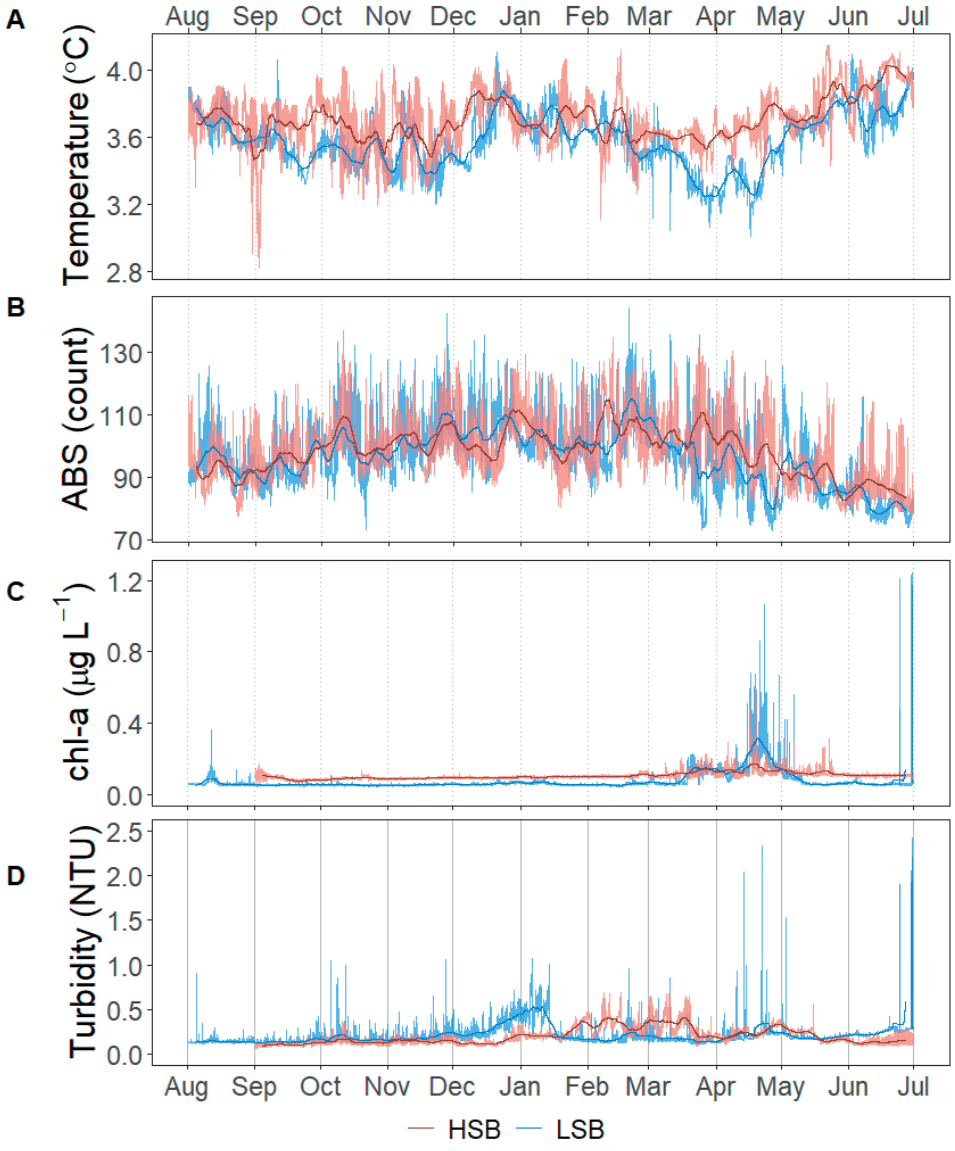

Figure 5.9 Time series for temperature in °C (A), acoustic backscatter (ABS) in arbitrary units (counts) (B), Chl-a concentration in µg L^{-1} (C), and turbidity in NTU (D). Plots C and D are limited on the y-axis to 1.25 µg L^{-1} and 2.5 NTU, respectively, for clarity. Chl-a and turbidity data without the Y-axis cut-offs are plotted in Figure S5.9

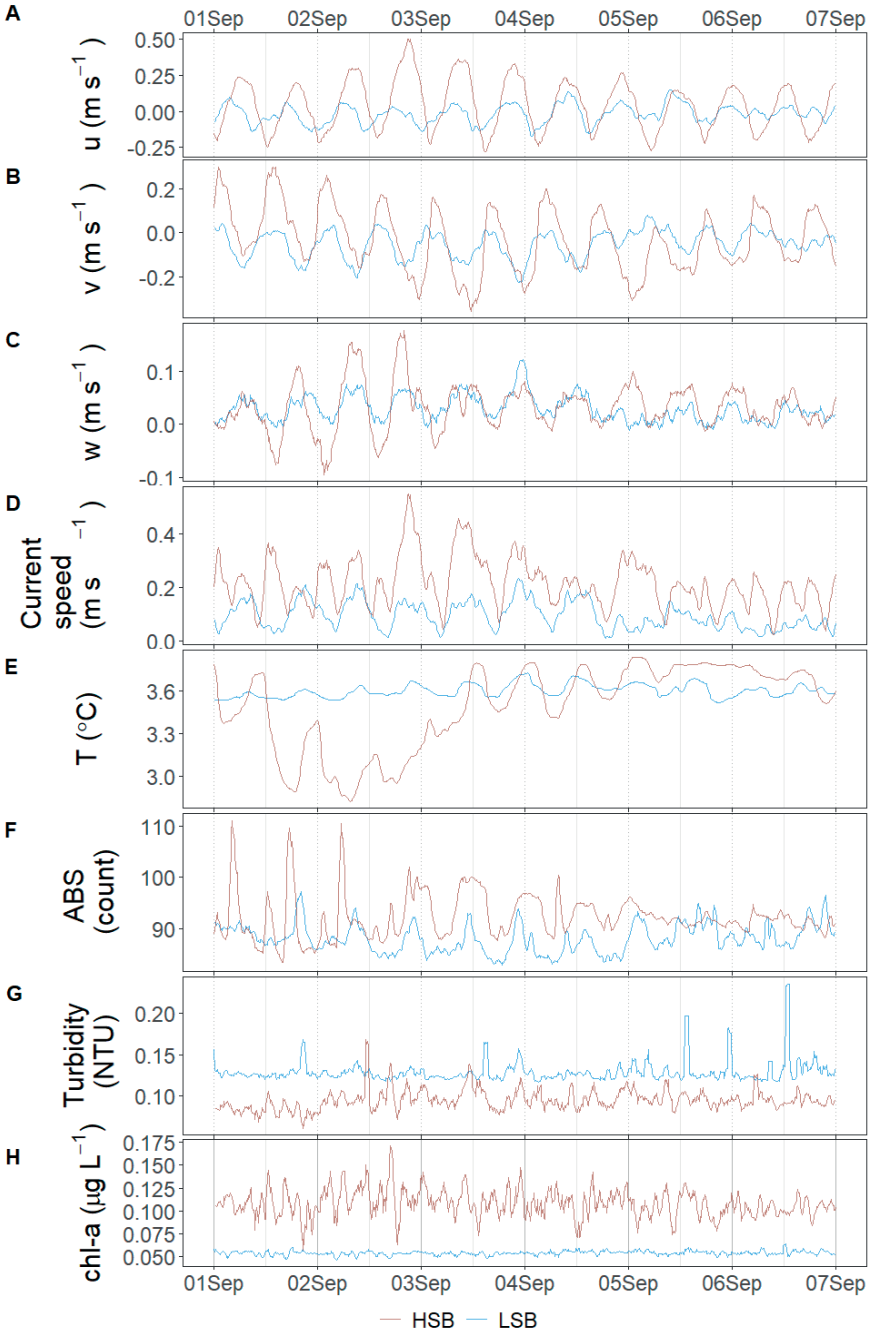

Figure 5.10 Expanded detail for the first week of September for the eastward velocity u (A), northward velocity v (B), vertical velocity (C), bottom current speed (D), temperature (E), acoustic backscatter signal (ABS; F), turbidity (G), and chl-a concentration (H)

Mass deposition and organic carbon fluxes

The average mass fluxes were higher at HSB (2.46 ± 1.76 g m^{-2} day^{-1}) than at LSB (1.43 ± 0.93 g m^{-2} day^{-1}), with highest fluxes in winter (October to April) at both sites and lower rates in spring. Average POC fluxes were also higher at HSB (3.07 ± 1.91 mmol C m^{-2} d^{-1}) than at LSB (1.91 ± 0.71 mmol C m^{-2} d^{-1}). Organic carbon content was highest in autumn/summer months at HSB and highest in autumn at LSB (data not shown). Average C:N ratios were lower at HSB (8.6 ± 3.2) than at LSB (10.8 ± 2.7) and were higher in winter and also in May 2018 (Figure 5.11C). The $\delta^{13}C$ ratios of trapped material were relatively enriched at HSB in winter and relatively enriched at LSB in summer (Figure 5.11D). The $\delta^{15}N$ of trapped material was comparable between sites, although slightly higher at LSB. Winter $\delta^{15}N$ values were higher than spring values, and at LSB the September and summer samples showed increased $\delta^{15}N$ (Figure 5.11E). The lipid flux was slightly higher at LSB, with low values in winter and peak values during the spring bloom (Figure 5.11F). Unsaturated alcohols comprised the largest fraction of lipids at LSB, especially in autumn and winter (S5.12B). Peak lipid flux in April consisted of 25% polyunsaturated fatty acids (PUFAs) at HSB (Figure S5.12C). Sterols made up the largest fraction of total lipids at HSB and LSB in May (Figure S5.12D). The sterol fraction was lower in spring at both sites. Swimmers were found in the sediment trap bottles, especially in the autumn months at LSB. These consisted mostly of copepods (e.g., *Calanus* sp.), mysids (e.g., *Boreomysis* sp.), amphipods (e.g., Eusiridae) and chaetognaths (i.e., arrow worms). Numbers of trapped swimmers were lowest during winter at both sites. In addition, several large sponge spicules were found in the bottles at HSB, but not at LSB.

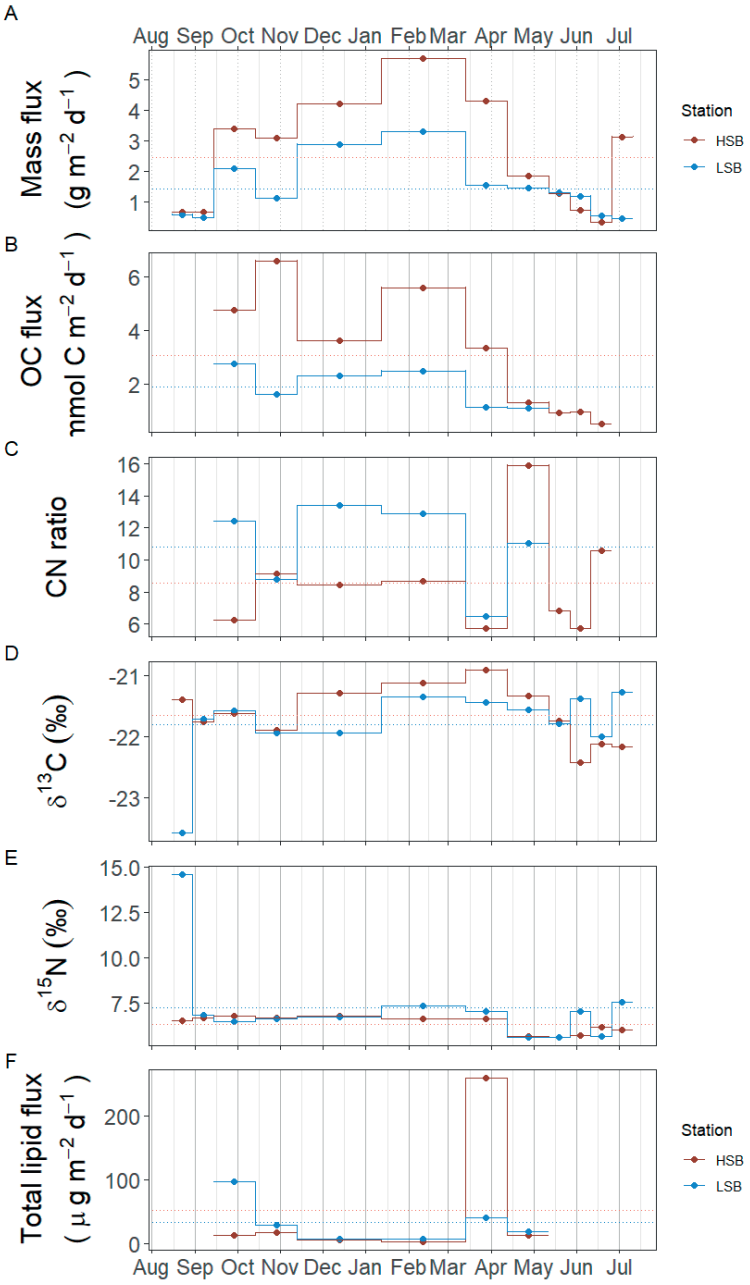

Figure 5.11 Sediment trap content from the two benthic landers. HSB = high sponge biomass lander, LSB = low sponge biomass lander. A) mass flux in g $m^{-2}d^{-1}$, B) organic carbon flux in mmol C m^{-2} d^{-1}, C) molar C:N ratio of trapped material, D) $\delta^{13}C$ of trapped material, E) $\delta^{15}N$ of trapped material, F) total lipid flux in µg m^{-2} d^{-1}

$\delta^{13}C$ and $\delta^{15}N$ isotopic ratios of benthic fauna and trapped material

The massive sponge *Geodia* spp. sampled at HSB showed a distinct isotopic signal compared to the other benthic organisms, with a relatively enriched $\delta^{13}C$ (-18.55 ± 0.17 ‰) and a low $\delta^{15}N$ (8.24 ± 0.16 ‰; Figure 5.12). The gorgonian coral *Primnoa resedaeformis* had a $\delta^{13}C$ (-21.19 ± 0.59 ‰) and a $\delta^{15}N$ (10.54 ± 0.33 ‰), values that indicated a lower trophic level than the Decapoda sp. ($\delta^{13}C$: -20.48 ± 0.31 ‰, and $\delta^{15}N$: 11.97 ± 0.43 ‰) and the glass sponge *Asconema* sp. ($\delta^{13}C$: -20.27 ± 0.36 ‰, and $\delta^{15}N$: 12.57 ± 0.31 ‰). The sponge *Mycale* sp., sampled at LSB, had a high $\delta^{15}N$ isotopic ratio (13.05 ± 0.41 ‰), and a $\delta^{13}C$ ratio of -19.47 ± 0.06 ‰. Sediment trap samples had the lowest $\delta^{15}N$ and $\delta^{13}C$ isotopic ratios, with only small differences between HSB and LSB (Figure 5.11D & E; Figure 5.12).

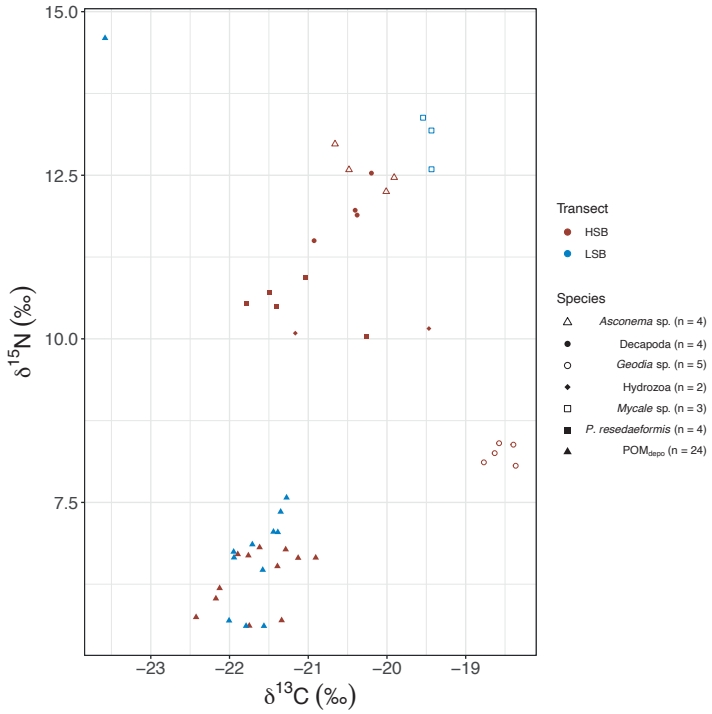

Figure 5.12 Carbon and nitrogen isotope biplots of megafauna and sediment trap samples. HSB = high sponge biomass, LSB = low sponge biomass

Discussion

In this study, hydrodynamic- and environmental conditions and food availability were compared at two contrasting high- and low sponge biomass sites along the northern Labrador shelf-break. More specifically, the aim of this study was to compare differences between the two sites in terms of (i) seawater properties, (ii) bottom currents and environmental conditions, including seasonal variations over the course of a year, and (iii) organic matter supply and uptake by benthic macrofauna.

Hydrography and bottom nutrients on the northern Labrador Shelf and Slope

The northern Labrador Shelf and Labrador Slope is known to be subject to strong tidal forcing which causes vertical mixing, high bottom current speeds (Griffiths et al., 1981; Drinkwater and Jones, 1987), and reduced stratification compared to the more northerly Baffin Island Shelf (Lazier 1982; Sutcliffe et al. 1983; Drinkwater and Harding 2001). Our CTD transects are similar to earlier cross-shelf transects (Petrie et al., 1988; Fissel and Lemon, 1991; Drinkwater and Harding, 2001), and captured all important hydrographic features described in previous studies in this area, including the fresh Arctic and Hudson Strait outflows, the cold intermediate layer on the Labrador Shelf and Slope, the West Greenland Current extension, the underlying partially diluted core of warmer and saltier Irminger Water, and at the deepest point, Labrador Sea Water (Figure 5.3). Hudson Strait outflow water and Arctic Water heading south from the Davis Strait are most prominent at the shelf stations of the HSB transect, and their signal is diluted moving offshore from the Hudson Strait. Bottom temperatures are well correlated at the two sites, with a time lag of five days at the LSB site. This time lag corresponds to an along slope velocity of ±0.3 m s^{-1}, which is within range of the mean bottom current speeds measured at HSB (0.25 m s^{-1}) and on the Labrador Slope (0.11 – 0.23 m s^{-1}; Lazier and Wright, 1993). This also agrees with earlier studies on the Labrador Shelf that found a connection between the Hudson Strait outflow strength and the southern Labrador Shelf water salinity (Sutcliffe et al., 1983; Myers et al., 1990).

Both the LSB and HSB lander sites show higher nutrient concentrations in the bottom water compared with the other shelf/deep CTD stations, and this difference was more pronounced at the HSB site. These observations are thought to be related to the sources of the bottom water and circulation. Thus, intermediate water flows from Baffin Bay via the Davis Strait southward along the continental slope (Curry et al., 2014). This water mass, referred to as Baffin Bay Water (BBW), contains higher nutrient concentrations (e.g., 41.6 ± 25.5 µM $Si(OH)_4$, 18.5 ± 2.6 µM NO_3^-; Sherwood et al., 2021) due to *in situ* remin-

eralization of deep water circulating in the Baffin Bay basin (Jones et al., 1984; Tremblay et al., 2002; Lehmann et al., 2019). BBW mixes with water masses on the Labrador Shelf and Slope and Hudson Strait outflow water while flowing southward along the Labrador Slope, resulting in lower nutrient concentrations at the LSB compared to the HSB (Figure S5.4). The absence of high nutrient concentrations at the shelf/deep CTD station at both sites supports this interpretation. The elevated nutrient concentrations could be beneficial for benthic organisms, for example, deep-sea sponges, which readily take up the silicic acid needed for spicule formation and skeletal growth (Whitney et al., 2005; Maldonado et al., 2011, 2020b; López-Acosta et al., 2016). Published kinetic uptake curves, describing silicic acid uptake rate *versus* concentration, suggests the concentration at the HSB lander (13.6 µM) compared to LSB shelf (9.3 µM), could increase silicic acid uptake rates of glass sponges by 39% for *Axinella* spp. and by 40% for *V. pourtalesii* (Maldonado et al., 2011, 2020b). Furthermore, elevated silicic acid concentrations on the spatial scale of kilometres are thought to allow the persistence of sponge grounds and build-up of (glass) sponge biomass over long timescales (Whitney et al., 2005; Maldonado et al., 2020a). It has also been suggested, however, that biogenic silica efflux from the sediments could cause higher bottom water silicic acid (Maldonado et al., 2020a), but this is unlikely for our study sites, because such an efflux would be quickly advected away by the high bottom tidal currents, while nutrient concentrations were elevated up to 100 metres above the bottom (Figure 5.4B & C). Overall, our study shows that bottom water between the LSB and HSB sites are connected, with higher nutrient availability at the HSB station, linked to large-scale circulation patterns.

Bottom hydrodynamics and environmental conditions over a year

This study provides the first concurrent long-term measurements of hydrodynamic- and environmental conditions at a high- and low sponge biomass site. Our measurements show high bottom currents at both sites with distinct differences in tidal dynamics. Tidal ellipses (northeast-southwest for HSB, north-south for LSB) align well with bathymetry and the OTIS modelled barotropic tide (Figure S5.13) and the tidal amplitude is around five times higher at HSB than at LSB. This outcome is contrary to White (2003) who measured high current speeds in areas where no sponges were recorded, and vice versa, at the Porcupine Sea Bight. Although bottom currents are higher at HSB than at LSB (Table 5.1), the bottom currents at LSB are still comparable with current speeds found at other sponge grounds on the Scotian Shelf (mean: 0.12 m s^{-1}; Hanz et al., 2021a) and on the Arctic mid-Atlantic ridge (mean: 0.14 m s^{-1}; Hanz et al., 2021b). However, the high bottom tidal currents seem to have a more pronounced effect on the environmental conditions at HSB compared to LSB.

Bottom water temperatures at both sites (3.5 – 4 °C) are within range of values reported for boreal deep-sea sponge grounds previously (<0 – 8 °C; Kutti et al., 2013; Howell et al., 2016; Strand et al., 2017; Hanz et al., 2021b, 2021a). From a biological point of view, fluctuations in temperature over a year were in general low (<1 °C) and unlikely to affect the sponge distribution in the study area, contrary to a correlation between sponge grounds and high variation in temperature reported elsewhere (Davison et al., 2019). However, temperature fluctuations in bottom water reveal clear differences between the two sites in terms of hydrography. Tidal currents have a distinct effect on bottom temperature at both sites, and this effect depends on the season. For example, in the first week of September at HSB, the bottom temperature decreases after water moves in a northwest direction and increases after the current becomes southeastly. As the lander was placed ~500 m from the shelf break (Figure S5.2C & D), and bottom water could be transported ~5 km in the northeastly direction in one semidiurnal tidal cycle (Figure 5.8A), this means that colder bottom water is transported on to the Labrador Shelf from beyond the shelf break to the HSB lander site. Furthermore, the tidal currents in the southeastly direction bring warmer bottom water from the Labrador Shelf to the HSB lander (Figure 5.8A). Colder bottom water temperatures were also observed when water moved upslope at LSB (Figure 5.8C). Therefore, although higher variability in bottom water temperature has been attributed to the presence of internal waves for other sponge grounds (Roberts et al., 2018; Davison et al., 2019), we attribute the variability in our study area to tidal-induced cross-slope transport of bottom water. Nevertheless, high downward velocities (>0.2 m s^{-1}), which occurred while water was moving in a southeastly direction sometimes caused a drop in bottom temperature at HSB (Figure S5.7), which suggests that colder water from shallower depths mixes with bottom water.

High tidally induced bottom currents can benefit the benthic community at the HSB site in various ways. First, passive suspension feeders as the gorgonian *P. resedaeformis* benefit from high horizontal currents through an increased particulate organic matter flux (Shimeta and Jumars, 1991) and sponges could benefit from an increased water flow rate through their body plan (Vogel, 1977), thereby increasing food availability. Second, resuspension caused by high bottom current speeds could enhance organic matter availability in the benthic boundary layer and prevent smothering of sponges by sedimentation (Roberts et al., 2018). Here, high along-slope bottom currents at both sites were associated with increased ABS and turbidity, indicative of resuspension (Figure S5.8). The substrate at HSB consisted mostly of pebbles, cobbles, and boulders (Dinn et al., 2020) and a qualitative assessment of the sediment type at LSB suggested the dominance of muddy soft sediment (Coté et al., 2019; J. Vad, *pers. com.*). As higher bottom currents would increase bed shear stress and thereby enhance resuspension (Lesht, 1979; Jones et al., 1998), we argue that fine material is resuspended at HSB before its deposition and accumulation on the seafloor. This increases availability of organic matter to benthic suspension feeders in

the benthic boundary layer and prevent smothering. Resuspension has also been linked to high sponge biomass, although the mechanisms behind this link are still unclear (Davison et al., 2019). Third, the interaction of high bottom currents with rough topography causes turbulence and mixing of bottom waters (Witte et al., 1997, 97; Leys et al., 2011; Culwick et al., 2020). As the substrate is likely rougher and bottom currents are higher at HSB than at LSB, the bottom water probably experiences more intense mixing and turbulence at HSB. Finally, periodic supply of fresh phytoplankton derived material during the spring bloom (Figure S5.10, Figure S5.11) increases the food availability of passive suspension feeders living on the sponge grounds. In short, the stronger tidal currents at HSB enhance bottom water mixing which replenishes oxygen, dissolved organic matter, POM, and (inorganic) nutrients to the benthic boundary layer, and thereby increases food supply to benthic fauna (Davison et al., 2019; Hanz et al., 2021b, 2021a).

Primary production and benthic-pelagic coupling

The Hudson Strait outflow water is known to increase nutrient concentrations in the surface waters on the northern Labrador Shelf (Kollmeyer et al., 1967; Sutcliffe et al., 1983; Drinkwater and Harding, 2001). A thermal front, associated with the offshore branch of the Labrador Current, is located along the 1,000 m isobath of the Labrador slope/shelf (Cyr and Larouche, 2015). The increased nutrient supply support high primary productivity in an area extending from the Hudson Strait to the southern Labrador Shelf, bounded by the thermal front associated with the 1,000 m isobath (Frajka-Williams et al., 2009; Frajka-Williams and Rhines, 2010; Cyr and Larouche, 2015). Our CTD profiles show elevated chl-*a* concentrations in the CIL (~150 m depth), as was observed by Frajka-Williams et al., (2009). The fact that primary production rates are comparable above the two lander station sites (Frajka-Williams and Rhines, 2010), suggests that differences in primary production alone are insufficient to explain the differences sponge biomass between regions. Furthermore, studies elsewhere in the Canadian Arctic have shown that benthic biomass is explained not only by surface productivity but also by local hydrodynamics and benthic-pelagic coupling (Thomson, 1982; Grebmeier and Barry, 1991; Roy et al., 2014).

The lander fluorescence observations showed the arrival of relatively fresh phyto-detritus at the seafloor three months before the start of the phytoplankton bloom (Fuentes-Yaco et al., 2007; Frajka-Williams and Rhines, 2010). We suggest that this results from phytoplankton growth that had already started in early March in the Hudson Strait outflow (Harrison et al., 2013). At this time, the water column was still relatively cold and poorly stratified, allowing for relatively high export, which resulted in fluorescent material transported towards the seafloor at each semidiurnal tidal cycle (Figure S5.11B). Sea ice retreat in mid-April relaxed light limitation and further stimulated primary production

(Carmack et al., 2004), explaining the fluorescent material peaks at both landers at this time. In summer, there appears to be a decoupling between high surface primary production (Frajka-Williams and Rhines, 2010) and low chl-*a* concentration on the seafloor (this study), likely due to enhanced stratification and intense zooplankton grazing (Rivkin et al., 1996; Turner, 2015). Strong tidal mixing, including a strong neap-spring tidal cycle, at HSB could inhibit water column stratification for a longer period than at LSB, thereby extending the period of fluorescent material deposition at the seafloor (Sharples et al., 2006; Sharples, 2008; this study). Our findings suggest strong benthic-pelagic coupling started weeks before the peak of the phytoplankton bloom, supplying fresh fluorescent material to the seafloor in spring for a period of weeks to months. Since the timing of phytoplankton bloom for high-latitude seas is shifting to earlier in the year due to rising temperatures and earlier sea-ice retreat (Edwards and Richardson, 2004; Wu et al., 2007; Hunter-Cevera et al., 2016), and since deep-sea sessile organisms, such as cold-water corals and deep-sea sponges demonstrate seasonality in their phenology (Leys and Lauzon, 1998; Maldonado, 2011; Maier et al., 2020a), the early arrival of phytoplankton-derived material could have consequences for their overall fitness and survival. Nevertheless, the effect of a shift in spring bloom timing for benthic suspension feeders, including deep-sea sponges, remains unknown.

Recent ABS measurements reveal a layer of increased 300 kHz backscatter along the northern Labrador Shelf, indictive of high abundance of micronekton and macrozooplankton (Chawarski et al., 2022). Earlier studies showed a high zooplankton biomass on the Newfoundland Shelf from July onwards (Head et al., 2003, 2013). In our traps the highest flux of unsaturated alcohols, a marker for zooplankton material (Dalsgaard et al., 2003), and the highest numbers of swimmers were in summer and autumn. During the spring bloom, trapped material at LSB had the highest relative amount of unsaturated alcohols while at HSB the level of PUFAs, markers for phytoplankton derived-material, was highest (Dalsgaard et al., 2003). As well, our observations suggest that the number of trapped swimmers was higher at LSB than at HSB. These results are consistent with the hypothesis that zooplankton biomass is high over the northern Labrador Shelf (Saglek Bank) and that zooplankton are transported by the southerly current along the Labrador Shelf together with the high phytoplankton biomass plume (Sutcliffe et al., 1983; Drinkwater and Harding, 2001). Overall, there was a larger fraction of zooplankton marker lipids in trapped material at LSB, which implies that zooplankton play a more important role in benthic-pelagic coupling at LSB than at HSB.

Organic matter cycling at the seafloor

Organic matter fluxes were higher at HSB than at LSB. Overall, deposition was highest during the winter months and consisted of more degraded material than during summer, indicated by high C:N ratios, high $\delta^{15}N$ ratios, and low fluorescence. This increased deposition in winter is likely resuspended material, as bottom current speeds were also higher. The C:N ratio of deposited matter was higher at LSB (~13) compared to HSB (~8), indicating the material was more degraded at LSB. Hanz et al. (2021a, 2021b) also found higher mass and carbon fluxes during winter months and low carbon fluxes when the spring/summer phytoplankton bloom arrived. They attributed this to the fact that there was more degraded and resuspended material present in winter. Data concerning mass fluxes from sponge grounds remain scarce, but the fluxes measured here (HSB 2.46 ± 1.76 g m^{-2} day^{-1}, LSB: 1.43 ± 0.93 g m^{-2} day^{-1}) were between those of a *Vazella pourtalesii* sponge ground on the Scotian Shelf (3.17 ± 3.42 g m^{-2} day^{-1}; Hanz et al., 2021a) and a sponge ground on the Arctic mid-Atlantic ridge (0.03 – 0.30 g m^{-2} day^{-1}; Hanz et al., 2021b). Overall, our data suggest organic matter deposition fluxes are higher at HSB compared to LSB, and that the organic matter is of higher quality. The organic carbon fluxes (HSB: 3.07 ± 1.91 mmol C m^{-2} d^{-1}; LSB: 1.91 ± 0.71 mmol C m^{-2} d^{-1}) reported in our study are considerably lower than those of a more shallow (150 – 250 m depth) *V. pourtalesii* sponge ground on the Scotian Shelf (8.3 mmol C m^{-2} d^{-1}; Hanz et al., 2021a), but high compared to an Arctic mid-Atlantic ridge sponge ground (peak of 1.6 mmol C m^{-2} d^{-1}; Hanz et al., 2021b). The higher organic matter deposition rate and relative fresher material at HSB compared to LSB are likely related to its shallower position on the shelf and the more dynamic water column.

No estimates of organic carbon utilization by the sponge grounds on the Northern Labrador Shelf were available for comparison with these sediment trap data at the time of writing. Here, we estimate the organic matter requirements of the sponge grounds from published respiration rates and biomass estimates obtained from bottom trawls using a depth stratified random sampling design. Bottom-trawl estimates gave a biomass of 35 g WW sponge m^{-2} at HSB and 0.01 g WW sponge m^{-2} at LSB (Lirette and Kenchington, pers. com.). Assuming a sponge respiration rate of 0.010 mmol O_2 g^{-1} WW d^{-1} (measured at 6 - 9 °C; Kutti et al., 2013; Leys et al., 2018; Bart et al., 2021), which corresponds to a benthic respiration rate of 0.35 mmol O_2 m^{-2} d^{-1}. Image analysis from ROV transects suggested higher biomass levels: 500 g sponge WW m^{-2} at HSB and 50 g sponge WW m^{-2} at LSB (Wolff et al., 2020), equivalent to benthic respiration rates of 5 mmol O_2 m^{-2} d^{-1} and 0.5 mmol O_2 m^{-2} d^{-1} for HSB and LSB, respectively. The large differences in sponge biomass estimates between the trawl and ROV methods are surprising, and we cautiously attribute this to: 1) the different spatial scales over which both methods work combined with spatial heterogeneity within the area, 2) under-sampling of sponges by bottom trawling (Wassenberg et al., 2002), and 3) potential bias in ROV imaging, as sampling design in ROV transects

is usually not randomized. The high values derived from ROV transects are more in line with earlier observed sponge community benthic respiration values in Norway (Kutti et al., 2013; Cathalot et al., 2015). As bottom trawling data are the only sponge biomass estimates available on a shelf-wide scale, we consider the trawl-based respiration rates to be the most representative for sponge respiration on the northern Labrador Shelf, with the ROV-based respiration rates giving upper bounds.

Food sources of benthic macrofauna

Although the sample size was limited, the stable isotope data reveal interesting patterns of organic matter utilization by the benthic community. The gorgonian coral *P. resedaeformis* is found 3.4 ‰ $\delta^{15}N$ or one trophic level (Fry, 2006) above the sediment trap material and likely feeds on sinking organic matter, confirming previous observations (Sherwood et al., 2005, 2008). Sponges can generally be classified into two groups based on their associated microbial fauna, those with high microbial abundance (HMA) or those with low microbial abundance (LMA; Vacelet and Donadey, 1977). *Geodia* spp. can occur in high abundance and biomass on sponge grounds (Kutti et al., 2013). These sponges are considered HMA (Radax et al., 2012) and feed mostly on dissolved organic matter with additional particulate sources such as bacterioplankton (Bart et al., 2021). Many hexactinellidae that can form sponge grounds, for instance *Vazella pourtalessii* and *Aphrocallistes vastus*, are considered LMA sponges and feed mostly on bacterioplankton (Kahn et al., 2015). The high $\delta^{15}N$ isotopic ratios for the sponges *Asconema* spp. (12.6 ± 0.3 ‰ $\delta^{15}N$) and *Mycale* spp. (13.1 ± 0.4 ‰ $\delta^{15}N$), has been observed previously for LMA sponges (Iken et al., 2001; Polunin;, 2001; Kahn et al., 2018). Deep-sea LMA sponges typically have elevated $\delta^{15}N$ values in the benthic food web (Kahn et al., 2018), a phenomenon that is still poorly understood. Possible explanations could be selective feeding on $\delta^{15}N$-rich bacteria (Wilkinson et al., 1984), feeding on resuspended benthic bacteria (Kahn et al., 2018), or nitrogen cycling within the sponge holobiont (Rooks et al., 2020). Interestingly, the HMA massive sponge *Geodia* sp. has distinct $\delta^{13}C$ *and* $\delta^{15}N$ values, indicating different feeding or metabolic strategies. Recent research on *Geodia baretti* has indeed demonstrated that these sponges rely for a large part on DOM for their metabolic requirements (Bart et al., 2021; de Kluijver et al., 2021). In this study, *Geodia* spp. (8.2 ± 0.2 ‰ $\delta^{15}N$) was one trophic level higher than oceanic DOM $\delta^{15}N$ (~5 ‰; Benner et al., 2005; Sigman et al., 2009) and $\delta^{15}N\text{-}NO_3^-$ (~5‰; Sigman et al., 2009; Sherwood et al., 2021), constraining our ability to distinguish between DOM and NO_3^- (by i.e., denitrification; Hoffmann et al., 2009) as potential nitrogen sources. The $\delta^{13}C$ value of *Geodia* spp. (-18.4 ± 0.17 ‰ $\delta^{13}C$) is ±3.5‰ higher than bottom water $\delta^{13}C$-DOC values on the Labrador Shelf (Barber et al., 2017), i.e. more than four times higher than the expected 0.8‰ $\delta^{13}C$ step per trophic level

(Vander Zanden and Rasmussen, 2001). Alternatively, *Geodia* spp. could capitalize on DIC via their symbionts, as recently observed in Arctic *Geodia* spp. assemblages (Morganti et al., 2022) and other deep-sea sponges (van Duyl et al., 2020). Even limited chemoautotrophic assimilation of high δ^{13}C-DIC (~0 ‰ δ^{13}C) could explain the high δ^{13}C values of *Geodia* spp. These results indicate that passive suspension feeders benefit from high tidal currents through an increased particulate organic matter flux (Shimeta and Jumars, 1991), whereas sponges likely benefit from replenishment of nutrients, oxygen, and dissolved organic matter (Schläppy et al., 2010).

Conclusion

This study investigated the hydrodynamic- and environmental conditions at two contrasting high- and low biomass sponge grounds on the northern Labrador Shelf. We recorded strong tidal currents at the high sponge biomass site throughout the year, which is also reflected in tidal periodicity of environmental conditions. The high tidal currents increase the flux of available food resources to the benthic community. High nutrient concentrations were found at the high sponge biomass site, which were associated with the presence of Baffin Bay water and therefore related to large scale circulation patterns. The Northern Labrador Shelf exhibits tight benthic-pelagic coupling during spring, and high primary production alone seems to be a poor predictor for sponge biomass in this area. Intense vertical mixing at the high sponge biomass site extends the period of benthic-pelagic coupling by several months. High currents benefit the benthic community by increasing food availability and replenishing nutrients, oxygen, and dissolved organic matter in bottom waters.

Supplementary material *Chapter 5*

Tables

Table S5.1 Overview of lander deployment and CTD casts

station	instrument	date/period	latitude	longitude	depth
HSB_bl	benthic_lander	27-7-2018 to 2-7-2019	60.47	-61.29	410
LSB_bl	benthic_lander	27-7-2018 to 1-7-2019	59.38	-60.28	558
HSB_ctd1	CTD	2018-08-03 07:37:08	60.47	-59.26	2428
HSB_ctd2	CTD	2018-08-02 17:21:58	60.47	-60.38	1877
HSB_ctd3	CTD	2018-07-30 15:27:05	60.47	-61.30	391
HSB_ctd4	CTD	2018-07-30 07:31:07	60.46	-62.12	359
HSB_ctd5	CTD	2018-07-27 19:41:58	60.40	-62.90	289
LSB_ctd1	CTD	2018-07-29 04:30:19	59.53	-58.64	2563
LSB_ctd2	CTD	2018-07-28 23:25:52	59.48	-59.45	1938
LSB_ctd3	CTD	2018-07-28 09:52:11	59.38	-60.27	608
LSB_ctd4	CTD	2018-07-28 06:12:07	59.31	-61.02	192
LSB_ctd5	CTD	2018-07-28 03:10:24	59.22	-61.83	138

Table S5.2 Overview of rock dredge transects. HSB = high sponge biomass site, LSB = low sponge biomass site, (Coté et al., 2019)

Station Name	Start Lat	Start Long	End Lat	End Long	Logged bottom depth (m)	Time at bottom (min)	Length of cable out (m)	Max vessel speed (knots)	Comments
LSB_rd	59.38	-60.27	59.37	-60.29	552	10	1500	1	NA
HSB_rd	60.47	-61.28	60.48	-61.30	404	20	507	2	Small catch

Figures

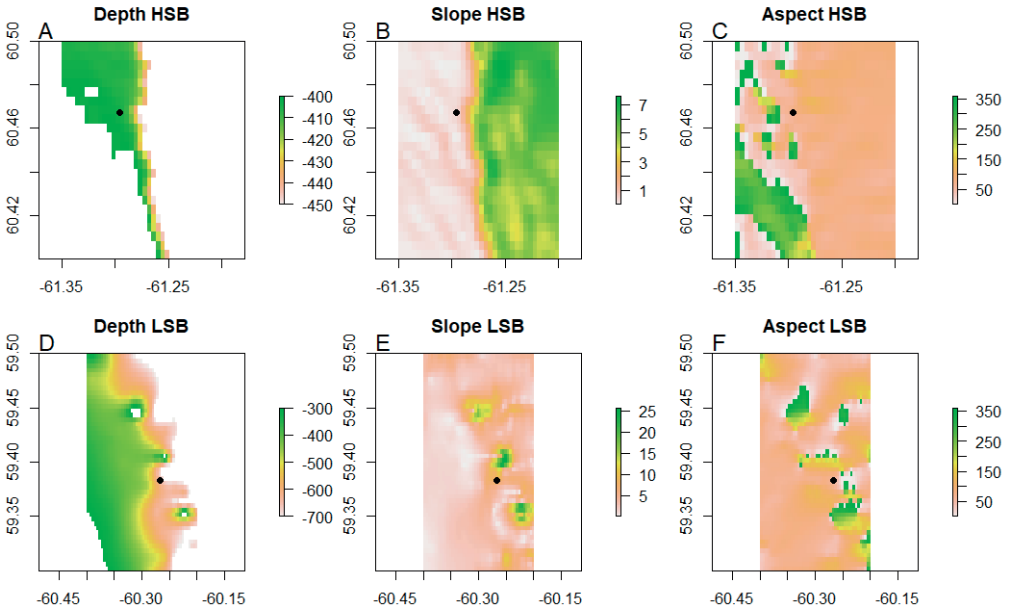

Figure S5.1 bathymetric characteristics of the areas around the high sponge biomass (HSB; A, B, C) and low sponge biomass (LSB; D, E, F) landers, with depth in metres (A,D), slope angle in degrees (B, E), and slope aspect in degrees (C, F). Note the different colour scales. Locations of lander is indicated by black dot

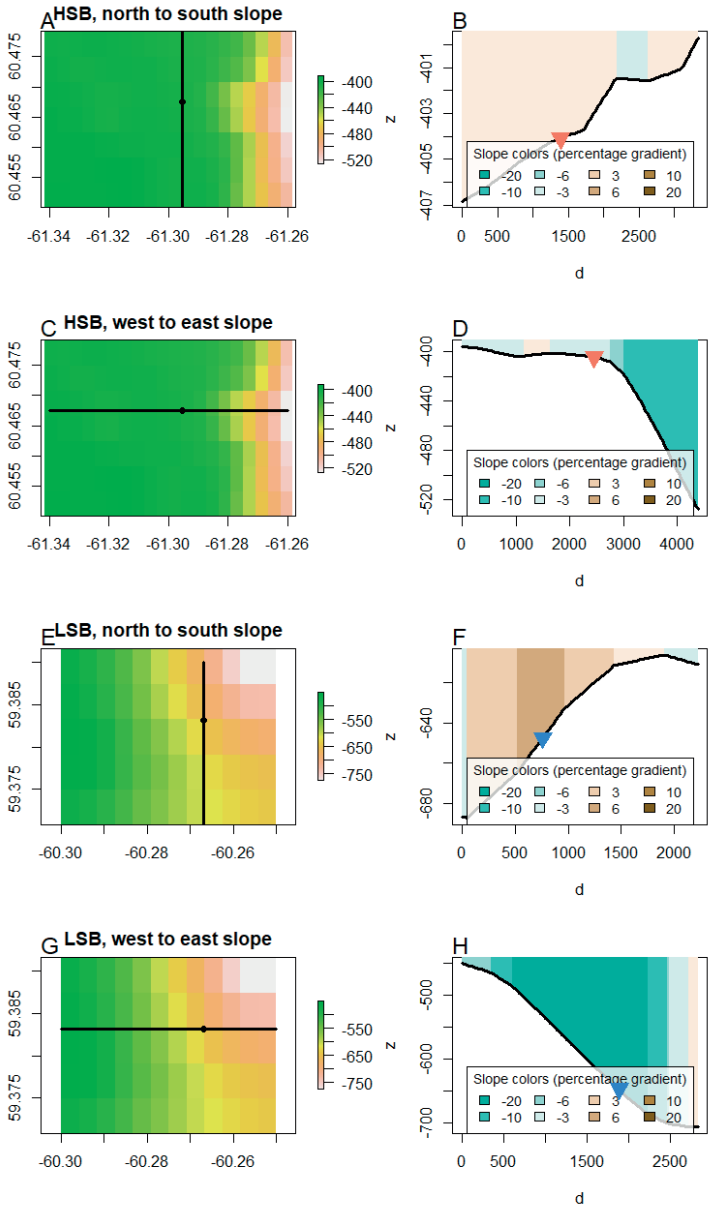

Figure S5.2 slope angle and direction in north- to-south and west-to-east direction close to the high sponge biomass (HSB) and low sponge biomass (LSB) landers. The left column shows the depth around the landers (A, C, E, G), and the transect line for which the slope is calculated and plotted. The right column shows the slope along the black line from either north to south (B, F), or west to east (D, H), blue colours represent downhill angle and brown colours an uphill angle, z = depth in metres, d = distance from start transect (north or west) in metres. Landers are indicated by black dots in the left column, and coloured triangles in the right column. Note the different colour scales for plots in the left column and different y-axis scale for the plots in the right column

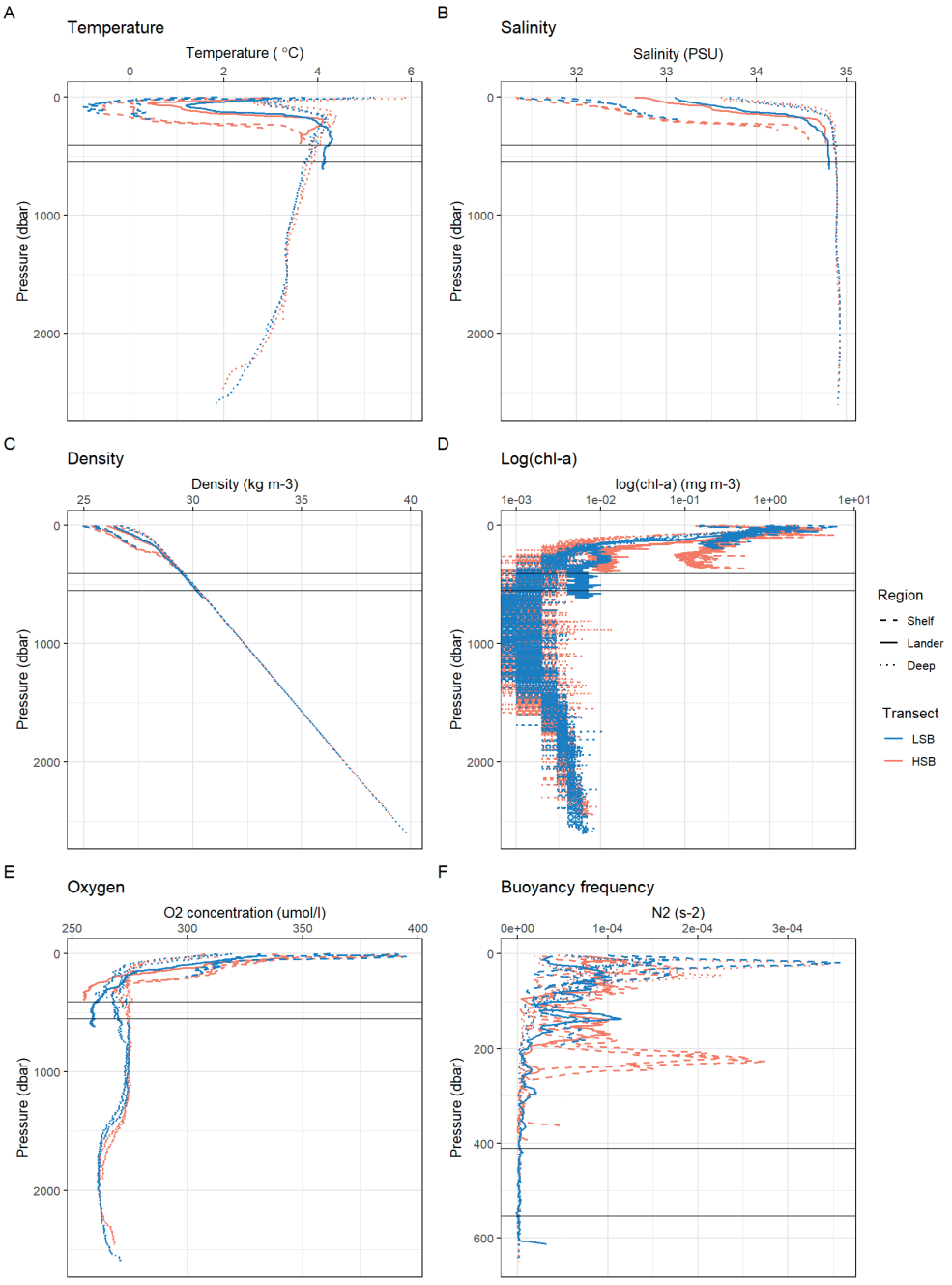

Figure S5.3 CTD profiles with temperature (A), salinity (B), density (C), chlorophyll-a (D), Oxygen (E), Buoyancy frequency (F). LSB = Low sponge transect, HSB = High sponge transect. Buoyancy frequency is smoothed over 15 m for visibility, and the plot only shows top 650 m of the water column, as deeper waters have values close to zero

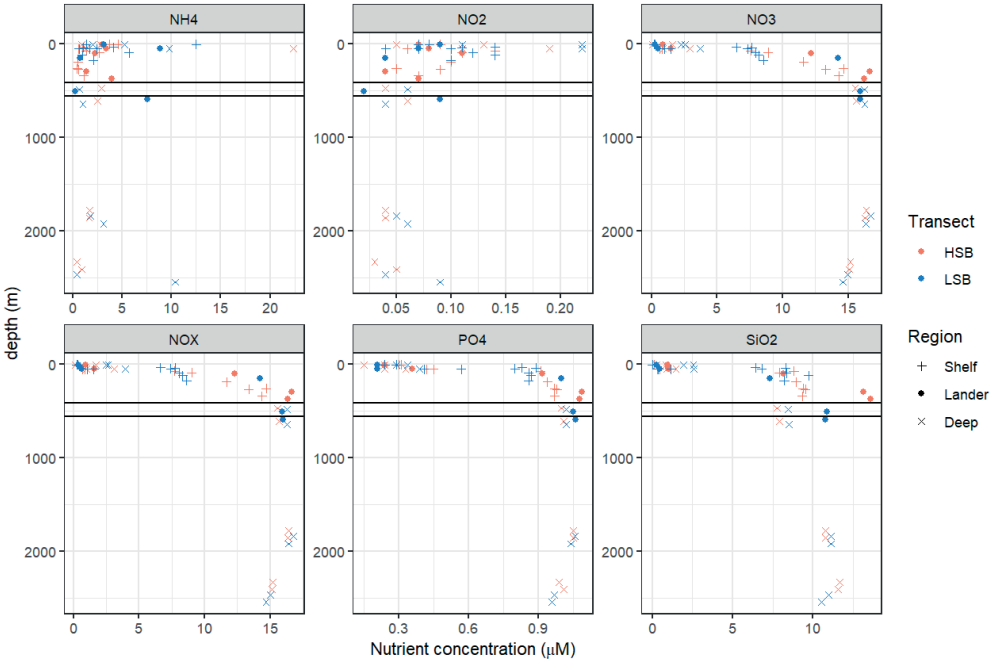

Figure S5.4 nutrient profiles for the two transects over the complete depth. HSB = high sponge biomass, LSB = low sponge biomass

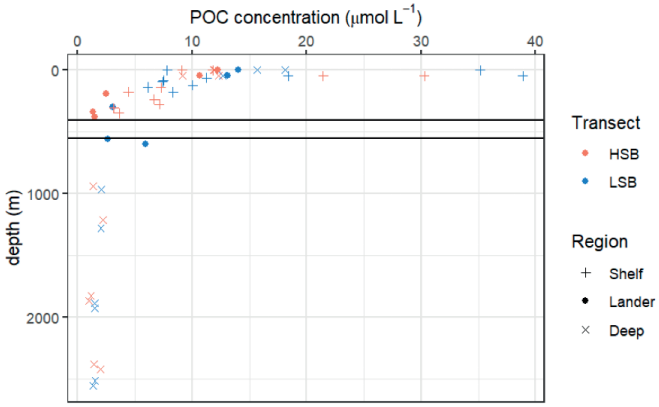

Figure S5.5 Particulate organic carbon (POC) profiles for the two transects. HSB = high sponge biomass lander, LSB = low sponge biomass lander

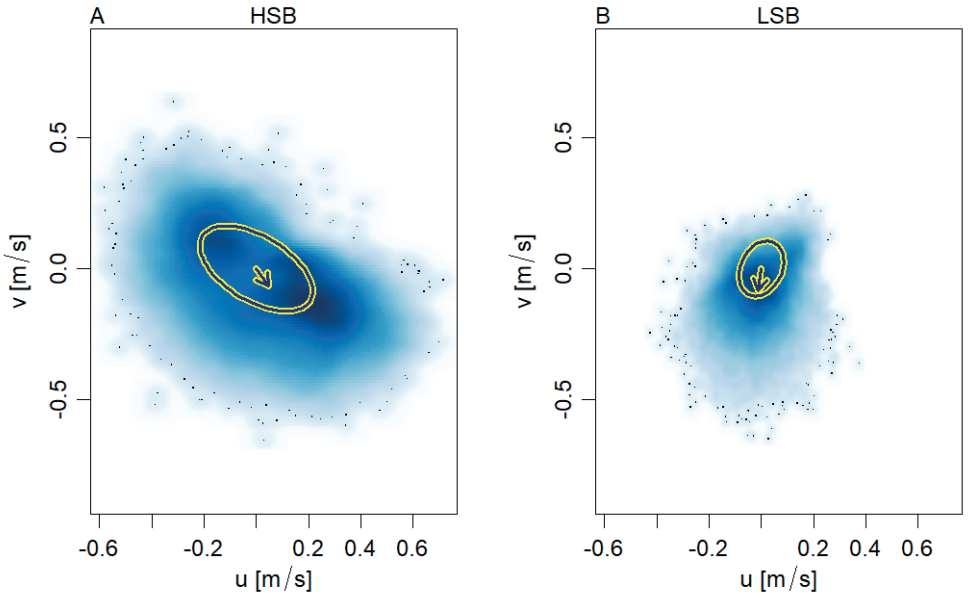

Figure S5.6 Frequency plots of bottom current velocities with eastward (u) velocity on the x-axis, and northward (v) velocity on the y-axis. A) high sponge biomass site (HSB), B) low sponge biomass site (LSB). The tidal ellipse and residual current strength/direction are indicated in yellow/black (Kelley and Richards, 2020)

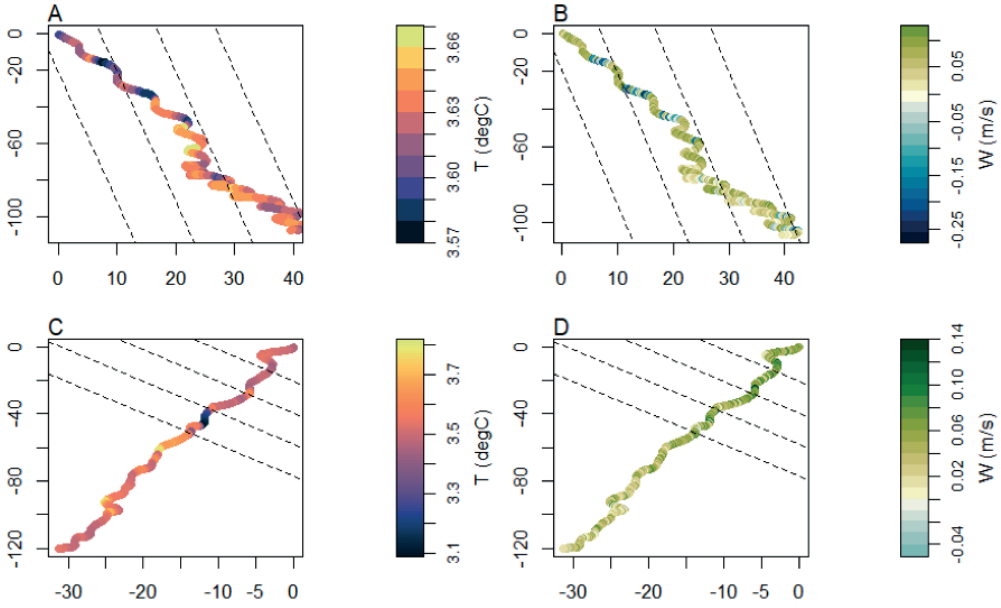

Figure S5.7 Bottom water temperature (A, C) and vertical velocity (B,D) for the high sponge biomass lander (A,B) and the low sponge biomass lander (C,D) from 1 – 7 March 2019

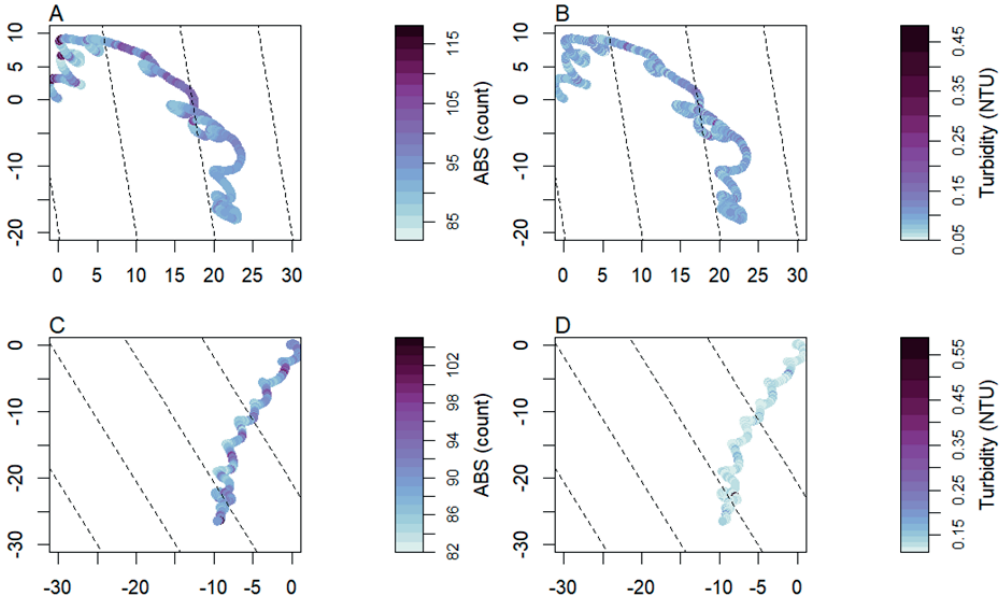

Figure S5.8 progressive vector plots of data from 1 to 7 September. A) the acoustic backscatter signal (ABS) at high sponge biomass lander (HSB), B) turbidity in Nepheloid Turbidity Units (NTU) at HSB, C) ABS at the LSB lander, D) turbidity at LSB lander

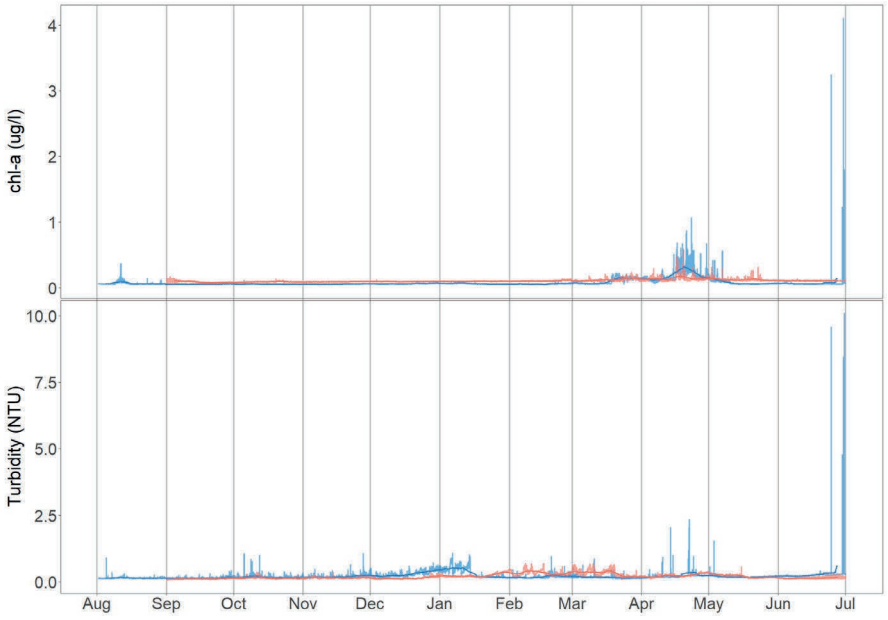

Figure S5.9 Chlorophyll-a and turbidity data without cutting the y-axis at 1.25 µg L^{-1}, and 2.5 NTU, respectively

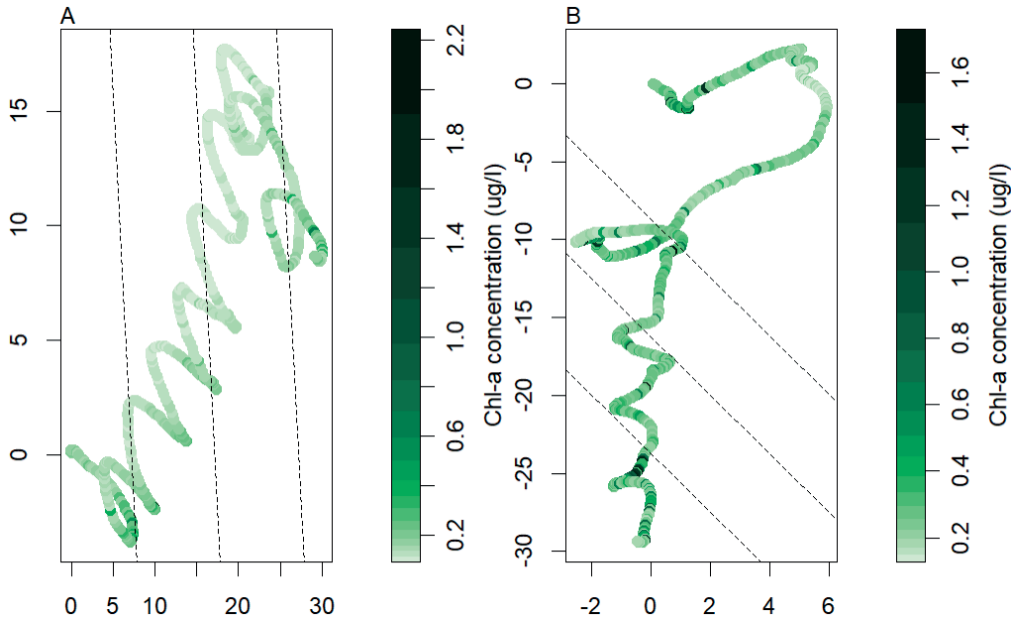

Figure S5.10 progressive vector plots with chlorophyll-a as colour variable from 19 to 24 April 2019. With A) the highs sponge biomass (HSB) lander and b) the low sponge biomass (LSB) lander. Dotted lines represent the along slope direction at the respective sites. Note colour is in log-scale

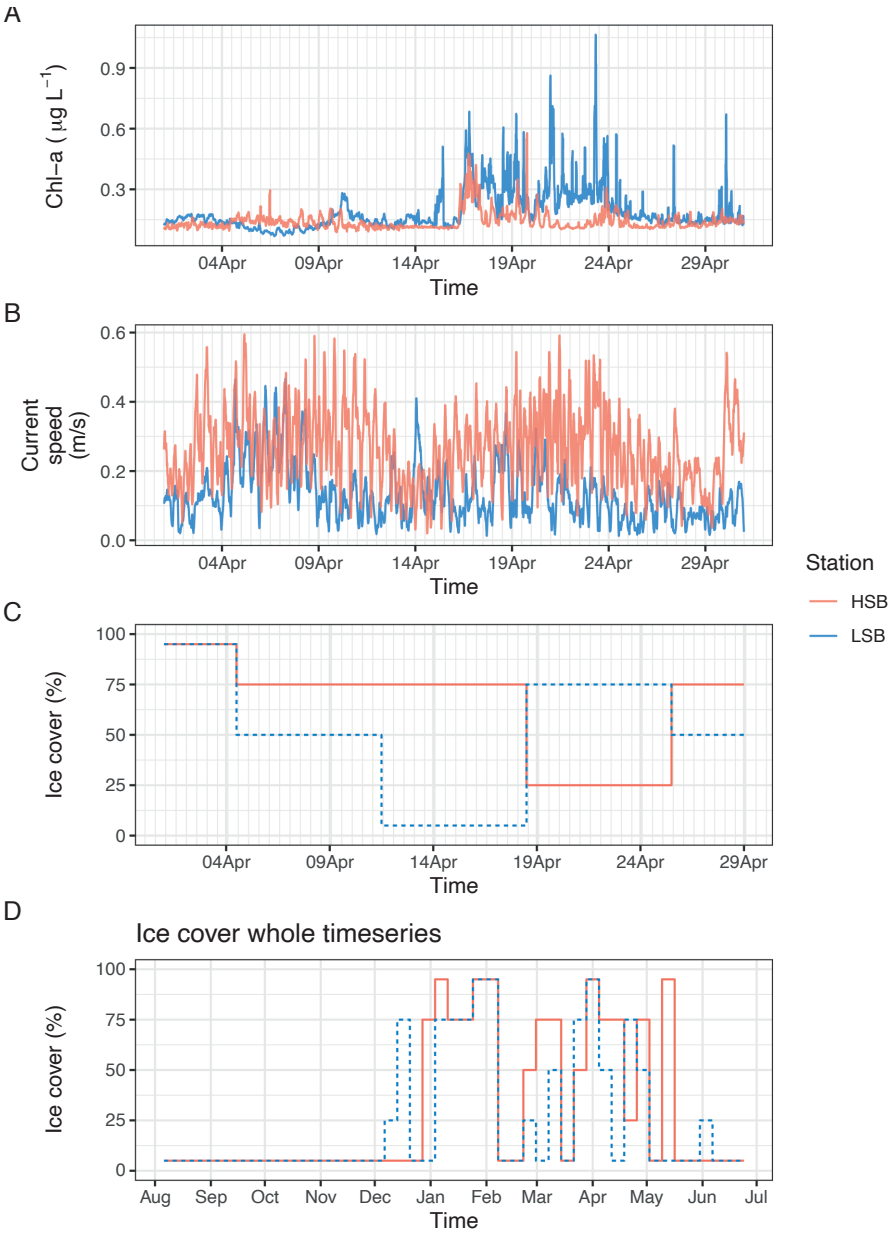

Figure S5.11 Spring Chlorophyll-a (A), bottom current speed (B), ice cover (C), during the spring bloom period (1 April-1 May, 2019), and ice cover for the whole deployment length (D)

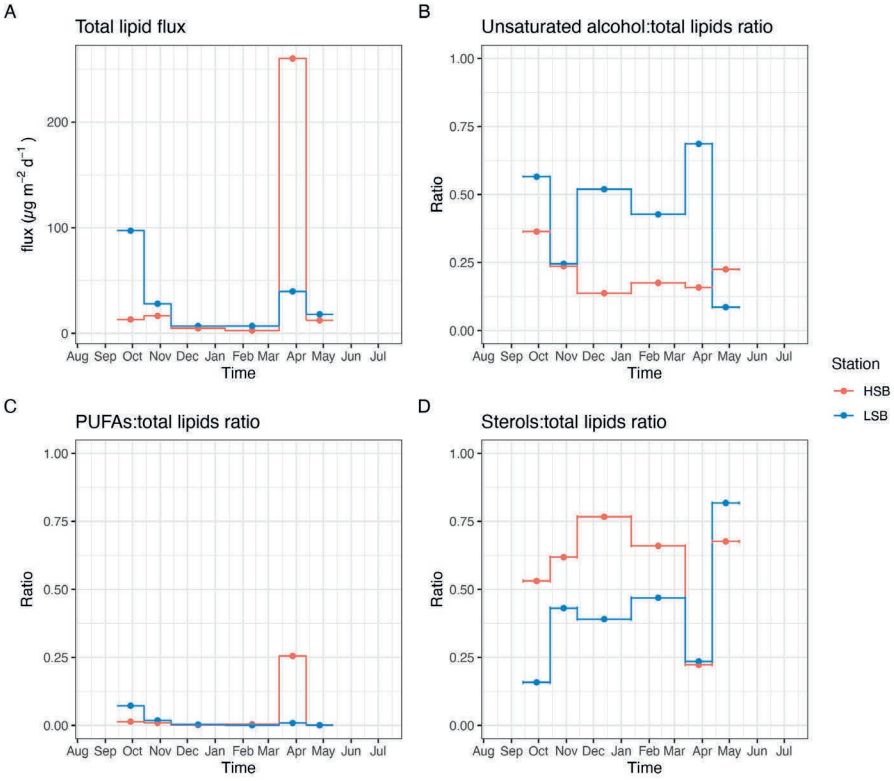

Figure S5.12 Sediment trap lipid fluxes. A) Total lipid flux, B) unsaturated alcohol:total lipids ratio, C) poly-unsaturated fatty acid:total lipids ratio, D) sterol:total lipids ratio

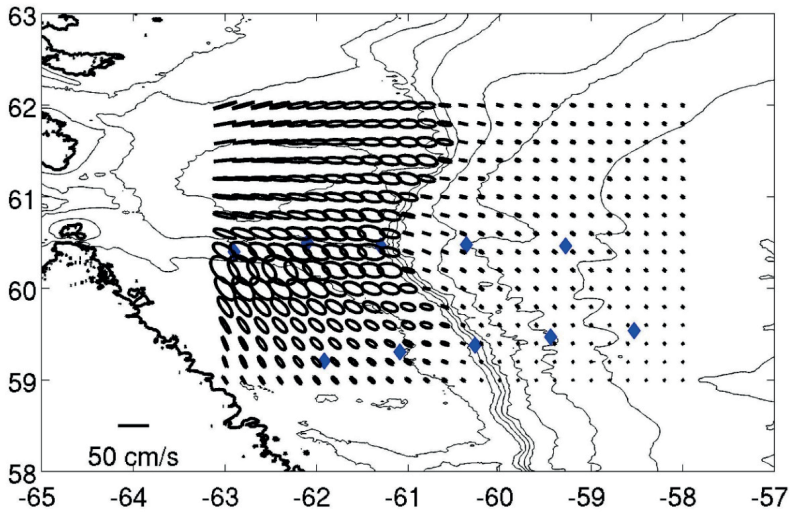

Figure S5.13 M_2 tidal current ellipses in the Davis Strait case study area (OTIS inverse tidal model, hourly data, July/August 2018)

References

Abelson, A., and Denny, M. (1997). Settlement of Marine Organisms in Flow. *Annu. Rev. Ecol. Syst.* 28, 317–339. doi: 10.1146/annurev.ecolsys.28.1.317.

Adams, C. E., and Weatherly, G. L. (1981). Suspended-sediment transport and benthic boundary-layer dynamics. *Marine Geology* 42, 1–18. doi: https://doi.org/10.1016/0025-3227(81)90155-9.

Addamo, A. M., Vertino, A., Stolarski, J., García-Jiménez, R., Taviani, M., and Machordom, A. (2016). Merging scleractinian genera: the overwhelming genetic similarity between solitary *Desmophyllum* and colonial *Lophelia*. *BMC Evolutionary Biology* 16, 108. doi: 10.1186/s12862-016-0654-8.

Ahyong, S., Boyko, C. B., Bailly, N., Bernot, J., Bieler, R., Brandão, S. N., et al. (2022). World Register of Marine Species (WoRMS). Available at: https://www.marinespecies.org.

Akima, H., and Gebhardt, A. (2020). *akima: Interpolation of Irregularly and Regularly Spaced Data*. Available at: https://CRAN.R-project.org/package=akima.

Alfaro, A. C., Thomas, F., Sergent, L., and Duxbury, M. (2006). Identification of trophic interactions within an estuarine food web (northern New Zealand) using fatty acid biomarkers and stable isotopes. *Estuarine, Coastal and Shelf Science* 70, 271–286. doi: 10.1016/j.ecss.2006.06.017.

Allaire, J. J., Xie, Y., McPherson, J., Luraschi, J., Ushey, K., Atkins, A., et al. (2021). *rmarkdown: Dynamic Documents for R*. Available at: https://github.com/rstudio/rmarkdown.

Alldredge, A. L., and Gotschalk, C. (1988). In situ settling behavior of marine snow1: Sinking rates of marine snow. *Limnol. Oceanogr.* 33, 339–351. doi: 10.4319/lo.1988.33.3.0339.

Allemand, D., Ferrier-Pagès, C., Furla, P., Houlbrèque, F., Puverel, S., Reynaud, S., et al. (2004). Biomineralisation in reef-building corals: from molecular mechanisms to environmental control. *Comptes Rendus Palevol* 3, 453–467. doi: 10.1016/j.crpv.2004.07.011.

Altabet, M. A. (1990). Organic C, N, and stable isotopic composition of particulate matter collected on glass-fiber and aluminum oxide filters. *Limnology and Oceanography* 35,

902–909. doi: 10.4319/lo.1990.35.4.0902.

Anderson, T. R., Hessen, D. O., Elser, J. J., and Urabe, J. (2005). Metabolic Stoichiometry and the Fate of Excess Carbon and Nutrients in Consumers. *The American Naturalist* 165, 1–15. doi: 10.1086/426598.

Andersson, J. H., Wijsman, J. W. M., Herman, P. M. J., Middelburg, J. J., Soetaert, K., and Heip, C. (2004). Respiration patterns in the deep ocean. *Geophysical Research Letters* 31, L03304. doi: 10.1029/2003GL018756.

Andrews, A. H., Cordes, E. E., Mahoney, M. M., Munk, K., Coale, K. H., Cailliet, G. M., et al. (2002). Age, growth and radiometric age validation of a deep-sea, habitat-forming gorgonian (Primnoa resedaeformis) from the Gulf of Alaska. *Hydrobiologia* 471, 101–110. doi: 10.1023/A:1016501320206.

Anthony, K. R. N. (1999). Coral suspension feeding on fine particulate matter. *Journal of Experimental Marine Biology and Ecology* 232, 85–106. doi: 10.1016/S0022-0981(98)00099-9.

Attard, K. M., Glud, R. N., McGinnis, D. F., and Rysgaard, S. (2014). Seasonal rates of benthic primary production in a Greenland fjord measured by aquatic eddy correlation. *Limnology & Oceanography* 59, 1555–1569. doi: 10.4319/lo.2014.59.5.1555.

Attard, K. M., Hancke, K., Sejr, M. K., and Glud, R. N. (2016). Benthic primary production and mineralization in a High Arctic fjord: in situ assessments by aquatic eddy covariance. *Marine Ecology Progress Series* 554, 35–50. doi: 10.3354/meps11780.

Attard, K. M., Stahl, H., Kamenos, N. A., Turner, G., Burdett, H. L., and Glud, R. N. (2015). Benthic oxygen exchange in a live coralline algal bed and an adjacent sandy habitat: an eddy covariance study. *Marine Ecology Progress Series* 535, 99–115. doi: 10.3354/meps11413.

Bakker, P., Schmittner, A., Lenaerts, J. T. M., Abe-Ouchi, A., Bi, D., van den Broeke, M. R., et al. (2016). Fate of the Atlantic Meridional Overturning Circulation: Strong decline under continued warming and Greenland melting. *Geophysical Research Letters* 43, 12,252-12,260. doi: 10.1002/2016GL070457.

Bandara, K., Varpe, Ø., Wijewardene, L., Tverberg, V., and Eiane, K. (2021). Two hundred years of zooplankton vertical migration research. *Biological Reviews* 96, 1547–1589. doi: 10.1111/brv.12715.

Barber, A., Sirois, M., Chaillou, G., and Gélinas, Y. (2017). Stable isotope analysis of dissolved organic carbon in Canada's eastern coastal waters. *Limnology and Oceanography* 62, S71–S84. doi: 10.1002/lno.10666.

Bargain, A., Foglini, F., Pairaud, I., Bonaldo, D., Carniel, S., Angeletti, L., et al. (2018). Predictive habitat modeling in two Mediterranean canyons including hydrodynamic variables. *Progress in Oceanography* 169, 151–168. doi: 10.1016/j.pocean.2018.02.015.

Barlow, R. G., Mantoura, R. F. C., Gough, M. A., and Fileman, T. W. (1993). Pigment signatures of the phytoplankton composition in the northeastern Atlantic during the 1990 spring bloom. *Deep Sea Research Part II: Topical Studies in Oceanography* 40, 459–477. doi: 10.1016/0967-0645(93)90027-K.

Bart, M. C., de Kluijver, A., Hoetjes, S., Absalah, S., Mueller, B., Kenchington, E., et al. (2020). Differential processing of dissolved and particulate organic matter by deep-sea sponges and their microbial symbionts. *Sci Rep* 10, 17515. doi: 10.1038/s41598-020-74670-0.

Bart, M. C., Mueller, B., Rombouts, T., van de Ven, C., Tompkins, G. J., Osinga, R., et al. (2021). Dissolved organic carbon (DOC) is essential to balance the metabolic demands of four dominant North-Atlantic deep-sea sponges. *Limnology and Oceanography* 66, 925–938. doi: 10.1002/lno.11652.

Beazley, L. I., Kenchington, E. L., Murillo, F. J., and Sacau, M. del M. (2013). Deep-sea sponge grounds enhance diversity and abundance of epibenthic megafauna in the Northwest Atlantic. *ICES Journal of Marine Science* 70, 1471–1490. doi: 10.1093/icesjms/fst124.

Beazley, L., Kenchington, E., Murillo, F., Brickman, D., Wang, Z., Davies, A., et al. (2021). Climate change winner in the deep sea? Predicting the impacts of climate change on the distribution of the glass sponge Vazella pourtalesii. *Mar. Ecol. Prog. Ser.* 657, 1–23. doi: 10.3354/meps13566.

Beazley, L., Kenchington, E., Yashayaev, I., and Murillo, F. J. (2015). Drivers of epibenthic megafaunal composition in the sponge grounds of the Sackville Spur, northwest

Atlantic. *Deep Sea Research Part I: Oceanographic Research Papers* 98, 102–114. doi: 10.1016/j.dsr.2014.11.016.

Beazley, L., Wang, Z., Kenchington, E., Yashayaev, I., Rapp, H. T., Xavier, J. R., et al. (2018). Predicted distribution of the glass sponge Vazella pourtalesi on the Scotian Shelf and its persistence in the face of climatic variability. *PLOS ONE* 13, e0205505. doi: 10.1371/journal.pone.0205505.

Belkin, I. M. (2009). Rapid warming of Large Marine Ecosystems. *Progress in Oceanography* 81, 207–213. doi: 10.1016/j.pocean.2009.04.011.

Benner, R., Louchouarn, P., and Amon, R. M. W. (2005). Terrigenous dissolved organic matter in the Arctic Ocean and its transport to surface and deep waters of the North Atlantic. *Global Biogeochemical Cycles*, 11.

Berg, P., Glud, R. N., Hume, A., Stahl, H., Oguri, K., Meyer, V., et al. (2009). Eddy correlation measurements of oxygen uptake in deep ocean sediments. *Limnology and Oceanography: Methods* 7, 576–584. doi: 10.4319/lom.2009.7.576.

Berg, P., Roy, H., Janssen, F., Meyer, V., Jorgensen, B. B., Huettel, M., et al. (2003). Oxygen uptake by aquatic sediments measured with a novel non-invasive eddy-correlation technique. *Marine Ecology Progress Series* 261, 75–83. doi: 10.3354/meps261075.

Berg, P., Roy, H., and Wiberg, P. L. (2007). Eddy correlation flux measurements: The sediment surface area that contributes to the flux. *Limnology & Oceanography* 52, 1672–1684. doi: 10.4319/lo.2007.52.4.1672.

Berggreen, U., Hansen, B., and Kiørboe, T. (1988). Food size spectra, ingestion and growth of the copepod *Acartia tonsa* during development: Implications for determination of copepod production. *Mar. Biol.* 99, 341–352. doi: 10.1007/BF02112126.

Bergquist, P. R. (1978). *Sponges*. University of California Press.

Bianchi, T. S., Rolff, C., Widbom, B., and Elmgren, R. (2002). Phytoplankton Pigments in Baltic Sea Seston and Sediments: Seasonal Variability, Fluxes, and Transformations. *Estuarine, Coastal and Shelf Science* 55, 369–383. doi: 10.1006/ecss.2001.0911.

Biber, M. F., Duineveld, G. C. A., Lavaleye, M. S. S., Davies, A. J., Bergman, M. J. N., and van den Beld, I. M. J. (2014). Investigating the association of fish abundance and biomass with cold-water corals in the deep Northeast Atlantic Ocean using a generalised linear modelling approach. *Deep Sea Research Part II: Topical Studies in Oceanography* 99, 134–145. doi: 10.1016/j.dsr2.2013.05.022.

Blaud, A., Lerch, T. Z., Chevallier, T., Nunan, N., Chenu, C., and Brauman, A. (2012). Dynamics of bacterial communities in relation to soil aggregate formation during the decomposition of 13C-labelled rice straw. *Applied Soil Ecology* 53, 1–9. doi: 10.1016/j.apsoil.2011.11.005.

Bloomfield, P. (2004). *Fourier analysis of time series: an introduction*. John Wiley & Sons.

Boers, N. (2021). Observation-based early-warning signals for a collapse of the Atlantic Meridional Overturning Circulation. *Nat. Clim. Chang.* 11, 680–688. doi: 10.1038/s41558-021-01097-4.

Böning, C. W., Behrens, E., Biastoch, A., Getzlaff, K., and Bamber, J. L. (2016). Emerging impact of Greenland meltwater on deepwater formation in the North Atlantic Ocean. *Nature Geosci* 9, 523–527. doi: 10.1038/ngeo2740.

Bopp, L., Monfray, P., Aumont, O., Dufresne, J.-L., Le Treut, H., Madec, G., et al. (2001). Potential impact of climate change on marine export production. *Global Biogeochem. Cycles* 15, 81–99. doi: 10.1029/1999GB001256.

Boschker, H. T. S., Brouwer, J. F. C. de, and Cappenberg, T. E. (1999). The contribution of macrophyte-derived organic matter to microbial biomass in salt-marsh sediments: Stable carbon isotope analysis of microbial biomarkers. *Limnology and Oceanography* 44, 309–319. doi: https://doi.org/10.4319/lo.1999.44.2.0309.

Bostock, H. C., Tracey, D. M., Currie, K. I., Dunbar, G. B., Handler, M. R., Mikaloff Fletcher, S. E., et al. (2015). The carbonate mineralogy and distribution of habitat-forming deep-sea corals in the southwest pacific region. *Deep Sea Research Part I: Oceanographic Research Papers* 100, 88–104. doi: 10.1016/j.dsr.2015.02.008.

Bourgault, D., Morsilli, M., Richards, C., Neumeier, U., and Kelley, D. E. (2014). Sediment resuspension and nepheloid layers induced by long internal solitary waves shoaling orthogonally on uniform slopes. *Continental Shelf Research* 72, 21–33. doi: 10.1016/j.csr.2013.10.019.

Boyd, P. W., and Newton, P. P. (1999). Does planktonic community structure determine downward particulate organic carbon flux in different oceanic provinces? *Deep Sea Research Part I: Oceanographic Research Papers* 46, 63–91. doi: 10.1016/S0967-0637(98)00066-1.

Boyd, P. W., and Trull, T. W. (2007). Understanding the export of biogenic particles in oceanic waters: Is there consensus? *Progress in Oceanography* 72, 276–312. doi: 10.1016/j.pocean.2006.10.007.

Brito-Morales, I., Schoeman, D. S., Molinos, J. G., Burrows, M. T., Klein, C. J., Arafeh-Dalmau, N., et al. (2020). Climate velocity reveals increasing exposure of deep-ocean biodiversity to future warming. *Nat. Clim. Chang.* 10, 576–581. doi: 10.1038/s41558-020-0773-5.

Brooke, S. D., Holmes, M. W., and Young, C. M. (2009). Sediment tolerance of two different morphotypes of the deep-sea coral Lophelia pertusa from the Gulf of Mexico. *Marine Ecology Progress Series* 390, 137–144. doi: 10.3354/meps08191.

Brussaard, C. P. D. (2004). Optimization of Procedures for Counting Viruses by Flow Cytometry. *Appl. Environ. Microbiol.* 70, 1506–1513. doi: 10.1128/AEM.70.3.1506-1513.2004.

Brussaard, C. P. D., Noordeloos, A. A. M., Witte, H., Collenteur, M. C. J., Schulz, K., Ludwig, A., et al. (2013). Arctic microbial community dynamics influenced by elevated CO2 levels. *Biogeosciences* 10, 719–731. doi: 10.5194/bg-10-719-2013.

Brzezinski, M. A. (1985). The Si:C:N Ratio Of Marine Diatoms: Interspecific Variability And The Effect Of Some Environmental Variables. *Journal of Phycology* 21, 347–357. doi: https://doi.org/10.1111/j.0022-3646.1985.00347.x.

Buesseler, K. O. (1998). The decoupling of production and particulate export in the surface ocean. *Global Biogeochem. Cycles* 12, 297–310. doi: 10.1029/97GB03366.

Buesseler, K. O., Lamborg, C. H., Boyd, P. W., Lam, P. J., Trull, T. W., Bidigare, R. R., et al. (2007). Revisiting Carbon Flux Through the Ocean's Twilight Zone. *Science* 316, 567–570. doi: 10.1126/science.1137959.

Buhl-Mortensen, L., Bøe, R., Dolan, M. F. J., Buhl-Mortensen, P., Thorsnes, T., Elvenes, S., et al. (2012). "51 - Banks, Troughs, and Canyons on the Continental Margin off Lofoten,

Vesterålen, and Troms, Norway," in *Seafloor Geomorphology as Benthic Habitat*, eds. P. T. Harris and E. K. Baker (London: Elsevier), 703–715. doi: 10.1016/B978-0-12-385140-6.00051-7.

Buhl-Mortensen, L., Vanreusel, A., Gooday, A. J., Levin, L. A., Priede, I. G., Buhl-Mortensen, P., et al. (2010). Biological structures as a source of habitat heterogeneity and biodiversity on the deep ocean margins. *Marine Ecology* 31, 21–50. doi: 10.1111/j.1439-0485.2010.00359.x.

Buitenhuis, E. T., Li, W. K. W., Vaulot, D., Lomas, M. W., Landry, M. R., Partensky, F., et al. (2012). Picophytoplankton biomass distribution in the global ocean. *Earth System Science Data*, 37–46. doi: 10.5194/essd-4-37-2012.

Caesar, L., McCarthy, G. D., Thornalley, D. J. R., Cahill, N., and Rahmstorf, S. (2021). Current Atlantic Meridional Overturning Circulation weakest in last millennium. *Nat. Geosci.* 14, 118–120. doi: 10.1038/s41561-021-00699-z.

Caesar, L., Rahmstorf, S., Robinson, A., Feulner, G., and Saba, V. (2018). Observed fingerprint of a weakening Atlantic Ocean overturning circulation. *Nature* 556, 191–196. doi: 10.1038/s41586-018-0006-5.

Caldeira, K., and Wickett, M. E. (2003). Anthropogenic carbon and ocean pH. *Nature* 425, 365–365. doi: 10.1038/425365a.

Campanyà-Llovet, N., Snelgrove, P. V. R., and Parrish, C. C. (2017). Rethinking the importance of food quality in marine benthic food webs. *Progress in Oceanography* 156, 240–251. doi: 10.1016/j.pocean.2017.07.006.

Canadian Government Latest Ice conditions. Available at: https://www.canada.ca/en/environment-climate-change/services/ice-forecasts-observations/latest-conditions.html [Accessed January 2, 2022].

Carlier, A., Le Guilloux, E., Olu, K., Sarrazin, J., Mastrototaro, F., Taviani, M., et al. (2009). Trophic relationships in a deep Mediterranean cold-water coral bank (Santa Maria di Leuca, Ionian Sea). *Mar. Ecol. Prog. Ser.* 397, 125–137. doi: 10.3354/meps08361.

Carmack, E. C., Macdonald, R. W., and Jasper, S. (2004). Phytoplankton productivity on the Canadian Shelf of the Beaufort Sea. *Marine Ecology Progress Series* 277, 37–50. doi: 10.3354/meps277037.

Caron, D. A., Dam, H. G., Kremer, P., Lessard, E. J., Madin, L. P., Malone, T. C., et al. (1995). The contribution of microorganisms to particulate carbon and nitrogen in surface waters of the Sargasso Sea near Bermuda. *Deep Sea Research Part I: Oceanographic Research Papers* 42, 943–972. doi: 10.1016/0967-0637(95)00027-4.

Casey, J. R., Aucan, J. P., Goldberg, S. R., and Lomas, M. W. (2013). Changes in partitioning of carbon amongst photosynthetic pico- and nano-plankton groups in the Sargasso Sea in response to changes in the North Atlantic Oscillation. *Deep Sea Research Part II: Topical Studies in Oceanography* 93, 58–70. doi: 10.1016/j.dsr2.2013.02.002.

Cathalot, C. C., Van Oevelen, D., Cox, T. J. S., Kutti, T., Lavaleye, M. S. S., Duineveld, G. C. A., et al. (2015). Cold-water coral reefs and adjacent sponge grounds: hotspots of benthic respiration and organic carbon cycling in the deep sea. *Frontiers in Marine Science* 2, 1–12. doi: 10.3389/fmars.2015.00037.

Chawarski, J., Klevjer, T., Coté, D., and Geoffroy, M. (2022). Evidence of temperature control on mesopelagic fish and zooplankton communities at high latitudes. Fronties in Marine Science 9, doi: https://doi.org/10.3389/fmars.2022.917985.

Cho, B. C., and Azam, F. (1988). Major role of bacteria in biogeochemical fluxes in the ocean's interior. *Nature* 332, 441–443. doi: 10.1038/332441a0.

Christie, W. W. (1982). A simple procedure for rapid transmethylation of glycerolipids and cholesteryl esters. *Journal of Lipid Research* 23, 1072–1075. doi: 10.1016/S0022-2275(20)38081-0.

Colaço, A., Rapp, H. T., Campanyà-Llovet, N., and Pham, C. K. (2022). Bottom trawling in sponge grounds of the Barents Sea (Arctic Ocean): A functional diversity approach. *Deep Sea Research Part I: Oceanographic Research Papers* 183, 103742. doi: 10.1016/j.dsr.2022.103742.

Conti, L. A., Lim, A., and Wheeler, A. J. (2019). High resolution mapping of a cold water coral mound. *Sci Rep* 9, 1016. doi: 10.1038/s41598-018-37725-x.

Correa, T. B. S., Eberli, G. P., Grasmueck, M., Reed, J. K., and Correa, A. M. S. (2012). Genesis and morphology of cold-water coral ridges in a unidirectional current regime. *Marine Geology* 326–328, 14–27. doi: 10.1016/j.margeo.2012.06.008.

Costello, M. J., McCrea, M., Freiwald, A., Lundälv, T., Jonsson, L., Bett, B. J., et al. (2005). "Role of cold-water Lophelia pertusa coral reefs as fish habitat in the NE Atlantic," in *Cold-Water Corals and Ecosystems* Erlangen Earth Conference Series., eds. A. Freiwald and J. M. Roberts (Berlin, Heidelberg: Springer), 771–805. doi: 10.1007/3-540-27673-4_41.

Coté, D., Edinger, E. N., and Mercier, A. (2018). CCGS Amundsen Field Report. Integrated studies and ecosystem characterization of the Labrador Sea Deep Ocean (ISECOLD).

Coté, D., Geoffroy, M., Sherwood, O. A., Neves, B. M., Mercier, A., Hubert, C., et al. (2019). CCGS Amundsen Field Report. Integrated studies and ecosystem characterization of the Labrador Sea Deep Ocean (ISECOLD).

Culwick, T., Phillips, J., Goodwin, C., Rayfield, E. J., and Hendry, K. R. (2020). Sponge Density and Distribution Constrained by Fluid Forcing in the Deep Sea. *Front. Mar. Sci.* 7, 395. doi: 10.3389/fmars.2020.00395.

Curry, B., Lee, C. M., and Petrie, B. (2011). Volume, Freshwater, and Heat Fluxes through Davis Strait, 2004–05. *Journal of Physical Oceanography* 41, 429–436. doi: 10.1175/2010JPO4536.1.

Curry, B., Lee, C. M., Petrie, B., Moritz, R. E., and Kwok, R. (2014). Multiyear Volume, Liquid Freshwater, and Sea Ice Transports through Davis Strait, 2004–10. *Journal of Physical Oceanography* 44, 1244–1266. doi: 10.1175/JPO-D-13-0177.1.

Cyr, F., Haren, H., Mienis, F., Duineveld, G., and Bourgault, D. (2016). On the influence of cold-water coral mound size on flow hydrodynamics, and vice versa. *Geophys. Res. Lett.* 43, 775–783. doi: 10.1002/2015GL067038.

Cyr, F., and Haren, H. van (2016). Observations of Small-Scale Secondary Instabilities during the Shoaling of Internal Bores on a Deep-Ocean Slope. *Journal of Physical Oceanography* 46, 219–231. doi: 10.1175/JPO-D-15-0059.1.

Cyr, F., and Larouche, P. (2015). Thermal Fronts Atlas of Canadian Coastal Waters. *Atmosphere-Ocean* 53, 212–236. doi: 10.1080/07055900.2014.986710.

Dalsgaard, J., St. John, M., Kattner, G., Müller-Navarra, D., and Hagen, W. (2003). "Fatty acid trophic markers in the pelagic marine environment," in *Advances in Marine Biology* (Elsevier), 225–340. doi: 10.1016/S0065-2881(03)46005-7.

Daly, M., Brugler, M. R., Cartwright, P., Collins, A. G., Dawson, M. N., Fautin, D. G., et al. (2007). The phylum Cnidaria: A review of phylogenetic patterns and diversity 300 years after Linnaeus*. *Zootaxa* 1668, 127–182. doi: 10.11646/zootaxa.1668.1.11.

Davies, A. J., Duineveld, G. C. A., Lavaleye, M. S. S., Bergman, M. J. N., van Haren, H., and Roberts, J. M. (2009). Downwelling and deep-water bottom currents as food supply mechanisms to the cold-water coral *Lophelia pertusa* (Scleractinia) at the Mingulay Reef Complex. *Limnol. Oceanogr.* 54, 620–629. doi: 10.4319/lo.2009.54.2.0620.

Davies, A. J., and Guinotte, J. M. (2011). Global Habitat Suitability for Framework-Forming Cold-Water Corals. *PLoS ONE* 6, e18483. doi: 10.1371/journal.pone.0018483.

Davies, A. J., Wisshak, M., Orr, J. C., and Murray Roberts, J. (2008). Predicting suitable habitat for the cold-water coral Lophelia pertusa (Scleractinia). *Deep Sea Research Part I: Oceanographic Research Papers* 55, 1048–1062. doi: 10.1016/j.dsr.2008.04.010.

Davison, J. J., van Haren, H., Hosegood, P., Piechaud, N., and Howell, K. L. (2019). The distribution of deep-sea sponge aggregations (Porifera) in relation to oceanographic processes in the Faroe-Shetland Channel. *Deep Sea Research Part I: Oceanographic Research Papers* 146, 55–61. doi: 10.1016/j.dsr.2019.03.005.

De Clippele, L. H., Gafeira, J., Robert, K., Hennige, S., Lavaleye, M. S., Duineveld, G. C. A., et al. (2017). Using novel acoustic and visual mapping tools to predict the small-scale spatial distribution of live biogenic reef framework in cold-water coral habitats. *Coral Reefs* 36, 255–268. doi: 10.1007/s00338-016-1519-8.

De Clippele, L. H., Huvenne, V. A. I., Molodtsova, T. N., and Roberts, J. M. (2019). The Diversity and Ecological Role of Non-scleractinian Corals (Antipatharia and Alcyonacea) on Scleractinian Cold-Water Coral Mounds. *Front. Mar. Sci.* 6, 184. doi: 10.3389/fmars.2019.00184.

De Clippele, L. H., Rovelli, L., Ramiro-Sánchez, B., Kazanidis, G., Vad, J., Turner, S., et al. (2021a). Mapping cold-water coral biomass: an approach to derive ecosystem functions. *Coral Reefs* 40, 215–231. doi: 10.1007/s00338-020-02030-5.

De Clippele, L. H., van der Kaaden, A.-S., Maier, S. R., de Froe, E., and Roberts, J. M. (2021b). Biomass Mapping for an Improved Understanding of the Contribution of Cold-Water Coral Carbonate Mounds to C and N Cycling. *Frontiers in Marine Science* 8. doi: 10.3389/fmars.2021.721062.

de Haas, H., Mienis, F., Frank, N., Richter, T. O., Steinacher, R., Stigter, H. De, et al. (2009). Morphology and sedimentology of (clustered) cold-water coral mounds at the south Rockall Trough margins , NE Atlantic Ocean. *Facies* 55, 1–26. doi: 10.1007/s10347-008-0157-1.

de Jonge, V. (1980). Fluctuations in the Organic Carbon to Chlorophyll a Ratios for Estuarine Benthic Diatom Populations. *Mar. Ecol. Prog. Ser.* 2, 345–353. doi: 10.3354/meps002345.

de Kluijver, A., Bart, M. C., van Oevelen, D., de Goeij, J. M., Leys, S. P., Maier, S. R., et al. (2021). An Integrative Model of Carbon and Nitrogen Metabolism in a Common Deep-Sea Sponge (Geodia barretti). *Frontiers in Marine Science* 7, 1131. doi: 10.3389/fmars.2020.596251.

De La Rocha, C. L., and Passow, U. (2007). Factors influencing the sinking of POC and the efficiency of the biological carbon pump. *Deep Sea Research Part II: Topical Studies in Oceanography* 54, 639–658. doi: 10.1016/j.dsr2.2007.01.004.

Dinn, C., Zhang, X., Edinger, E., and Leys, S. P. (2020). Sponge communities in the eastern Canadian Arctic: species richness, diversity and density determined using targeted benthic sampling and underwater video analysis. *Polar Biol* 43, 1287–1305. doi: 10.1007/s00300-020-02709-z.

Dodds, L. A., Roberts, J. M., Taylor, A. C., and Marubini, F. (2007). Metabolic tolerance of the cold-water coral Lophelia pertusa (Scleractinia) to temperature and dissolved oxygen change. *Journal of Experimental Marine Biology and Ecology* 349, 205–214. doi: 10.1016/J.Jembe.2007.05.013.

Dodds, L., Black, K., Orr, H., and Roberts, J. (2009). Lipid biomarkers reveal geographical differences in food supply to the cold-water coral *Lophelia pertusa* (Scleractinia). *Mar. Ecol. Prog. Ser.* 397, 113–124. doi: 10.3354/meps08143.

Dorschel, B., Hebbeln, D., Foubert, A., White, M., and Wheeler, A. J. (2007). Hydrodynamics and cold-water coral facies distribution related to recent sedimentary processes at Galway Mound west of Ireland. *Marine Geology* 244, 184–195. doi: 10.1016/j.margeo.2007.06.010.

Dorschel, B., Hebbeln, D., Rüggeberg, A., Dullo, W. C., and Freiwald, A. (2005a). Growth and erosion of a cold-water coral covered carbonate mound in the Northeast Atlantic

during the Late Pleistocene and Holocene. *Earth and Planetary Science Letters* 233, 33–44. doi: 10.1016/j.epsl.2005.01.035.

Dorschel, B., Hebbeln, D., Ruggeberg, A., Dullo, W., and Freiwald, A. (2005b). Growth and erosion of a cold-water coral covered carbonate mound in the Northeast Atlantic during the Late Pleistocene and Holocene. *Earth and Planetary Science Letters* 233, 33–44. doi: 10.1016/j.epsl.2005.01.035.

Drinkwater, K. F., and Harding, G. C. (2001). Effects of the Hudson Strait outflow on the biology of the Labrador Shelf. *Can. J. Fish. Aquat. Sci.* 58, 171–184. doi: 10.1139/f00-210.

Drinkwater, K. F., and Jones, E. P. (1987). Density stratification, nutrient and chlorophyll distributions in the Hudson Strait region during summer and their relation to tidal mixing. *Continental Shelf Research* 7, 599–607. doi: 10.1016/0278-4343(87)90025-2.

Ducklow, H. W., Steinberg, D. K., and Buesseler, K. O. (2001). Upper Ocean Carbon Export and the Biological Pump. *Oceanography* issue_volume. Available at: https://doi.org/10.5670/oceanog.2001.06.

Dugdale, R. C., and Goering, J. J. (1967). Uptake of new and regenerated forms of nitrogen in primary productivity. *Limnol. Oceanogr.* 12, 196–206. doi: 10.4319/lo.1967.12.2.0196.

Dugdale, R. C., and Wilkerson, F. P. (1998). Silicate regulation of new production in the equatorial Pacific upwelling. *Nature* 391, 270–273. doi: 10.1038/34630.

Duineveld, G. C. A., Lavaleye, M. S. S., and Berghuis, E. M. (2004). Particle flux and food supply to a seamount cold-water coral community (Galicia Bank, NW Spain). *Marine Ecology Progress Series* 277, 13–23. doi: 10.3354/meps277013.

Duineveld, G. C. A., Lavaleye, M. S. S., Bergman, M. J. N., de Stigter, H., and Mienis, F. (2007). Trophic structure of a cold-water coral mound community (Rockall Bank, NE Atlantic) in relation to the near-bottom particle supply and current regime. *BULLETIN OF MARINE SCIENCE* 81, 19.

Duineveld, G., Jeffreys, R., Lavaleye, M., Davies, A., Bergman, M., Watmough, T., et al. (2012). Spatial and tidal variation in food supply to shallow cold-water coral reefs of the Mingulay Reef complex (Outer Hebrides, Scotland). *Mar. Ecol. Prog. Ser.* 444, 97–115. doi: 10.3354/meps09430.

Dullo, W. C., Flögel, S., and Rüggeberg, A. (2008). Cold-water coral growth in relation to the hydrography of the Celtic and Nordic European continental margin. *Mar. Ecol. Prog. Ser.* 371, 165–176. doi: 10.3354/meps07623.

Dunbar, M. J. (1951). *Eastern Arctic waters: a summary of our present knowledge of the physical oceanography of the eastern arctic area, from Hudson bay to cape Farewell and from Bell Isle to Smith sound*. Ottawa: Fisheries Research Board of Canada.

Edwards, M., and Richardson, A. J. (2004). Impact of climate change on marine pelagic phenology and trophic mismatch. *Nature* 430, 881–884. doi: 10.1038/nature02808.

Egbert, G. D., and Erofeeva, S. Y. (2002). Efficient Inverse Modeling of Barotropic Ocean Tides. *Journal of Atmospheric and Oceanic Technology* 19, 183–204. doi: 10.1175/1520-0426(2002)019<0183:EIMOBO>2.0.CO;2.

Ellett, D. J., Edwards, A., and Bowers, R. (1986). The hydrography of the Rockall Channel—an overview. *Proceedings of the Royal Society of Edinburgh. Section B. Biological Sciences* 88, 61–81. doi: 10.1017/S0269727000004474.

Falkowski, P. G., Barber, R. T., and Smetacek, V. (1998). Biogeochemical Controls and Feedbacks on Ocean Primary Production. *Science* 281, 200–206. doi: 10.1126/science.281.5374.200.

Falk-Petersen, S., Dahl, T., Scott, C., Sargent, J., Gulliksen, B., Kwasniewski, S., et al. (2002). Lipid biomarkers and trophic linkages between ctenophores and copepods in Svalbard waters. *Mar. Ecol. Prog. Ser.* 227, 187–194. doi: 10.3354/meps227187.

Fanelli, E., Cartes, J. E., and Papiol, V. (2011a). Food web structure of deep-sea macrozooplankton and micronekton off the Catalan slope: Insight from stable isotopes. *Journal of Marine Systems* 87, 79–89. doi: 10.1016/j.jmarsys.2011.03.003.

Fanelli, E., Papiol, V., Cartes, J. E., Rumolo, P., Brunet, C., and Sprovieri, M. (2011b). Food web structure of the epibenthic and infaunal invertebrates on the Catalan slope (NW Mediterranean): Evidence from δ13C and δ15N analysis. *Deep Sea Research Part I:*

Oceanographic Research Papers 58, 98–109. doi: 10.1016/j.dsr.2010.12.005.

Findlay, H. S., Artioli, Y., Moreno Navas, J., Hennige, S. J., Wicks, L. C., Huvenne, V. A. I., et al. (2013). Tidal downwelling and implications for the carbon biogeochemistry of cold-water corals in relation to future ocean acidification and warming. *Glob Change Biol* 19, 2708–2719. doi: 10.1111/gcb.12256.

Findlay, H. S., Hennige, S. J., Wicks, L. C., Navas, J. M., Woodward, E. M. S., and Roberts, J. M. (2014). Fine-scale nutrient and carbonate system dynamics around cold-water coral reefs in the northeast Atlantic. *Scientific Reports* 4, 3671. doi: 10.1038/srep03671.

Fink, H. G., Wienberg, C., De Pol-Holz, R., Wintersteller, P., and Hebbeln, D. (2013). Cold-water coral growth in the Alboran Sea related to high productivity during the Late Pleistocene and Holocene. *Marine Geology* 339, 71–82. doi: 10.1016/j.margeo.2013.04.009.

Fissel, D. B., and Lemon, D. D. (1991). Analysis of physical oceanographic data from the Labrador Shelf, summer 1980. Available at: https://www.osti.gov/etdeweb/biblio/5105285 [Accessed December 17, 2021].

Flögel, S., Dullo, W.-Chr., Pfannkuche, O., Kiriakoulakis, K., and Rüggeberg, A. (2014). Geochemical and physical constraints for the occurrence of living cold-water corals. *Deep Sea Research Part II: Topical Studies in Oceanography* 99, 19–26. doi: 10.1016/j.dsr2.2013.06.006.

Fowler, S. W., and Knauer, G. A. (1986). Role of large particles in the transport of elements and organic compounds through the oceanic water column. *Progress in Oceanography* 16, 147–194. doi: 10.1016/0079-6611(86)90032-7.

Frajka-Williams, E., and Rhines, P. B. (2010). Physical controls and interannual variability of the Labrador Sea spring phytoplankton bloom in distinct regions. *Deep Sea Research Part I: Oceanographic Research Papers* 57, 541–552. doi: 10.1016/j.dsr.2010.01.003.

Frajka-Williams, E., Rhines, P. B., and Eriksen, C. C. (2009). Physical controls and mesoscale variability in the Labrador Sea spring phytoplankton bloom observed by Seaglider. *Deep Sea Research Part I: Oceanographic Research Papers* 56, 2144–2161. doi: 10.1016/j.dsr.2009.07.008.

Frank, N., Freiwald, A., Correa, M. L., Wienberg, C., Eisele, M., Hebbeln, D., et al. (2011). Northeastern Atlantic cold-water coral reefs and climate. *Geology* 39, 743–746.

Freiwald, A., Fossâ, J. H., Grehan, A., Koslow, T., and Roberts, J. M. (2004). *Cold-water coral reefs: out of sight-no longer out of mind*. UNEP-WCMC.

Freiwald, A., Hühnerbach, V., Lindberg, B., Wilson, J. B., and Campbell, J. (2002). The Sula Reef Complex, Norwegian shelf. *Facies* 47, 179–200. doi: 10.1007/BF02667712.

Freiwald, A., and Wilson, J. B. (1998). Taphonomy of modern deep, cold-temperate water coral reefs. *Historical Biology* 13, 37–52. doi: 10.1080/08912969809386571.

Friedlingstein, P., Jones, M. W., O'Sullivan, M., Andrew, R. M., Bakker, D. C. E., Hauck, J., et al. (2022). Global Carbon Budget 2021. *Earth System Science Data* 14, 1917–2005. doi: 10.5194/essd-14-1917-2022.

Friedlingstein, P., Jones, M. W., O'Sullivan, M., Andrew, R. M., Hauck, J., Peters, G. P., et al. (2019). Global Carbon Budget 2019. *Earth System Science Data* 11, 1783–1838. doi: 10.5194/essd-11-1783-2019.

Fry, B. (2006). *Stable Isotope Ecology*. New York: Springer-Verlag doi: 10.1007/0-387-33745-8.

Fuentes-Yaco, C., Koeller, P. A., Sathyendranath, S., and Platt, T. (2007). Shrimp (Pandalus borealis) growth and timing of the spring phytoplankton bloom on the Newfoundland–Labrador Shelf. *Fisheries Oceanography* 16, 116–129. doi: 10.1111/j.1365-2419.2006.00402.x.

Fuhrman, J., Sleeter, T., Carlson, C., and Proctor, L. (1989). Dominance of bacterial biomass in the Sargasso Sea and its ecological implications. *Mar. Ecol. Prog. Ser.* 57, 207–217. doi: 10.3354/meps057207.

Gage, J. D., and Tyler, P. A. (1991). *Deep-Sea Biology: A Natural History of Organisms at the Deep-Sea Floor*. Cambridge University Press doi: 10.1017/CBO9781139163637.

Galand, P. E., Remize, M., Meistertzheim, A., Pruski, A. M., Peru, E., Suhrhoff, T. J., et al. (2020). Diet shapes cold-water corals bacterial communities. *Environ Microbiol* 22, 354–368. doi: 10.1111/1462-2920.14852.

Galli, G., Bramanti, L., Priori, C., Rossi, S., Santangelo, G., Tsounis, G., et al. (2016). Model-

ling red coral (Corallium rubrum) growth in response to temperature and nutrition. *Ecological Modelling* 337, 137–148. doi: 10.1016/j.ecolmodel.2016.06.010.

Gasbarro, R., Sowers, D., Margolin, A., and Cordes, E. E. (2022). Distribution and predicted climatic refugia for a reef-building cold-water coral on the southeast US margin. *Global Change Biology*. doi: 10.1111/gcb.16415.

Gehlen, M., Séférian, R., Jones, D. O. B., Roy, T., Roth, R., Barry, J., et al. (2014). Projected pH reductions by 2100 might put deep North Atlantic biodiversity at risk. *Biogeosciences* 11, 6955–6967. doi: 10.5194/bg-11-6955-2014.

Genin, A., Dayton, P. K., Lonsdale, P. F., and Spiess, F. N. (1986). Corals on seamount peaks provide evidence of current acceleration over deep-sea topography. *Nature* 322, 59–61. doi: 10.1038/322059a0.

Gerkema, T. (2019). *An Introduction to Tides*. Cambridge: Cambridge University Press doi: 10.1017/9781316998793.

Gislason, A. (2018). Life cycles and seasonal vertical distributions of copepods in the Iceland Sea. *Polar Biol* 41, 2575–2589. doi: 10.1007/s00300-018-2392-4.

Glud, R. N. (2008). Oxygen dynamics of marine sediments. *Marine Biology Research* 4, 243–289. doi: 10.1080/17451000801888726.

Glud, R. N., Berg, P., Hume, A., Batty, P., Blicher, M. E., Lennert, K., et al. (2010). Benthic O2 exchange across hard-bottom substrates quantified by eddy correlation in a sub-Arctic fjord. *Marine Ecology Progress Series* 417, 1–12. doi: 10.3354/meps08795.

Glud, R. N., Berg, P., Stahl, H., Hume, A., Larsen, M., Eyre, B. D., et al. (2016). Benthic Carbon Mineralization and Nutrient Turnover in a Scottish Sea Loch: An Integrative In Situ Study. *Aquatic Geochemistry* 22, 443–467. doi: 10.1007/s10498-016-9300-8.

Gooday, A. J. (2002). Biological Responses to Seasonally Varying Fluxes of Organic Matter to the Ocean Floor: A Review. *Journal of Oceanography* 58, 305–332. doi: 10.1023/A:1015865826379.

Gori, A., Ferrier-Pagès, C., Hennige, S. J., Murray, F., Rottier, C., Wicks, L. C., et al. (2016). Physiological response of the cold-water coral *Desmophyllum dianthus* to thermal stress and ocean acidification. *PeerJ* 4, e1606. doi: 10.7717/peerj.1606.

Gori, A., Grover, R., Orejas, C., Sikorski, S., and Ferrier-Pagès, C. (2014). Uptake of dissolved free amino acids by four cold-water coral species from the Mediterranean Sea. *Deep Sea Research Part II: Topical Studies in Oceanography* 99, 42–50. doi: 10.1016/j.dsr2.2013.06.007.

Gori, A., Reynaud, S., Orejas, C., and Ferrier-Pagès, C. (2015). The influence of flow velocity and temperature on zooplankton capture rates by the cold-water coral Dendrophyllia cornigera. *Journal of Experimental Marine Biology and Ecology* 466, 92–97. doi: 10.1016/j.jembe.2015.02.004.

Grebmeier, J. M., and Barry, J. P. (1991). The influence of oceanographic processes on pelagic-benthic coupling in polar regions: A benthic perspective. *Journal of Marine Systems* 2, 495–518. doi: 10.1016/0924-7963(91)90049-Z.

Griffiths, D. K., Pingree, R. D., and Sinclair, M. (1981). Summer tidal fronts in the near-arctic regions of Foxe Basin and Hudson Bay. *Deep Sea Research Part A. Oceanographic Research Papers* 28, 865–873. doi: 10.1016/S0198-0149(81)80006-4.

Grolemund, G., and Wickham, H. (2011). Dates and Times Made Easy with lubridate. *Journal of Statistical Software* 40, 1–25.

Guihen, D., White, M., and Lundälv, T. (2013). Boundary layer flow dynamics at a cold-water coral reef. *Journal of Sea Research* 78, 36–44. doi: 10.1016/j.seares.2012.12.007.

Guillot, P. (2018). Cruise Bright/SN/Atlas 1802 (leg 2) CTD processing notes. Amundsen Science.

Guinotte, J. M., and Davies, A. J. (2014). Predicted Deep-Sea Coral Habitat Suitability for the U.S. West Coast. *PLoS ONE* 9, e93918. doi: 10.1371/journal.pone.0093918.

Guinotte, J. M., Orr, J., Cairns, S., Freiwald, A., Morgan, L., and George, R. (2006). Will human-induced changes in seawater chemistry alter the distribution of deep-sea scleractinian corals? *Frontiers in Ecology and the Environment* 4, 141–146. doi: 10.1890/1540-9295(2006)004[0141:WHCISC]2.0.CO;2.

Hansen, B., and Østerhus, S. (2000). North Atlantic–Nordic Seas exchanges. *Progress in Oceanography* 45, 109–208. doi: 10.1016/S0079-6611(99)00052-X.

Hanz, U., Beazley, L., Kenchington, E., Duineveld, G., Rapp, H. T., and Mienis, F. (2021a).

Seasonal Variability in Near-bed Environmental Conditions in the Vazella pourtalesii Glass Sponge Grounds of the Scotian Shelf. *Front. Mar. Sci.* 7, 597682. doi: 10.3389/fmars.2020.597682.

Hanz, U., Riekenberg, P., de Kluijver, A., van der Meer, M., Middelburg, J. J., de Goeij, J. M., et al. (2022). The important role of sponges in carbon and nitrogen cycling in a deep-sea biological hotspot. *Functional Ecology* 36, 2188–2199. doi: 10.1111/1365-2435.14117.

Hanz, U., Roberts, E. M., Duineveld, G., Davies, A., Haren, H. van, Rapp, H. T., et al. (2021b). Long-term Observations Reveal Environmental Conditions and Food Supply Mechanisms at an Arctic Deep-Sea Sponge Ground. *Journal of Geophysical Research: Oceans* 126, e2020JC016776. doi: https://doi.org/10.1029/2020JC016776.

Hanz, U., Wienberg, C., Hebbeln, D., Duineveld, G., Lavaleye, M., Juva, K., et al. (2019). Environmental factors influencing benthic communities in the oxygen minimum zones on the Angolan and Namibian margins. *Biogeosciences* 16, 4337–4356. doi: 10.5194/bg-16-4337-2019.

Harrison, G. W., Yngve Børsheim, K., Li, W. K. W., Maillet, G. L., Pepin, P., Sakshaug, E., et al. (2013). Phytoplankton production and growth regulation in the Subarctic North Atlantic: A comparative study of the Labrador Sea-Labrador/Newfoundland shelves and Barents/Norwegian/Greenland seas and shelves. *Progress in Oceanography* 114, 26–45. doi: 10.1016/j.pocean.2013.05.003.

Hawkes, N., Korabik, M., Beazley, L., Rapp, H., Xavier, J., and Kenchington, E. (2019). Glass sponge grounds on the Scotian Shelf and their associated biodiversity. *Mar. Ecol. Prog. Ser.* 614, 91–109. doi: 10.3354/meps12903.

Head, E. J. H., Harris, L. R., and Yashayaev, I. (2003). Distributions of Calanus spp. and other mesozooplankton in the Labrador Sea in relation to hydrography in spring and summer (1995–2000). *Progress in Oceanography* 59, 1–30. doi: 10.1016/S0079-6611(03)00111-3.

Head, E. J. H., Melle, W., Pepin, P., Bagøien, E., and Broms, C. (2013). On the ecology of Calanus finmarchicus in the Subarctic North Atlantic: A comparison of population dynamics and environmental conditions in areas of the Labrador Sea-Labrador/Newfoundland Shelf and Norwegian Sea Atlantic and Coastal Waters. *Progress in Oceanography* 114, 46–63. doi: 10.1016/j.pocean.2013.05.004.

Heath, M. R., Boyle, P. R., Gislason, A., Gurney, W. S. C., Hay, S. J., Head, E. J. H., et al. (2004). Comparative ecology of over-wintering Calanus finmarchicus in the northern North Atlantic, and implications for life-cycle patterns. *ICES Journal of Marine Science* 61, 698–708. doi: 10.1016/j.icesjms.2004.03.013.

Hebbeln, D., Portilho-Ramos, R. da C., Wienberg, C., and Titschack, J. (2019). The Fate of Cold-Water Corals in a Changing World: A Geological Perspective. *Front. Mar. Sci.* 6, 119. doi: 10.3389/fmars.2019.00119.

Hebbeln, D., Van Rooij, D., and Wienberg, C. (2016). Good neighbours shaped by vigorous currents: Cold-water coral mounds and contourites in the North Atlantic. *Marine Geology* 378, 171–185. doi: 10.1016/j.margeo.2016.01.014.

Hebbeln, D., Wienberg, C., Wintersteller, P., Freiwald, A., Becker, M., Beuck, L., et al. (2014). Environmental forcing of the Campeche cold-water coral province, southern Gulf of Mexico. *Biogeosciences* 11, 1799–1815. doi: 10.5194/bg-11-1799-2014.

Heifetz, J. (2002). Coral in Alaska: distribution, abundance, and species associations. *Hydrobiologia* 471, 19–28. doi: 10.1023/A:1016528631593.

Hennige, S. J., Wicks, L. C., Kamenos, N. A., Perna, G., Findlay, H. S., and Roberts, J. M. (2015). Hidden impacts of ocean acidification to live and dead coral framework. *Proc. R. Soc. B* 282, 20150990. doi: 10.1098/rspb.2015.0990.

Hennige, S. J., Wolfram, U., Wickes, L., Murray, F., Roberts, J. M., Kamenos, N. A., et al. (2020). Crumbling Reefs and Cold-Water Coral Habitat Loss in a Future Ocean: Evidence of "Coralporosis" as an Indicator of Habitat Integrity. *Front. Mar. Sci.* 7. doi: 10.3389/fmars.2020.00668.

Hennige, S., Larsson, A., Orejas, C., Gori, A., De Clippele, L., Lee, Y., et al. (2021). Using the Goldilocks Principle to model coral ecosystem engineering. *Proceedings of the Royal Society B* 288, 20211260.

Henry, L. A., and Roberts, J. M. (2007). Biodiversity and ecological composition of macrobenthos on cold-water coral mounds and adjacent off-mound habitat in the bathyal Porcupine Seabight, NE Atlantic. *Deep-Sea Research Part I: Oceanographic Research Papers* 54, 654–672. doi: 10.1016/j.dsr.2007.01.005.

Henson, S. A., Yool, A., and Sanders, R. (2015). Global Biogeochemical Cycles

carbon export : A model study. *Global Biogeochemical Cycles* 29, 33–45. doi: 10.1002/2014GB004965.Received.

Herring, P. J. (2002). *The biology of the deep ocean*. Oxford; New York: Oxford University Press.

Hirche, H.-J., and Mumm, N. (1992). Distribution of dominant copepods in the Nansen Basin, Arctic Ocean, in summer. *Deep Sea Research Part A, Oceanographic Research Papers* 39, S485–S505. doi: 10.1016/S0198-0149(06)80017-8.

Hoffmann, F., Radax, R., Woebken, D., Holtappels, M., Lavik, G., Rapp, H. T., et al. (2009). Complex nitrogen cycling in the sponge Geodia barretti. *Environmental Microbiology* 11, 2228–2243. doi: 10.1111/j.1462-2920.2009.01944.x.

Hogg, M., Tendal, O., Conway, K., Pomponi, S., Gutt, J., Krautter, M., et al. (2010). Deep-sea sponge grounds: Reservoirs of biodiversity.

Holliday, N. P., Pollard, R. T., Read, J. F., and Leach, H. (2000). Water mass properties and fluxes in the Rockall Trough, 1975 - 1998. *Deep Sea Research Part I: Oceanographic Research Papers*, 1303–1332.

Holtappels, M., Glud, R. N., Donis, D., Liu, B., Hume, A., Wenzhöfer, F., et al. (2013). Effects of transient bottom water currents and oxygen concentrations on benthic exchange rates as assessed by eddy correlation measurements. *Journal of Geophysical Research: Oceans*, 1157–1169. doi: 10.1002/jgrc.20112.

Hosegood, P., and van Haren, H. (2004). Near-bed solibores over the continental slope in the Faeroe-Shetland Channel. *Deep Sea Research Part II: Topical Studies in Oceanography* 51, 2943–2971. doi: 10.1016/j.dsr2.2004.09.016.

Howell, K., Pond, D., Billett, D., and Tyler, P. (2003). Feeding ecology of deep-sea seastars (Echinodermata: Asteroidea): a fatty-acid biomarker approach. *Mar. Ecol. Prog. Ser.* 255, 193–206. doi: 10.3354/meps255193.

Howell, K.-L., Piechaud, N., Downie, A.-L., and Kenny, A. (2016). The distribution of deep-sea sponge aggregations in the North Atlantic and implications for their effective spatial management. *Deep Sea Research Part I: Oceanographic Research Papers* 115, 309–320. doi: 10.1016/j.dsr.2016.07.005.

Hunter, T. (1989). Suspension Feeding in Oscillating Flow: The Effect of Colony Morphology and Flow Regime on Plankton Capture by the Hydroid *Obelia longissima*. *The Biological Bulletin* 176, 41–49. doi: 10.2307/1541887.

Hunter-Cevera, K. R., Neubert, M. G., Olson, R. J., Solow, A. R., Shalapyonok, A., and Sosik, H. M. (2016). Physiological and ecological drivers of early spring blooms of a coastal phytoplankter. *Science* 354, 326–329. doi: 10.1126/science.aaf8536.

Husebø, Å., Nøttestad, L., Fosså, J. H., Furevik, D. M., and Jørgensen, S. B. (2002). Distribution and abundance of fish in deep-sea coral habitats. *Hydrobiologia* 471, 91–99. doi: 10.1023/A:1016549203368.

Huthnance, J. M. (1973). On the diurnal tidal currents over Rockall Bank. *Deep Sea Research* 21, 23–35.

Hygum, B. H., Rey, C., and Hansen, B. W. (2000). Growth and development rates of *Calanus finmarchicus* nauplii during a diatom spring bloom. *Marine Biology* 136, 1075–1085. doi: 10.1007/s002270000313.

Iken, K., Brey, T., Wand, U., Voigt, J., and Junghans, P. (2001). Food web structure of the benthic community at the Porcupine Abyssal Plain (NE Atlantic): a stable isotope analysis. *Progress in Oceanography* 50, 383–405. doi: 10.1016/S0079-6611(01)00062-3.

Inoue, T., Glud, R. N., Stahl, H., and Hume, A. (2011). Comparison of three different methods for assessing in situ friction velocity: A case study from Loch Etive, Scotland. *Limnology and Oceanography: Methods* 9, 275–287. doi: 10.4319/lom.2011.9.275.

Iversen, M. H., and Lampitt, R. S. (2020). Size does not matter after all: No evidence for a size-sinking relationship for marine snow. *Progress in Oceanography* 189, 102445. doi: 10.1016/j.pocean.2020.102445.

Iversen, M. H., and Ploug, H. (2010). Ballast minerals and the sinking carbon flux in the ocean: carbon-specific respiration rates and sinking velocity of marine snow aggregates. *Biogeosciences* 7, 2613–2624. doi: 10.5194/bg-7-2613-2010.

Jeffrey, S. W., Mantoura, R. F. C., and Wright, S. W. (2005). *Phytoplankton pigments in oceanography: guidelines to modern methods*. Unesco Pub. Paris, France.

Jensen, A., and Frederiksen, R. (1992). The fauna associated with the bank-forming deep-water coral Lophelia pertusa (Scleractinaria) on the Faroe shelf. *Sarsia* 77, 53–69. doi: 10.1080/00364827.1992.10413492.

Johnson, C., Sherwin, T., Cunningham, S., Dumont, E., Houpert, L., and Holliday, N. P. (2017). Transports and pathways of overflow water in the Rockall Trough. *Deep Sea Research Part I: Oceanographic Research Papers* 122, 48–59. doi: 10.1016/j.dsr.2017.02.004.

Johnson, C., Sherwin, T., Smythe-Wright, D., Shimmield, T., and Turrell, W. (2010). Wyville Thomson Ridge Overflow Water: Spatial and temporal distribution in the Rockall Trough. *Deep Sea Research Part I: Oceanographic Research Papers* 57, 1153–1162. doi: 10.1016/j.dsr.2010.07.006.

Jones, C. G., Lawton, J. H., and Shachak, M. (1994). Organisms as Ecosystem Engineers. *Oikos* 69, 373–386. doi: 10.2307/3545850.

Jones, D. O. B., Yool, A., Wei, C.-L., Henson, S. A., Ruhl, H. A., Watson, R. A., et al. (2014). Global reductions in seafloor biomass in response to climate change. *Global Change Biology* 20, 1861–1872. doi: 10.1111/gcb.12480.

Jones, E. P., Dyrssen, D., and Coote, A. R. (1984). Nutrient Regeneration in Deep Baffin Bay with Consequences for Measurements of the Conservative Tracer NO and Fossil Fuel CO2 in the Oceans. *Can. J. Fish. Aquat. Sci.* 41, 30–35. doi: 10.1139/f84-003.

Jones, S. E., Jago, C. F., Bale, A. J., Chapman, D., Howland, R. J. M., and Jackson, J. (1998). Aggregation and resuspension of suspended particulate matter at a seasonally stratified site in the southern North Sea: physical and biological controls. *Continental Shelf Research* 18, 1283–1309. doi: 10.1016/S0278-4343(98)00044-2.

Jonsson, L. G., Nilsson, P. G., Floruta, F., and Lundälv, T. (2004). Distributional patterns of macro- and megafauna associated with a reef of the cold-water coral Lophelia pertusa on the Swedish west coast. 284, 163–171. doi: 10.3354/meps284163.

Jorda, G., Marbà, N., Bennett, S., Santana-Garcon, J., Agusti, S., and Duarte, C. M. (2020). Ocean warming compresses the three-dimensional habitat of marine life. *Nat Ecol Evol* 4, 109–114. doi: 10.1038/s41559-019-1058-0.

Juva, K., Flögel, S., Karstensen, J., Linke, P., and Dullo, W.-C. (2020). Tidal Dynamics Control on Cold-Water Coral Growth: A High-Resolution Multivariable Study on Eastern Atlantic Cold-Water Coral Sites. *Front. Mar. Sci.* 7, 132. doi: 10.3389/fmars.2020.00132.

Juva, K., Kutti, T., Chierici, M., Dullo, W.-C., and Flögel, S. (2021). Cold-Water Coral Reefs in the Langenuen Fjord, Southwestern Norway—A Window into Future Environmental Change. *Oceans* 2, 583–610. doi: 10.3390/oceans2030033.

Kahn, A. S., Chu, J. W. F., and Leys, S. P. (2018). Trophic ecology of glass sponge reefs in the Strait of Georgia, British Columbia. *Sci Rep* 8, 756. doi: 10.1038/s41598-017-19107-x.

Kahn, A. S., Yahel, G., Chu, J. W. F., Tunnicliffe, V., and Leys, S. P. (2015). Benthic grazing and carbon sequestration by deep-water glass sponge reefs: Deep-water glass sponge reefs. *Limnol. Oceanogr.* 60, 78–88. doi: 10.1002/lno.10002.

Karl, D. M., Wirsen, C. O., and Jannasch, H. W. (1980). Deep-Sea Primary Production at the Galápagos Hydrothermal Vents. *Science* 207, 1345–1347. doi: 10.1126/science.207.4437.1345.

Kazanidis, G., van Oevelen, D., Veuger, B., and Witte, U. F. M. (2018). Unravelling the versatile feeding and metabolic strategies of the cold-water ecosystem engineer Spongosorites coralliophaga (Stephens, 1915). *Deep Sea Research Part I: Oceanographic Research Papers* 141, 71–82. doi: 10.1016/j.dsr.2018.07.009.

Kelley, D., and Richards, C. (2020). *oce: Analysis of Oceanographic Data*. Available at: https://CRAN.R-project.org/package=oce.

Kelly, J., and Scheibling, R. (2012). Fatty acids as dietary tracers in benthic food webs. *Mar. Ecol. Prog. Ser.* 446, 1–22. doi: 10.3354/meps09559.

Kenchington, E. L., Lirette, C., Cogswell, A., Archambault, D., Archambault, P., Benoit, H., et al. (2010). Delineating Coral and Sponge Concentrations in the Biogeographic Regions of the East Coast of Canada Using Spatial Analyses. *DFO Can. Sci. Advis. Sec. Res. Doc.*, vi + 202 pp.

Kenchington, E., Power, D., and Koen-Alonso, M. (2013). Associations of demersal fish with sponge grounds on the continental slopes of the northwest Atlantic. *Mar. Ecol. Prog. Ser.* 477, 217–230. doi: 10.3354/meps10127.

Kenyon, N. H., Akhmetzhanov, A. M., Wheeler, A. J., van Weering, T. C. E., de Haas, H., and Ivanov, M. K. (2003). Giant carbonate mud mounds in the southern Rockall Trough. *Marine Geology* 195, 5–30. doi: 10.1016/S0025-3227(02)00680-1.

Khripounoff, A., Caprais, J.-C., Le Bruchec, J., Rodier, P., Noel, P., and Cathalot, C. (2014). Deep cold-water coral ecosystems in the Brittany submarine canyons (Northeast Atlantic): Hydrodynamics, particle supply, respiration, and carbon cycling. *Limnology & Oceanography* 59, 87–98. doi: 10.4319/lo.2014.59.01.0087.

Kim, K., and Lasker, H. R. (1998). Allometry of resource capture in colonial cnidarians and constraints on modular growth. *Funct Ecology* 12, 646–654. doi: 10.1046/j.1365-2435.1998.00228.x.

Kiriakoulakis, K., Bett, B. J., White, M., and Wolff, G. A. (2004). Organic biogeochemistry of the Darwin Mounds, a deep-water coral ecosystem, of the NE Atlantic. *Deep Sea Research Part I: Oceanographic Research Papers* 51, 1937–1954. doi: 10.1016/j.dsr.2004.07.010.

Kiriakoulakis, K., Fisher, E., Wolff, G. A., Freiwald, A., Grehan, A., and Roberts, J. M. (2005). "Lipids and nitrogen isotopes of two deep-water corals from the North-East Atlantic: initial results and implications for their nutrition," in *Cold-Water Corals and Ecosystems*, eds. A. Freiwald and J. M. Roberts (Berlin/Heidelberg: Springer-Verlag), 715–729. doi: 10.1007/3-540-27673-4_37.

Kiriakoulakis, K., Freiwald, A., Fisher, E., and Wolff, G. A. (2007). Organic matter quality and supply to deep-water coral/mound systems of the NW European Continental Margin. *Int J Earth Sci (Geol Rundsch)* 96, 159–170. doi: 10.1007/s00531-006-0078-6.

Klein Breteler, W. C. M. (1982). The life stages of four pelagic copepods (Copepoda: Calanoida), illustrated by a series of photographs: Klein Breteler, W.C.M., 1982. (Acartia clausi, Temora longicornis, Centropages hamatus and Pseudocalanus sp.). Publ. Ser. Neth. Inst. Sea Res., 6:32pp. *Deep Sea Research Part B. Oceanographic Literature Review* 30, 934. doi: 10.1016/0198-0254(83)96590-1.

Klitgaard, A. B. (1995). The fauna associated with outer shelf and upper slope sponges (Porifera, Demospongiae) at the Faroe Islands, northeastern Atlantic. *Sarsia* 80, 1–22. doi: 10.1080/00364827.1995.10413574.

Klitgaard, A. B., and Tendal, O. S. (2004). Distribution and species composition of mass occurrences of large-sized sponges in the northeast Atlantic. *Progress in Oceanography* 61, 57–98. doi: 10.1016/j.pocean.2004.06.002.

Knudby, A., Kenchington, E., and Murillo, F. J. (2013). Modeling the Distribution of Geodia Sponges and Sponge Grounds in the Northwest Atlantic. *PLoS ONE* 8, e82306. doi: 10.1371/journal.pone.0082306.

Kollmeyer, R. C., United States. Coast Guard. Oceanographic Unit, McGill, D. A. (David A.), and Corwin, N. (1967). *Oceanography of the Labrador Sea in the vicinity of Hudson Strait in 1965*. Washington, D.C. : U.S. Coast Guard Oceanographic Unit Available at: http://archive.org/details/oceanographyoflaOOkoll [Accessed January 28, 2022].

Krieger, K. J., and Wing, B. L. (2002). Megafauna associations with deepwater corals (Primnoa spp.) in the Gulf of Alaska. *Hydrobiologia* 471, 83–90. doi: 10.1023/A:1016597119297.

Krumhansl, K. A., Head, E. J. H., Pepin, P., Plourde, S., Record, N. R., Runge, J. A., et al. (2018). Environmental drivers of vertical distribution in diapausing Calanus copepods in the Northwest Atlantic. *Progress in Oceanography* 162, 202–222. doi: 10.1016/j.pocean.2018.02.018.

Kutti, T., Bannister, R. J., and Fosså, J. H. (2013). Community structure and ecological function of deep-water sponge grounds in the Traenadypet MPA—Northern Norwegian continental shelf. *Continental Shelf Research* 69, 21–30. doi: 10.1016/j.csr.2013.09.011.

Kutti, T., Fosså, J., and Bergstad, O. (2015). Influence of structurally complex benthic habitats on fish distribution. *Mar. Ecol. Prog. Ser.* 520, 175–190. doi: 10.3354/meps11047.

Lalli, C., and Parsons, T. (1997). *Biological oceanography: an introduction*. Elsevier.

Lampitt, R. S., Wishner, K. F., Turley, C. M., and Angel, M. V. (1993). Marine snow studies in the Northeast Atlantic Ocean: distribution, composition and role as a food source for migrating plankton. *Marine Biology* 116, 689–702. doi: 10.1007/BF00355486.

Larsson, A. I., Lundälv, T., and van Oevelen, D. (2013). Skeletal growth, respiration rate and fatty acid composition in the cold-water coral *Lophelia pertusa* under varying food conditions. *Mar. Ecol. Prog. Ser.* 483, 169–184. doi: 10.3354/meps10284.

Lavaleye, M., Duineveld, G., Lundälv, T., White, M., Guihen, D., Kiriakoulakis, K., et al. (2009). Cold-water corals on the Tisler reef: preliminary observations on the dynamic reef environment. *Oceanography* 22, 76–84.

Lavaleye, M. S. S., Duineveld, G. C. A., Berghuis, E. M., Kok, A., and Witbaard, R. (2002). A comparison between the megafauna communities on the N.W. Iberian and Celtic continental margins—effects of coastal upwelling? *Progress in Oceanography* 52, 459–476. doi: 10.1016/S0079-6611(02)00019-8.

Laws, E. A., Falkowski, P. G., Smith, W. O., Ducklow, H., and McCarthy, J. J. (2000). Temperature effects on export production in the open ocean. *Global Biogeochem. Cycles* 14, 1231–1246. doi: 10.1029/1999GB001229.

Lazier, J. R. N., and Wright, D. G. (1993). Annual Velocity Variations in the Labrador Current. *Journal of Physical Oceanography* 23, 659–678. doi: 10.1175/1520-0485(1993)023<0659:AVVITL>2.0.CO;2.

Lee, R. F., Hagen, W., and Kattner, G. (2006). Lipid storage in marine zooplankton. *Marine Ecology Progress Series* 307, 273–306. doi: 10.3354/meps307273.

Lee, S., and Fuhrman, J. A. (1987). Relationships between Biovolume and Biomass of Naturally Derived Marine Bacterioplankton. *Appl. Environ. Microbiol.* 53, 1298–1303.

Lehmann, N., Kienast, M., Granger, J., Bourbonnais, A., Altabet, M. A., and Tremblay, J.-É. (2019). Remote Western Arctic Nutrients Fuel Remineralization in Deep Baffin Bay. *Global Biogeochemical Cycles* 33, 649–667. doi: 10.1029/2018GB006134.

Lesht, B. M. (1979). Relationship between sediment resuspension and the statistical frequency distribution of bottom shear stress. *Marine Geology* 32, M19–M27. doi: 10.1016/0025-3227(79)90142-7.

Levin, L. A. (2003). *Oxygen minimum zone benthos: adaptation and community response to hypoxia*. CRC Press doi: 10.1201/9780203180570-3.

Levin, L. A., and Le Bris, N. (2015). The deep ocean under climate change. *Science* 350, 766–768. doi: 10.1126/science.aad0126.

Levin, L. A., and Sibuet, M. (2012). Understanding Continental Margin Biodiversity: A New Imperative. *Annu. Rev. Mar. Sci.* 4, 79–112. doi: 10.1146/annurev-marine-120709-142714.

Levitus, S., Antonov, J., and Boyer, T. (2005). Warming of the world ocean, 1955–2003. *Geophysical Research Letters* 32. doi: 10.1029/2004GL021592.

Leys, S. P., Kahn, A. S., Fang, J. K. H., Kutti, T., and Bannister, R. J. (2018). Phagocytosis of microbial symbionts balances the carbon and nitrogen budget for the deep-water boreal sponge Geodia barretti: Metabolism of Geodia barretti. *Limnol. Oceanogr.* 63, 187–202. doi: 10.1002/lno.10623.

Leys, S. P., and Lauzon, N. R. J. (1998). Hexactinellid sponge ecology: growth rates and seasonality in deep water sponges. *Journal of Experimental Marine Biology and Ecology* 230, 111–129. doi: 10.1016/S0022-0981(98)00088-4.

Leys, S. P., Yahel, G., Reidenbach, M. A., Tunnicliffe, V., Shavit, U., and Reiswig, H. M. (2011). The Sponge Pump: The Role of Current Induced Flow in the Design of the Sponge Body Plan. *PLoS ONE* 6, e27787. doi: 10.1371/journal.pone.0027787.

Li, G., Cheng, L., Zhu, J., Trenberth, K. E., Mann, M. E., and Abraham, J. P. (2020). Increasing ocean stratification over the past half-century. *Nat. Clim. Chang.* doi: 10.1038/s41558-020-00918-2.

Libes, S. M. (2009). *Introduction to marine biogeochemistry*. Academic Press.

Lim, A., Wheeler, A. J., and Arnaubec, A. (2017). High-resolution facies zonation within a cold-water coral mound: The case of the Piddington Mound, Porcupine Seabight, NE Atlantic. *Marine Geology* 390, 120–130. doi: 10.1016/j.margeo.2017.06.009.

Lim, A., Wheeler, A. J., Price, D. M., O'Reilly, L., Harris, K., and Conti, L. (2020). Influence of benthic currents on cold-water coral habitats: a combined benthic monitoring and 3D photogrammetric investigation. *Sci Rep* 10, 19433. doi: 10.1038/s41598-020-76446-y.

Lomas, M. W., and Moran, S. B. (2011). Evidence for aggregation and export of cyanobacteria and nano-eukaryotes from the Sargasso Sea euphotic zone. *Biogeosciences* 8, 203–2016. doi: 10.5194/bg-8-203-2011.

López-Acosta, M., Leynaert, A., and Maldonado, M. (2016). Silicon consumption in two shallow-water sponges with contrasting biological features. *Limnology and Oceanography* 61, 2139–2150. doi: 10.1002/lno.10359.

Louda, J. W., Liu, L., and Baker, E. W. (2002). Senescence- and death-related alteration of chlorophylls and carotenoids in marine phytoplankton. *Organic Geochemistry* 33, 1635–1653. doi: 10.1016/S0146-6380(02)00106-7.

Lovelace, R., Félix, R., and Talbot, J. (2022). *slopes: Calculate Slopes of Roads, Rivers and Trajectories*.

Madsen, S. D., Nielsen, T. G., and Hansen, B. W. (2001). Annual population development and production by Calanus finmarchicus , C. glacialis and C. hyperboreus in Disko Bay, western Greenland. *Marine Biology* 139, 75–93. doi: 10.1007/s002270100552.

Maier, C., de Kluijver, A., Agis, M., Brussaard, C. P. D., van Duyl, F. C., and Weinbauer, M. G. (2011). Dynamics of nutrients, total organic carbon, prokaryotes and viruses in onboard incubations of cold-water corals. *Biogeosciences* 8, 2609–2620. doi: 10.5194/bg-8-2609-2011.

Maier, S. R., Bannister, R. J., van Oevelen, D., and Kutti, T. (2020a). Seasonal controls on the diet, metabolic activity, tissue reserves and growth of the cold-water coral *Lophelia pertusa*. *Coral Reefs* 39, 173–187. doi: 10.1007/s00338-019-01886-6.

Maier, S. R., Kutti, T., Bannister, R. J., Fang, J. K.-H., van Breugel, P., van Rijswijk, P., et al. (2020b). Recycling pathways in cold-water coral reefs: Use of dissolved organic matter and bacteria by key suspension feeding taxa. *Scientific Reports* 10, 9942. doi: 10.1038/s41598-020-66463-2.

Maier, S. R., Kutti, T., Bannister, R. J., van Breugel, P., van Rijswijk, P., and van Oevelen, D. (2019). Survival under conditions of variable food availability: Resource utilization and storage in the cold-water coral *Lophelia pertusa*. *Limnology & Oceanography* 0, 1–21. doi: 10.1002/lno.11142.

Maier, S. R., Mienis, F., de Froe, E., Soetaert, K., Lavaleye, M., Duineveld, G., et al. (2021). Reef communities associated with 'dead' cold-water coral framework drive resource retention and recycling in the deep sea. *Deep Sea Research Part I: Oceanographic Research Papers* 175. doi: 10.1016/j.dsr.2021.103574.

Maldonado, M. (2011). The ecology of the sponge larva. *Canadian Journal of Zoology*. doi: 10.1139/z05-177.

Maldonado, M., Aguilar, R., Bannister, R. J., Bell, J. J., Conway, K. W., Dayton, P. K., et al. (2017). "Sponge Grounds as Key Marine Habitats: A Synthetic Review of Types, Structure, Functional Roles, and Conservation Concerns," in *Marine Animal Forests: The Ecology of Benthic Biodiversity Hotspots*, eds. S. Rossi, L. Bramanti, A. Gori, and C. Orejas (Cham: Springer International Publishing), 145–183. doi: 10.1007/978-3-319-21012-4_24.

Maldonado, M., Beazley, L., López-Acosta, M., Kenchington, E., Casault, B., Hanz, U., et al. (2020a). Massive silicon utilization facilitated by a benthic-pelagic coupled feedback sustains deep-sea sponge aggregations. *Limnol Oceanogr*, lno.11610. doi: 10.1002/lno.11610.

Maldonado, M., López-Acosta, M., Beazley, L., Kenchington, E., Koutsouveli, V., and Riesgo, A. (2020b). Cooperation between passive and active silicon transporters clarifies the ecophysiology and evolution of biosilicification in sponges. *Science Advances* 6, eaba9322. doi: 10.1126/sciadv.aba9322.

Maldonado, M., Navarro, L., Grasa, A., Gonzalez, A., and Vaquerizo, I. (2011). Silicon uptake by sponges: a twist to understanding nutrient cycling on continental margins. *Sci Rep* 1, 30. doi: 10.1038/srep00030.

Maldonado, M., Ribes, M., and van Duyl, F. C. (2012). "Nutrient Fluxes Through Sponges," in *Advances in Marine Biology* (Elsevier), 113–182. doi: 10.1016/B978-0-12-394283-8.00003-5.

Marie, D., Partensky, F., Vaulot, D., and Brussaard, C. (1999). Enumeration of Phytoplankton, Bacteria, and Viruses in Marine Samples. *Current Protocols in Cytometry* 10, 11.11.1-11.11.15. doi: https://doi.org/10.1002/0471142956.cy1111s10.

Martin, J. H., Knauer, G. A., Karl, D. M., and Broenkow, W. W. (1987). VERTEX: carbon cycling in the northeast Pacific. *Deep Sea Research Part A. Oceanographic Research Papers* 34, 267–285. doi: 10.1016/0198-0149(87)90086-0.

MATLAB (2010). *version 7.10.0 (R2010a)*. Natick, Massachusetts: The MathWorks Inc.

Matos, L., Wienberg, C., Titschack, J., Schmiedl, G., Frank, N., Abrantes, F., et al. (2017). Coral mound development at the Campeche cold-water coral province, southern Gulf of Mexico: Implications of Antarctic Intermediate Water increased influence during interglacials. *Marine Geology* 392, 53–65. doi: 10.1016/j.margeo.2017.08.012.

Mauchline, J. (1998). *The biology of calanoid copepods*. San Diego: Academic Press.

McCulloch, M., Falter, J., Trotter, J., and Montagna, P. (2012a). Coral resilience to ocean acidification and global warming through pH up-regulation. *Nature Clim Change* 2, 623–627. doi: 10.1038/nclimate1473.

McCulloch, M., Trotter, J., Montagna, P., Falter, J., Dunbar, R., Freiwald, A., et al. (2012b). Resilience of cold-water scleractinian corals to ocean acidification: Boron isotopic systematics of pH and saturation state up-regulation. *Geochimica et Cosmochimica Acta* 87, 21–34. doi: 10.1016/j.gca.2012.03.027.

McGinnis, D. F., Cherednichenko, S., Sommer, S., Berg, P., Rovelli, L., Schwarz, R., et al. (2011). Simple, robust eddy correlation amplifier for aquatic dissolved oxygen and hydrogen sulfide flux measurements. *Limnology and Oceanography: Methods* 9, 340–347. doi: 10.4319/lom.2011.9.340.

McGinnis, D. F., Sommer, S., Lorke, A., Glud, R. N., and Linke, P. (2014). Quantifying tidally driven benthic oxygen exchange across permeable sediments: An aquatic eddy correlation study. *Journal of Geophysical Research: Oceans* 119, 6918–6932. doi: 10.1002/2014JC010303.

McGrath, T., Nolan, G., and McGovern, E. (2012). Chemical characteristics of water masses in the Rockall Trough. *Deep Sea Research Part I: Oceanographic Research Papers* 61, 57–73. doi: 10.1016/j.dsr.2011.11.007.

McIntyre, F. D., Drewery, J., Eerkes-Medrano, D., and Neat, F. C. (2016). Distribution and diversity of deep-sea sponge grounds on the Rosemary Bank Seamount, NE Atlantic. *Mar Biol* 163, 143. doi: 10.1007/s00227-016-2913-z.

Meyer, H. K., Roberts, E. M., Rapp, H. T., and Davies, A. J. (2019). Spatial patterns of arctic sponge ground fauna and demersal fish are detectable in autonomous underwater vehicle (AUV) imagery. *Deep Sea Research Part I: Oceanographic Research Papers* 153, 103137. doi: 10.1016/j.dsr.2019.103137.

Michna, P., and Woods, M. (2019). *RNetCDF: Interface to "NetCDF" Datasets*. Available at: https://CRAN.R-project.org/package=RNetCDF.

Middelbo, A. B., Sejr, M. K., Arendt, K. E., and Møller, E. F. (2018). Impact of glacial meltwater on spatiotemporal distribution of copepods and their grazing impact in Young Sound NE, Greenland. *Limnology and Oceanography* 63, 322–336. doi: 10.1002/lno.10633.

Middelburg, J. J. (2019). *Marine Carbon Biogeochemistry: A Primer for Earth System Scientists*. Cham, Switzerland: Springer International Publishing doi: 10.1007/978-3-030-10822-9.

Middelburg, J. J., Mueller, C. E., Veuger, B., Larsson, A. I., Form, A., and van Oevelen, D. (2015). Discovery of symbiotic nitrogen fixation and chemoautotrophy in cold-water corals. *Scientific reports* 5, 17962. doi: 10.1038/srep17962.

Mienis, F., Bouma, T. J., Witbaard, R., Van Oevelen, D., and Duineveld, G. C. A. (2019). Experimental assessment of the effects of cold-water coral patches on water flow. *Marine Ecology Progress Series* 609, 101–117. doi: https://doi.org/10.3354/meps12815.

Mienis, F., de Stigter, H. C., de Haas, H., and van Weering, T. C. E. (2009a). Near-bed particle deposition and resuspension in a cold-water coral mound area at the Southwest Rockall Trough margin, NE Atlantic. *Deep Sea Research Part I: Oceanographic Research Papers* 56, 1026–1038. doi: 10.1016/j.dsr.2009.01.006.

Mienis, F., van der Land, C., de Stigter, H. C., van de Vorstenbosch, M., de Haas, H., Richter, T., et al. (2009b). Sediment accumulation on a cold-water carbonate mound at the Southwest Rockall Trough margin. *Marine Geology* 265, 40–50. doi: 10.1016/j.margeo.2009.06.014.

Mienis, F., de Stigter, H. C., White, M., Duineveld, G., de Haas, H., and van Weering, T. C. E. (2007). Hydrodynamic controls on cold-water coral growth and carbonate-mound development at the SW and SE Rockall Trough Margin, NE Atlantic Ocean. *Deep Sea Research Part I: Oceanographic Research Papers* 54, 1655–1674. doi: 10.1016/j.dsr.2007.05.013.

Mienis, F., Duineveld, G. C. A., Davies, A. J., Ross, S. W., Seim, H., Bane, J., et al. (2012). The influence of near-bed hydrodynamic conditions on cold-water corals in the Viosca Knoll area, Gulf of Mexico. *Deep Sea Research Part I: Oceanographic Research Papers*

60, 32–45. doi: 10.1016/j.dsr.2011.10.007.

Mienis, F., van Weering, T., de Haas, H., de Stigter, H., Huvenne, V., and Wheeler, A. (2006). Carbonate mound development at the SW Rockall Trough margin based on high resolution TOBI and seismic recording. *Marine Geology* 233, 1–19. doi: 10.1016/j.margeo.2006.08.003.

Mohn, C., Rengstorf, A., White, M., Duineveld, G. C. A., Mienis, F., Soetaert, K., et al. (2014). Linking benthic hydrodynamics and cold-water coral occurrences: A high-resolution model study at three cold-water coral provinces in the NE Atlantic. *Progress in Oceanography* 122, 92–104. doi: 10.1016/j.pocean.2013.12.003.

Mohn, C., and White, M. (2007). Remote sensing and modelling of bio-physical distribution patterns at Porcupine and Rockall Bank, Northeast Atlantic. *Continental Shelf Research* 27, 1875–1892. doi: 10.1016/j.csr.2007.03.006.

Mojica, K. D. A., van de Poll, W. H., Kehoe, M., Huisman, J., Timmermans, K. R., Buma, A. G. J., et al. (2015). Phytoplankton community structure in relation to vertical stratification along a north-south gradient in the Northeast Atlantic Ocean: Phytoplankton and vertical stratification. *Limnol. Oceanogr.* 60, 1498–1521. doi: 10.1002/lno.10113.

Mora, C., Wei, C.-L., Rollo, A., Amaro, T., Baco, A. R., Billett, D., et al. (2013). Biotic and Human Vulnerability to Projected Changes in Ocean Biogeochemistry over the 21st Century. *PLOS Biology* 11, e1001682. doi: 10.1371/journal.pbio.1001682.

Morato, T., González-Irusta, J.-M., Dominguez-Carrió, C., Wei, C.-L., Davies, A., Sweetman, A. K., et al. (2020). Climate-induced changes in the suitable habitat of cold-water corals and commercially important deep-sea fishes in the North Atlantic. *Global Change Biology* 26, 2181–2202. doi: 10.1111/gcb.14996.

Morganti, T. M., Slaby, B. M., de Kluijver, A., Busch, K., Hentschel, U., Middelburg, J. J., et al. (2022). Giant sponge grounds of Central Arctic seamounts are associated with extinct seep life. *Nat Commun* 13, 638. doi: 10.1038/s41467-022-28129-7.

Mortensen, P. B. (2001). Aquarium observations on the deep-water coral *Lophelia pertusa* (L., 1758) (scleractinia) and selected associated invertebrates. *Ophelia* 54, 83–104. doi: 10.1080/00785236.2001.10409457.

Mortensen, P. B., and Buhl-Mortensen, L. (2005). Morphology and growth of the deep-water gorgonians Primnoa resedaeformis and Paragorgia arborea. *Marine Biology* 147, 775–788. doi: 10.1007/s00227-005-1604-y.

Mueller, C. E., Larsson, A. I., Veuger, B., Middelburg, J. J., and van Oevelen, D. (2014). Opportunistic feeding on various organic food sources by the cold-water coral *Lophelia pertusa*. *Biogeosciences* 11, 123–133. doi: 10.5194/bg-11-123-2014.

Mueller, C. E., Lundälv, T., Middelburg, J. J., and van Oevelen, D. (2013). The Symbiosis between *Lophelia pertusa* and *Eunice norvegica* Stimulates Coral Calcification and Worm Assimilation. *PLoS ONE* 8, e58660. doi: 10.1371/journal.pone.0058660.

Murillo, F. J., Muñoz, P. D., Cristobo, J., Ríos, P., González, C., Kenchington, E., et al. (2012). Deep-sea sponge grounds of the Flemish Cap, Flemish Pass and the Grand Banks of Newfoundland (Northwest Atlantic Ocean): Distribution and species composition. *Marine Biology Research* 8, 842–854. doi: 10.1080/17451000.2012.682583.

Murillo, F., Kenchington, E., Tompkins, G., Beazley, L., Baker, E., Knudby, A., et al. (2018). Sponge assemblages and predicted archetypes in the eastern Canadian Arctic. *Mar. Ecol. Prog. Ser.* 597, 115–135. doi: 10.3354/meps12589.

Murray, F., Clippele, L. H. D., Hiley, A., Wicks, L., Roberts, J. M., and Hennige, S. (2019). Multiple feeding strategies observed in the cold-water coral Lophelia pertusa. *Journal of the Marine Biological Association of the United Kingdom* 99, 1281–1283. doi: 10.1017/S0025315419000298.

Murray, J. W., Barber, R. T., Roman, M. R., Bacon, M. P., and Feely, R. A. (1994). Physical and Biological Controls on Carbon Cycling in the Equatorial Pacific. *Science* 266, 58–65. doi: 10.1126/science.266.5182.58.

Myers, R. A., Akenhead, S. A., and Drinkwater, K. (1990). The influence of Hudson Bay runoff and ice-melt on the salinity of the inner Newfoundland Shelf. *Atmosphere-Ocean* 28, 241–256. doi: 10.1080/07055900.1990.9649377.

Naumann, M. S., Orejas, C., Wild, C., and Ferrier-Pages, C. (2011). First evidence for zooplankton feeding sustaining key physiological processes in a scleractinian cold-water coral. *Journal of Experimental Biology* 214, 3570–3576. doi: 10.1242/jeb.061390.

Neuwirth, E. (2014). *RColorBrewer: ColorBrewer Palettes*. Available at: https://CRAN.R-project.org/package=RColorBrewer.

Newton, P. P., Lampitt, R. S., Jickells, T. D., King, P., and Boutle, C. (1994). Temporal and spatial variability of biogenic particles fluxes during the JGOFS northeast Atlantic process studies at 47°N, 20°W. *Deep Sea Research Part I: Oceanographic Research Papers* 41, 1617–1642. doi: 10.1016/0967-0637(94)90065-5.

Ogle, D. H., Wheeler, P., and Dinno, A. (2021). *FSA: Fisheries Stock Analysis*. Available at: https://github.com/droglenc/FSA.

Orejas, C., Ferrier-Pagès, C., Reynaud, S., Tsounis, G., Allemand, D., and Gili, J. M. (2011). Experimental comparison of skeletal growth rates in the cold-water coral Madrepora oculata Linnaeus, 1758 and three tropical scleractinian corals. *Journal of Experimental Marine Biology and Ecology* 405, 1–5. doi: 10.1016/j.jembe.2011.05.008.

Orejas, C., Gori, A., Rad-Menéndez, C., Last, K. S., Davies, A. J., Beveridge, C. M., et al. (2016). The effect of flow speed and food size on the capture efficiency and feeding behaviour of the cold-water coral Lophelia pertusa. *Journal of Experimental Marine Biology and Ecology* 481, 34–40. doi: 10.1016/j.jembe.2016.04.002.

Osterloff, J., Nilssen, I., Järnegren, J., Van Engeland, T., Buhl-Mortensen, P., and Nattkemper, T. W. (2019). Computer vision enables short- and long-term analysis of Lophelia pertusa polyp behaviour and colour from an underwater observatory. *Sci Rep* 9, 6578. doi: 10.1038/s41598-019-41275-1.

Papadimitriou, S., Kennedy, H., Bentaleb, I., and Thomas, D. N. (2002). Dissolved organic carbon in sediments from the eastern North Atlantic. *Marine Chemistry* 79, 37–47. doi: 10.1016/S0304-4203(02)00055-5.

Parrish, C. C. (2013). Lipids in Marine Ecosystems. *ISRN Oceanography* 2013, 604045. doi: 10.5402/2013/604045.

Pawlowicz, R., Beardsley, B., and Lentz, S. (2002). Classical tidal harmonic analysis including error estimates in MATLAB using T_TIDE. *Computers & Geosciences* 28, 929–937. doi: 10.1016/S0098-3004(02)00013-4.

Pearman, T. R. R., Robert, K., Callaway, A., Hall, R., Lo Iacono, C., and Huvenne, V. A. I. (2020). Improving the predictive capability of benthic species distribution models by incorporating oceanographic data – Towards holistic ecological modelling of a submarine canyon. *Progress in Oceanography* 184, 102338. doi: 10.1016/j.pocean.2020.102338.

Pearson, T., and Rosenberg, R. (1978). Macrobenthic succession in relation to organic enrichment and pollution of the marine environment. in *Oceanography and Marine Biology—An Annual Review*, 229–311. doi: 10.2983/035.034.0121U1.10.

Pedersen, T. L. (2019). *patchwork: The Composer of Plots*. Available at: https://CRAN.R-project.org/package=patchwork.

Petrie, B., Akenhead, S. A., Lazier, J., and Loder, J. (1988). The cold intermediate layer on the Labrador and Northeast Newfoundland Shelves, 1978–86.

Pham, C. K., Murillo, F. J., Lirette, C., Maldonado, M., Colaço, A., Ottaviani, D., et al. (2019). Removal of deep-sea sponges by bottom trawling in the Flemish Cap area: conservation, ecology and economic assessment. *Sci Rep* 9, 15843. doi: 10.1038/s41598-019-52250-1.

Pile, A. J., and Young, C. M. (2006). The natural diet of a hexactinellid sponge: Benthic–pelagic coupling in a deep-sea microbial food web. *Deep Sea Research Part I: Oceanographic Research Papers* 53, 1148–1156. doi: 10.1016/j.dsr.2006.03.008.

Pingree, R. D., and Griffiths, D. K. (1984). Trapped diurnal waves on Porcupine and Rockall Banks. *Journal of the Marine Biological Association of the United Kingdom* 64, 889–897. doi: 10.1017/S0025315400047305.

Polunin; (2001). Feeding relationships in Mediterranean bathyal assemblages elucidated by stable nitrogen and carbon isotope data. *Mar Ecol Prog Ser* 220, 13–23.

Pomar, L., Morsilli, M., Hallock, P., and Bádenas, B. (2012). Internal waves, an under-explored source of turbulence events in the sedimentary record. *Earth-Science Reviews* 111, 56–81. doi: 10.1016/j.earscirev.2011.12.005.

Portilho-Ramos, R. da C., Titschack, J., Wienberg, C., Rojas, M. G. S., Yokoyama, Y., and Hebbeln, D. (2022). Major environmental drivers determining life and death of cold-water corals through time. *PLOS Biology* 20, e3001628. doi: 10.1371/journal.

pbio.3001628.

Puerta, P., Johnson, C., Carreiro-Silva, M., Henry, L.-A., Kenchington, E., Morato, T., et al. (2020). Influence of Water Masses on the Biodiversity and Biogeography of Deep-Sea Benthic Ecosystems in the North Atlantic. *Frontiers in Marine Science* 7, 239. doi: 10.3389/fmars.2020.00239.

Purser, A., Larsson, A. I., Thomsen, L., and van Oevelen, D. (2010). The influence of flow velocity and food concentration on *Lophelia pertusa* (Scleractinia) zooplankton capture rates. *Journal of Experimental Marine Biology and Ecology* 395, 55–62. doi: 10.1016/j.jembe.2010.08.013.

R Core Team (2019). R: A Language and Environment for Statistical Computing. Available at: https://www.R-project.org/.

Radax, R., Rattei, T., Lanzen, A., Bayer, C., Rapp, H. T., Urich, T., et al. (2012). Metatranscriptomics of the marine sponge Geodia barretti: tackling phylogeny and function of its microbial community. *Environmental Microbiology* 14, 1308–1324. doi: 10.1111/j.1462-2920.2012.02714.x.

Raddatz, J., Rüggeberg, A., Liebetrau, V., Foubert, A., Hathorne, E. C., Fietzke, J., et al. (2014). Environmental boundary conditions of cold-water coral mound growth over the last 3 million years in the Porcupine Seabight, Northeast Atlantic. *Deep Sea Research Part II: Topical Studies in Oceanography* 99, 227–236. doi: 10.1016/j.dsr2.2013.06.009.

Ramirez-Llodra, E., Brandt, A., Danovaro, R., De Mol, B., Escobar, E., German, C. R., et al. (2010). Deep, diverse and definitely different: unique attributes of the world's largest ecosystem. *Biogeosciences* 7, 2851–2899. doi: 10.5194/bg-7-2851-2010.

Ramirez-Llodra, E., Tyler, P. A., Baker, M. C., Bergstad, O. A., Clark, M. R., Escobar, E., et al. (2011). Man and the Last Great Wilderness: Human Impact on the Deep Sea. *PLOS ONE* 6, e22588. doi: 10.1371/journal.pone.0022588.

Ranasinghe, R., Swinkels, C., Luijendijk, A., Roelvink, D., Bosboom, J., Stive, M., Walstra, D. (2011), Morphodynamic upscaling with the MORFAC approach: Dependencies and sensitivities, *Coastal Engineering*.

Ravet, J. L., Brett, M. T., and Arhonditsis, G. B. (2010). The effects of seston lipids on zooplankton fatty acid composition in Lake Washington, Washington, USA. *Ecology* 91, 180–190. doi: 10.1890/08-2037.1.

Reid, P. C., Fischer, A. C., Lewis-Brown, E., Meredith, M. P., Sparrow, M., Andersson, A. J., et al. (2009). Impacts of the oceans on climate change. *Advances in marine biology* 56, 1–150.

Renaud, P. E., Morata, N., Carroll, M. L., Denisenko, S. G., and Reigstad, M. (2008). Pelagic–benthic coupling in the western Barents Sea: Processes and time scales. *Deep Sea Research Part II: Topical Studies in Oceanography* 55, 2372–2380. doi: 10.1016/j.dsr2.2008.05.017.

Rengstorf, A. M., Mohn, C., Brown, C., Wisz, M. S., and Grehan, A. J. (2014). Predicting the distribution of deep-sea vulnerable marine ecosystems using high-resolution data: Considerations and novel approaches. *Deep Sea Research Part I: Oceanographic Research Papers* 93, 72–82. doi: 10.1016/j.dsr.2014.07.007.

Rex, M. A., Etter, R. J., Morris, J. S., Crouse, J., McClain, C. R., Johnson, N. A., et al. (2006). Global bathymetric patterns of standing stock and body size in the deep-sea benthos. *Marine Ecology Progress Series* 317, 1–8. doi: 10.3354/meps317001.

Ribeiro, C., Lopes dos Santos, A., Marie, D., Helena Pellizari, V., Pereira Brandini, F., and Vaulot, D. (2016). Pico and nanoplankton abundance and carbon stocks along the Brazilian Bight. *PeerJ* 4, e2587. doi: 10.7717/peerj.2587.

Rice, A. L., Thurston, M. H., and New, A. L. (1990). Dense aggregations of a hexactinellid sponge, Pheronema carpenteri, in the Porcupine Seabight (northeast Atlantic Ocean), and possible causes. *Progress in Oceanography* 24, 179–196. doi: 10.1016/0079-6611(90)90029-2.

Richardson, T. L. (2019). Mechanisms and Pathways of Small-Phytoplankton Export from the Surface Ocean. *Annu. Rev. Mar. Sci.* 11, 57–74. doi: 10.1146/annurev-marine-121916-063627.

Rietkerk, M., and van de Koppel, J. (2008). Regular pattern formation in real ecosystems. *Trends in Ecology & Evolution* 23, 169–175. doi: 10.1016/j.tree.2007.10.013.

Riley, J. S., Sanders, R., Marsay, C., Le Moigne, F. A. C., Achterberg, E. P., and Poulton, A. J. (2012). The relative contribution of fast and slow sinking particles to ocean carbon export: EXPORT OF FAST AND SLOW SINKING POC. *Global Biogeochem. Cycles* 26, n/a-n/a. doi: 10.1029/2011GB004085.

Risk, M. J., Heikoop, J. M., Snow, M. G., and Beukens, R. (2002). Lifespans and growth patterns of two deep-sea corals: Primnoa resedaeformis and Desmophyllum cristagalli. *Hydrobiologia* 471, 125–131. doi: 10.1023/A:1016557405185.

Rivkin, R. B., Legendre, L., Deibel, D., Tremblay, J.-É., Klein, B., Crocker, K., et al. (1996). Vertical Flux of Biogenic Carbon in the Ocean: Is There Food Web Control? *Science* 272, 1163–1166. doi: 10.1126/science.272.5265.1163.

Rix, L., de Goeij, J. M., Mueller, C. E., Struck, U., Middelburg, J. J., van Duyl, F. C., et al. (2016). Coral mucus fuels the sponge loop in warm- and cold-water coral reef ecosystems. *Sci Rep* 6, 18715. doi: 10.1038/srep18715.

Roberts, E. M., Bowers, D. G., Meyer, H. K., Samuelsen, A., Rapp, H. T., and Cárdenas, P. (2021). Water masses constrain the distribution of deep-sea sponges in the North Atlantic Ocean and Nordic Seas. *Marine Ecology Progress Series* 659, 75–96. doi: 10.3354/meps13570.

Roberts, E. M., Mienis, F., Rapp, H. T., Hanz, U., Meyer, H. K., and Davies, A. J. (2018). Oceanographic setting and short-timescale environmental variability at an Arctic seamount sponge ground. *Deep Sea Research Part I: Oceanographic Research Papers* 138, 98–113. doi: 10.1016/j.dsr.2018.06.007.

Roberts, J., Davies, A., Henry, L., Dodds, L., Duineveld, G., Lavaleye, M., et al. (2009a). Mingulay reef complex: an interdisciplinary study of cold-water coral habitat, hydrography and biodiversity. *Mar. Ecol. Prog. Ser.* 397, 139–151. doi: 10.3354/meps08112.

Roberts, J. M., Wheeler, A., Freiwald, A., and Cairns, S. (2009b). *Cold-Water Corals: The Biology and Geology of Deep-Sea Coral Habitats*. Cambridge University Press doi: 10.1017/CBO9780511581588.

Roberts, J. M., Wheeler, A. J., and Freiwald, A. (2006). Reefs of the Deep: The Biology and Geology of Cold-Water Coral Ecosystems. *Science* 312, 543–547. doi: 10.1126/science.1119861.

Robertson, L. M., Hamel, J.-F., and Mercier, A. (2017). Feeding in deep-sea demosponges: Influence of abiotic and biotic factors. *Deep Sea Research Part I: Oceanographic Research Papers* 127, 49–56. doi: 10.1016/j.dsr.2017.07.006.

Rogers, A. D. (1999). The Biology of *Lophelia pertusa* (L innaeus 1758) and Other Deep-Water Reef-Forming Corals and Impacts from Human Activities. *International Review of Hydrobiology* 84, 315–406. doi: 10.1002/iroh.199900032.

Rogers, A. D. (2018). "Chapter Four - The Biology of Seamounts: 25 Years on," in *Advances in Marine Biology*, ed. C. Sheppard (Academic Press), 137–224. doi: 10.1016/bs.amb.2018.06.001.

Roman, M. R., Caron, D. A., Kremer, P., Lessard, E. J., Madin, L. P., Malone, T. C., et al. (1995). Spatial and temporal changes in the partitioning of organic carbon in the plankton community of the Sargasso Sea off Bermuda. *Deep Sea Research Part I: Oceanographic Research Papers* 42, 973–992. doi: 10.1016/0967-0637(95)00028-5.

Rooks, C., Fang, J. K.-H., Mørkved, P. T., Zhao, R., Rapp, H. T., Xavier, J. R., et al. (2020). Deep-sea sponge grounds as nutrient sinks: denitrification is common in boreo-Arctic sponges. *Biogeosciences* 17, 1231–1245. doi: 10.5194/bg-17-1231-2020.

Rovelli, L., Attard, K., Bryant, L., Flögel, S., Stahl, H., Roberts, J., et al. (2015). Benthic O2 uptake of two cold-water coral communities estimated with the non-invasive eddy correlation technique. *Mar. Ecol. Prog. Ser.* 525, 97–104. doi: 10.3354/meps11211.

Rowe, G. T., Wei, C., Nunnally, C., Haedrich, R., Montagna, P., Baguley, J. G., et al. (2008). Comparative biomass structure and estimated carbon flow in food webs in the deep Gulf of Mexico. *Deep Sea Research Part II: Topical Studies in Oceanography* 55, 2699–2711. doi: 10.1016/j.dsr2.2008.07.020.

Roy, V., Iken, K., and Archambault, P. (2014). Environmental Drivers of the Canadian Arctic Megabenthic Communities. *PLOS ONE* 9, e100900. doi: 10.1371/journal.pone.0100900.

Rüggeberg, A., Flögel, S., Dullo, W.-C., Hissmann, K., and Freiwald, A. (2011). Water mass characteristics and sill dynamics in a subpolar cold-water coral reef setting at Stjernsund, northern Norway. *Marine Geology* 282, 5–12. doi: 10.1016/j.margeo.2010.05.009.

Rüggeberg, A., Flögel, S., Dullo, W.-C., Raddatz, J., and Liebetrau, V. (2016). Paleoseawater density reconstruction and its implication for cold-water coral carbonate mounds in the northeast Atlantic through time: seawater density and carbonate mounds. *Paleoceanography* 31, 365–379. doi: 10.1002/2015PA002859.

Sabatini, M., and Kiørboe, T. (1994). Egg production, growth and development of the cyclopoid copepod Oithona similis. *Journal of Plankton Research* 16, 1329–1351. doi: 10.1093/plankt/16.10.1329.

Sabine, C. L., Feely, R. A., Gruber, N., Key, R. M., Lee, K., Bullister, J. L., et al. (2004). The Oceanic Sink for Anthropogenic CO2. *Science* 305, 367–371. doi: 10.1126/science.1097403.

Sanna, G., and Freiwald, A. (2021). Deciphering the composite morphological diversity of Lophelia pertusa, a cosmopolitan deep-water ecosystem engineer. *Ecosphere* 12, e03802. doi: 10.1002/ecs2.3802.

Sarmiento, J. L., and Gruber, N. (2013). *Ocean Biogeochemical Dynamics*. Princeton University Press doi: doi:10.1515/9781400849079.

Satapoomin, S. (1999). Carbon content of some common tropical Andaman Sea copepods. *Journal of Plankton Research* 21, 2117–2123.

Sathyendranath, S., Stuart, V., Nair, A., Oka, K., Nakane, T., Bouman, H., et al. (2009). Carbon-to-chlorophyll ratio and growth rate of phytoplankton in the sea. *Mar. Ecol. Prog. Ser.* 383, 73–84. doi: 10.3354/meps07998.

Schläppy, M.-L., Weber, M., Mendola, D., Hoffmann, F., and de Beer, D. (2010). Heterogeneous oxygenation resulting from active and passive flow in two Mediterranean sponges, Dysida avara and Chondrosia reniformis. *Limnology and Oceanography* 55, 1289–1300. doi: 10.4319/lo.2010.55.3.1289.

Schulz, K., Soetaert, K., Mohn, C., Korte, L., Mienis, F., Duineveld, G., et al. (2020). Linking large-scale circulation patterns to the distribution of cold water corals along the eastern Rockall Bank (northeast Atlantic). *Journal of Marine Systems* 212, 103456. doi: 10.1016/j.jmarsys.2020.103456.

Sharples, J. (2008). Potential impacts of the spring-neap tidal cycle on shelf sea primary production. *Journal of Plankton Research* 30, 183–197. doi: 10.1093/plankt/fbm088.

Sharples, J., Ross, O. N., Scott, B. E., Greenstreet, S. P. R., and Fraser, H. (2006). Inter-annual variability in the timing of stratification and the spring bloom in the North-western North Sea. *Continental Shelf Research* 26, 733–751. doi: 10.1016/j.csr.2006.01.011.

Shchepetkin, A. F., and McWilliams, J. C. (2005). The regional oceanic modeling system (ROMS): a split-explicit, free-surface, topography-following-coordinate oceanic model. *Ocean Modelling* 9, 347–404. doi: 10.1016/j.ocemod.2004.08.002.

Sheridan, C. C., Lee, C., Wakeham, S. G., and Bishop, J. K. B. (2002). Suspended particle organic composition and cycling in surface and midwaters of the equatorial Pacific Ocean. *Deep Sea Research Part I: Oceanographic Research Papers* 49, 1983–2008. doi: 10.1016/S0967-0637(02)00118-8.

Sherwood, O. A., Davin, S. H., Lehmann, N., Buchwald, C., Edinger, E. N., Lehmann, M. F., et al. (2021). Stable isotope ratios in seawater nitrate reflect the influence of Pacific water along the northwest Atlantic margin. *Biogeosciences* 18, 4491–4510. doi: 10.5194/bg-18-4491-2021.

Sherwood, O. A., Heikoop, J. M., Scott, D. B., Risk, M. J., Guilderson, T. P., and McKinney, R. A. (2005). Stable isotopic composition of deep-sea gorgonian corals Primnoa spp.: a new archive of surface processes. *Marine Ecology Progress Series* 301, 135–148. doi: 10.3354/meps301135.

Sherwood, O. A., Jamieson, R. E., Edinger, E. N., and Wareham, V. E. (2008). Stable C and N isotopic composition of cold-water corals from the Newfoundland and Labrador continental slope: Examination of trophic, depth and spatial effects. *Deep Sea Research Part I: Oceanographic Research Papers* 55, 1392–1402. doi: 10.1016/j.dsr.2008.05.013.

Shimeta, J., and Jumars, P. A. (1991). Physical mechanisms and rates of particle capture by suspension feeders. *Oceanogr. Mar. Biol. Annu. Rev.*, 191–257.

Shumway, R. H., Stoffer, D. S., and Stoffer, D. S. (2000). *Time series analysis and its applications*. Springer.

Sigman, D. M., and Boyle, E. A. (2000). Glacial/interglacial variations in atmospheric carbon dioxide. *Nature* 407, 859–869. doi: 10.1038/35038000.

Sigman, D. M., Karsh, K. L., and Casciotti, K. L. (2009). "Nitrogen Isotopes in the Ocean,"

in *Encyclopedia of Ocean Sciences* (Elsevier Ltd), 40–54. doi: 10.1016/B978-012374473-9.00632-9.

signal developers (2014). *signal: Signal processing*. Available at: http://r-forge.r-project.org/projects/signal/.

Simpson, J. H., and McCandliss, R. R. (2013). "The Ekman Drain": a conduit to the deep ocean for shelf material. *Ocean Dynamics* 63, 1063–1072. doi: 10.1007/s10236-013-0644-y.

Smith, C., Deleo, F., Bernardino, A., Sweetman, A., and Arbizu, P. (2008). Abyssal food limitation, ecosystem structure and climate change. *Trends in Ecology & Evolution* 23, 518–528. doi: 10.1016/j.tree.2008.05.002.

Smith, E. J., Soule, F. M., and Mosby, O. (1937). The Marion and General Greene expeditions to Davis Strait and Labrador Sea. *U.S. Coast Guard Bull.* 19.

Soetaert, K. (2017). plot3D: Plotting Multi-Dimensional Data.

Soetaert, K. (2019a). *OceanView: Visualisation of Oceanographic Data and Model Output*. Available at: https://CRAN.R-project.org/package=OceanView.

Soetaert, K. (2019b). *plot3D: Plotting Multi-Dimensional Data*. Available at: https://CRAN.R-project.org/package=plot3D.

Soetaert, K., Mohn, C., Rengstorf, A., Grehan, A., and van Oevelen, D. (2016a). Ecosystem engineering creates a direct nutritional link between 600-m deep cold-water coral mounds and surface productivity. *Sci Rep* 6, 35057. doi: 10.1038/srep35057.

Soetaert, K., Petzoldt, T., and Meysman, F. (2016b). marelac: Tools for Aquatic Sciences. R package version 2.1.6.

Soetaert, K., Petzoldt, T., and Woodrow Setzer, R. (2010). Solving Differential Equations in R: Package deSolve. *Journal of Statistical Software* 33. doi: 10.18637/jss.v033.i09.

Sonnekus, M. J., Bornman, T. G., and Campbell, E. E. (2017). Phytoplankton and nutrient dynamics of six South West Indian Ocean seamounts. *Deep-Sea Research Part II: Topical Studies in Oceanography* 136, 59–72. doi: 10.1016/j.dsr2.2016.12.008.

Steinberg, D. K. (1995). Diet of copepods (Scopalatum vorax) associated with mesopelagic detritus (giant larvacean houses) in Monterey Bay, California. *Marine Biology* 122, 571–584. doi: 10.1007/BF00350679.

Stoffer, D. (2020). *astsa: Applied Statistical Time Series Analysis*. Available at: https://CRAN.R-project.org/package=astsa.

Strand, R., Whalan, S., Webster, N. S., Kutti, T., Fang, J. K. H., Luter, H. M., et al. (2017). The response of a boreal deep-sea sponge holobiont to acute thermal stress. *Sci Rep* 7, 1660. doi: 10.1038/s41598-017-01091-x.

Straneo, F., and Saucier, F. (2008). The outflow from Hudson Strait and its contribution to the Labrador Current. *Deep Sea Research Part I: Oceanographic Research Papers* 55, 926–946. doi: 10.1016/j.dsr.2008.03.012.

Sutcliffe, W. H. Jr., Loucks, R. H., Drinkwater, K. F., and Coote, A. R. (1983). Nutrient Flux onto the Labrador Shelf from Hudson Strait and its Biological Consequences. *Can. J. Fish. Aquat. Sci.* 40, 1692–1701. doi: 10.1139/f83-196.

Suttle, C. A. (2005). Viruses in the sea. *Nature* 437, 356–361. doi: 10.1038/nature04160.

Sweetman, A. K., Thurber, A. R., Smith, C. R., Levin, L. A., Mora, C., Wei, C.-L., et al. (2017). Major impacts of climate change on deep-sea benthic ecosystems. *Elem Sci Anth* 5, 4. doi: 10.1525/elementa.203.

Talley, L. D., Pickard, G. L., Emery, W. J., and Swift, J. H. (2011). *Descriptive physical oceanography: an introduction*. Academic press.

Tarran, G. A., Heywood, J. L., and Zubkov, M. V. (2006). Latitudinal changes in the standing stocks of nano- and picoeukaryotic phytoplankton in the Atlantic Ocean. *Deep Sea Research Part II: Topical Studies in Oceanography* 53, 1516–1529.

Taylor, A., Geider, R., and Gilbert, F. (1997). Seasonal and latitudinal dependencies of phytoplankton carbon-to-chlorophyll a ratios:results of a modelling study. *Mar. Ecol. Prog. Ser.* 152, 51–66. doi: 10.3354/meps152051.

Thamdrup, B., and Dalsgaard, T. (2008). "Nitrogen cycling in sediments," in *Microbial ecology of the oceans*, ed. D. L. Kirchman (John Wiley & Sons, Inc), 527–567.

Thiem, Ø., Ravagnan, E., Fosså, J. H., and Berntsen, J. (2006). Food supply mechanisms for cold-water corals along a continental shelf edge. *Journal of Marine Systems* 60, 207–219. doi: 10.1016/j.jmarsys.2005.12.004.

Thomson, D. H. (1982). Marine Benthos in the Eastern Canadian High Arctic: Multivariate Analyses of Standing Crop and Community Structure. *Arctic* 35, 61–74.

Thorpe, S. A., and White, M. (1988). A deep intermediate nepheloid layer. *Deep Sea Research Part A. Oceanographic Research Papers* 35, 1665–1671. doi: 10.1016/0198-0149(88)90109-4.

Titschack, J., Baum, D., De Pol-Holz, R., López Correa, M., Forster, N., Flögel, S., et al. (2015). Aggradation and carbonate accumulation of Holocene Norwegian cold-water coral reefs. *Sedimentology* 62, 1873–1898. doi: 10.1111/sed.12206.

Tittensor, D. P., Baco, A. R., Hall-Spencer, J. M., Orr, J. C., and Rogers, A. D. (2010). Seamounts as refugia from ocean acidification for cold-water stony corals: Seamounts as refugia from ocean acidification. *Marine Ecology* 31, 212–225. doi: 10.1111/j.1439-0485.2010.00393.x.

Tolosa, I., Vescovali, I., LeBlond, N., Marty, J.-C., de Mora, S., and Prieur, L. (2004). Distribution of pigments and fatty acid biomarkers in particulate matter from the frontal structure of the Alboran Sea (SW Mediterranean Sea). *Marine Chemistry* 88, 103–125. doi: 10.1016/j.marchem.2004.03.005.

Tremblay, J.-É., Gratton, Y., Carmack, E. C., Payne, C. D., and Price, N. M. (2002). Impact of the large-scale Arctic circulation and the North Water Polynya on nutrient inventories in Baffin Bay. *Journal of Geophysical Research: Oceans* 107, 26-1-26–14. doi: 10.1029/2000JC000595.

Turner, J. T. (2015). Zooplankton fecal pellets, marine snow, phytodetritus and the ocean's biological pump. *Progress in Oceanography* 130, 205–248. doi: 10.1016/j.pocean.2014.08.005.

Vacelet, J., and Donadey, C. (1977). Electron microscope study of the association between some sponges and bacteria. *Journal of Experimental Marine Biology and Ecology* 30, 301–314. doi: 10.1016/0022-0981(77)90038-7.

Vad, J., Orejas, C., Moreno-Navas, J., Findlay, H. S., and Roberts, J. M. (2017). Assessing the living and dead proportions of cold-water coral colonies: implications for deep-water Marine Protected Area monitoring in a changing ocean. *PeerJ* 5, e3705. doi: 10.7717/peerj.3705.

Van Bleijswijk, J. D. L., Whalen, C., Duineveld, G. C. A., Lavaleye, M. S. S., Witte, H. J., and Mienis, F. (2015). Microbial assemblages on a cold-water coral mound at the SE Rockall Bank (NE Atlantic): Interactions with hydrography and topography. *Biogeosciences* 12, 4483–4496. doi: 10.5194/bg-12-4483-2015.

van de Koppel, J., Rietkerk, M., Dankers, N., and Herman, P. M. J. (2005). Scale-Dependent Feedback and Regular Spatial Patterns in Young Mussel Beds. *The American Naturalist* 165, E66–E77. doi: 10.1086/428362.

van der Kaaden, A.-S., Mohn, C., Gerkema, T., Maier, S. R., de Froe, E., van de Koppel, J., et al. (2021). Feedbacks between hydrodynamics and cold-water coral mound development. *Deep Sea Research Part I: Oceanographic Research Papers* 178, 103641. doi: 10.1016/j.dsr.2021.103641.

van der Kaaden, A.-S., van Oevelen, D., Rietkerk, M., Soetaert, K., and van de Koppel, J. (2020). Spatial Self-Organization as a New Perspective on Cold-Water Coral Mound Development. *Front. Mar. Sci.* 7, 631. doi: 10.3389/fmars.2020.00631.

van der Land, C., Eisele, M., Mienis, F., de Haas, H., Hebbeln, D., Reijmer, J. J. G., et al. (2014). Carbonate mound development in contrasting settings on the Irish margin. *Deep Sea Research Part II: Topical Studies in Oceanography* 99, 297–306. doi: 10.1016/j.dsr2.2013.10.004.

van Duyl, F. C., Lengger, S. K., Schouten, S., Lundälv, T., van Oevelen, D., and Müller, C. E. (2020). Dark CO_2 fixation into phospholipid-derived fatty acids by the cold-water coral associated sponge *Hymedesmia* (*Stylopus*) *coriacea* (Tisler Reef, NE Skagerrak). *Marine Biology Research*, 1–17. doi: 10.1080/17451000.2019.1704019.

van Duyl, F., Hegeman, J., Hoogstraten, A., and Maier, C. (2008). Dissolved carbon fixation by sponge–microbe consortia of deep water coral mounds in the northeastern Atlantic Ocean. *Mar. Ecol. Prog. Ser.* 358, 137–150. doi: 10.3354/meps07370.

Van Engeland, T., Godø, O. R., Johnsen, E., Duineveld, G. C. A., and van Oevelen, D. (2019). Cabled ocean observatory data reveal food supply mechanisms to a cold-water coral

reef. *Progress in Oceanography* 172, 51–64. doi: 10.1016/j.pocean.2019.01.007.

van Haren, H., and Gostiaux, L. (2012). Energy Release Through Internal Wave Breaking. *oceanog* 25, 124–131. doi: 10.5670/oceanog.2012.47.

van Haren, H., Mienis, F., Duineveld, G. C. A., and Lavaleye, M. S. S. (2014). High-resolution temperature observations of a trapped nonlinear diurnal tide influencing cold-water corals on the Logachev mounds. *Progress in Oceanography* 125, 16–25. doi: 10.1016/j.pocean.2014.04.021.

van Oevelen, D., Duineveld, G. C. A., Lavaleye, M. S. S., Kutti, T., and Soetaert, K. (2018). Trophic structure of cold-water coral communities revealed from the analysis of tissue isotopes and fatty acid composition. *Marine Biology Research* 14, 287–306. doi: 10.1080/17451000.2017.1398404.

van Oevelen, D., Duineveld, G. C. A., Lavaleye, M. S. S., Mienis, F., Soetaert, K., and Heip, C. H. R. (2009). The cold-water coral community as hotspot of carbon cycling on continental margins: A food-web analysis from Rockall Bank (northeast Atlantic). *Limnology & Oceanography* 54, 1829–1844. doi: 10.4319/lo.2009.54.6.1829.

van Oevelen, D., Mueller, C. E., Lundälv, T., and Middelburg, J. J. (2016). Food selectivity and processing by the cold-water coral *Lophelia pertusa*. *Biogeosciences* 13, 5789–5798. doi: 10.5194/bg-13-5789-2016.

Van Soest, R. W. M., and Lavaleye, M. S. S. (2005). Diversity and abundance of sponges in bathyal coral reefs of Rockall Bank, NE Atlantic, from boxcore samples. *Marine Biology Research* 1, 338–349. doi: 10.1080/17451000500380322.

van Weering, T. C. E., de Haas, H., de Stigter, H. C., Lykke-Andersen, H., and Kouvaev, I. (2003). Structure and development of giant carbonate mounds at the SW and SE Rockall Trough margins, NE Atlantic Ocean. *Marine Geology* 198, 67–81. doi: 10.1016/S0025-3227(03)00095-1.

Vander Zanden, M. J., and Rasmussen, J. B. (2001). Variation in δ15N and δ13C trophic fractionation: Implications for aquatic food web studies. *Limnology and Oceanography* 46, 2061–2066. doi: 10.4319/lo.2001.46.8.2061.

Vaughan, D., and Dancho, M. (2020). *tibbletime: Time Aware Tibbles*. Available at: https://CRAN.R-project.org/package=tibbletime.

Verity, P. G., Robertson, C. Y., Tronzo, C. R., Andrews, M. G., Nelson, J. R., and Sieracki, M. E. (1992). Relationships between cell volume and the carbon and nitrogen content of marine photosynthetic nanoplankton. *Limnol. Oceanogr.* 37, 1434–1446. doi: 10.4319/lo.1992.37.7.1434.

Vetter, E. W., Smith, C. R., and De Leo, F. C. (2010). Hawaiian hotspots: enhanced megafaunal abundance and diversity in submarine canyons on the oceanic islands of Hawaii. *Marine Ecology* 31, 183–199. doi: 10.1111/j.1439-0485.2009.00351.x.

Vic, C., Naveira Garabato, A. C., Green, J. A. M., Waterhouse, A. F., Zhao, Z., Melet, A., et al. (2019). Deep-ocean mixing driven by small-scale internal tides. *Nat Commun* 10, 2099. doi: 10.1038/s41467-019-10149-5.

Vieira, R. P., Bett, B. J., Jones, D. O. B., Durden, J. M., Morris, K. J., Cunha, M. R., et al. (2020). Deep-sea sponge aggregations (Pheronema carpenteri) in the Porcupine Seabight (NE Atlantic) potentially degraded by demersal fishing. *Progress in Oceanography* 183, 102189. doi: 10.1016/j.pocean.2019.102189.

Vlasenko, V., and Stashchuk, N. (2018). Tidally Induced Overflow of the Faroese Channels Bottom Water Over the Wyville Thomson Ridge. *Journal of Geophysical Research: Oceans* 123, 6753–6765. doi: 10.1029/2018JC014365.

Vogel, S. (1977). Current-induced flow through living sponges in nature. *Proceedings of the National Academy of Sciences* 74, 2069–2071. doi: 10.1073/pnas.74.5.2069.

Volk, T., and Hoffert, M. I. (1985). "Ocean Carbon Pumps: Analysis of Relative Strengths and Efficiencies in Ocean-Driven Atmospheric CO2 Changes," in *The Carbon Cycle and Atmospheric CO2: Natural Variations Archean to Present* (American Geophysical Union (AGU), 99–110. doi: 10.1029/GM032p0099.

Volkman, J. K., Jeffrey, S. W., Nichols, P. D., Rogers, G. I., and Garland, C. D. (1989). Fatty acid and lipid composition of 10 species of microalgae used in mariculture. *Journal of Experimental Marine Biology and Ecology* 128, 219–240. doi: 10.1016/0022-0981(89)90029-4.

Wagner, H., Purser, A., Thomsen, L., Jesus, C. C., and Lundälv, T. (2011). Particulate organic matter fluxes and hydrodynamics at the Tisler cold-water coral reef. *Journal of Marine Systems* 85, 19–29. doi: 10.1016/j.jmarsys.2010.11.003.

Wassenberg, T. J., Dews, G., and Cook, S. D. (2002). The impact of fish trawls on megabenthos (sponges) on the north-west shelf of Australia. *Fisheries Research* 58, 141–151. doi: 10.1016/S0165-7836(01)00382-4.

Wehrmann, L. M., Knab, N. J., Pirlet, H., Unnithan, V., Wild, C., and Ferdelman, T. G. (2009). Carbon mineralization and carbonate preservation in modern cold-water coral reef sediments on the Norwegian shelf. *Biogeosciences* 6, 663–680. doi: 10.5194/bg-6-663-2009.

Weinbauer, M., Ogier, J., and Maier, C. (2012). Microbial abundance in the coelenteron and mucus of the cold-water coral *Lophelia pertusa* and in bottom water of the reef environment. *Aquat. Biol.* 16, 209–216. doi: 10.3354/ab00443.

Weiss, R. F. (1970). The solubility of nitrogen, oxygen and argon in water and seawater. 17.

Westrich, J. T., and Berner, R. A. (1984). The role of sedimentary organic matter in bacterial sulfate reduction: The G model tested1. *Limnology and Oceanography* 29, 236–249. doi: 10.4319/lo.1984.29.2.0236.

White, M. (2003). Comparison of near seabed currents at two locations in the Porcupine Sea Bight—implications for benthic fauna. *Journal of the Marine Biological Association of the United Kingdom* 83, 683–686. doi: 10.1017/S0025315403007641h.

White, M., Mohn, C., de Stigter, H., and Mottram, G. (2005). "Deep-water coral development as a function of hydrodynamics and surface productivity around the submarine banks of the Rockall Trough, NE Atlantic," in *Cold-Water Corals and Ecosystems*, eds. A. Freiwald and J. M. Roberts (Berlin, Heidelberg: Springer Berlin Heidelberg), 503–514. doi: 10.1007/3-540-27673-4_25.

White, M., Roberts, J. M., and van Weering, T. (2007). Do bottom-intensified diurnal tidal currents shape the alignment of carbonate mounds in the NE Atlantic? *Geo-Mar Lett* 27, 391–397. doi: 10.1007/s00367-007-0060-8.

White, M., Wolff, G. A., Lundälv, T., Guihen, D., Kiriakoulakis, K., Lavaleye, M. S. S., et al. (2012). Cold-water coral ecosystem (Tisler Reef, Norwegian shelf) may be a hotspot for carbon cycling. *Marine Ecology Progress Series* 465, 11–23. doi: 10.3354/meps09888.

Whitney, F., Conway, K., Thomson, R., Barrie, V., Krautter, M., and Mungov, G. (2005). Oceanographic habitat of sponge reefs on the Western Canadian Continental Shelf. *Continental Shelf Research* 25, 211–226. doi: 10.1016/j.csr.2004.09.003.

Wickham, H. (2007). Reshaping Data with the reshape Package. *Journal of Statistical Software* 21, 1–20.

Wickham, H. (2016a). *ggplot2: Elegant Graphics for Data Analysis*. Springer-Verlag New York Available at: https://ggplot2.tidyverse.org.

Wickham, H. (2016b). ggplot2: Elegant Graphics for Data Analysis.

Wickham, H., and Bryan, J. (2019). *readxl: Read Excel Files*. Available at: https://CRAN.R-project.org/package=readxl.

Wickham, H., Francois, R., Henry, L., and Moller, K. (2021). *dplyr: A Grammar of Data Manipulation*. Available at: https://CRAN.R-project.org/package=dplyr.

Wienberg, C., Titschack, J., Frank, N., De Pol-Holz, R., Fietzke, J., Eisele, M., et al. (2020). Deglacial upslope shift of NE Atlantic intermediate waters controlled slope erosion and cold-water coral mound formation (Porcupine Seabight, Irish margin). *Quaternary Science Reviews* 237, 106310. doi: 10.1016/j.quascirev.2020.106310.

Wienberg, C., Titschack, J., Freiwald, A., Frank, N., Lundälv, T., Taviani, M., et al. (2018). The giant Mauritanian cold-water coral mound province: Oxygen control on coral mound formation. *Quaternary Science Reviews* 185, 135–152. doi: 10.1016/j.quascirev.2018.02.012.

Wijffels, S., Roemmich, D., Monselesan, D., Church, J., and Gilson, J. (2016). Ocean temperatures chronicle the ongoing warming of Earth. *Nature Clim Change* 6, 116–118. doi: 10.1038/nclimate2924.

Wild, C., Mayr, C., Wehrmann, L., Schöttner, S., Naumann, M., Hoffmann, F., et al. (2008). Organic matter release by cold water corals and its implication for fauna–microbe interaction. *Mar. Ecol. Prog. Ser.* 372, 67–75. doi: 10.3354/meps07724.

Wilke, C. O. (2019). *cowplot: Streamlined Plot Theme and Plot Annotations for "ggplot2."* Available at: https://CRAN.R-project.org/package=cowplot.

Wilkinson, C. R., Garrone, R., Vacelet, J., and Smith, D. C. (1984). Marine sponges discriminate between food bacteria and bacterial symbionts: electron microscope radioautography and in situ evidence. *Proceedings of the Royal Society of London. Series B. Biological Sciences* 220, 519–528. doi: 10.1098/rspb.1984.0018.

Wilson, J. B. (1979). 'Patch' development of the deep-water coral Lophelia Pertusa (L.) on Rockall Bank. *Journal of the Marine Biological Association of the United Kingdom* 59, 165–177. doi: 10.1017/S0025315400046257.

Witbaard, R., Duineveld, G. C. A., Van der Weele, J. A., Berghuis, E. M., and Reyss, J. P. (2000). The benthic response to the seasonal deposition of phytopigments at the Porcupine Abyssal Plain in the North East Atlantic. *Journal of Sea Research* 43, 15–31. doi: 10.1016/S1385-1101(99)00040-4.

Witte, U., Brattegard, T., Graf, G., and Springer, B. (1997). Particle capture and deposition by deep-sea sponges from the Norwegian-Greenland Sea. *Marine Ecology Progress Series* 154, 241–252. doi: 10.3354/meps154241.

Wohlers, J., Engel, A., Zöllner, E., Breithaupt, P., Jürgens, K., Hoppe, H.-G., et al. (2009). Changes in biogenic carbon flow in response to sea surface warming. *PNAS* 106, 7067–7072. doi: 10.1073/pnas.0812743106.

Wolff, G. A., Boardman, D., Horsfall, I., Sutton, I., Davis, N., Chester, R., et al. (1995). The Biogeochemistry of Sediments from the Madeira Abyssal Plain - Preliminary Results. *Int. Revue Ges. Hydrobiol.* 80, 333–349.

Wolff, G., van Oevelen, D., Glud, R., Rovelli, L., Carreiro-Silva, M., Mohn, C., et al. (2020). *ATLAS Deliverable 2.3 Community respiration rates, biogeochemical characteristics of organic matter and fauna at ATLAS Case Study Sites.* Zenodo doi: 10.5281/zenodo.4243873.

Wright, P. A. (1995). Nitrogen excretion: three end products, many physiological roles. *The Journal of experimental biology* 198, 273–81.

Wright, S. W., and Jeffrey, S. W. (1987). Fucoxanthin pigment markers of marine phytoplankton analysed by HPLC and HPTLC. *Marine Ecology Progress Series* 38, 259–266.

Wright, S. W., Jeffrey, S. W., Mantoura, R. F. C., Llewellyn, C. A., Bjornland, T., Repeta, D., et al. (1991). Improved HPLC method for the analysis of chlorophylls and carotenoids from marine phytoplankton. *Marine Ecology Progress Series* 77, 183–196.

Wu, Y., Peterson, I. K., Tang, C. C. L., Platt, T., Sathyendranath, S., and Fuentes-Yaco, C. (2007). The impact of sea ice on the initiation of the spring bloom on the Newfoundland and Labrador Shelves. *Journal of Plankton Research* 29, 509–514. doi: 10.1093/plankt/fbm035.

Xie, Y. (2020). *knitr: A General-Purpose Package for Dynamic Report Generation in R*. Available at: https://yihui.org/knitr/.

Yahel, G., Whitney, F., Reiswig, H. M., Eerkes-Medrano, D. I., and Leys, S. P. (2007). In situ feeding and metabolism of glass sponges (Hexactinellida, Porifera) studied in a deep temperate fjord with a remotely operated submersible. *Limnol. Oceanogr.* 52, 428–440. doi: 10.4319/lo.2007.52.1.0428.

Yamamuro, M., and Kayanne, H. (1995). Rapid direct determination of organic carbon and nitrogen in carbonate-bearing sediments with a Yanaco MT-5 CHN analyzer. *Limnology and Oceanography* 40, 1001–1005. doi: 10.4319/lo.1995.40.5.1001.

Yashayaev, I. (2007). Hydrographic changes in the Labrador Sea, 1960–2005. *Progress in Oceanography* 73, 242–276. doi: 10.1016/j.pocean.2007.04.015.

Yool, A., Popova, E. E., and Anderson, T. R. (2011). MEDUSA-2.0: An intermediate complexity biogeochemical model of the marine carbon cycle for climate change and ocean acidification studies. *Geoscientific Model Development*. doi: 10.5194/gmd-6-1767-2013.

Youngbluth, M. J., Bailey, T. G., Davoll, P. J., Jacoby, C. A., Blades-Eckelbarger, P. I., and Griswold, C. A. (1989). Fecal pellet production and diel migratory behavior by the euphausiid *Meganyctiphanes norvegica* effect benthic-pelagic coupling. *Deep Sea Research Part A. Oceanographic Research Papers* 36, 1491–1501. doi: 10.1016/0198-0149(89)90053-8.

Zamer, W. E., and Shick, J. M. (1987). Physiological energetics of the intertidal sea anemone Anthopleura elegantissima. *Mar. Biol.* 93, 481–491. doi: 10.1007/BF00392785.

Zapata, M., Rodríguez, F., and Garrido, J. L. (2000). Separation of chlorophylls and carot-

enoids from marine phytoplankton: a new HPLC method using a reversed phase C8 column and pyridine-containing mobile phases. *Marine Ecology Progress Series* 195, 29–45. doi: 10.3354/meps195029.

Zaret, T. M., and Suffern, J. S. (1976). Vertical migration in zooplankton as a predator avoidance mechanism. *Limnology and Oceanography* 21, 804–813. doi: 10.4319/lo.1976.21.6.0804.

Zibrowius, H. (1980). Les Scléractiniaires de la Méditerranée et de l'Atlantique nord-oriental. *Mémoires de l'Institut océanographique, Monaco*.

Zimmerman, A. R., and Canuel, E. A. (2001). Bulk Organic Matter and Lipid Biomarker Composition of Chesapeake Bay Surficial Sediments as Indicators of Environmental Processes. *Estuarine, Coastal and Shelf Science* 53, 319–341. doi: 10.1006/ecss.2001.0815.

Authors affiliation and addresses

Sabena Blackbird

School of Environmental Sciences
University of Liverpool
4 Brownlow Street
Liverpool, L69 3GP
United Kingdom

Chiu H. Cheng

NIOZ Royal Netherlands Institute for Sea Research
Department of Estuarine and Delta Systems
PO Box 140
4400 AC, Yerseke
The Netherlands

Wageningen Marine Research
Wageningen University & Research
4400 AB Yerseke
The Netherlands

Laurence H. De Clippele

Changing Oceans Research Group, School of GeoSciences
The University of Edinburgh
Edinburgh, United Kingdom

Gerard Duineveld

NIOZ Royal Netherlands Institute for Sea Research
Department of Ocean Systems
The Netherlands

Furu Mienis

NIOZ Royal Netherlands Institute for Sea Research
Department of Ocean Systems
The Netherlands

Ronnie N. Glud

Nordcee, Department of Biology
University of Southern Denmark
Odense, Denmark

Department of Ocean and Environmental Sciences
Tokyo University of Marine Science and Technology
Tokyo, Japan

Britt van Haastregt

NIOZ Royal Netherlands Institute for Sea Research
Department of Estuarine and Delta Systems
PO Box 140
4400 AC, Yerseke
The Netherlands

Erica Head

Bedford Institute of Oceanography
Department of Fisheries and Oceans
PO Box 1006
Dartmouth, NS, B2Y 4A2
Canada

Henriette G. Horn

NIOZ Royal Netherlands Institute for Sea Research
Department of Estuarine and Delta Systems
PO Box 140
4400 AC, Yerseke
The Netherlands

Centre for Coastal Research
University of Agder
PO Box 422
4604 Kristiansand
Norway

Anna-Selma van der Kaaden

NIOZ Royal Netherlands Institute for Sea Research
Department of Estuarine and Delta Systems
PO Box 140
4400 AC, Yerseke
The Netherlands

Ellen Kenchington

Bedford Institute of Oceanography
Department of Fisheries and Oceans
PO Box 1006
Dartmouth, NS, B2Y 4A2
Canada

Marc Lavaleye

NIOZ Royal Netherlands Institute for Sea Research
Department of Ocean Systems
PO Box 59
1790 AB, Den Burg
The Netherlands

Sandra R. Maier

NIOZ Royal Netherlands Institute for Sea Research
Department of Estuarine and Delta Systems
PO Box 140
4400 AC, Yerseke
The Netherlands

Greenland Climate Research Centre
Greenland Institute of Natural Resources
Kivioq 2, PO Box 570, 3900, Nuuk
Greenland

Barry McDonald

Bedford Institute of Oceanography
Department of Fisheries and Oceans
PO Box 1006
Dartmouth, NS, B2Y 4A2
Canada

Christian Mohn

Department of Ecoscience
Aarhus University
Frederiksborgvej 399
4000 Roskilde
Denmark

Eva Friis Moller

Department of Ecoscience
Aarhus University
Frederiksborgvej 399
4000 Roskilde
Denmark

Dick van Oevelen

NIOZ Royal Netherlands Institute for Sea Research
Department of Estuarine and Delta Systems
PO Box 140
4400 AC, Yerseke
The Netherlands

Gert-Jan Reichart

NIOZ Royal Netherlands Institute for Sea Research
Department of Ocean Systems
PO Box 59
1790 AB, Den Burg
The Netherlands

Department of Earth Sciences, Faculty of Geosciences
Utrecht University
Princetonlaan 8a
3584 CB Utrecht
The Netherlands

Murray Roberts

Changing Oceans Research Group, School of GeoSciences
The University of Edinburgh
Edinburgh, United Kingdom

Steve W. Ross

University of North Carolina at Wilmington
Center for Marine Science
5600 Marvin Moss Ln.,
Wilmington, NC, 28409
USA

Lorenzo Rovelli

Institute for Environmental Sciences
University of Koblenz-Landau
Landau, Germany

Mads Schultz

NORD University
Faculty of Biosciences and Aquaculture
Post Box 1490, 8049 Bodø

Karline Soetaert

NIOZ Royal Netherlands Institute for Sea Research
Department of Estuarine and Delta Systems
PO Box 140
4400 AC, Yerseke

Graham Tulloch

British Geological Survey
Lyell Centre
Research Avenue North, Edinburgh, EH14 4AP
United Kingdom

Johanne Vad

Changing Oceans Research Group, School of GeoSciences
The University of Edinburgh
Edinburgh
United Kingdom

George A. Wolff

School of Environmental Sciences
University of Liverpool
4 Brownlow Street
Liverpool L69 3GP
United Kingdom

Evi Wubben

Department of Earth Sciences, Faculty of Geosciences
Utrecht University
Princetonlaan 8a
3584 CB Utrecht
The Netherlands

Igor Yashayaev

Bedford Institute of Oceanography
Department of Fisheries and Oceans
PO Box 1006
Dartmouth, NS, B2Y 4A2
Canada

Summary

The deep sea encompasses more than 99% of available habitat on earth but is yet one of the most understudied ecosystems on earth. Starting below 200 metre depth, light levels in the deep sea are too low for photosynthesis. Organisms living on the seafloor below the deep sea are therefore mostly dependent on organic matter produced at the ocean's surface as a food source. As only a small percentage of the organic matter produced at the surface reaches the seafloor (1 – 3%), large parts of the ocean are considered food limited ecosystems and sometimes seen as deserts in the deep sea (**chapter 1**). However, at certain locations in the deep sea, thriving cold-water coral reefs and sponge grounds are found, which support numerous species and are seen as hotspots of biological activity. This thesis investigates how these hotspots can persist in an otherwise food limited environment as the deep sea.

Cold-water corals and deep-sea sponges are considered ecosystem engineers, as their body plan provides structure and habitat for associated species. Cold-water corals and deep-sea sponges are known as filter feeding animals, whereby corals are seen as passive filter feeders and sponges as active filter feeders. Corals filter (food) particles out of the overlaying water and thereby depend on strong bottom currents for food supply. Sponges filter the water for food particles by actively pumping water through their body plan. Both organisms are often found in the deep sea in areas where specific oceanic conditions cause downward transport of fresh organic matter from the surface to the seafloor. Under sustained favourable environmental conditions, cold-water corals and deep-sea sponges can form, respectively, large reefs/mounds and sponge grounds in the deep sea (**chapter 1**).

Although past research efforts have increased our knowledge on these ecosystems, currently little is known on under which environmental conditions cold-water corals and sponges thrive and what controls the spatial distribution of these organisms. As pressure from anthropogenic stressors, e.g., climate change and fisheries, on the deep sea is currently increasing, understanding in which environment these valuable ecosystems thrive is key in predicting their fate in future oceanic conditions. This thesis aims at understanding the mechanisms that control the spatial distribution of cold-water corals and sponges in the deep sea. More specifically, this thesis investigates: i) food supply mechanisms towards cold-water coral reefs (**chapter 2**), ii) how much food is required for a cold-water coral reef to sustain itself (**chapter 3**), iii) if the spatial distribution of cold-water coral biomass can be predicted based solely on hydrodynamics, organic matter transport, and cold-water coral physiology (**chapter 4**), the environmental conditions that support high sponge biomass at a deep-sea sponge ground (**chapter 5**).

Past research on food supply mechanisms towards cold-water coral reefs mostly reported snapshots of data (a few hours) or long-term measurements (seasonal cycles). Few studies looked at the organic matter distribution in the water column over a diur-

nal tidal cycle, while no studies report this over the full organic matter spectrum (e.g., bacteria, virus, dissolved-, and particulate organic matter). This thesis presents data on four 24-hour water column profile measurements along a transect over a cold-water coral mound on Rockall Bank, Northeast Atlantic Ocean (**chapter 2**). The water column above the cold-water coral mound was more dynamic compared to the station on the slope of Rockall Bank. The results of this study suggest fresh organic matter transport towards the cold-water coral reef is enhanced by three pathways: i) advective transport of phytoplankton derived material from mid-water depths with help of 200-300 m amplitude internal waves, ii) replenishment of nutrients in the surface water might promote production of diatoms, iii) formation of zooplankton faecal pellets could speed-up downward transport of particulate matter. Cold-water corals and their associated reef fauna utilize a variety of food sources, but ultimately depend on surface produced organic matter. Results of this study (**chapter 2**) show variability in organic matter quality and composition is high over a diurnal tidal cycle and this should be considered in future sampling campaigns.

Quantitative measurements of the metabolic requirements of cold-water coral reefs are scarce, and absent for reefs located at >250 metre depth. Furthermore, little is known on nitrogen cycling at cold-water coral reefs. In this thesis, benthic fluxes of oxygen and nitrogen were measured at two deeper cold-water coral mounds and sediment reference sites at Rockall Bank (600 – 750 m depth; **chapter 3**). *In situ* measurements of benthic oxygen uptake were performed by the non-invasive *in situ* Aquatic Eddy Covariance technique and *ex situ* measurements of oxygen uptake and nitrogen fluxes were done by on-board box core incubations. Results shows that oxygen uptake on cold-water coral reefs is on average five times higher than sediments from comparable depth. Furthermore, cold-water coral reefs are a source of ammonium and nitrate in the deep sea. This high oxygen uptake and ammonium excretion is mostly driven by presence of living corals and, but to a lesser extent, by dead coral framework. The results of this study show that cold-water coral reefs are hotspots of carbon and nitrogen cycling in the deep sea.

A mechanistic modelling approach was used to predict cold-water coral biomass and benthic respiration based on hydrodynamics, organic matter transport, and cold-water coral physiology (**chapter 4**). So far, efforts on predicting the spatial distribution of cold-water corals have been based on statistical methods. While these models provide good predictions of suitable habitat for cold-water corals, they often only predict coral presence/absence and are dependent on the availability of high-quality observational data. As oceanic conditions in the deep sea are subject to change, new tools to evaluate and predict the effect of these changes on cold-water corals are needed. Results of our modelling approach show cold-water coral biomass is highest on the upper slopes of the cold-water coral mounds in the area, where organic matter gets replenished at sufficient rate, and where bottom currents are strong. Competition for organic matter between cold-water corals proved key in adequately predicting the spatial distribution

of cold-water corals. The model predictions compared well with observational data, and benthic respiration rates were in line with measurements (**chapter 3**). The here presented modelling approach can be used to obtain a mechanistic understanding on the effects of changing environmental conditions as temperature, surface production export, or ocean currents on cold-water coral biomass and can be applied to other study areas or species. Bottom currents and environmental conditions were measured by benthic landers for a yearlong at two contrasting high- and low sponge biomass sponge grounds on the Labrador Shelf, Northeast Canada (**chapter 5**). Little is known on environmental conditions at sponge grounds and what controls sponge biomass on the seafloor. Strong semidiurnal tidal currents were recorded at the high sponge biomass site which transport water cross-shelf over a diurnal tidal cycle. Tidal currents were on average two times lower bottom current speeds at the low sponge biomass site. High bottom nutrient concentrations (silicic acid, SiO_2) were measured at the high sponge biomass site, which was likely related water flowing southward from Baffin Bay. The landers recorded the arrival of fresh phytoplankton derived material in February, suggesting strong benthic-pelagic coupling during spring months. In summer, while phytoplankton concentrations in the surface water were likely still higher, no chlorophyll-a fluorescence was recorded at the seafloor, which suggest a decoupling of the benthic and pelagic ecosystem in summer months. These results indicate that strong bottom tidal currents likely benefit benthic filter feeders as sponges and gorgonians on the Labrador Shelf, by increasing food supply and replenishing nutrients in bottom waters.

Nederlandse samenvatting

De diepzee beslaat meer dan 99% van het totaal beschikbaar leefbare habitat op aarde, maar is tot nog toe één van de minst goed bestudeerde ecosystemen. In het algemeen begint de diepzee bij 200 meter diepte, een diepte waaronder de hoeveelheid licht die doordringt in de waterkolom te laag is voor het plaatsvinden van fotosynthese. Organismes die op de zeebodem leven in de diepzee zijn daarom voor het grootste deel afhankelijk van organisch materiaal geproduceerd aan het zeeoppervlak (bijv., fytoplankton) voor hun voedselbronnen. Omdat maar een klein deel van dit aan de oppervlakte geproduceerd organisch materiaal de zeebodem bereikt (één tot drie procent), worden grote delen van de oceaan gezien als voedselgelimiteerd en in sommige gevallen omschreven als woestijnen in de diepzee (**hoofdstuk 1**). Desalniettemin zijn er bepaalde gebieden in de diepzee waar levendige en bloeiende koudwaterkoraalriffen en diepzeesponsvelden aangetroffen kunnen worden. Deze riffen en sponsvelden bieden onderdak aan talrijke soorten (bijv., vissen, krabben) en worden daarom gezien als knooppunten van biologische activiteit. Dit proefschrift onderzoekt hoe deze knooppunten kunnen bestaan in een anderzijds voedselgelimiteerde omgeving als de diepzee.

Koudwaterkoralen en diepzeesponzen worden gezien als biobouwers of ecosysteemingenieurs, omdat ze met hun lichaamsplan een leefgebied bieden voor andere soorten in de diepzee. Ze staan beide bekend als filtervoeders, waarbij koralen onder de passieve filtervoeders vallen en sponzen onder de actieve filtervoeders. Koralen filteren (organisch) zwevende stofdeeltjes uit de bovenliggende waterkolom en zijn daarbij afhankelijk van een (sterke) bodemstroom voor de aanvoer van voldoende voedsel. Sponzen filteren (voedsel) deeltjes uit het water door actief water door hun lichaamsplan te pompen. Beide organismes worden vaak gevonden in de diepzee in gebieden waar specifieke omgevingscondities ervoor zorgen dat vers organisch materiaal wordt getransporteerd van het zeeoppervlak naar de zeebodem. Als deze gunstige omgevingsomstandigheden voor een langere tijd aanhouden, kunnen de koudwaterkoralen en diepzeesponzen op de zeebodem respectievelijk grote riffen/bergen of sponsvelden vormen (**hoofdstuk 1**).

Hoewel onze kennis van deze ecosystemen in de afgelopen jaren significant is toegenomen, is er momenteel nog weinig bekend onder welke milieuomstandigheden waaronder koudwaterkoralen en sponzen goed gedijen en wat de ruimtelijke verspreiding van deze dieren bepaald. Aangezien de druk op deze ecosystemen door antropogene stressoren, zoals klimaatverandering en visserij, op dit moment toeneemt, is kennis over de omstandigheden waarin deze waardevolle ecosystemen gedijen essentieel in het voorspellen van hun toekomst. Dit proefschrift beoogt de mechanismes te begrijpen achter de ruimtelijke verdeling van koudwaterkoralen en sponzen in de diepzee. In het bijzonder onderzoekt deze thesis: i) mechanismes van voedseltoevoer naar koudwaterkoraalriffen (**hoofdstuk 2**), ii) hoeveel voedsel is er nodig voor een koudwaterkoraalrif om zichzelf in stand te hou-

den (**hoofdstuk 3**), iii) of de ruimtelijke verspreiding van koudwaterkoraalbiomassa kan worden voorspeld op basis van hydrodynamica (stromingen), het transport van organisch materiaal, en koudwaterkoraalfysiologie (**hoofdstuk 4**), de milieuomstandigheden die een hoge biomassa van sponzen op een diepzeesponsveld ondersteunen (**hoofdstuk 5**).

Eerder onderzoek naar voedselvoorzieningsmechanismes bij koudwaterkoraalriffen rapporteerde meestal gegevens van momentopnames (bijv. enkele uren) of langetermijnmetingen (maanden/jaar). Weinig studies hebben gekeken naar de organische stofverdeling (voedsel) over een dagelijkse getijdencycles, en geen enkele studie rapporteerd dit over het volledige organisch stofspectrum (bijv., bacteriën, virussen, opgelost– en stoffelijk organische deeltjes). Dit proefschrift presenteert gegevens van vier 24-uurs waterkolommetingen langs een transect over een koudwaterkoraalheuvel op Rockall Bank, Noordoost-Atlantische Oceaan (**hoofdstuk 2**). De waterkolom boven de koudwaterkoraalheuvel was dynamischer dan op de helling van Rockall Bank. De resultaten van dit hoofstuk wijzen erop dat het transport van vers organisch materiaal naar het koudwaterkoraalrif op de zeebodem wordt bevorderd via drie routes: i) advectief transport van fytoplankton van middenwaterdieptes met behulp van interne golven met amplitudes van 200 – 300 m, ii) de aanvuling van voedingstoffen in het oppervlaktewater zou de productie van diatomeeën kunnen bevorderen, iii) de vorming van fecale zoöplanktonpellets kan het neerwaartse transport van organische deeltjes versnellen. Koudwaterkoralen en de bijbehorende riffauna maken gebruik van verscheidene voedselbronnen, maar zijn uiteindelijk afhankelijk van aan de oppervlakte geproduceerd organisch materiaal. Daarbij toont deze studie (**hoofdstuk 2**) aan dat de variabiliteit in de kwaliteit en de samenstelling van het organisch materiaal groot is gedurende een dagelijkse getijdencyclus en dat hiermee rekening moet worden gehouden in toekomstige onderzoeksexpedities.

Kwantitatieve metingen van de stofwisselingsbehoeften van koudwaterkoraalriffen zijn schaars, en ontbreken momenteel geheel voor riffen op >250 meter diepte. Daarnaast is er weinig bekend over de stikstofcyclus op koudwaterkoraalriffen. In dit proefschrift zijn de benthische fluxen van zuurstof en stikstof gemeten op twee diepere koudwaterkoraalriffen en sediment gedomineerde referentielocaties op Rockall Bank (600 – 700 m diepte; **hoofdstuk 3**). *In situ* metingen van de benthische zuurstofopname werden uitgevoerd met de niet-invasieve *in situ* 'Aquatic eddy covariance' techniek. *Ex situ* metingen van de benthische zuurstofopname en stikstoffluxen werden gedaan door middel van 'box core' incubaties aan boord van het onderzoeksschip. De zuurstofopname van koudwaterkoraalriffen op Rockall Bank is gemiddeld vijf keer zo hoog als van sedimenten van vergelijkbare diepte. Bovendien zijn koudwaterkoraalriffen een bron van ammonium en nitraat in de diepzee. Deze hoge zuurstofopname en stikstofexcretie wordt voornamelijk veroorzaakt door de aanwezigheid van levende koralen en, alhoewel in mindere mate, door dode koraalstructuren. De resultaten van deze studie (**hoofdstuk 3**) tonen aan dat koudwaterkoraalriffen knooppunten zijn in de koolstof- and stikstofkringloop in de diepzee.

Een mechanistische modelbenadering werd gebruikt om de biomassa van koudwaterkoraal en de benthische respiratie te voorspellen op basis van hydodynamica, het transport van organisch materiaal, en de fysiologie van koudwaterkoralen (**hoofdstuk 4**). Tot dusver zijn de onderzoeksinspanningen om de ruimtelijke verdeling van koudwaterkoralen te voorspellen gebaseerd op statistische methoden. Hoewel deze statistische modellen goede voorspellingen geven van de verspreiding van geschikte habitats voor koudwaterkoralen, voorspellen deze modellen vaak alleen de aan- en afwezigheid van koralen en zijn zij afhankelijk van de beschikbaarheid van gedetailleerde waarnemingsgegevens. Omdat de milieuomstandigheden in de diepzee aan het veranderen zijn, zijn er nieuwe instrumenten nodig om het effect van deze veranderingen op koudwaterkoralen te evalueren en te voorspellen. Uit de resultaten van dit model blijkt dat de biomasssa van koudwaterkoralen het hoogst is op de bovenste hellingen van de koudwaterkoraalheuvels in het studiegebied. Dit zijn de locaties waar organisch materiaal dichtbij de zeebodem in voldoende mate wordt aangevuld en waar de bodemstromingen sterk zijn. Concurrentie tussen koudwaterkoralen voor organisch materiaal bleek de sleutel te zijn om tot een goede voorspelling te komen van de ruimtelijke verspreiding van koudwaterkoraalbiomassa. De modelvoorspellingen kwamen goed overeen met observaties en de benthische respiratiewaarden kwamen overeen met veldmetingen (**hoofdstuk 3**). De hier gepresenteerde modelbenadering kan worden gebruikt om een mechanistisch inzicht te krijgen in de effecten van veranderende milieuomstandigheden zoals temperatuur, fytoplankton export van het oceaanoppervlak, of veranderende oceaanstromingen op de biomassa van koudwaterkoralen in de diepzee en kan daarbij worden toegepast op andere studiegebieden en soorten.

Bodemstromingen en milieuomstandigheden werden voor een jaar lang gemeten op twee contrasterende diepzeesponsvelden met hoge- en lage sponsbiomassa op de continentale plaat van Labrador, Noordoost-Canada (**hoofdstuk 5**). Tot nu toe is er weinig bekend over de milieuomstandigheden op diepzeesponsvelden en wat de biomass van sponzen in de diepzee bepaalt. In dit proefschrift werden sterke semidiurnale getijdestromingen gemeten op een diepzeesponsveld met hoge sponsbiomassa. Deze stromingen transporteerden het bodemwater heen- en weer over de continentale plaat tijdens een dagelijkse getijdencyclus. De getijdestromingen waren gemiddeld twee keer zo sterk op het sponsveld met hoge biomassa vergeleken met het sponsveld met lage biomass. Daarnaast werden er verhoogde nutriëntconcentraties (kiezelzuur, SiO_2) gemeten in het bodemwater boven het hoge biomassa sponsveld, wat waarschijnlijk verband hield met water dat zuidwaarts stroomde vanuit de Baffinbaai. De benthische landers registreerde de aanwezigheid van vers fytoplankton in februari, wat wijst op een sterke benthisch-pelagische koppeling in het voorjaar. In de zomer, terwijl de fytoplanktonconcentraties in het oppervlaktewater waarschijnlijk nog steeds hoger waren, werd er geen chlorophyll-a gerelateerde fluorescentie gemeten op zeebodem op beide sponsvelden, wat wijst op

een ontkoppeling van het benthische en pelagische ecosysteem in de zomermaanden. De resultaten van **hoofdstuk 5** suggereren dat sterke getijdenstromingen op de zeebodem van de continentale plaat van Labrador gunstig zijn voor benthische filtervoeders zoals sponzen en gorgonen doordat zij het voedselaanbod vergroten en de voedingsstoffen in het bodemwater aanvullen.

Acknowledgements

First of all, I would like to thank you, the reader, for having stuck with me to the end of this thesis and for only starting to read the acknowledgements after reading the whole book. For the ones that are here to look up their name, that's okay, you can start reading hereafter.

Then, I would first and most especially like to thank my supervisor **Dick** for his guidance and support (and patience) throughout my PhD. **Dick**, thanks a lot for taking a chance with me for this PhD project and introducing me to the world of deep-sea research, biogeochemistry, and modelling. In these past years I've learned a lot from you (don't know where to start), not only in terms of scientific writing/thinking and modelling, but also in believing in the significance of my own results. Thank you also for giving me the chance to follow my own interests, as the original plan for this PhD was a lot more model focused, I recall. We've had some great times on the many conferences, ATLAS general assemblies, and research cruises we've participated in. I really enjoyed watching (especially for you nail-biting) Ajax – Olympique Lyon in the top of a small bar in Galway after a long and intense research cruise or exploring the *Ramen* scene in Monterrey and San Diego. I hope we'll get to eat some Ramen again on a conference in the near future! **Karline**, thank you very much for all your help with questions I had on biogeochemistry and mathematical modelling in the past years. Whenever I had any (modelling) issues, you seemed to solve them on the back of an envelop and with a big laugh. This thesis, and especially chapter 4, would not be there without you. **Furu and Gerard & Marc** (aka 'the grumpy muppets', not my words!)**,** thanks a lot for your help with my incubation experiments, on research cruises, sediment trap samples, and revising or commenting on my manuscripts. I had a great time with you on Texel setting-up the box core incubations and onboard of the Pelagia, and always enjoyed our discussions on the Rockall Bank' cold-water corals. **Gert-Jan**, thank you for being my promotor during this PhD. Especially at the end you helped a lot during our (online) discussions, and I want to thank you (and **Dick**) for keep supporting me to the end to finish this thesis when life wasn't so smooth.

This thesis would not be here without the help and company of my fellow PhD students and colleagues at NIOZ. **Sandra**, a big thank you for your help in the lab, for cruise preparations, on writing, and on thinking critically. The on-board incubation experiment in this thesis would not have happened without you. Besides, I enjoyed our (Amaaazing) time off during conferences and cruises in Monterey and Galway. I always admired your passion for (and persistence in!) cold-water coral research and science in general and I hope we can collaborate on some cool project in the future. **Anna**, also a member of the Yerseke cold-water coral research team, and you are, I think, the smart one. You helped me a lot understanding theoretical ecology and the use of mathematical modelling. Thank you for all your help and let's keep exchanging (very cute) pictures of our little boys! **Tanja,** my

office mate for the first (three?) years and one the few deep-sea crew in Yerseke. Thank you for all our discussions on science, football, and deep-sea creatures. Your determination and (impressive) work ethic have both amazed and inspired me. Also, thank you for being in my reading committee, who would have thought that a few years ago! I would like to thank **Pieter, Peter, Jurian, Yvonne, Jan, Anton** from the NIOZ lab for all your work processing my samples, helping me in the lab, and helping to interpret the results**.** A big thanks also the **crews of the R/V Pelagia and CCGS Amundsen**, for making this line of work possible. **Yvo Witte**, thank you for helping me set-up the incubation experiments on-board the Pelagia, we had especially fun with the inventive cooling system, I think. Then, I want to thank the following NIOZ colleagues, staff, students, and technicians I've met over the years, from Texel and from Yerseke, some while playing soccer, some during conferences or over a coffee break, you've made this PhD a lot more fun (in no particular order): **Justin, Chiu, Emil, Rob, Kiki, Lorenz, Jaco, Tim, Greg, Marieke, Marieke, Camilla, Aimée, Christine, Elly, Jan, Long, Rosanna, Tisja, Sofia, Ulrike, Manuel, Beatriz, Hans, Alexander, Lauren, Jetze, Alice, Jacco, Roeland, Tim, Anna, Dunia, Christiaan, Carolina, Jim, Bas, Jette, Celine, Koen, Laura, Sharyn, Loreta,** and **Tom.** Special thanks to the two students I helped supervise **Britt** and **Jerry,** it was a pleasure working with you. A big thanks also to all the colleagues from the EU Horizon 2020 ATLAS project. **Christian**, thank your for your help during (many) online meetings to interpret CTD-yoyos and ADCP data. I can't think of another person who can explain physical oceanography in a more understandable way. I also enjoyed our discussions over dinner/beers during the ATLAS assemblies in Mallorca and Edinburgh. It's a pity that COVID blocked my visit to Roskilde (already had booked the tickets!), but maybe we can change that in the near future. **George**, thank you for helping me to grasp the world of lipids and fatty acids, and improving my academic (English) writing skills. But most of all, and I am sure you have forgotten this, you helped me by saying the words: "you're a clever guy" to me during a whiskey "tasting" night in a Scottish castle. This is one of the things that helped me through my thesis during the more difficult period thereafter. The general assemblies of ATLAS were always a lot of fun, I would like to thank the following ATLAS folks that I've met over the years in Mallorca or Edinburgh: **Laurence, Johanne, Maria, Cova, Georgios, Stephanie, Marina, Murray, Dierk, Stuart, Igor, Erica, Ellen, Sabena, Steve, Lorenzo, Ronnie, Carlos,** and **the people I am forgetting at this moment (thousand apologies)**. Finally, I would like to thank all the other co-authors on my manuscripts: **Mads, Eva, Evi, Graham,** and **Barry**.

Migle, thanks a million for your beautiful illustrations for this thesis and putting the whole thing together. I am sure I will get a lot of compliments for actually your work!

Omdat een proefschrift veel werk is, en er zonder momenten van ontspanning ook geen inspanning kan plaatsvinden, wil ik de volgende vrienden bedanken voor hun steun,

maar vooral ook voor hun afleiding: **Paul**, **Pim, Luc, Jan, Didier, David, Roland, Merlijn, Jelle, Jurian, Koen, Tobie, Jori, Knillis, Stefan, Antoon, Jirka, Thijs, Luuk,** en **Jonah**. Daarnaast, mochten jullie dit ooit lezen, de jongens van (voormalig) **Athena Heren 4** bedankt voor de nodige lichamelijke ontspanning in de afgelopen jaren.

Dan wil ik graag mijn lieve familie de Froe/Wijnberg/Jacobs bedanken voor de interesse in mijn onderzoek tijdens (voornamelijk) de verjaardagen en kerstdiners: **Beatrijs, Charlotte, Elie** (merci)**, Martijn, Marjo, Ellen, Piet, Laurelin, Melian, Quinten, Arthur, Martine, Zina, Max, Frans, Marieke, Michaël, Tanya** (спасибо), en vooruit, **Nick & Tim**. Gracias **a mi familia colombiana** que siempre estuvo a mi lado apoyándome. En especial, a **Sandra**, gracias por todo, me/nos has ayudado enormemente en los últimos años y esta tesis no habría sido posible sin ti.

Heleen & papa, bedankt voor al jullie steun de afgelopen jaren. Het is niet altijd makkelijk geweest de afgelopen jaren met het verlies van mama, maar jullie 'krullende neuzen' hebben me erdoorheen geholpen. Ik hou van jullie. Zonder jullie was dit boekje nooit gedrukt (wel lezen hé).

Es, ik zou niet weten waar ik moet beginnnen om jou te bedanken. Je hebt me aangespoord om een PhD te gaan doen en mijn interesses te volgen. Ik leer nog elke dag van jouw enthousiasme voor dieren en natuur. Bedankt voor al je steun en begrip als ik weer eens, zeker de laatste maanden, aan mijn thesis moest werken. Ik hou heel veel van je, en ik hoop dat we samen nog vele avonturen gaan beleven samen met onze hapsnurkers. Daarover gesproken, als laatste, **Bruno en Matías**, bedankt dat jullie in mijn leven zijn gekomen. Het is elke dag een feest.

About the author

Evert de Froe was born on the 10th of June 1990 in Breda (the south of the Netherlands) and raised in a close-by village called Ulvenhout. He moved to the big city of Wageningen in 2008 to study environmental sciences, but then in 2012 took a definitive detour towards the world of marine ecology. He completed his master's in Aquaculture and Marine Resources Management with projects investigating the state of the tropical coral reef on Bonaire, Dutch Antilles, and small-scale tuna fishery in the north of Celebes, Indonesia. In 2016, Evert joined the Netherlands Institute for Sea Research (NIOZ) to work under the supervision of Dick van Oevelen, Karline Soetaert, and Gert-Jan Reichart on a PhD project that investigated how cold-water corals and deep-sea sponges can thrive in an otherwise food limited environment as the deep sea. He joined two research cruises towards the cold-water coral reefs of Rockall Bank, North Atlantic Ocean. Currently, he is working as a postdoctoral fellow at the Fisheries and Marine Institute of Memorial University in St. John's, Newfoundland, Canada. Together with Maxime Geoffroy and Evan Edinger he is investigating if glacial troughs are hotspots of biodiversity, abundance, and benthic-pelagic coupling in the Northeast Canadian (sub-) Arctic region. To this end, he joined a research expedition on the CCGS Amundsen in 2022 visiting glacial troughs on the continental shelf of the Labrador Sea.

List of publications

Scientific peer-reviewed articles

De Froe, E., Rovelli, L. Glud, R. N., Maier, S., Duineveld, G., Lavaleye, M., Van Oevelen, D. (2019), Benthic Oxygen and Nitrogen Exchange on a Cold-Water Coral Reef in the North-East Atlantic Ocean. Frontiers in Marine Sciences, DOI: 10.3389/fmars.2019.00665

Maier, S. R., Mienis, F., de Froe, E., Soetaert, K., Lavaleye, M., Duineveld, G., et al. (2021). Reef communities associated with 'dead' cold-water coral framework drive resource retention and recycling in the deep sea. Deep Sea Research Part I: Oceanographic Research Papers, doi: 10.1016/j.dsr.2021.103574.

van der Kaaden, A.-S., Mohn, C., Gerkema, T., Maier, S. R., de Froe, E., van de Koppel, J., et al. (2021). Feedbacks between hydrodynamics and cold-water coral mound development. Deep Sea Research Part I: Oceanographic Research Papers, doi: 10.1016/j.dsr.2021.103641.

De Clippele, L. H., van der Kaaden, A.-S., Maier, S. R., de Froe, E., and Roberts, J. M. (2021). Biomass Mapping for an Improved Understanding of the Contribution of Cold-Water Coral Carbonate Mounds to C and N Cycling. Frontiers in Marine Science, doi: 10.3389/fmars.2021.721062

de Froe, E., Maier, S. R., Horn, H. G., Wolff, G. A., Blackbird, S., Mohn, C., et al. (2022). Hydrography and food distribution during a tidal cycle above a cold-water coral-mound. Deep Sea Research Part I: Oceanographic Research Papers, doi: 10.1016/j.dsr.2022.103854.

Mohn, C., Hansen, J. L. S., Carreiro-Silva, M., Cunningham S. A., **de Froe, E**., Dominguez-Carrió, C., Gary, S., Glud., R. N., Göke, C., Johnson, C., Morato, T., Friis Møller, E., Rovelli, L., Schulz, K., Soetaert, K., van Oevelen, D., (*in review*). Tidal to decadal scale hydrodynamics at two contrasting cold-water coral sites in the Northeast Atlantic. Submitted to *Progress in Oceanography*.

Maier, S. R., Brooke, S., De Clippele, L. H., **de Froe, E.**, van der Kaaden, A. S., Kutti, T., Mienis, F., van Oevelen, D. (*in review*). On the paradox of flourishing cold-water coral reefs in the food-limited deep sea. *Biological reviews*.

de Froe, E., Yashayaev, Mohn, C., Vad, J., Mienis, F., Duineveld, G., Kenchington, E., Head, E., Ross, S., Wolff, G., Blackbird, S., Roberts, J. M., McDonald, B, Tulloch, G., van Oevelen, D., (*in preparation*). Year-long benthic measurements of environmental conditions indicate high sponge biomass is related to strong bottom currents over the Northern Labrador shelf.

De Froe, E., Soetaert, K., van der Kaaden, A., Mohn, C., de Clippele, L. H., van Oevelen, D., (*in preparation*). Modelling cold-water coral biomass and respiration based on physiology, hydrodynamics, and organic matter transport.

Reports

Orejas, C., de Froe, E., van Oevelen, D., ATLAS Deliverable 2.1: Compilation of existing physiological data on CWC response to different conditions of food supply and oceanographic change scenarios. DOI: https://doi.org/10.5281/zenodo.321898.

Wolff, G; van Oevelen, D; Glud, RN; Rovelli, L; Carreiro-Silva, M; Mohn, C; Blackbird, S; de Froe, E; Korte, L; Rakka, M; Bilan, M; Dominguez-Carrió, C; Tulloch, G; Vad, J; MacDonald, B; Kenchington, E; Cote, D; Ross, S; Roberts, JM, ATLAS Deliverable 2.3 Community respiration rates, biogeochemical characteristics of organic matter and fauna at ATLAS Case Study Sites. DOI: https://doi.org/10.5281/zenodo.4243873.

Van Oevelen, D., de Froe, E., Mohn, C., Soetaert, K., ATLAS Deliverable 2.5: Integrative and coupled model based on hydrodynamics, biogeochemistry and physiology for the prediction of biomass and biogeochemical dynamics, projections under future oceanic conditions and marine spatial planning. DOI: https://doi.org/10.5281/zenodo.4095448.

Van Oevelen D., Mohn, C., Schulz, K., van Rijswijk, P., de Froe, E., S. Maier, Cheng C., Horn, H., van der Kaaden, A. S., van Haastregt, B., Wubben, E. 2018. Cruise report 64PE436 – NICO leg 9A Untangling the topography – hydrography interaction that sustains cold-water coral reefs https://doi.org/10.5281/zenodo.1454097

Van Oevelen D., Reichart, G-J, Mienis, F., Duineveld, G., Lavaleye, M., Maier, S., de Froe, E., Rovelli, L., Blackbird, S., Versteeg, W., T'Jampens, M.. 2018. Cruise report 64PE420 ATLAS cold-water coral carbon cycling. https://doi.org/10.5281/zenodo.1454465

Zanke, F., de Froe, E., (2015) Small-scale variation in coral reef quality on the leeward side of Bonaire, IMARES report. https://www.dcbd.nl/document/small-scale-variation-coral-reef-quality-leeward-side-bonaire

Data products

de Froe, E., Mohn, C., Soetaert, K., van Oevelen, D. (2020). ATLAS Deliverable 2.5: Model code for the Rockall Bank case study area. DOI: https://doi.org/10.5281/zenodo.4250150.

De Froe, E., Rovelli, L. Glud, R. N., Maier, S., Duineveld, G., Lavaleye, M., Van Oevelen, D. (2019), Benthic Oxygen and Nitrogen Exchange on a Cold-Water Coral Reef in the North-East Atlantic Ocean. DOI: https://doi.org/10.1594/PANGAEA.911412.

de Froe, E., Zanke, F., Meis, R., Scholten, Y. (2017) Coral inventory Bonaire, 2014 and 2017, https://www.dcbd.nl/document/coral-inventory-bonaire-2014-and-2017-0

Conference talks and posters

de Froe, E., Maier, S., Bannister, R., Kutti, T., van Oevelen, D. (2017), Modelling a feeding experiment of the cold-water coral Lophelia pertusa, *Netherlands Annual Ecology Meeting*, Lunteren, the Netherlands. Poster.

de Froe, E., S. Maier, F. Mienis, G. Duineveld, M. Lavaleye, D. van Oevelen: Oxygen and nutrient dynamics of a cold-water coral reef in the North-East Atlantic Ocean. 15th Deep-Sea Biology Symposium, Monterey, CA, USA, September 2018. Oral presentation.

De Froe, E., Soetaert, K., van der Kaaden, A., Mohn, C., van Oevelen, D. (2020) A Mechanistic Modelling Approach to Predict Cold-Water Coral Biomass Based on Organic Matter and Hydrodynamics. *Ocean Sciences meeting*, San Diego, CA, USA, February 2020. Oral presentation.

Outreach

Radio-interview with regional broadcasting channel Omroep Zeeland (in Dutch): https://www.omroepzeeland.nl/nieuws/10658455/zeeuwse-wetenschappers-op-expeditie-om-oceanen-te-redden

Podcast (by Edda Heinsman) on a research cruise on the R/V Pelagia, broadcasted on Dutch national radio: https://www.nporadio1.nl/podcasts/docs/84059/109-het-wonder-van-het-koraal

Utrecht University
Faculty of Geosciences
Department of Earth Sciences

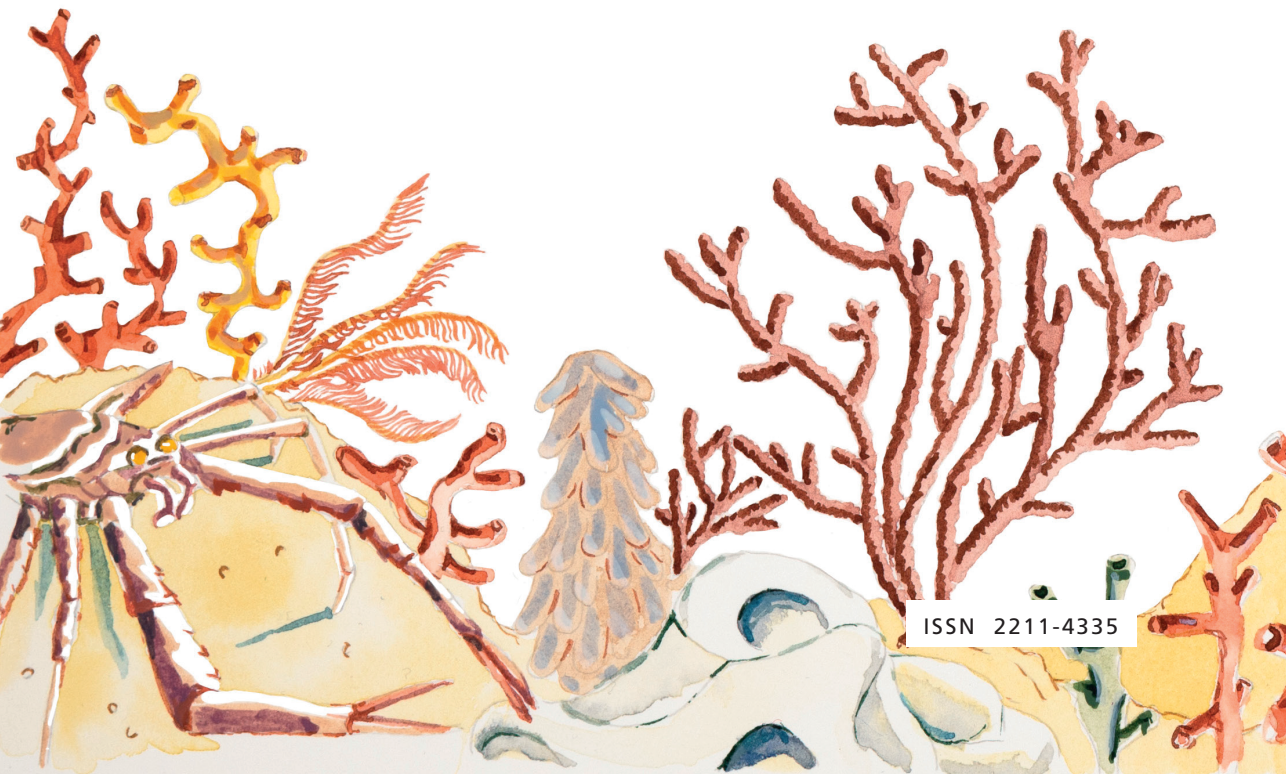

ISSN 2211-4335